NASA-CR-197934

THE OHIO STATE UNIVERSITY

A Uniform Geometrical Optics and an Extended Uniform Geometrical Theory of Diffraction for Evaluating High Frequency EM Fields Near Smooth Caustics and Composite Shadow Boundaries

E.D. Constantinides and R.J. Marhefka

The Ohio State University

ElectroScience Laboratory

Department of Electrical Engineering
Columbus, Ohio 43212

Final Report 725311-3
Grant No. NSG-1498 Supplement 2
October 1994

National Aeronautics and Space Administration
Langley Research Center
Hampton, VA 23665

and

AFEWC/EST
San Antonio, TX

A. Approved for public release; Distribution is unlimited

NOTICES

When Government drawings, specifications, or other data are used for any purpose other than in connection with a definitely related Government procurement operation, the United States Government thereby incurs no responsibility nor any obligation whatsoever, and the fact that the Government may have formulated, furnished, or in any way supplied the said drawings, specifications, or other data, is not to be regarded by implication or otherwise as in any manner licensing the holder or any other person or corporation, or conveying any rights or permission to manufacture, use, or sell any patented invention that may in any way be related thereto.

50272-101

REPORT DOCUMENTATION PAGE	1. REPORT NO.	2.	3. Recipient's Accession No.

4. Title and Subtitle
A Uniform Geometrical Optics and An Extended Uniform Geometrical Theory of Diffraction for Evaluating High Frequency EM Fields Near Smooth Caustics and Composite Shadow Boundaries

5. Report Date
October 1994

6.

7. Author(s)
E.D. Constantinides and R.J. Marhefka

8. Performing Org. Rept. No.
725311-3

9. Performing Organization Name and Address
The Ohio State University
ElectroScience Laboratory
1320 Kinnear Road
Columbus, OH 43212

10. Project/Task/Work Unit No.

11. Contract(C) or Grant(G) No.
(C)
(G) NSG-1498 Supplement 2

12. Sponsoring Organization Name and Address
NASA Lewis Research Center, Hampton, VA 23665
and
AFEWC/EST, San Antonio, TX

13. Report Type/Period Covered
Final

14.

15. Supplementary Notes

16. Abstract (Limit: 200 words)

A uniform geometrical optics (UGO) and an extended uniform geometrical theory of diffraction (EUTD) are developed for evaluating high frequency electromagnetic (EM) fields within transition regions associated with a two and three dimensional smooth caustic of reflected rays and a composite shadow boundary formed by the caustic termination or the confluence of the caustic with the reflection shadow boundary (RSB). The UGO is a uniform version of the classic geometrical optics (GO). It retains the simple ray optical expressions of classic GO and employs a new set of uniform reflection coefficients. The UGO also includes a uniform version of the complex GO ray field that exists on the dark side of the smooth caustic. The EUTD is an extension of the classic uniform geometrical theory of diffraction (UTD) and accounts for the non-ray optical behavior of the UGO reflected field near caustics by using a two-variable transition function in the expressions for the edge diffraction coefficients. It also uniformly recovers the classic UTD behavior of the edge diffracted field outside the composite shadow boundary transition region.

The approach employed for constructing the UGO/EUTD solution is based on a spatial domain physical optics (PO) radiation integral representation for the fields which is then reduced using uniform asymptotic procedures. The UGO/EUTD analysis is also employed to investigate the far-zone RCS problem of plane wave scattering from two and three dimensional polynomial defined surfaces, and uniform reflection, zero-curvature, and edge diffraction coefficients are derived. Numerical results for the scattering and diffraction from cubic and fourth order polynomial strips are also shown and the UGO/EUTD solution is validated by comparison to an independent moment method (MM) solution. The UGO/EUTD solution is also compared with the classic GO/UTD solution. The failure of the classic techniques near caustics and composite shadow boundaries is clearly demonstrated and it is shown that the UGO/EUTD results remain valid and uniformly reduce to the classic results away from the transition regions. Mathematical details on the asymptotic properties and efficient numerical evaluation of the canonical functions involved in the UGO/EUTD expressions are also provided.

17. Document Analysis a. Descriptors
ASYMPTOTIC
RCS
UTD (UNIFORM THEORY OF DIFFRACTION)
DIFFRACTION

b. Identifiers/Open-Ended Terms

c. COSATI Field/Group

18. Availability Statement
A. Approved for public release;
Distribution is unlimited.

19. Security Class (This Report)
Unclassified

21. No. of Pages
215

20. Security Class (This Page)
Unclassified

22. Price

(See ANSI-Z39.18) *See Instructions on Reverse* OPTIONAL FORM 272 (4-77)
Department of Commerce

Contents

List of Figures

List of Tables

Chapter 1

Introduction

A uniform geometrical optics (UGO) and an extended uniform geometrical theory of diffraction (EUTD) are developed for evaluating high frequency electromagnetic (EM) fields within transition regions associated with smooth caustics of reflected rays and composite shadow boundaries. Although such transition regions usually occupy a small portion of the coordinate space surrounding an opaque scattering object, they contain some very complicated and yet most interesting wave phenomena. Composite shadow boundaries occur when a smooth caustic formed by an envelope of geometrical optics (GO) [1] reflected rays is terminated due to an edge in the reflecting boundary, or when the smooth caustic is in the immediate vicinity of the reflection shadow boundary (RSB). Figures 1.1 and 1.2 depict radiation/scattering problems that represent typical situations of interest for this analysis. In the concave surface example of Figure 1.1 the composite shadow boundary is formed by the termination of the smooth caustic occurring at T. This termination also generates a complex ray shadow boundary (CRSB) on the dark side of the smooth caustic. In the case of the concave-convex boundary of Figure 1.2 the smooth caustic is not terminated and therefore a CRSB does not exist; however, a transition region is formed when the edge at Q_a is near the point of inflection, Q_p, and the RSB is in close proximity of the smooth caustic.

The UGO is a uniform version of the classic GO. It retains the simple ray optical expressions of classic GO and employs a new set of uniform high frequency reflection coefficients that provide for a finite reflected field near a smooth caustic on the lit

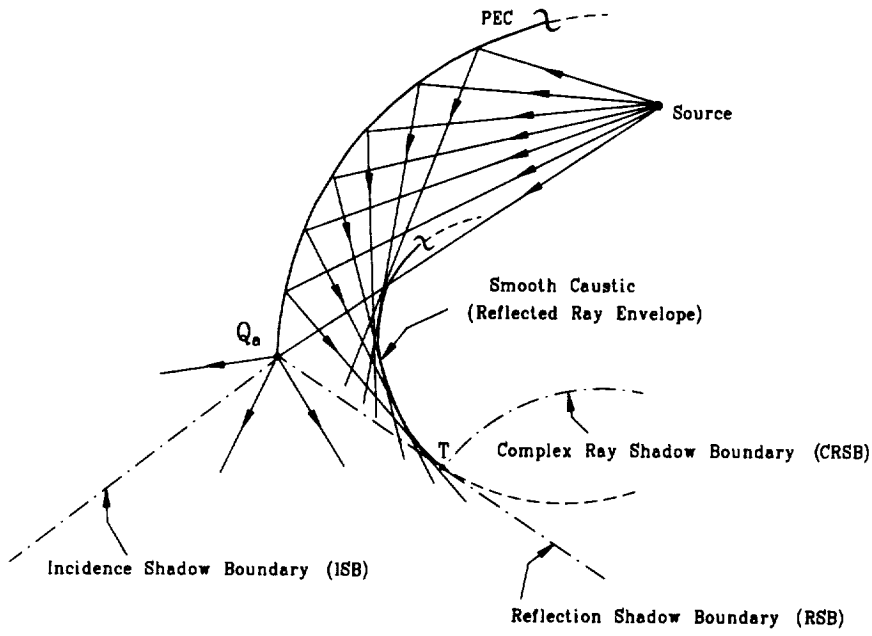

Figure 1.1: Scattering and diffraction from a concave boundary containing an edge.

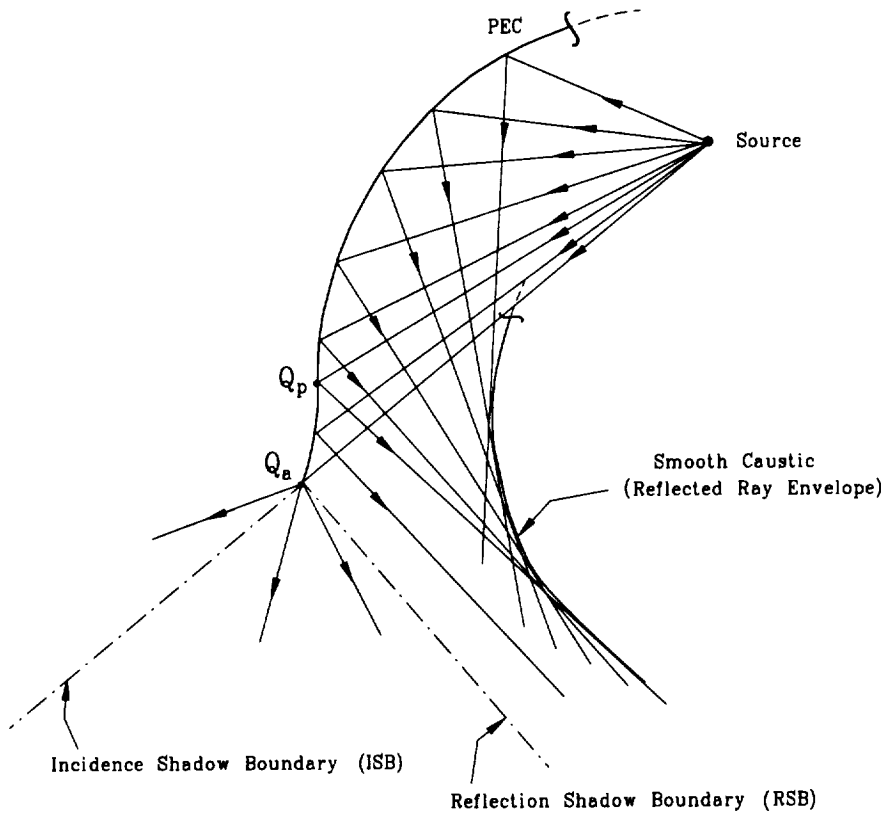

Figure 1.2: Scattering and diffraction from a concave-convex boundary containing an edge.

side. The UGO also encompasses a uniform version of the complex GO (CGO) ray field of Ikuno and Felsen [2, 3] that exists on the dark side of the smooth caustic. The EUTD is meant as an extension of the classic uniform geometrical theory of diffraction (UTD) of Kouyoumjian and Pathak [4] which is regarded as a uniform version of Keller's geometrical theory of diffraction (GTD) [5]. The UTD provides for a finite field associated with the diffracted rays and also compensates the discontinuities of the classic GO fields across the optical boundaries. However, in the immediate vicinity of caustics the incident and/or reflected fields do not exhibit the simple ray optical behavior predicted by classic GO and therefore the UTD fails to provide the necessary corrections near a composite shadow boundary formed by the confluence of a smooth caustic and a ray shadow boundary. The EUTD developed in this report accounts for the non-ray optical behavior of the UGO reflected field near caustics by using a more sophisticated transition function in the expression for the edge diffraction coefficient. It also uniformly recovers the classic UTD behavior of the diffracted field outside the composite shadow boundary transition region.

The approach employed in this report to construct the UGO/EUTD solution for the high frequency EM fields near smooth caustics and composite shadow boundaries is based on a spatial domain radiation integral representation for the fields scattered by a perfectly conducting smoothly indented surface containing an edge. The radiation integral is then evaluated using uniform asymptotic procedures to recover the uniform reflected, complex ray, and edge diffracted fields. The asymptotic estimate for the surface current in the radiation integral representation is found using the physical optics (PO) [6] approximation and therefore the resulting solution only includes first order scattering mechanisms that remain valid away from regions where grazing fields exist. In addition, the resulting expressions for the edge diffracted field are heuristically modified to satisfy reciprocity and the local boundary condition on the scattering surface. Two methods are employed for the asymptotic reduction of the PO radiation integral. The first method employs the Chester et al. expansion [7] which results in a rigorous asymptotic reduction of the PO radiation integral. Although the resulting solution is not in a UGO/EUTD format, that is the expression for the fields

is not in terms of the conventional ray optical GO/GTD description multiplied by an appropriate transition function, it provides for a systematic approach for obtaining the higher order terms in the uniform asymptotic expansion for the fields in cases where slope scattering effects are present. The second method for the asymptotic reduction of the PO radiation integral employs the method of steepest descent [8]. The resulting expressions in this case are indeed in a UGO/EUTD format and are in agreement with the results of the first method to the first order term. Both solutions reduce to the conventional GO/UTD and CGO expressions outside the transition regions associated with the smooth caustic and composite shadow boundary.

The subject of high frequency field behavior near a terminated caustic of a composite shadow boundary was investigated by Levey and Felsen [9] using a boundary layer expansion. However, they did not provide a useful engineering solution since they only concentrated on the mathematical aspects of the problem and specifically on the asymptotic reduction of the relevant diffraction integral and the asymptotic properties of the incomplete Airy functions that serve as canonical functions in the uniform asymptotic representation for the fields. On the other hand, the subject of evaluating fields in regions of smooth caustics but away from caustic terminations has been investigated extensively in the past. The solution obtained by Rahnavard and Rusch [10] is strictly valid in the caustic transition region, where Albertsen et al. [11] heuristically modified their solution near caustics of the diffracted rays from a curved edge to reduce to the non-uniform result on the deep lit side of the caustic. Other solutions which use Maslov's method [12, 13] and uniformly recover the non-uniform fields outside the caustic transition regions are not very useful for engineering purposes since the relevant parameters involved in the solutions depend on the details of the caustic geometry. A uniform asymptotic high frequency solution which remains valid across smooth caustics of reflected rays, uniformly recovers the non-uniform expressions outside the caustic transition region, and is useful for engineering purposes was recently developed by Pathak and Liang [14]. Their solution, however, is not cast in a UGO format, that is the scattered field contributions do not retain the GO ray optical expressions multiplied by an appropriate transition function, and also the

effects of the caustic termination of a composite shadow boundary are not accounted for.

The ultimate goal of the work presented in this report is to develop a useful and efficient engineering solution for treating high frequency radiation and scattering problems involving higher order geometric primitives such as polynomial or spline defined surfaces that are commonly used in computer aided design (CAD) systems for the modeling of complex structures such as aircraft, ships, reflectors, etc. Such higher order surfaces often exhibit rapid curvature variation and discontinuities in surface derivatives which in turn create caustics and phase catastrophes that cannot be handled by the classic GO/UTD techniques. Numerical techniques for treating these problems such as the method of moments (MM) or PO with numerical integration still require vast amounts of computer resources for even intermediate size objects. Uniform asymptotic closed form solutions on the other hand are inherently very efficient provided the canonical functions involved are efficiently computed. They also provide significant physical insight into the various scattering and radiation processes, a fact that proves useful in radar cross section (RCS) as well as antenna pattern analysis and design.

The outline of this report is as follows: In Chapter 2, the near-zone problem for the scattered EM fields near a two dimensional smooth caustic and composite shadow boundary is formulated in terms of a spatial domain radiation integral which is then reduced using two different uniform asymptotic procedures. The first method yields a rigorous uniform asymptotic solution that provides for a systematic approach in obtaining the higher order terms in the uniform asymptotic expansion for the fields. The second method yields the desired UGO/EUTD expressions for the reflected, complex ray, and edge diffracted fields which are in agreement to the first order term with the results of the first method. The same procedure is repeated in Chapter 3 for the near-zone problem for the scattered EM fields near a three dimensional smooth caustic and composite shadow boundary. In Chapter 4, the far-zone RCS problem for the plane wave scattering from two and three dimensional polynomial defined surfaces is formulated using the procedures developed in Chapters 2 and 3. In the

far-zone problem the two methods introduced in Chapters 2 and 3 produce the same results for the reflection and zero-curvature diffraction mechanisms with the associated field expressions cast in the UGO/EUTD format. However, they result in slightly different expressions for the EUTD edge diffraction coefficient. Although the zero-curvature diffraction contribution in the far-zone problem is equivalent to the complex ray mechanism in the near-zone problem, it is easier to use since it eliminates the need for a complex extension of the scattering surface. In Chapter 5, some indicative numerical results for the scattering from cubic and fourth order polynomial strips are presented. The UGO/EUTD results are validated by comparison with results obtained using an independent method of moments (MM) solution. The UGO/EUTD results are also compared with classic GO/UTD results to demonstrate the need for the new solution. Chapter 6 summarizes the accomplishments of this report, offers some concluding remarks, and briefly discusses topics for future research. All the new UGO/EUTD reflection and diffraction coefficients are also tabulated in Chapter 6. Several appendices are also included in this report. Appendices A–E provide important mathematical details on the asymptotic properties and efficient numerical evaluation of the canonical functions involved in the UGO/EUTD reflection and diffraction coefficients. Appendices F and G provide some background derivations for the uniform asymptotic reduction of the spatial domain PO radiation integral.

All fields are time harmonic with an assumed $e^{j\omega t}$ time dependance that is suppressed throughout this report. Also the wavenumber, k, of free space is assumed to have a small negative imaginary part to ensure that the radiation condition at infinity is satisfied.

Chapter 2

Near-Zone Uniform Asymptotic Analysis and UGO/EUTD Formulation for the Scattered Fields near a Two Dimensional Smooth Caustic and Composite Shadow Boundary

In this chapter, the behavior of near-zone high frequency scattered EM fields near a two dimensional smooth caustic and composite shadow boundary is investigated and a UGO/EUTD solution is developed for the description of the scattering mechanisms. A composite shadow boundary occurs when a smooth caustic formed by an envelope of GO reflected rays is terminated due to an edge in the reflecting boundary, or when the smooth caustic is in the immediate vicinity of the RSB as shown in Figures 1.1 and 1.2. The caustic termination also generates a complex ray shadow boundary (CRSB) on the dark side of the smooth caustic. When the RSB is not in the immediate vicinity of the smooth caustic, the conventional UTD edge diffraction solution [4] which involves the Fresnel integral as a canonical function can be used effectively together with the solution in [14] to describe the fields away from the composite shadow boundary. However, near the composite shadow boundary where a confluence of both reflected and caustic type shadowing occurs, the Fresnel integral is not adequate to describe

the diffracted field behavior and it must be appropriately replaced by the incomplete Airy functions [9] via a uniform asymptotic procedure.

The present analysis is based on a spatial domain radiation integral representation for the fields scattered by an analytically described smoothly indented perfectly conducting boundary containing an edge. The asymptotic estimate for the surface current induced by the incident field from a source whose vector pattern function can also be described analytically is found using the PO approximation. The PO radiation integral is subsequently reduced using two uniform asymptotic methods to recover the uniform expressions for the scattering mechanisms. The first method employs the Chester et al. expansion [7] and results in a rigorous uniform asymptotic reduction of the PO radiation integral. Although the resulting solution is not in the desired UGO/EUTD format, that is the expression for the fields is not in terms of the conventional ray optical GO/GTD description multiplied by an appropriate transition function, it provides for a systematic approach for obtaining the higher order terms in the uniform asymptotic expansion for the fields in cases where slope scattering effects are present. The second method for the uniform asymptotic reduction of the PO radiation integral employs the method of steepest descent [8] and the resulting expressions in this case are indeed in a UGO/EUTD format.

The PO integral for finite concave or concave-convex shaped boundaries is characterized by two stationary phase points that are arbitrarily close to one another or to the integration endpoint associated with the edge. The stationary points are real and correspond to the two points of reflection when the observation point is on the lit side of the caustic. For observation points near the smooth caustic itself, the two stationary points coalesce to form a second order stationary point that moves near the integration endpoint for observation points near the caustic termination or composite shadow boundary. For observation points on the dark side of the smooth caustic, the two stationary points become a pair of complex conjugate stationary phase points with only one of them satisfying the radiation condition and eventually contributing to the fields on the dark side. Away from the caustic transition region the contribution from the complex stationary point was interpreted by Ikuno and Felsen [2, 3]

as a complex GO ray field reflected from the complex extension of the boundary. This complex GO ray field obeys a generalized form of Fermat's principle with all the parameters involved computed in complex space through analytic continuation and in precisely the same manner as for real GO rays as shown in [14]. In the case of a caustic termination as in Figure 1.1, the complex ray field only exists in the illuminated side of the CRSB, and therefore the edge diffracted field has to provide continuity in the total field across this boundary as well as the optical boundaries associated with the real GO rays on the lit side of the caustic.

Although higher order mechanisms such as edge excited creeping waves and whispering gallery modes may also exist and contribute significantly to the scattered field from the geometries considered, they will not be addressed in the analysis that follows. The problem formulation and the derivation of a uniform asymptotic solution using the Chester expansion for the asymptotic reduction of the PO radiation integral are presented in Section 2.1. In Section 2.2 the method of steepest descent is employed for the asymptotic reduction of the PO radiation integral and the UGO/EUTD expressions for the reflection, complex ray, and edge diffraction mechanisms are formulated.

2.1 Derivation of a uniform asymptotic solution using the Chester expansion

In this section, the spatial domain PO radiation integral is formulated and then asymptotically evaluated using a rigorous uniform asymptotic procedure that employs the Chester expansion. The canonical geometry for the analysis that follows is a semi-infinite two dimensional concave or concave-convex boundary as shown in Figures 2.1a and 2.1b, respectively. The scattered electric field at any point P exterior to the surface boundary C can be expressed in terms of the usual radiation integral over the electric current $\vec{J}$ induced on C by the source at P' as follows:

$$\vec{E}^s(P) \approx \frac{kZ_0}{4} \int_C \left[\hat{R} \times \hat{R} \times \vec{J}(Q')\right] H_0^{(2)}(kR) dl' \tag{2.1}$$

where

$$\vec{R} = \overline{Q'P}, \; R = |\vec{R}|, \; \hat{R} = \vec{R}/R,$$

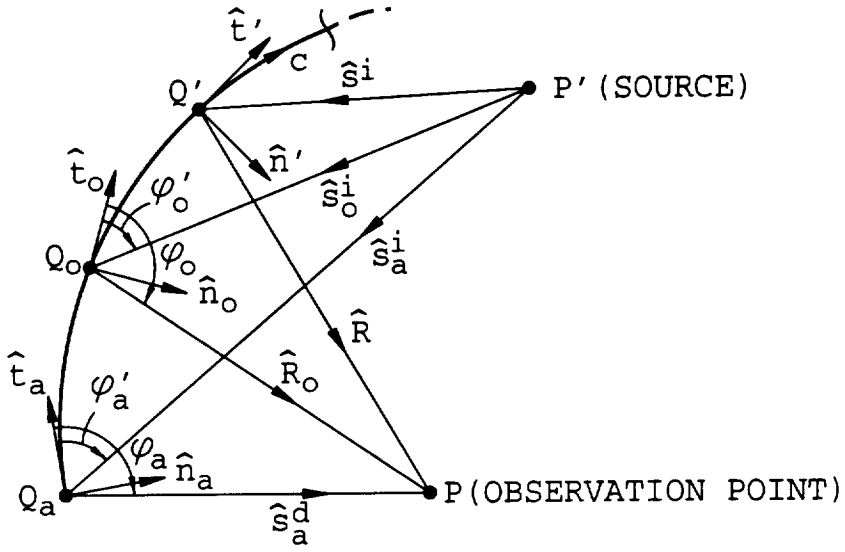

(a)

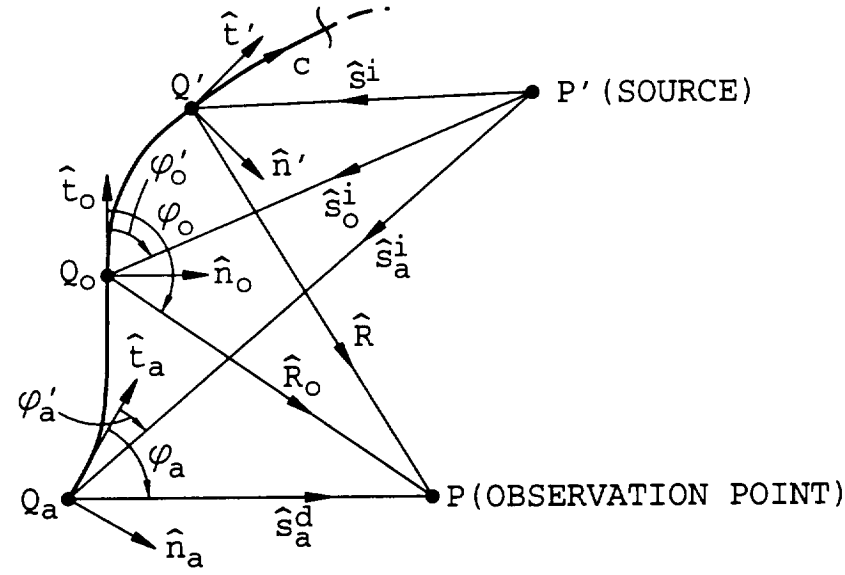

(b)

Figure 2.1: Canonical geometries for the uniform asymptotic analysis: (a) semi-infinite concave boundary, and (b) semi-infinite concave-convex boundary.

$\vec{J}(Q')$ = value of $\vec{J}$ at any point Q' on the surface,

$H_0^{(2)}(kR)$ = cylindrical Hankel function of the second kind of order zero,

Z_0 = impedance of free space,

k = wavenumber of free space, and

$d\ell'$ = line integration element.

Also, the observation point P cannot be too close to the scattering boundary for Equation (2.1) to be valid. When the scattering boundary is electrically large and well illuminated, one can use the PO approximation to (2.1) in which the induced current is assumed to be given by GO as follows:

$$\vec{J}(Q') \approx \begin{cases} 2\hat{n}' \times \vec{H}^i(Q'), & \text{on the lit portion of the boundary} \\ 0, & \text{on the shadowed portion of the boundary} \end{cases} \tag{2.2}$$

in which $\hat{n}'$ is the outward unit normal to the surface at Q', and $\vec{H}^i(Q')$ is the direct incident magnetic field from the source whose phase center is at P' and may expressed ray optically as follows:

$$\vec{H}^i(Q') \sim Z_0^{-1}(\hat{s}^i \times \vec{A})\frac{e^{-jks^i}}{\sqrt{s^i}}; \quad \hat{s}^i \cdot \vec{A} = 0, \tag{2.3}$$

$$= Z_0^{-1}\hat{s}^i \times \vec{E}^i(Q'), \tag{2.4}$$

$$\vec{E}^i(Q') = \vec{A}(Q')\frac{e^{-jks^i}}{\sqrt{s^i}}, \tag{2.5}$$

where $\vec{A}$ is the vector source pattern, $\vec{s}^i = \overline{P'Q'}$, $s^i = |\vec{s}^i|$, and $\hat{s}^i = \vec{s}^i/s^i$. Using the assumed current in (2.2) and the large argument form of Hankel function given by

$$H_0^{(2)}(kR) \sim \sqrt{\frac{2j}{\pi kR}}\, e^{-jkR}, \quad \text{for } kR \gg 1, \tag{2.6}$$

$\vec{E}^s(P)$ is given by the following stationary phase integral:

$$\vec{E}^s(P) \approx \int_{\ell_a}^{\infty} \vec{F}(\ell')\, e^{-jk\phi(\ell')}\, d\ell' \tag{2.7}$$

where

$$\vec{F}(\ell') = \sqrt{\frac{jk}{2\pi}}\, \frac{\hat{R}(\ell') \times \hat{R}(\ell') \times \left[\hat{n}(\ell') \times \hat{s}^i(\ell') \times \vec{A}(\ell')\right]}{\sqrt{s^i(\ell')R(\ell')}}, \text{ and} \tag{2.8}$$

$$\phi(\ell') = s^i(\ell') + R(\ell'). \tag{2.9}$$

The phase function contains two real or complex stationary phase points $\ell_{1,2}$ satisfying the condition $\dot{\phi}(\ell_{1,2}) = 0$, and are arbitrarily close to one another or to the integration endpoint ℓ_a. Before proceeding with the asymptotic reduction of the integral in (2.7), we choose the reference point on the scattering surface to be Q_0, which is a first order stationary point of the derivative of the phase function, that is $\ddot{\phi}(\ell_0) = 0$ and must necessarily lie between the two stationary phase points on the concave part of C. For the moment, we assume that this point is real without losing the generality of the analysis. Then, the quantities $R(\ell')$ and $s^i(\ell')$ are given by

$$R(\ell') = \left|\vec{R}_0 - \vec{r}(\ell')\right|, \text{ and} \tag{2.10}$$

$$s^i(\ell') = \left|\vec{s}^i_0 + \vec{r}(\ell')\right|, \tag{2.11}$$

where $\vec{R}_0 = \overline{Q_0P}$, $\vec{s}^i_0 = \overline{P'Q_0}$, and $\vec{r}(\ell') = \overline{Q_0Q'}$ is the natural representation of the scattering boundary.

The first step in the asymptotic reduction of the stationary phase integral in Equation (2.7) is to expand the phase function in a Taylor series around ℓ_0, that is

$$\phi(\ell') \simeq \phi(\ell_0) + (\ell' - \ell_0)\dot{\phi}(\ell_0) + \frac{(\ell' - \ell_0)^2}{2!}\ddot{\phi}(\ell_0) + \frac{(\ell' - \ell_0)^3}{3!}\dddot{\phi}(\ell_0). \tag{2.12}$$

The derivatives of the phase function can be expressed in terms of the geometric parameters of the surface and using (F.9), (F.14), and (F.19) they are given by

$$\dot{\phi}(\ell_0) = (\hat{s}^i_0 - \hat{R}_0)\cdot\hat{t}_0, \tag{2.13}$$

$$\ddot{\phi}(\ell_0) = \hat{n}_0\cdot(\hat{R}_0 - \hat{s}^i_0)\,\kappa_g(Q_0) + \frac{(\hat{s}^i_0\cdot\hat{n}_0)^2}{s^i_0} + \frac{\hat{R}_0\cdot\hat{n}_0)^2}{R_0} = 0, \tag{2.14}$$

$$\begin{aligned}\dddot{\phi}(\ell_0) &= \hat{n}_0\cdot(\hat{R}_0 - \hat{s}^i_0)\,\kappa_g'(Q_0) + \hat{t}_0\cdot(\hat{R}_0 - \hat{s}^i_0)\,\kappa_g^2(Q_0) \\ &+ \frac{3(\hat{s}^i_0\cdot\hat{n}_0)(\hat{s}^i_0\cdot\hat{t}_0)}{s^i_0}\left[\kappa_g(Q_0) - \frac{\hat{s}^i_0\cdot\hat{n}_0}{s^i_0}\right] \\ &+ \frac{3(\hat{R}_0\cdot\hat{n}_0)(\hat{R}_0\cdot\hat{t}_0)}{R_0}\left[\kappa_g(Q_0) + \frac{\hat{R}_0\cdot\hat{n}_0}{R_0}\right] = m(Q_0),\end{aligned} \tag{2.15}$$

where $\hat{t}_0$ and $\hat{n}_0$ are the unit tangent and normal vectors to C at Q_0, respectively, and $\kappa_g(Q_0) = 1/\rho_g(Q_0)$ is the normal surface curvature at Q_0. From Equation (2.14) one can observe that the point ℓ_0 is real for a concave or concave-convex boundary, with $\kappa_g(Q_0) < 0$. On the other hand, for a strictly convex boundary, the point ℓ_0,

if it exists, must be complex. In the special case of plane wave incidence with the observer in the Fraünhofer region of the boundary, that is s_0^i, $R_0 \to \infty$, the point Q_0 is a zero-curvature (inflection) point that satisfies $\kappa_g(Q_0) = 0$. For this case, ℓ_0 may be real for strictly convex boundaries as well.

Next, we make the following linear transformation:

$$s = (\ell' - \ell_0)\left[\frac{m(Q_0)}{2}\right]^{\frac{1}{3}}, \tag{2.16}$$

where $m(Q_0)$ is given in (2.15), and Equation (2.9) becomes

$$\phi(\ell') = \tau(s) = \alpha + \beta s + s^3/3, \tag{2.17}$$

where

$$\begin{aligned}
\alpha &= \phi(\ell_0) = \frac{1}{2}\left[\phi(\ell_1) + \phi(\ell_2)\right], \text{ or} && (2.18)\\
&= \phi(\ell_{1,2}) \pm \frac{2}{3}(-\beta)^{3/2}, \text{ or} && (2.19)\\
&= \phi(\ell_a) - \beta s_a - s_a^3/3, && (2.20)\\
\beta &= \dot{\phi}(\ell_0)\left[\frac{2}{m(Q_0)}\right]^{\frac{1}{3}}, \text{ or} && (2.21)\\
&= -\left\{\frac{3}{4}\left[\phi(\ell_2) - \phi(\ell_1)\right]\right\}^{2/3}, \text{ or} && (2.22)\\
&= \mp\left\{\frac{3}{2}\left[\phi(\ell_0) - \phi(\ell_{1,2})\right]\right\}^{2/3}, \text{ and} && (2.23)\\
s_a &= (\ell_a - \ell_0)\left[\frac{m(Q_0)}{2}\right]^{\frac{1}{3}}, \text{ or} && (2.24)\\
&= \pm\left[\dot{\phi}(\ell_a) - \dot{\phi}(\ell_0)\right]^{1/2}\left[\frac{2}{m(Q_0)}\right]^{\frac{1}{3}}; \begin{cases} + \text{ if } Q_0 \ni C \\ - \text{ if } Q_0 \in C. \end{cases} && (2.25)
\end{aligned}$$

The proper branches for β and s_a depend on the sign of $m(Q_0)$. Thus, using (2.17) Equation (2.7) transforms to the following expression:

$$\vec{E}^s(P) \approx e^{-jk\alpha} \int_{s_a}^{"\infty"} \vec{G}(s)\, e^{-jk(\beta s + s^3/3)}\, ds \tag{2.26}$$

where

$$\vec{G}(s) = \vec{F}(\ell')\frac{d\ell'}{ds}, \tag{2.27}$$

$$\frac{d\ell'}{ds} = \left[\frac{2}{m(Q_0)}\right]^{\frac{1}{3}}, \text{ and} \tag{2.28}$$

$$\text{“}\infty\text{”} = \infty \exp\left[-j\arg\left(\frac{d\ell'}{ds}\right)\right]. \tag{2.29}$$

The proper branch for $\frac{d\ell'}{ds}$ also depends on the sign of $m(Q_0)$.

Next we employ the Chester et al. expansion [7] for the amplitude function in Equation (2.26), that is

$$\begin{aligned}\vec{G}(s) &= \sum_{m=0}^{\infty}\left[\vec{a}_m(s^2+\beta)^m + \vec{b}_m s(s^2+\beta)^m\right] \\ &= \vec{a}_0 + s\vec{b}_0 + (s^2+\beta)\vec{g}(s),\end{aligned} \tag{2.30}$$

where

$$\vec{a}_0 = \frac{1}{2}\left[\vec{G}(s_1) + \vec{G}(s_2)\right], \tag{2.31}$$

$$\vec{b}_0 = \frac{1}{2s_1}\left[\vec{G}(s_1) - \vec{G}(s_2)\right], \tag{2.32}$$

$$\vec{g}(s) = \sum_{m=1}^{\infty}\left[\vec{a}_m(s^2+\beta)^{m-1} + \vec{b}_m s(s^2+\beta)^{m-1}\right], \tag{2.33}$$

$$s_{1,2} = \pm(-\beta)^{1/2};\ \ \tau'(s_{1,2}) = 0, \tag{2.34}$$

$$\vec{G}(s_{1,2}) = \vec{F}(\ell_{1,2})\left.\frac{d\ell'}{ds}\right|_{s_{1,2}}, \tag{2.35}$$

$$\left.\frac{d\ell'}{ds}\right|_{s_{1,2}} = (-\beta)^{1/4}\sqrt{\frac{\pm 2}{\ddot{\phi}(\ell_{1,2})}}, \tag{2.36}$$

and thus Equation (2.26) becomes

$$\begin{aligned}\vec{E}^s(P) \simeq\ & e^{-jk\alpha}\left[\vec{a}_0\int_{s_a}^{\text{“}\infty\text{”}} e^{-jk(\beta s + s^3/3)}\,ds + \vec{b}_0\int_{s_a}^{\text{“}\infty\text{”}} s\,e^{-jk(\beta s+s^3/3)}\,ds\right. \\ &+ \left.\int_{s_a}^{\text{“}\infty\text{”}}(s^2+\beta)\,\vec{g}(s)\,e^{-jk(\beta s+s^3/3)}\,ds\right].\end{aligned} \tag{2.37}$$

The third integral on the right hand side of Equation (2.37) is regular over the entire path of integration, thus employing integration by parts for this integral we get

$$\begin{aligned}\vec{E}^s(P) \simeq\ & e^{-jk\alpha}\left[\vec{a}_0\int_{s_a}^{\text{“}\infty\text{”}} e^{-jk(\beta s + s^3/3)}\,ds + \vec{b}_0\int_{s_a}^{\text{“}\infty\text{”}} s\,e^{-jk(\beta s+s^3/3)}\,ds\right. \\ &+ \left.\frac{1}{jk}\,\vec{g}(s_a)\,e^{-jk(\beta s_a + s_a^3/3)}\right] + O(k^{-2}).\end{aligned} \tag{2.38}$$

Now, from Equation (2.30) we have that

$$\vec{g}(s_a) = \frac{\vec{G}(s_a) - \vec{a}_0 - s_a\vec{b}_0}{s_a^2 + \beta} \tag{2.39}$$

and omitting the $O(k^{-2})$ terms, Equation (2.38) becomes

$$\begin{aligned}\vec{E}^s(P) \;\sim\; & e^{-jk\alpha}\left[\vec{a}_0 \int_{s_a}^{\text{"}\infty\text{"}} e^{-jk(\beta s + s^3/3)}\,ds + \vec{b}_0 \int_{s_a}^{\text{"}\infty\text{"}} s\, e^{-jk(\beta s + s^3/3)}\,ds\right] \\ & + e^{-jk\tau(s_a)}\left[\frac{\vec{G}(s_a)}{jk\tau'(s_a)} - \frac{\vec{a}_0 + s_a\vec{b}_0}{jk(\beta + s_a^2)}\right].\end{aligned} \tag{2.40}$$

Next, we let $s = k^{-1/3}t$, $\beta = k^{-2/3}\gamma$, and $s_a = k^{-1/3}\zeta_a$ in (2.40), thus

$$\begin{aligned}\vec{E}^s(P) \;\sim\; & \frac{e^{-jk\alpha}}{\sqrt{k}}\left[\vec{a}_0 \int_{\zeta_a}^{\text{"}\infty\text{"}} e^{-j(\gamma t + t^3/3)}\,dt + \vec{b}_0 \int_{\zeta_a}^{\text{"}\infty\text{"}} t\, e^{-j(\gamma t + t^3/3)}\,dt\right] \\ & + e^{-jk\tau(s_a)}\left[\frac{\vec{G}(s_a)}{jk\tau'(s_a)} + \frac{j(\vec{a}_0 + \zeta_a\vec{b}_0)}{\sqrt{k}(\gamma + \zeta_a^2)}\right].\end{aligned} \tag{2.41}$$

Finally, depending on the sign of $m(Q_0)$ the scattered electric field $\vec{E}^s(P)$ is given by

$$\begin{aligned}\vec{E}^s(P) \;\sim\; & \frac{e^{-jk\alpha}}{\sqrt{k}}\left[\vec{a}_0\overline{\mathrm{Ai}}^*(\gamma,\zeta_a) + j\vec{b}_0\frac{\partial}{\partial\gamma}\overline{\mathrm{Ai}}^*(\gamma,\zeta_a)\right] \\ & + e^{-jk\phi(\ell_a)}\left[\frac{\vec{F}(\ell_a)}{jk\dot{\phi}(\ell_a)} + \frac{j\left(\vec{a}_0 + \zeta_a\vec{b}_0\right)}{\sqrt{k}\,(\gamma + \zeta_a^2)}\right], \quad \text{if } m(Q_0) > 0 \end{aligned} \tag{2.42}$$

$$\begin{aligned}\vec{E}^s(P) \;\sim\; & \frac{e^{-jk\alpha}}{\sqrt{k}}\left[\vec{a}_0\overline{\mathrm{Ai}}(\gamma,\zeta_a) - j\vec{b}_0\frac{\partial}{\partial\gamma}\overline{\mathrm{Ai}}(\gamma,\zeta_a)\right] \\ & + e^{-jk\phi(\ell_a)}\left[\frac{\vec{F}(\ell_a)}{jk\dot{\phi}(\ell_a)} - \frac{j\left(\vec{a}_0 + \zeta_a\vec{b}_0\right)}{\sqrt{k}\,(\gamma + \zeta_a^2)}\right], \quad \text{if } m(Q_0) < 0, \end{aligned} \tag{2.43}$$

where $(*)$ denotes the complex conjugate operator, $\gamma = k^{2/3}\beta$, $\zeta_a = k^{1/3}s_a$, and α, $\vec{a}_0$, and $\vec{b}_0$ are given by the following expressions:

$$\alpha = \phi(\ell_a) - \delta k^{-1}\left(\gamma\zeta_a + \zeta_a^3/3\right), \text{ or} \tag{2.44}$$

$$= \phi(\ell_{1,2}) \pm \delta k^{-1}\frac{2}{3}(-\gamma)^{3/2}, \tag{2.45}$$

$$\delta = \mathrm{sgn}[m(Q_0)], \tag{2.46}$$

$$\left\{\begin{array}{c}\vec{a}_0 \\ \vec{b}_0\end{array}\right\} = \frac{(-\gamma)^{\pm 1/4}}{2}\left[\vec{F}(\ell_1)\sqrt{\frac{2}{|\ddot{\phi}(\ell_1)|}} \pm \vec{F}(\ell_2)\sqrt{\frac{2}{|\ddot{\phi}(\ell_2)|}}\right]. \tag{2.47}$$

The function $\overline{\mathrm{Ai}}(\gamma,\zeta)$ is the incomplete Airy integral defined by

$$\overline{\mathrm{Ai}}(\gamma,\zeta) \triangleq \int_{\zeta}^{\infty} e^{j(\gamma z+z^3/3)}\,dz\,. \tag{2.48}$$

The second term in both Equations (2.42) and (2.43) is an edge diffraction contribution where the first term in (2.42) and (2.43) appears to be a contribution from the two real or complex stationary points. If left in this form, the solution would clearly be in a UAT format [15], since the necessary corrections to the fields near the optical boundaries are performed on the reflected field as opposed to the edge diffracted field in a UTD type solution [4]. In fact, the first term in Equations (2.42) and (2.43) besides containing reflection and complex ray mechanisms, it also contains edge diffraction contributions implicitly embedded in the incomplete Airy integral. Therefore, in order to obtain a UTD type solution it is necessary to separate the edge diffraction contributions in (2.42) and (2.43) by using the properties and complex plane topology of the incomplete Airy integral found in Appendix C. In this form, the solution would be applicable to more general problems and also provide important physical insight into the individual scattering processes.

2.1.1 Scattered field solution on the lit side of the caustic

On the lit side of the caustic, the two stationary phase points $\ell_{1,2}$ are real and correspond to real reflection points $Q_{1,2}$ on C. Therefore, the parameter γ in Equations (2.42) and (2.43) must be negative. Using (C.9)-(C.11), the scattered field solution on the lit side of the smooth caustic is given by

1. $m(Q_0) > 0$:

$$\begin{aligned}
\vec{E}^s(P_L) \;\sim\;& j\sqrt{\frac{\pi}{k}}\,e^{-jk\alpha}\left\{\left[\vec{a}_0 \mathrm{W}_1^s(\gamma)+j\vec{b}_0\mathrm{W}_1'^s(\gamma)\right]-\left[\vec{a}_0\mathrm{W}_2^s(\gamma)+j\vec{b}_0\mathrm{W}_2'^s(\gamma)\right]\right\}\\
&+\; e^{-jk\phi(\ell_a)}\left\{\frac{\vec{F}(\ell_a)}{jk\dot{\phi}(\ell_a)}+\frac{\vec{a}_0}{\sqrt{k}}\left[e^{j(\gamma\zeta_a+\zeta_a^3/3)}\mathrm{g}_2^s(\gamma,\zeta_a)+\frac{j}{\gamma+\zeta_a^2}\right]\right.\\
&\left.+\; j\frac{\vec{b}_0}{\sqrt{k}}\left[e^{j(\gamma\zeta_a+\zeta_a^3/3)}\frac{\partial}{\partial\gamma}\mathrm{g}_2^s(\gamma,\zeta_a)+\frac{\zeta_a}{\gamma+\zeta_a^2}\right]\right\}, \qquad (2.49)\\
&\text{if}\quad \zeta_a \le -(-\gamma)^{-1/2},\\
\vec{E}^s(P_L) \;\sim\;& -j\sqrt{\frac{\pi}{k}}\,e^{-jk\alpha}\left[\vec{a}_0\mathrm{W}_2^s(\gamma)+j\vec{b}_0\mathrm{W}_2'^s(\gamma)\right]
\end{aligned}$$

$$+ \quad e^{-jk\phi(\ell_a)} \left\{ \frac{\vec{F}(\ell_a)}{jk\dot{\phi}(\ell_a)} + \frac{\vec{a}_0}{\sqrt{k}} \left[e^{j(\gamma\zeta_a + \zeta_a^3/3)} g_3^*(\gamma, \zeta_a) + \frac{j}{\gamma + \zeta_a^2} \right] \right.$$

$$\left. + \quad j\frac{\vec{b}_0}{\sqrt{k}} \left[e^{j(\gamma\zeta_a + \zeta_a^3/3)} \frac{\partial}{\partial\gamma} g_3^*(\gamma, \zeta_a) + \frac{\zeta_a}{\gamma + \zeta_a^2} \right] \right\}, \tag{2.50}$$

$$\text{if} \quad -(-\gamma)^{1/2} < \zeta_a \leq (-\gamma)^{-1/2},$$

$$\vec{E}^s(P_L) \sim e^{-jk\phi(\ell_a)} \left\{ \frac{\vec{F}(\ell_a)}{jk\dot{\phi}(\ell_a)} + \frac{\vec{a}_0}{\sqrt{k}} \left[e^{j(\gamma\zeta_a + \zeta_a^3/3)} g_1^*(\gamma, \zeta_a) + \frac{j}{\gamma + \zeta_a^2} \right] \right.$$

$$\left. + \quad j\frac{\vec{b}_0}{\sqrt{k}} \left[e^{j(\gamma\zeta_a + \zeta_a^3/3)} \frac{\partial}{\partial\gamma} g_1^*(\gamma, \zeta_a) + \frac{\zeta_a}{\gamma + \zeta_a^2} \right] \right\}, \tag{2.51}$$

$$\text{if} \quad \zeta_a > (-\gamma)^{-1/2}.$$

2. $m(Q_0) < 0$:

$$\vec{E}^s(P_L) \sim -j\sqrt{\frac{\pi}{k}}\, e^{-jka} \left\{ \left[\vec{a}_0 W_1(\gamma) - j\vec{b}_0 W_1'(\gamma) \right] - \left[\vec{a}_0 W_2(\gamma) - j\vec{b}_0 W_2'(\gamma) \right] \right\}$$

$$+ \quad e^{-jk\phi(\ell_a)} \left\{ \frac{\vec{F}(\ell_a)}{jk\dot{\phi}(\ell_a)} + \frac{\vec{a}_0}{\sqrt{k}} \left[e^{-j(\gamma\zeta_a + \zeta_a^3/3)} g_2(\gamma, \zeta_a) - \frac{j}{\gamma + \zeta_a^2} \right] \right.$$

$$\left. - \quad j\frac{\vec{b}_0}{\sqrt{k}} \left[e^{-j(\gamma\zeta_a + \zeta_a^3/3)} \frac{\partial}{\partial\gamma} g_2(\gamma, \zeta_a) + \frac{\zeta_a}{\gamma + \zeta_a^2} \right] \right\}, \tag{2.52}$$

$$\text{if} \quad \zeta_a \leq -(-\gamma)^{-1/2}$$

$$\vec{E}^s(P_L) \sim j\sqrt{\frac{\pi}{k}}\, e^{-jka} \left[\vec{a}_0 W_2(\gamma) - j\vec{b}_0 W_2'(\gamma) \right]$$

$$+ \quad e^{-jk\phi(\ell_a)} \left\{ \frac{\vec{F}(\ell_a)}{jk\dot{\phi}(\ell_a)} + \frac{\vec{a}_0}{\sqrt{k}} \left[e^{-j(\gamma\zeta_a + \zeta_a^3/3)} g_3(\gamma, \zeta_a) - \frac{j}{\gamma + \zeta_a^2} \right] \right.$$

$$\left. - \quad j\frac{\vec{b}_0}{\sqrt{k}} \left[e^{-j(\gamma\zeta_a + \zeta_a^3/3)} \frac{\partial}{\partial\gamma} g_3(\gamma, \zeta_a) + \frac{\zeta_a}{\gamma + \zeta_a^2} \right] \right\}, \tag{2.53}$$

$$\text{if} \quad -(-\gamma)^{1/2} < \zeta_a \leq (-\gamma)^{-1/2}$$

$$\vec{E}^s(P_L) \sim e^{-jk\phi(\ell_a)} \left\{ \frac{\vec{F}(\ell_a)}{jk\dot{\phi}(\ell_a)} + \frac{\vec{a}_0}{\sqrt{k}} \left[e^{-j(\gamma\zeta_a + \zeta_a^3/3)} g_1(\gamma, \zeta_a) - \frac{j}{\gamma + \zeta_a^2} \right] \right.$$

$$\left. - \quad j\frac{\vec{b}_0}{\sqrt{k}} \left[e^{-j(\gamma\zeta_a + \zeta_a^3/3)} \frac{\partial}{\partial\gamma} g_1(\gamma, \zeta_a) + \frac{\zeta_a}{\gamma + \zeta_a^2} \right] \right\}, \tag{2.54}$$

$$\text{if} \quad \zeta_a > (-\gamma)^{-1/2},$$

where $W_{1,2}(\gamma)$ are the Fock-type Airy functions [16], and $g_i(\gamma, \zeta_a)$, $i = 1, 2, 3$ are the incomplete Airy functions [9]. From (2.8), (2.9), (F.9), and (F.28) we have the

following relations on the lit side of the caustic:

$$\vec{F}(\ell_{1,2}) = \sqrt{\frac{jk}{2\pi}} \frac{\hat{s}^r_{1,2} \times \hat{s}^r_{1,2} \times \left[\hat{n}_{1,2} \times \hat{s}^i_{1,2} \times \vec{A}(Q_{1,2})\right]}{\sqrt{s^i_{1,2}\, s^r_{1,2}}}, \tag{2.55}$$

$$\phi(\ell_{1,2}) = s^i_{1,2} + s^r_{1,2}, \tag{2.56}$$

$$\ddot{\phi}(\ell_{1,2}) = \cos^2\theta^i_{1,2} \left(\frac{1}{\rho^r_{1,2}} + \frac{1}{s^r_{1,2}}\right), \text{ and} \tag{2.57}$$

$$\dot{\phi}(\ell_0) = \left(\hat{s}^i_0 - \hat{R}_0\right) \cdot \hat{t}_0 = -(\cos\varphi'_0 + \cos\varphi_0), \tag{2.58}$$

where $\theta^i_{1,2}$ is the usual angle of incidence at $Q_{1,2}$, φ'_0, φ_0 are defined in Figure 2.1, and $\rho^r_{1,2}$ is the radius of curvature of the reflected wavefront from $Q_{1,2}$ given in (F.29). Also, the vector expression in the numerator of (2.55) may be written as follows:

$$\hat{s}^r_{1,2} \times \hat{s}^r_{1,2} \times \left[\hat{n}_{1,2} \times \hat{s}^i_{1,2} \times \vec{A}(Q_{1,2})\right] = \cos\theta^i_{1,2} \vec{A}(Q_{1,2}) \cdot \bar{\bar{R}}\,(Q_{1,2}), \tag{2.59}$$

where $\bar{\bar{R}}\,(Q_{1,2})$ is the dyadic GO reflection coefficient and is given by

$$\bar{\bar{R}}\,(Q_{1,2}) = \hat{n}_{1,2}\,\hat{n}_{1,2} - \bar{\bar{I}} = R_s\,\hat{e}_\perp \hat{e}_\perp + R_h\,\hat{e}^i_\parallel(Q_{1,2})\hat{e}^r_\parallel(Q_{1,2}), \tag{2.60}$$

$$R_{s,h} = \mp 1\,; \text{ for a perfectly conducting boundary,} \tag{2.61}$$

$\bar{\bar{I}}$ is the unit dyad, and the vectors $\hat{e}_\perp$ and $\hat{e}^{i,r}_\parallel$ are defined in Figure F.2. Thus, using (2.21)–(2.23), (2.45), (2.47), and (2.55)–(2.59), the parameters α, γ, $\vec{a}_0$, and $\vec{b}_0$ for the lit side of the caustic are given by

$$\alpha = s^i_{1,2} + s^r_{1,2} \pm \delta k^{-1} \frac{2}{3}(-\gamma)^{3/2}, \tag{2.62}$$

$$\gamma = -k^{2/3} \left|\cos\varphi'_0 + \cos\varphi_0\right| \left|\frac{2}{m(Q_0)}\right|^{\frac{1}{3}}, \text{ or} \tag{2.63}$$

$$= -\left[\frac{3}{4}k \left|(s^i_2 + s^r_2) - (s^i_1 + s^r_1)\right|\right]^{\frac{2}{3}}, \text{ or} \tag{2.64}$$

$$= -\left[\frac{3}{2}k \left|(s^i_0 + R_0) - \left(s^i_{1,2} + s^r_{1,2}\right)\right|\right]^{\frac{2}{3}}, \tag{2.65}$$

$$\left\{ \begin{array}{c} \vec{a}_0 \\ \vec{b}_0 \end{array} \right\} = \sqrt{\frac{k}{\pi}} \frac{(-\gamma)^{\pm 1/4}\, e^{j\frac{\pi}{4}}}{2} \left[\frac{\vec{A}(Q_1) \cdot \bar{\bar{R}}\,(Q_1)}{\sqrt{s^i_1}} \left|\sqrt{\frac{\rho^r_1}{\rho^r_1 + s^r_1}}\right| \right.$$

$$\left. \pm \frac{\vec{A}(Q_2) \cdot \bar{\bar{R}}\,(Q_2)}{\sqrt{s^i_2}} \left|\sqrt{\frac{\rho^r_2}{\rho^r_2 + s^r_2}}\right| \right]. \tag{2.66}$$

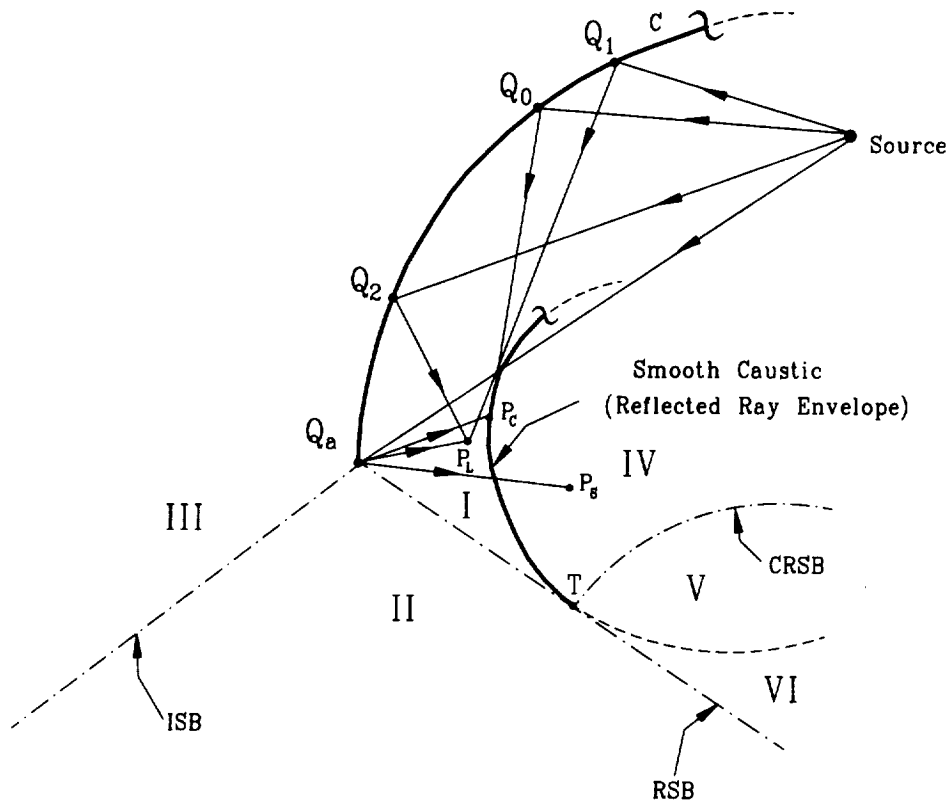

Figure 2.2: Scattered field regions associated with a concave boundary containing an edge.

Before proceeding with the scattered field solution on the dark side of the caustic, a few observations on Equations (2.49)–(2.54) are in order. First, Equations (2.49) and (2.52) apply on the illuminated side of the reflection shadow boundary (RSB) designated as region I in Figures 2.2 and 2.3, where two reflected ray contributions exist and are represented by the first term in (2.49) and (2.52) involving the Fock-type Airy functions and their derivatives. The second term in (2.49) and (2.52) represents the diffracted field contribution from the edge. Equations (2.50) and (2.53) apply on the shadow side of the RSB designated as region II in Figures 2.2 and 2.3, where only a single reflected ray contribution exists and is represented by the first term in (2.50) and (2.53). The second term in (2.50) and (2.53) represents the diffracted field contribution from the edge. Equations (2.51) and (2.54) apply in regions III and VI in Figures 2.2 and 2.3 where only edge diffracted rays exist.

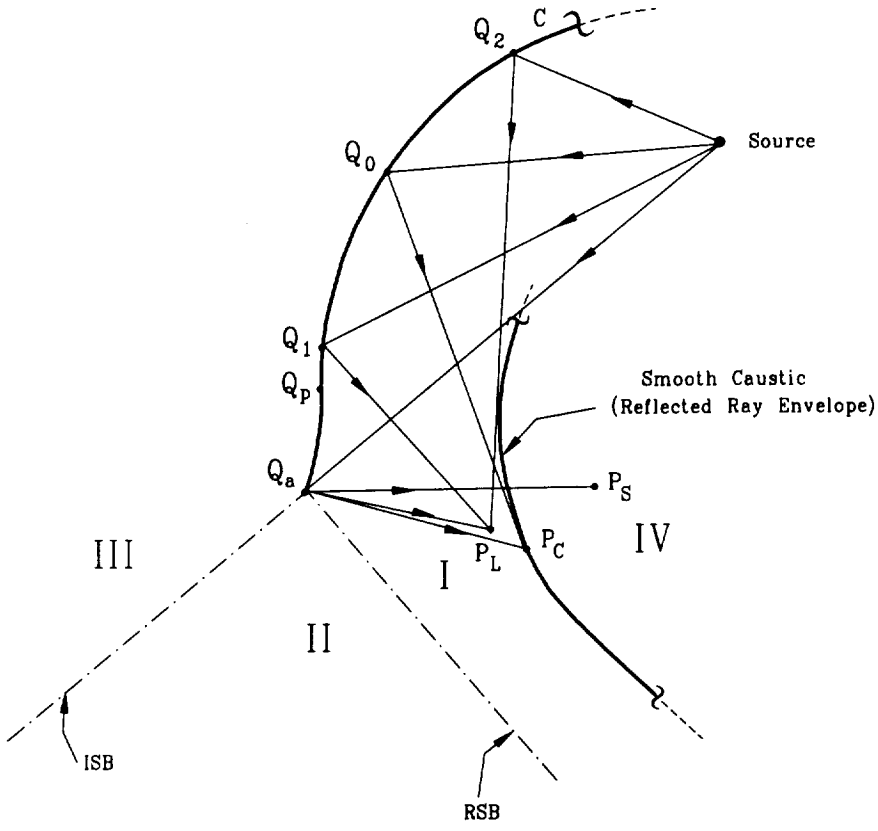

Figure 2.3: Scattered field regions associated with a concave-convex boundary containing an edge.

2.1.2 Scattered field solution on the dark side of the caustic

On the dark side of the caustic, the two stationary phase points $\ell_{1,2}$ are complex and correspond to complex reflection points $Q^c_{1,2}$ which are interpreted to lie on the complex extension of C. Therefore, the parameter γ in Equations (2.42) and (2.43) must be positive. Using (C.12) and (C.13), the scattered field solution on the dark side of the smooth caustic is given by

1. $m(Q_0) > 0$:

$$\begin{aligned}
\vec{E}^s(P_s) \;\sim\; & \frac{2\pi}{\sqrt{k}}\, e^{-jks}\left[\vec{a}_0 \mathrm{Ai}(\gamma) + j\vec{b}_0 \mathrm{Ai}'(\gamma)\right] \\
+\; & e^{-jk\phi(\ell_a)}\left\{\frac{\vec{F}(\ell_a)}{jk\dot{\phi}(\ell_a)} + \frac{\vec{a}_0}{\sqrt{k}}\left[e^{j(\gamma\zeta_a+\zeta_a^3/3)}\mathrm{g}_2^*(\gamma,\zeta_a) + \frac{j}{\gamma+\zeta_a^2}\right]\right. \\
+\; & \left. j\frac{\vec{b}_0}{\sqrt{k}}\left[e^{j(\gamma\zeta_a+\zeta_a^3/3)}\frac{\partial}{\partial\gamma}\mathrm{g}_2^*(\gamma,\zeta_a) + \frac{\zeta_a}{\gamma+\zeta_a^2}\right]\right\}, \qquad (2.67) \\
& \text{if} \quad \zeta_a < 0\,, \\
\vec{E}^s(P_s) \;\sim\; & e^{-jk\phi(\ell_a)}\left\{\frac{\vec{F}(\ell_a)}{jk\dot{\phi}(\ell_a)} + \frac{\vec{a}_0}{\sqrt{k}}\left[e^{j(\gamma\zeta_a+\zeta_a^3/3)}\mathrm{g}_1^*(\gamma,\zeta_a) + \frac{j}{\gamma+\zeta_a^2}\right]\right. \\
+\; & \left. j\frac{\vec{b}_0}{\sqrt{k}}\left[e^{j(\gamma\zeta_a+\zeta_a^3/3)}\frac{\partial}{\partial\gamma}\mathrm{g}_1^*(\gamma,\zeta_a) + \frac{\zeta_a}{\gamma+\zeta_a^2}\right]\right\}, \qquad (2.68) \\
& \text{if} \quad \zeta_a > 0\,.
\end{aligned}$$

2. $m(Q_0) < 0$:

$$\begin{aligned}
\vec{E}^s(P_s) \;\sim\; & \frac{2\pi}{\sqrt{k}}\, e^{-jks}\left[\vec{a}_0 \mathrm{Ai}(\gamma) - j\vec{b}_0 \mathrm{Ai}'(\gamma)\right] \\
+\; & e^{-jk\phi(\ell_a)}\left\{\frac{\vec{F}(\ell_a)}{jk\dot{\phi}(\ell_a)} + \frac{\vec{a}_0}{\sqrt{k}}\left[e^{-j(\gamma\zeta_a+\zeta_a^3/3)}\mathrm{g}_2(\gamma,\zeta_a) - \frac{j}{\gamma+\zeta_a^2}\right]\right. \\
-\; & \left. j\frac{\vec{b}_0}{\sqrt{k}}\left[e^{-j(\gamma\zeta_a+\zeta_a^3/3)}\frac{\partial}{\partial\gamma}\mathrm{g}_2(\gamma,\zeta_a) + \frac{\zeta_a}{\gamma+\zeta_a^2}\right]\right\}, \qquad (2.69) \\
& \text{if} \quad \zeta_a < 0\,, \\
\vec{E}^s(P_s) \;\sim\; & e^{-jk\phi(\ell_a)}\left\{\frac{\vec{F}(\ell_a)}{jk\dot{\phi}(\ell_a)} + \frac{\vec{a}_0}{\sqrt{k}}\left[e^{-j(\gamma\zeta_a+\zeta_a^3/3)}\mathrm{g}_1(\gamma,\zeta_a) - \frac{j}{\gamma+\zeta_a^2}\right]\right. \\
-\; & \left. j\frac{\vec{b}_0}{\sqrt{k}}\left[e^{-j(\gamma\zeta_a+\zeta_a^3/3)}\frac{\partial}{\partial\gamma}\mathrm{g}_1(\gamma,\zeta_a) + \frac{\zeta_a}{\gamma+\zeta_a^2}\right]\right\}, \qquad (2.70) \\
& \text{if} \quad \zeta_a > 0\,,
\end{aligned}$$

where $\mathrm{Ai}(\gamma)$ is the ordinary or Miller-type Airy function [17]. In the dark side of the caustic we have the following relations:

$$\vec{F}(\ell_{1,2}) = \sqrt{\frac{jk}{2\pi}}\,\frac{\cos\theta^{ic}_{1,2}\,\vec{A}(Q^c_{1,2})\cdot\bar{\bar{R}}^c(Q^c_{1,2})}{\sqrt{s^{ic}_{1,2}\,s^{rc}_{1,2}}}\,, \tag{2.71}$$

$$\phi(\ell_{1,2}) = s^{ic}_{1,2} + s^{rc}_{1,2}\,,\ \text{and} \tag{2.72}$$

$$\ddot{\phi}(\ell_{1,2}) = \cos^2\theta^{ic}_{1,2}\left(\frac{1}{\rho^{rc}_{1,2}} + \frac{1}{s^{rc}_{1,2}}\right), \tag{2.73}$$

where $\bar{\bar{R}}^c(Q^c_{1,2})$ is the dyadic complex GO reflection coefficient and is given by

$$\bar{\bar{R}}^c(Q^c_{1,2}) = \hat{n}^c_{1,2}\,\hat{n}^c_{1,2} - \bar{\bar{I}} = R^c_s\,\hat{e}^{\,c}_{\perp}\hat{e}^{\,c}_{\perp} + R^c_h\,\hat{e}^{\,ic}_{\parallel}(Q^c_{1,2})\hat{e}^{\,rc}_{\parallel}(Q^c_{1,2})\,, \tag{2.74}$$

$$R^c_{s,h} = \mp 1\,;\ \text{for a perfectly conducting boundary.} \tag{2.75}$$

Notice that all the quantities in (2.71)–(2.75) with the superscript c are associated with the complex reflection points $Q^c_{1,2}$ and are analytic continuations along the complex extension of C [2] of the quantities associated with the real reflection points $Q_{1,2}$ in the lit side of the caustic. They are evaluated in precisely the same fashion as the quantities associated with the real reflection points. Thus, using (2.21)–(2.23), (2.45), (2.47), and (2.71)–(2.73), the parameters α, γ, $\vec{a}_0$, and $\vec{b}_0$ for the dark side of the caustic are given by

$$\alpha = s^{ic}_{1,2} + s^{rc}_{1,2} \mp j\delta k^{-1}\frac{2}{3}\gamma^{3/2}\,, \tag{2.76}$$

$$\gamma = k^{2/3}\,|\cos\varphi'_0 + \cos\varphi_0|\left|\frac{2}{m(Q_0)}\right|^{\frac{1}{3}},\ \text{or} \tag{2.77}$$

$$= \left[\frac{3}{4}k\,|(s^{ic}_2 + s^{rc}_2) - (s^{ic}_1 + s^{rc}_1)|\right]^{\frac{2}{3}},\ \text{or} \tag{2.78}$$

$$= \left[\frac{3}{2}k\,\left|(s^{i}_0 + R_0) - \left(s^{ic}_{1,2} + s^{rc}_{1,2}\right)\right|\right]^{\frac{2}{3}}, \tag{2.79}$$

$$\vec{a}_0 = \frac{j\sqrt{k}\,\gamma^{1/4}}{2\sqrt{\pi}}\left[\frac{\vec{A}(Q^c_1)\cdot\bar{\bar{R}}^c(Q^c_1)}{\sqrt{s^{ic}_1}}\left|\sqrt{\frac{\rho^{rc}_1}{\rho^{rc}_1 + s^{rc}_1}}\right|\right.$$
$$\left. + \frac{\vec{A}(Q^c_2)\cdot\bar{\bar{R}}^c(Q^c_2)}{\sqrt{s^{ic}_2}}\left|\sqrt{\frac{\rho^{rc}_2}{\rho^{rc}_2 + s^{rc}_2}}\right|\right], \tag{2.80}$$

$$\vec{b}_0 = \frac{\sqrt{k}\,\gamma^{-1/4}}{2\sqrt{\pi}}\left[\frac{\vec{A}(Q^c_1)\cdot\bar{\bar{R}}^c(Q^c_1)}{\sqrt{s^{ic}_1}}\left|\sqrt{\frac{\rho^{rc}_1}{\rho^{rc}_1 + s^{rc}_1}}\right|\right.$$

$$- \frac{\vec{A}(Q_2^c)\cdot\bar{\bar{R}}^c(Q_2^c)}{\sqrt{s_2^{ic}}}\left|\sqrt{\frac{\rho_2^{rc}}{\rho_2^{rc}+s_2^{rc}}}\right|\Bigg]\,. \tag{2.81}$$

A few observations on the nature of the scattered field solution on the dark side of the caustic are as follows: First, Equations (2.67) and (2.69) apply on the illuminated side of the CRSB designated as region IV of the dark side in Figures 2.2 and 2.3, where both complex ray and edge diffraction contributions exist. The complex ray contribution is represented by the first term in Equations (2.67) and (2.69) involving the ordinary Airy function and its derivative. Although the values associated with both complex stationary points are present in the expression for the complex ray contribution, as will be shown later in this section, in its asymptotic limit it contains only the reflected field from one of the complex stationary points. The second term in (2.67) and (2.69) involving the incomplete Airy function and its derivative represents the edge diffraction contribution in region IV. Equations (2.68) and (2.70) apply in shadow side of the CRSB designated as region V of the dark side in Figure 2.2, where only edge diffracted field contribution exists.

2.1.3 The reflected field and its limiting forms on the lit side of the caustic

From Equations (2.49)–(2.54) and using the fact that $\mathrm{W}_1(\gamma) = \mathrm{W}_2^*(\gamma)$ the reflected field on the lit side of the caustic may be written as follows:

$$\begin{aligned}
\vec{E}^r(P_L) \;\sim\; & \frac{e^{-j\frac{\pi}{4}}}{2}\Big\{u_1\, e^{-jka_1}\left[\vec{A}_\ell\,\gamma_\ell^{1/4}\,\mathrm{W}_1(-\gamma_\ell) - j\vec{B}_\ell\,\gamma_\ell^{-1/4}\,\mathrm{W}_1'(-\gamma_\ell)\right] \\
& - u_2\, e^{-jka_2}\left[\vec{A}_\ell\,\gamma_\ell^{1/4}\,\mathrm{W}_2(-\gamma_\ell) - j\vec{B}_\ell\gamma_\ell^{-1/4}\,\mathrm{W}_2'(-\gamma_\ell)\right]\Big\} \qquad (2.82) \\
& \text{if}\quad m(Q_0) > 0\,, \\
\vec{E}^r(P_L) \;\sim\; & -\frac{e^{-j\frac{\pi}{4}}}{2}\Big\{u_1\, e^{-jka_1}\left[\vec{A}_\ell\,\gamma_\ell^{1/4}\,\mathrm{W}_1^*(-\gamma_\ell) + j\vec{B}_\ell\,\gamma_\ell^{-1/4}\,\mathrm{W}_1'^*(-\gamma_\ell)\right] \\
& - u_2\, e^{-jka_2}\left[\vec{A}_\ell\,\gamma_\ell^{1/4}\,\mathrm{W}_2^*(-\gamma_\ell) + j\vec{B}_\ell\,\gamma_\ell^{-1/4}\,\mathrm{W}_2'^*(-\gamma_\ell)\right]\Big\} \qquad (2.83) \\
& \text{if}\quad m(Q_0) < 0\,, \\
u_{1,2} \;=\; & u(-\zeta_a \pm \gamma_\ell^{1/2})\,, \qquad (2.84)
\end{aligned}$$

where $u(x)$ is the Heaviside unit step function and from (2.62), (2.64), and (2.66) the parameters γ_ℓ, $\alpha_{1,2}$, $\vec{A}_\ell$, and $\vec{B}_\ell$ are given by

$$\gamma_\ell = \left[\frac{3}{4}k\left|(s_2^i + s_2^r) - (s_1^i + s_1^r)\right|\right]^{2/3}, \tag{2.85}$$

$$\alpha_{1,2} = s_{1,2}^i + s_{1,2}^r \pm \delta k^{-1}\frac{2}{3}\gamma_\ell^{3/2}, \tag{2.86}$$

$$\left\{\begin{array}{c}\vec{A}_\ell \\ \vec{B}_\ell\end{array}\right\} = \frac{\vec{A}(Q_1)\cdot\bar{\bar{R}}(Q_1)}{\sqrt{s_1^i}}\left|\sqrt{\frac{\rho_1^r}{\rho_1^r + s_1^r}}\right| \pm \frac{\vec{A}(Q_2)\cdot\bar{\bar{R}}(Q_2)}{\sqrt{s_2^i}}\left|\sqrt{\frac{\rho_2^r}{\rho_2^r + s_2^r}}\right|, \tag{2.87}$$

with δ given in (2.46). The first term in (2.82) and (2.83) is non-zero in regions I and II of Figures 2.2 and 2.3 and represents the uniform reflected field contribution from Q_1. The second term in (2.82) and (2.83) is non-zero only in region I of Figures 2.2 and 2.3 and represents the uniform reflected field contribution from Q_2. Both terms in (2.82) and (2.83) are zero in the remaining regions of Figures 2.2 and 2.3 where only edge diffracted and/or complex ray fields exist. Also, it should be noted from Equations (2.82) and (2.83) that the uniform contributions from each reflection point are not completely independent of each other since the values from both reflection points are explicitly contained in the parameters $\vec{A}_\ell$, and $\vec{B}_\ell$.

Next, let us investigate the behavior of the reflected field by examining two limiting cases.

Limiting case 1 : Observation point on the deep lit side of the caustic.

In this case, the parameter $\gamma_\ell \gg 1$, and using the large negative argument forms of the Fock-type Airy functions and their derivatives given in (A.21)-(A.24) Equations (2.82) and (2.83) become

$$\begin{aligned}\vec{E}^r(P_L) &\sim \frac{1}{2}e^{-jk(s_1^i+s_1^r)}\left(\vec{A}_\ell + \vec{B}_\ell\right)u(-\zeta_a + \gamma_\ell^{1/2}) \\ &+ \frac{j}{2}e^{-jk(s_2^i+s_2^r)}\left(\vec{A}_\ell - \vec{B}_\ell\right)u(-\zeta_a - \gamma_\ell^{1/2}) \ ; \ \text{if } m(Q_0) > 0, \end{aligned}\tag{2.88}$$

$$\begin{aligned}\vec{E}^r(P_L) &\sim \frac{j}{2}e^{-jk(s_1^i+s_1^r)}\left(\vec{A}_\ell + \vec{B}_\ell\right)u(-\zeta_a + \gamma_\ell^{1/2}) \\ &+ \frac{1}{2}e^{-jk(s_2^i+s_2^r)}\left(\vec{A}_\ell - \vec{B}_\ell\right)u(-\zeta_a - \gamma_\ell^{1/2}) \ ; \ \text{if } m(Q_0) < 0. \end{aligned}\tag{2.89}$$

From (2.5) and (2.87), we have that

$$\frac{1}{2}e^{-jks_{1,2}^i}\left(\vec{A}_\ell \pm \vec{B}_\ell\right) = \vec{E}^i(Q_{1,2})\cdot\bar{\bar{R}}(Q_{1,2})\left|\sqrt{\frac{\rho_{1,2}^r}{\rho_{1,2}^r + s_{1,2}^r}}\right|, \tag{2.90}$$

and the reflected field on the deep lit side of the smooth caustic is given by the following expression:

$$\begin{aligned}\vec{E}^r(P_L) \;\sim\; & u_1\,\vec{E}^i(Q_1)\cdot\bar{\bar{R}}\,(Q_1)\sqrt{\frac{\rho_1^r}{\rho_1^r+s_1^r}}\,e^{-jks_1^r} \\ & +\; u_2\,\vec{E}^i(Q_2)\cdot\bar{\bar{R}}\,(Q_2)\sqrt{\frac{\rho_2^r}{\rho_2^r+s_2^r}}\,e^{-jks_2^r} \qquad (2.91)\end{aligned}$$

with the understanding that

$$\begin{aligned}&\frac{\rho_1^r}{\rho_1^r+s_1^r}\gtrless 0 \quad \text{for} \quad m(Q_0)\gtrless 0\,, \\ &\frac{\rho_2^r}{\rho_2^r+s_2^r}\lessgtr 0 \quad \text{for} \quad m(Q_0)\gtrless 0\,, \quad \text{and} \\ &\sqrt{\frac{\rho^r}{\rho^r+s^r}} \;=\; j\left|\sqrt{\frac{\rho^r}{\rho^r+s^r}}\,\right| \;\text{ if }\; \frac{\rho^r}{\rho^r+s^r}<0\,.\end{aligned}$$

Equation (2.91) shows that the reflected field solution on the deep lit side of the smooth caustic reduces to the classic GO expression as expected.

Limiting case 2 : Observation point lies on the smooth caustic of reflected rays.

In this case, $\gamma_\ell \to 0$ in (2.82) and (2.83), where the spread factors in (2.87) become singular for observation points at the caustic, that is $\rho_{1,2}^r \to -s_{1,2}^r$. From (2.28) and (2.36) the reflected ray spread factor near the caustic assumes the following form:

$$\left|\sqrt{\frac{\rho_0^r}{\rho_0^r+s_0^r}}\,\right| \to \frac{\cos\theta_0^i\,(k/2)^{1/6}\,\gamma_\ell^{-1/4}}{\sqrt{s_0^r}\,|m(Q_0)|^{1/3}}\,, \qquad (2.92)$$

and thus using (2.87) and (2.92) we have

$$\gamma_\ell^{1/4}\,\vec{A}_\ell \;=\; \frac{2\cos\theta_0^i\,(k/2)^{1/6}}{\sqrt{s_0^r}\,|m(Q_0)|^{1/3}}\left[\frac{\vec{A}(Q_0)\cdot\bar{\bar{R}}\,(Q_0)}{\sqrt{s_0^i}}\right],\ \text{and} \qquad (2.93)$$

$$\gamma_\ell^{-1/4}\,\vec{B}_\ell \;\approx\; 0\,. \qquad (2.94)$$

Also, the Fock-type Airy functions, $W_{1,2}$, assume the following small argument form:

$$W_{1,2}(0) = \frac{3^{-2/3}\,\Gamma(1/3)}{2\sqrt{\pi}}\left(3^{1/3}\pm j\sqrt{3}\right), \qquad (2.95)$$

and thus the uniform asymptotic expression for the reflected field close to the smooth caustic is as follows:

$$\vec{E}^r(P_C)\sim u(-\zeta_a)\left[\frac{e^{j\frac{\pi}{4}}\,\cos\theta_0^i\,(k/6)^{1/6}\,\Gamma(1/3)}{\sqrt{\pi}\,|m(Q_0)|^{1/3}}\right]\vec{E}^i(Q_0)\cdot\bar{\bar{R}}\,(Q_0)\frac{e^{-jks_0^r}}{\sqrt{s_0^r}}\,. \qquad (2.96)$$

2.1.4 The complex ray field and its limiting form on the dark side of the caustic

From Equations (2.67)–(2.70) the complex ray field on the dark side of the caustic is given by the following expression:

$$\vec{E}^c(P_S) \sim j\sqrt{\pi}\, e^{-jk\alpha^c_{1,2}} \left[\vec{A}_s\, \gamma_s^{1/4}\, \mathrm{Ai}(\gamma_s) \mp \vec{B}_s\, \gamma_s^{-1/4}\, \mathrm{Ai}'(\gamma_s)\right] u(-\zeta_a)\,, \quad \text{for} \quad m(Q_0) \lesseqgtr 0\,, \tag{2.97}$$

where from (2.76), (2.78), (2.80), and (2.81) the parameters γ_s, $\alpha^c_{1,2}$, $\vec{A}_s$, and $\vec{B}_s$ are given by

$$\gamma_s = \left[\frac{3}{4}k\left|(s_2^{ic} + s_2^{rc}) - (s_1^{ic} + s_1^{rc})\right|\right]^{2/3}, \tag{2.98}$$

$$\alpha^c_{1,2} = s^{ic}_{1,2} + s^{rc}_{1,2} \mp j\delta k^{-1}\frac{2}{3}\gamma_s^{3/2}, \tag{2.99}$$

$$\left\{\begin{array}{c}\vec{A}_s \\ \vec{B}_s\end{array}\right\} = \frac{\vec{A}(Q_1^c)\cdot\bar{\bar{R}}\,(Q_1^c)}{\sqrt{s_1^{ic}}}\left|\sqrt{\frac{\rho_1^{rc}}{\rho_1^{rc}+s_1^{rc}}}\right| \pm \frac{\vec{A}(Q_2^c)\cdot\bar{\bar{R}}\,(Q_2^c)}{\sqrt{s_2^{ic}}}\left|\sqrt{\frac{\rho_2^{rc}}{\rho_2^{rc}+s_2^{rc}}}\right|, \tag{2.100}$$

The uniform complex ray field solution in (2.97) is non-zero only in region IV of Figures 2.2 and 2.3. Although the values associated with both complex reflection points are present in the expression for the complex ray field through the parameters $\vec{A}_s$, and $\vec{B}_s$, on the deep dark side of the caustic only the contribution from one of the complex reflection points should be present in the solution since the contribution from its complex conjugate counterpart violates the radiation condition and produces an unbounded result. On the deep dark side of the caustic the parameter $\gamma_s \gg 1$, and using the large argument form of the ordinary Airy function and its derivative given in (A.10) and (A.11) the complex ray field in the deep dark side of the smooth caustic is given by the following expression:

$$\vec{E}^c(P_S) \sim u(-\zeta_a)\,\vec{E}^i(Q^c_{1,2})\cdot\bar{\bar{R}}\,(Q^c_{1,2})\sqrt{\frac{\rho^{rc}_{1,2}}{\rho^{rc}_{1,2}+s^{rc}_{1,2}}}\, e^{-jks^{rc}_{1,2}}\,;\ m(Q_0)\lesseqgtr 0\,, \tag{2.101}$$

with the understanding that $\rho^{rc}_{1,2}/\left(\rho^{rc}_{1,2}+s^{rc}_{1,2}\right) < 0$ on the dark side of the caustic. Equation (2.101) indeed shows that the complex ray field solution in the deep dark

side of the smooth caustic reduces to the non-uniform complex GO expression of Ikuno and Felsen [2, 3] obtained independently via the complex stationary phase method [18].

2.1.5 The edge diffracted field and its limiting forms

The edge diffracted field may be written as follows:

$$\vec{E}^d(P) = \vec{E}^d_{nu}(P) + \vec{E}^d_c(P), \tag{2.102}$$

where $\vec{E}^d_{nu}(P)$ and $\vec{E}^d_c(P)$ are the non-uniform and curvature correction terms, respectively. From Equations (2.49)–(2.54) and (2.67)–(2.70) they are given by the following expressions:

$$\vec{E}^d_{nu}(P) \sim \frac{\vec{F}(\ell_a)}{jk\dot{\phi}(\ell_a)} e^{-jk(s^i_a + s^d_a)}, \tag{2.103}$$

$$\begin{aligned}\vec{E}^d_c(P) \sim\ & e^{-jk(s^i_a+s^d_a)} \left\{ \vec{A}_d \left[e^{j(\gamma_a\zeta_a+\zeta_a^3/3)} \mathrm{g}^*_i(\gamma_a,\zeta_a) + \frac{j}{\gamma_a+\zeta_a^2} \right] \right. \\ & \left. + \ j\vec{B}_d \left[e^{j(\gamma_a\zeta_a+\zeta_a^3/3)} \frac{\partial}{\partial\gamma_a} \mathrm{g}^*_i(\gamma_a,\zeta_a) + \frac{\zeta_a}{\gamma_a+\zeta_a^2} \right] \right\}, \\ & \text{if} \quad m(Q_0) > 0,\end{aligned} \tag{2.104}$$

$$\begin{aligned}\vec{E}^d_c(P) \sim\ & e^{-jk(s^i_a+s^d_a)} \left\{ \vec{A}_d \left[e^{-j(\gamma_a\zeta_a+\zeta_a^3/3)} \mathrm{g}_i(\gamma_a,\zeta_a) - \frac{j}{\gamma_a+\zeta_a^2} \right] \right. \\ & \left. - \ j\vec{B}_d \left[e^{-j(\gamma_a\zeta_a+\zeta_a^3/3)} \frac{\partial}{\partial\gamma_a} \mathrm{g}_i(\gamma_a,\zeta_a) + \frac{\zeta_a}{\gamma_a+\zeta_a^2} \right] \right\}, \\ & \text{if} \quad m(Q_0) < 0,\end{aligned} \tag{2.105}$$

$$i = \begin{cases} 1 \text{ in regions III, V, and VI} \\ 2 \text{ in region I and IV} \\ 3 \text{ in region II} \end{cases}$$

where γ_a, ζ_a, $\vec{A}_d$, and $\vec{B}_d$ are given by

$$\gamma_a = -\delta k^{\frac{2}{3}} (\cos\varphi'_0 + \cos\varphi_0) \left| \frac{2}{m(Q_0)} \right|^{\frac{1}{3}}, \tag{2.106}$$

$$\zeta_a = u_0 k^{\frac{1}{3}} \left| (\cos\varphi'_0 + \cos\varphi_0) - (\cos\varphi'_a + \cos\varphi_a) \right|^{1/2} \left| \frac{2}{m(Q_0)} \right|^{\frac{1}{6}}, \tag{2.107}$$

$$u_0 = \begin{cases} +1 & \text{if } Q_0 \ni C \\ -1 & \text{if } Q_0 \in C, \end{cases} \tag{2.108}$$

$$\begin{Bmatrix} \vec{A}_d \\ \vec{B}_d \end{Bmatrix} = \frac{e^{j\frac{\pi}{4}}(-\gamma_a)^{\pm 1/4}}{2\sqrt{\pi}} \begin{Bmatrix} \vec{A}_\ell \\ \vec{B}_\ell \end{Bmatrix}, \text{ if } \gamma_a < 0 \tag{2.109}$$

$$= \frac{\gamma_a^{\pm 1/4}}{2\sqrt{\pi}} \begin{Bmatrix} j\vec{A}_s \\ \vec{B}_s \end{Bmatrix}, \text{ if } \gamma_a > 0, \tag{2.110}$$

where $\vec{A}_\ell$, $\vec{B}_\ell$ and $\vec{A}_s$, $\vec{B}_s$ are given in (2.87) and (2.100), respectively. The non-uniform term in the diffracted field expression of Equation (2.103) can be recognized as the non-uniform PO solution for the edge diffracted field from a half-plane. The curvature correction term given by Equations (2.104)–(2.105) cancels the singular non-uniform term near the real ray optical boundaries, namely the RSB and ISB. It also compensates the discontinuities of the incident, reflected, and complex ray field components at the ISB, RSB, and CRSB, respectively, thus ensuring continuity in the total field. As will be shown in more detail later in this subsection, the curvature correction term reduces to zero away from all optical boundaries. Before proceeding with a more detailed examination of the two terms comprising the edge diffracted field, some disadvantages of the formulation in Equation (2.102) should be mentioned. First, the singularity near the real ray optical boundaries is subtracted by the curvature correction term. For practical implementations this could result in numerical instabilities due to the subtraction of two large numbers that tend to infinity at the aforementioned boundaries, and therefore it might be necessary to take special limiting procedures near these boundaries. Second, the expression for the curvature correction term involves information about the reflection points explicitly contained in the vector quantities $\vec{A}_d$ and $\vec{B}_d$, and at least from a philosophical point of view, the locality ansatz of GTD/UTD postulating that the edge diffracted field only depends on the geometrical properties of the surface near the edge is clearly violated. Nevertheless, this non-local nature of the diffracted field is a direct result of the rigorous Chester et al. expansion [7] employed at the outset of the asymptotic analysis which provides for a systematic method for obtaining the higher order terms in the asymptotic expansion for the fields in the vicinity of the smooth caustic.

Next, let us proceed with a more in depth examination of the two terms comprising the edge diffracted field. The non-uniform term will be examined first. From Equations (2.8) and (F.9) we have

$$\vec{F}(\ell_a) = \sqrt{\frac{jk}{2\pi}} \frac{\hat{s}_a^d \times \hat{s}_a^d \times \left[\hat{n}_a \times \hat{s}_a^i \times \vec{A}(Q_a)\right]}{\sqrt{s_a^i s_a^d}}, \tag{2.111}$$

$$\dot{\phi}(\ell_a) = -\cos\varphi_a' - \cos\varphi_a, \tag{2.112}$$

where the vector quantity in the numerator of (2.111) can be written as follows:

$$\hat{s}_a^d \times \hat{s}_a^d \times \left[\hat{n}_a \times \hat{s}_a^i \times \vec{A}(Q_a)\right] = -\vec{A}(Q_a) \cdot \left[\sin\varphi_a' \hat{e}_\perp \hat{e}_\perp - \sin\varphi_a \hat{e}_\parallel^i \hat{e}_\parallel^d\right], \tag{2.113}$$

with φ_a' and φ_a being the angles of incidence and observation, respectively, measured from the edge-fixed coordinate system, and $\hat{e}_\perp$, $\hat{e}_\parallel^{i,d}$ are the unit vectors fixed in the incident and diffracted rays as shown in Figure 2.4. Thus, using (2.111)–(2.113) the non-uniform term of the diffracted field is given by

$$\vec{E}_{nu}^d(P) \sim \vec{E}^i(Q_a) \cdot \bar{\bar{D}}_{nu}(Q_a) \frac{e^{-jks_a^d}}{\sqrt{s_a^d}}, \tag{2.114}$$

where $\vec{E}^i(Q_a)$ is the incident electric field at the edge and $\bar{\bar{D}}_{nu}$ is the non-uniform dyadic PO diffraction coefficient given by

$$\bar{\bar{D}}_{nu}(Q_a) = D_s(\varphi_a', \varphi_a)\hat{e}_\perp \hat{e}_\perp + D_h(\varphi_a', \varphi_a)\hat{e}_\parallel^i \hat{e}_\parallel^d, \tag{2.115}$$

$$D_{s,h}(\varphi_a', \varphi_a) = \pm \frac{e^{-j\frac{\pi}{4}}}{\sqrt{2\pi k}} \frac{\left\{ \begin{array}{c} \sin\varphi_a' \\ \sin\varphi_a \end{array} \right\}}{(\cos\varphi_a' + \cos\varphi_a)}. \tag{2.116}$$

It is well known that the PO diffraction coefficient does not satisfy reciprocity nor does it satisfy the local boundary condition on the surface for the soft acoustic or TM polarization case. These shortcomings are expected to produce erroneous results for observation points away from the optical boundaries where the total diffracted field would equal the non-uniform PO part. A rigorous method of providing the necessary corrections to the PO approximation is to employ the PTD technique [19] at the outset of the analysis. PTD introduces a non-uniform induced current near the edge in addition to the GO current. However, this addition most often makes the asymptotic

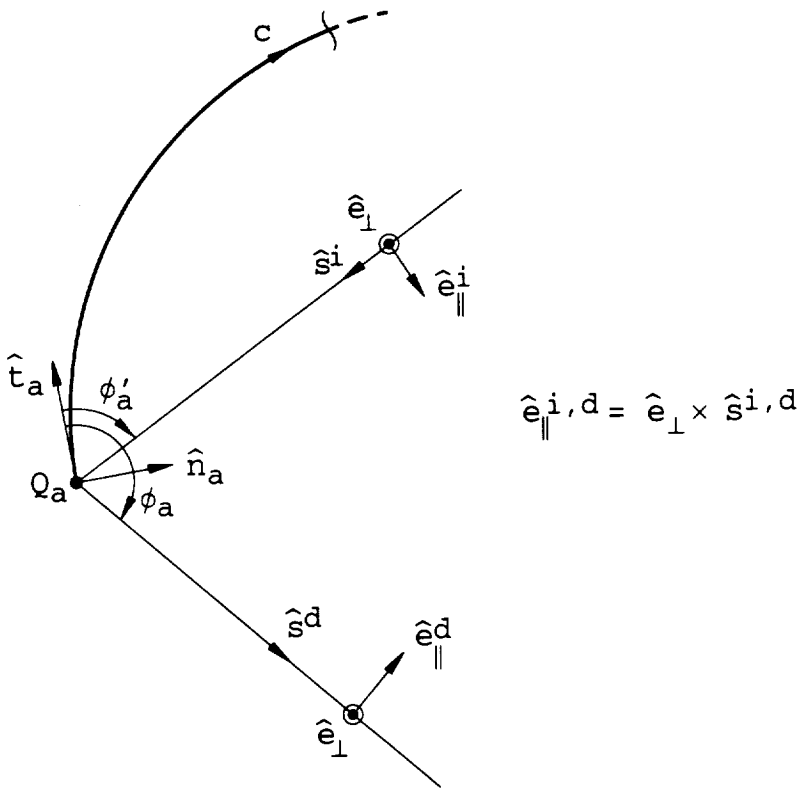

Figure 2.4: Edge diffracted field geometry.

reduction of the resulting radiation integral quite difficult if not impossible, thus necessitating the use of time consuming numerical integrations. A rather heuristic but indeed simpler approach for correcting the edge diffracted field contribution is to improve the PO diffraction coefficient by introducing a pair of multiplicative correction terms (one for each polarization) derived by James [20], that is

$$C_s(\varphi',\varphi) = \sin(\varphi/2)\sec(\varphi'/2), \text{ and} \tag{2.117}$$

$$C_h(\varphi',\varphi) = \cos(\varphi'/2)\csc(\varphi/2), \tag{2.118}$$

which enforce reciprocity and the local boundary condition for the soft acoustic or TM polarization case so that the PO diffraction coefficient yields the exact diffraction coefficient outside the optical boundaries. A plot of the PO correction factors appears in Figure 2.5. The correction factors are approximately unity near the real ray optical boundaries ($\varphi = \pi \pm \varphi'$), and therefore they do not affect the cancellation of singularities or the compensation of discontinuities in the incident, reflected, and complex ray field components provided by the curvature correction term in the edge diffracted field.

Next, we will investigate the behavior of the curvature correction term of the edge diffracted field by examining certain limiting cases. The curvature correction term is expected to cancel the singular non-uniform term and enforce total field continuity near the optical and composite shadow boundaries, while reducing to zero for observation points far removed from such regions.

Limiting case 1a : Observation point on the deep lit side of the smooth caustic of reflected rays.

In this case $\gamma_a \ll -1$ in Equations (2.104) and (2.105), and using the asymptotic formulas for the incomplete Airy functions and their derivatives in Appendix B, the curvature correction term assumes the following form:

$$\vec{E}_c^d(P_L) \sim e^{-jk(s_a^i + s_a^d)}\left(\vec{A}_d + \zeta_a \vec{B}_d\right)\left[\frac{F(\eta^2)-1}{2j\eta(-\gamma_a)^{1/4}}\right] ; \text{ if } m(Q_0) > 0, \tag{2.119}$$

$$\vec{E}_c^d(P_L) \sim e^{-jk(s_a^i + s_a^d)}\left(\vec{A}_d + \zeta_a \vec{B}_d\right)\left[\frac{1-F^*(\eta^2)}{2j\eta(-\gamma_a)^{1/4}}\right] ; \text{ if } m(Q_0) < 0, \tag{2.120}$$

(2.121)

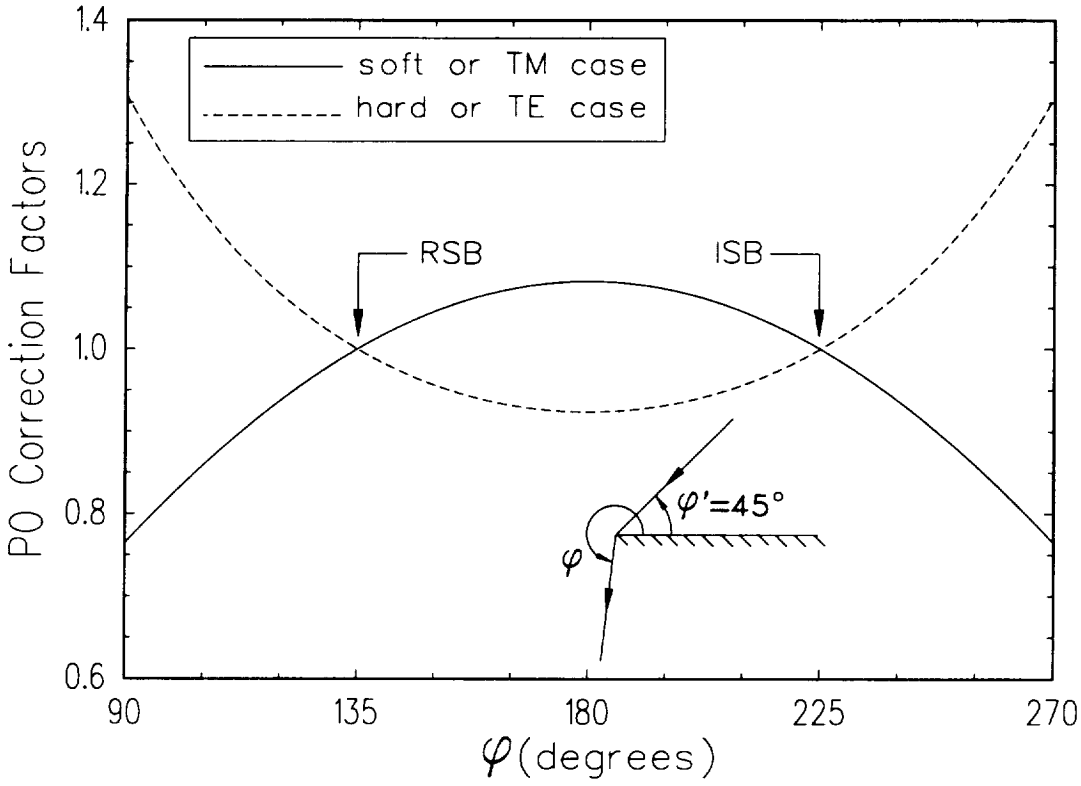

Figure 2.5: Plot of the PO correction factors $C_{s,h}(\varphi', \varphi)$ with $\varphi' = 45°$.

where

$$\eta = \pm\left[\gamma_a\zeta_a + \zeta_a^3/3 + \frac{2}{3}(-\gamma_a)^{3/2}\right]^{\frac{1}{2}} \;;\; \zeta_a \gtrless (-\gamma_a)^{1/2}\,\mathrm{sgn}(\zeta_a)\,, \tag{2.122}$$

and $F(x)$ is the UTD transition function [4]. Note that when the observation point is far removed from the optical boundaries, that is $|\eta| \gg 1$, $F(\eta^2) \to 1$ and the curvature correction term reduces to zero as expected.

Limiting case 1b : Observation point on the deep lit side of the smooth caustic of reflected rays and close to the RSB.

In this case, $\zeta_a \approx -(-\gamma_a)^{1/2}$ with $\gamma_a \ll -1$ in Equations (2.104) and (2.105) or $\eta \approx 0$ in (2.119) and (2.120). Again using the asymptotic formulas for the incomplete Airy functions and their derivatives in Appendix B, the curvature correction term assumes the following form:

$$\vec{E}_c^{\,d}(P_L) \;\sim\; e^{-jk(s_a^i+s_a^d)}\left[\vec{A}_d - (-\gamma_a)^{1/2}\,\vec{B}_d\right]\left\{\frac{j}{\gamma_a+\zeta_a^2} \pm \frac{\sqrt{\pi}e^{j\frac{\pi}{4}}}{2(-\gamma_a)^{1/4}}\right\}, \tag{2.123}$$

$$\text{if} \quad m(Q_0) > 0\,,$$

$$\vec{E}_c^{\,d}(P_L) \;\sim\; e^{-jk(s_a^i+s_a^d)}\left[\vec{A}_d - (-\gamma_a)^{1/2}\,\vec{B}_d\right]\left\{\frac{-j}{\gamma_a+\zeta_a^2} \pm \frac{\sqrt{\pi}e^{-j\frac{\pi}{4}}}{2(-\gamma_a)^{1/4}}\right\}, \tag{2.124}$$

$$\text{if} \quad m(Q_0) < 0\,.$$

Now, from Equations (2.28), (2.36), (2.87), (2.106)–(2.109), (2.115), and (2.116) we have that

$$\vec{A}_d - (-\gamma_a)^{1/2}\,\vec{B}_d \;=\; \frac{e^{j\frac{\pi}{4}}(-\gamma_a)^{1/4}}{\sqrt{\pi}}\left[\frac{\vec{A}(Q_a)\cdot\bar{\bar{R}}\,(Q_a)}{\sqrt{s_a^r}}\right]\left|\sqrt{\frac{\rho_a^r}{\rho_a^r+s_a^r}}\,\right|, \tag{2.125}$$

$$\gamma_a + \zeta_a^2 \;=\; -\delta\sqrt{k}(-\gamma_a)^{1/4}\left(\frac{\cos\varphi_a' + \cos\varphi_a}{\sin\varphi_a'}\right)\left|\sqrt{\frac{2\rho_a^r\,s_a^r}{\rho_a^r+s_a^r}}\,\right|, \tag{2.126}$$

$$\bar{\bar{D}}_{nu}\,(Q_a)\Big|_{RSB} \;=\; -\frac{e^{-j\frac{\pi}{4}}\sin\varphi_a'\;\bar{\bar{R}}\,(Q_a)}{\sqrt{2\pi k}(\cos\varphi_a' + \cos\varphi_a)}\,, \tag{2.127}$$

and using the fact that $s_a^r = s_a^d$ at the RSB, the curvature correction term is given by

$$\begin{aligned}\vec{E}_c^{\,d}(P_L) \;&\sim\; -\vec{E}^i(Q_a)\cdot\bar{\bar{D}}_{nu}\,(Q_a)\,\frac{e^{-jks_a^d}}{\sqrt{s_a^d}} \pm \frac{1}{2}\vec{E}^i(Q_a)\cdot\bar{\bar{R}}\,(Q_a)\sqrt{\frac{\rho_a^r}{\rho_a^r+s_a^r}}\,e^{-jks_a^r} \\ &=\; -\vec{E}_{nu}^{\,d}(P_L) \pm \frac{1}{2}\vec{E}^r(P_L)\,,\end{aligned} \tag{2.128}$$

with the $\pm$ sign for the shadowed and illuminated sides of the RSB, respectively. Therefore, the singular non-uniform term is cancelled, and the discontinuity in the reflected field is appropriately compensated to provide continuity in the total field.

Limiting case 1c : Observation point is close to the ISB.

In this case, $\zeta_a \approx (-\gamma_a)^{1/2}$ with $\gamma_a \ll -1$ in (2.104) and (2.105) or $\eta \approx 0$ in (2.119) and (2.120). Again using the asymptotic formulas for the incomplete Airy functions and their derivatives in Appendix B, the curvature correction term assumes the following form:

$$\vec{E}_c^d(P_L) \sim e^{-jk(s_a^i+s_a^d)}\left[\vec{A}_d + (-\gamma_a)^{1/2}\,\vec{B}_d\right]\left\{\frac{j}{\gamma_a+\zeta_a^2} \pm \frac{\sqrt{\pi}e^{-j\frac{\pi}{4}}}{2(-\gamma_a)^{1/4}}\right\}, \quad (2.129)$$

$$\text{if} \quad m(Q_0) > 0\,,$$

$$\vec{E}_c^d(P_L) \sim e^{-jk(s_a^i+s_a^d)}\left[\vec{A}_d + (-\gamma_a)^{1/2}\,\vec{B}_d\right]\left\{\frac{-j}{\gamma_a+\zeta_a^2} \pm \frac{\sqrt{\pi}e^{j\frac{\pi}{4}}}{2(-\gamma_a)^{1/4}}\right\}, \quad (2.130)$$

$$\text{if} \quad m(Q_0) < 0\,.$$

Now, from (2.87), (2.109), (2.111), (2.115), and (2.116) we have that

$$\vec{A}_d + (-\gamma_a)^{1/2}\,\vec{B}_d = -\frac{e^{j\frac{\pi}{4}}\,(-\gamma_a)^{1/4}}{\sqrt{\pi}}\left[\frac{\vec{A}(Q_a)\cdot\bar{\bar{I}}}{\sqrt{s_a^i+s_a^d}}\right], \quad (2.131)$$

$$\gamma_a + \zeta_a^2 = -\delta\sqrt{k}(-\gamma_a)^{1/4}\left(\frac{\cos\varphi_a' + \cos\varphi_a}{\sin\varphi_a'}\right)\sqrt{\frac{2s_a^i\,s_a^d}{s_a^i+s_a^d}}, \quad (2.132)$$

$$\bar{\bar{D}}_{nu}\,(Q_a)\Big|_{ISB} = \frac{e^{-j\frac{\pi}{4}}\,\sin\varphi_a'\;\bar{\bar{I}}}{\sqrt{2\pi k}(\cos\varphi_a' + \cos\varphi_a)}, \quad (2.133)$$

$$\bar{\bar{I}} = \hat{e}_\perp\hat{e}_\perp + \hat{e}_\parallel^i\hat{e}_\parallel^d, \quad (2.134)$$

and using the fact that $s_a^i + s_a^d = |\overline{P'P_L}| = s_p^i$ and $\vec{A}(Q_a) = \vec{A}(P_L)$ at the ISB, the curvature correction term is given by

$$\vec{E}_c^d(P_L) \sim -\vec{E}^i(Q_a)\cdot\bar{\bar{D}}_{nu}\,(Q_a)\frac{e^{-jks_a^d}}{\sqrt{s_a^d}} \pm \frac{1}{2}\vec{A}(P_L)\,\frac{e^{-jks_p^i}}{\sqrt{s_p^i}} \quad (2.135)$$

$$= -\vec{E}_{nu}^d(P_L) \pm \frac{1}{2}\vec{E}^i(P_L)\,, \quad (2.136)$$

with the $\pm$ sign for the shadowed and illuminated sides of the ISB, respectively. Therefore, the singular non-uniform term is cancelled, and the discontinuity in the incident field is appropriately compensated to produce a continuous total field.

Limiting case 2a : Observation point lies on the smooth caustic of reflected rays.

In this case $Q_{1,2} \to Q_0$ thus, $\gamma_a = 0$ with $\zeta_a < 0$. Also, $\vec{B}_d \approx 0$ and using the small argument form of the incomplete Airy functions in Appendix B, the curvature

correction term is given by

$$\vec{E}_c^d(P) \sim \vec{A}_d e^{-jk(s_a^i+s_a^d)}\left[-e^{j\zeta_a^3/3}e^{j\frac{\pi}{6}}3^{-2/3}\,\Gamma\left(1/3, j\zeta_a^3/3\right)+\frac{j}{\zeta_a^2}\right], \quad (2.137)$$

$$\text{if } m(Q_0) > 0,$$

$$\vec{E}_c^d(P) \sim \vec{A}_d e^{-jk(s_a^i+s_a^d)}\left[-e^{-j\zeta_a^3/3}e^{-j\frac{\pi}{6}}3^{-2/3}\,\Gamma\left(1/3, -j\zeta_a^3/3\right)-\frac{j}{\zeta_a^2}\right], \quad (2.138)$$

$$\text{if } m(Q_0) < 0,$$

where $\Gamma(x,y)$ is the incomplete Gamma function [21]. When $\zeta_a \ll -1$ or the observation point is far removed from the RSB, the incomplete Gamma function assumes the following large argument form:

$$\Gamma(x,y) \sim (-y)^{x-1}\,e^{-y}, \quad (2.139)$$

and letting $x = 1/3$ and $y = j\zeta_a^3/3$ one can show that $\vec{E}_c^d(P) \to 0$.

Limiting case 2b : Observation point coincides with the caustic termination point T.

In this case $Q_{1,2} = Q_0 \to Q_a$, thus $\gamma_a = 0$, $\zeta_a = 0^{\mp}$, and (2.137), (2.138) become

$$\vec{E}_c^d(T^-) \sim \vec{A}_d\, e^{-jk(s_a^i+s_a^d)}\left[-e^{j\delta\frac{\pi}{6}}\,3^{-2/3}\,\Gamma(1/3)+\frac{j\delta}{\zeta_a^2}\right], \quad (2.140)$$

$$\vec{E}_c^d(T^+) \sim \vec{A}_d\, e^{-jk(s_a^i+s_a^d)}\left[e^{-j\delta\frac{\pi}{6}}\,3^{-2/3}\,\Gamma(1/3)+\frac{j\delta}{\zeta_a^2}\right]. \quad (2.141)$$

Now, from (2.92), (2.93), and (2.107)–(2.109) we have

$$\vec{A}_d = \frac{e^{j\frac{\pi}{4}}\,(k/2)^{1/6}\,\cos\theta_0^i}{\sqrt{\pi}\,|m(Q_0|^{1/3}}\left[\frac{\vec{A}(Q_0)\cdot\bar{\bar{R}}\,(Q_0)}{\sqrt{s_0^i\,s_0^r}}\right], \quad (2.142)$$

$$\zeta_a^2 = -\delta k^{2/3}(\cos\varphi_a' + \cos\varphi_a)\left|\frac{2}{m(Q_0)}\right|^{\frac{1}{3}}, \quad (2.143)$$

$$\bar{\bar{D}}_{nu}\,(Q_a)\Big|_T = -\frac{e^{-j\frac{\pi}{4}}\sin\varphi_a'\;\bar{\bar{R}}\,(Q_a)}{\sqrt{2\pi k}\,(\cos\varphi_a' + \cos\varphi_a)}, \quad (2.144)$$

and using the fact that $s_a^{i,d} = s_0^{i,r}$ and $\cos\theta_0^i = \sin\varphi_a'$ near T, the curvature correction term assumes the following form:

$$\vec{E}_c^d(T^{\pm}) \sim -\vec{E}^i(Q_a)\cdot\bar{\bar{D}}_{nu}\,(Q_a)\frac{e^{-jks_a^d}}{\sqrt{s_a^d}} \pm \frac{e^{\mp j\delta\pi/6}}{\sqrt{3}}\left[\frac{\cos\theta_0^i\,(k/6)^{1/6}\,\Gamma(1/3)\,e^{j\frac{\pi}{4}}}{\sqrt{\pi}\,|m(Q_0)|^{1/3}}\right]$$
$$\times\ \vec{E}^i(Q_0)\cdot\bar{\bar{R}}\,(Q_0)\frac{e^{-jks_0^r}}{\sqrt{s_0^r}} \quad (2.145)$$

$$= -\vec{E}_{nu}^d(T) \pm \left(\frac{1}{2} \mp \frac{j\delta}{2\sqrt{3}}\right)\vec{E}^r(T), \quad (2.146)$$

where $\vec{E}^r(T)$ is given in (2.96). The curvature correction term cancels the singular non-uniform term and also compensates the discontinuity of the reflected field to ensure continuity in the total field.

Limiting case 3a : Observation point on the deep dark side of the smooth caustic of reflected rays.

In this last case, $\gamma_a \gg 1$ and using the asymptotic formulas for the incomplete Airy functions in Appendix B, the curvature correction term assumes the following form:

$$\vec{E}_c^d(P_S) \sim \mathrm{sgn}(\zeta_a)\, e^{-jk(s_a^i+s_a^d)} \left(\vec{A}_d + \zeta_a \vec{B}_d\right) \left\{ \frac{\left[\tilde{F}(\xi) - 1\right] e^{j\frac{\pi}{4}}}{2j\xi\gamma_a^{1/4}} \right\}, \qquad (2.147)$$

$$\text{if} \quad m(Q_0) > 0\,,$$

$$\vec{E}_c^d(P_S) \sim \mathrm{sgn}(\zeta_a)\, e^{-jk(s_a^i+s_a^d)} \left(\vec{A}_d + \zeta_a \vec{B}_d\right) \left\{ \frac{\left[\tilde{F}(\xi) - 1\right] e^{j\frac{\pi}{4}}}{2j\xi\gamma_a^{1/4}} \right\}^*, \qquad (2.148)$$

$$\text{if} \quad m(Q_0) < 0\,,$$

where

$$\xi = \mathrm{sgn}(\zeta_a) \left[\gamma_a\zeta_a + \zeta_a^3/3 + j\frac{2}{3}\gamma_a^{3/2}\right]^{\frac{1}{2}}, \qquad (2.149)$$

and $\tilde{F}(\xi)$ is the Fresnel transition function of complex argument defined in Appendix E. When the observation point is far removed from the CRSB on either side, $\Re(\xi e^{j\pi/4}) \gg 0$ with $|\xi| \gg 1$ and $\tilde{F}(\xi) \to 1$, thus the curvature correction term reduces to zero.

Limiting case 3b : Observation point near the CRSB.

In this case, $\zeta_a = 0^{\pm}$, $\Re(\xi e^{j\pi/4}) \approx 0$, $\tilde{F}(\xi)$ assumes the following form:

$$\tilde{F}(\xi) = \sqrt{\pi}\,\xi\, e^{j\frac{\pi}{4}}\, e^{j\xi^2} + 1\,, \qquad (2.150)$$

and the curvature correction term in Equations (2.147) and (2.148) becomes

$$\vec{E}_c^d(P_S) \sim \frac{\mathrm{sgn}(\zeta_a)\sqrt{\pi}}{2\gamma_a^{1/4}}\, \vec{A}_d\, e^{-jk(s_a^i+s_a^d)-\frac{2}{3}\gamma_a^{3/2}}. \qquad (2.151)$$

Now, from Equations (2.44) and (2.76) with $\zeta_a = 0$, (2.100), and (2.110) we have

$$s_a^i + s_a^d = s_{1,2}^{ic} + s_{1,2}^{rc} + jk^{-1}\frac{2}{3}\gamma_a^{3/2}, \qquad (2.152)$$

$$\vec{A}_d = \frac{j\gamma_a^{1/4}}{\sqrt{\pi}} \left[\frac{\vec{A}(Q_{1,2}^c)\cdot\bar{\bar{R}}\,(Q_{1,2}^c)}{\sqrt{s_{1,2}^{ic}}}\right] \left|\sqrt{\frac{\rho_{1,2}^c}{\rho_{1,2}^c + s_{1,2}^{rc}}}\right|, \qquad (2.153)$$

and the curvature correction term near the CRSB is given by

$$\vec{E}_c^d(P_S) \sim \frac{1}{2}\mathrm{sgn}(\zeta_a)\vec{E}^i(Q_{1,2}^c)\cdot\bar{\bar{R}}(Q_{1,2}^c)\sqrt{\frac{\rho_{1,2}^{rc}}{\rho_{1,2}^{rc}+s_{1,2}^{rc}}}\,e^{-jks_{1,2}^{rc}};\ m(Q_0)\lesseqgtr 0, \quad (2.154)$$

$$= \frac{1}{2}\mathrm{sgn}(\zeta_a)\vec{E}^c(P_S), \quad (2.155)$$

where $\vec{E}^c(P_S)$ is the complex GO ray field. Since $\zeta_a < 0$ in the illuminated side of the CRSB and $\zeta_a > 0$ in the shadow side of the CRSB, the curvature correction term indeed compensates the discontinuity in the complex ray field across the CRSB.

2.2 Derivation of the UGO/EUTD solution using the method of steepest descent

In this section, the UGO/EUTD solution for the reflected, complex ray, and edge diffracted fields is derived using the method of steepest descent [8] for the asymptotic reduction of the PO radiation integral representation for the scattered field formulated in the previous section. We begin with the expression for the scattered field in Equation (2.26), that is

$$\vec{E}^s(P) \approx e^{-jk\alpha}\,\vec{I}(\beta, s_a; k), \quad (2.156)$$

where α is given in (2.18)–(2.20) and $\vec{I}(\beta, s_a; k)$ is a stationary phase integral in the s-plane given by

$$\vec{I}(\beta, s_a; k) = \int_{s_a}^{\infty} \vec{G}(s)\, e^{-jk(\beta s + s^3/3)}\, ds, \quad (2.157)$$

where β, s_a, and $\vec{G}(s)$ are given in (2.21)–(2.23), (2.25) and (2.27), respectively. Only the case of $m(Q_0) > 0$ will be considered here since the results for $m(Q_0) < 0$ can be easily obtained by letting $\beta = \beta\exp(j2\pi/3)$ and $s_a = s_a\exp(j\pi/3)$ in (2.157). The complex plane topology of the stationary phase integral in (2.157) for the lit side of the caustic ($\beta < 0$) is shown in Figure 2.6. The original path of integration, P_0, running from s_a to ∞ is deformed into the appropriate steepest descent paths through the endpoint and the two real saddle points $s_{1,2} = \pm(-\beta)^{1/2}$, and Equation (2.157) may be written as follows:

$$\vec{I}(\beta, s_a; k) = u(s_2 - s_a)\int_{L_{21}} \vec{G}(s)\, e^{-jk(\beta s + s^3/3)}\, ds$$

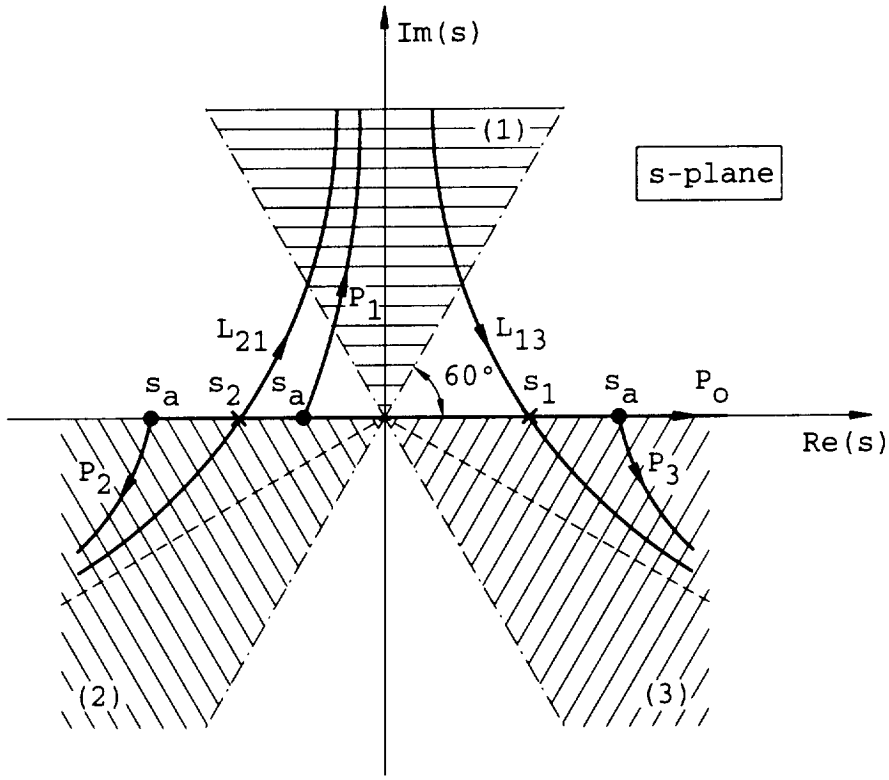

Figure 2.6: Complex plane topology of the stationary phase integral $\vec{I}(\beta, s_a; k)$ for observation points in the lit side of the smooth caustic ($\beta < 0$).

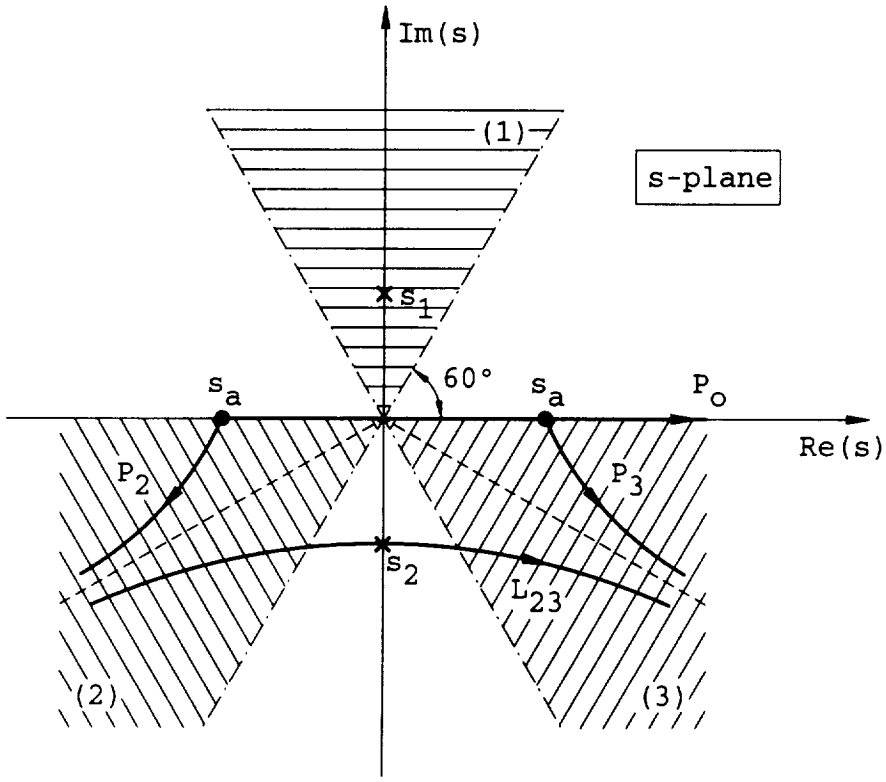

Figure 2.7: Complex plane topology of the stationary phase integral $\vec{I}(\beta, s_a; k)$ for observation points in the dark side of the smooth caustic ($\beta > 0$).

$$+ \quad u(s_1 - s_a) \int_{L_{13}} \vec{G}(s)\, e^{-jk(\beta s + s^3/3)}\, ds$$

$$+ \int_{P_n} \vec{G}(s)\, e^{-jk(\beta s + s^3/3)}\, ds\,, \tag{2.158}$$

$$n = \begin{cases} 1 \text{ if } s_2 < s_a < s_1 \\ 2 \text{ if } s_a < s_2 \\ 3 \text{ if } s_a > s_1. \end{cases} \tag{2.159}$$

In a similar fashion, in the dark side of the caustic ($\beta > 0$), the original path of integration P_0 is deformed into the steepest descent paths through the endpoint and the complex saddle point s_2 as shown in Figure 2.7 and Equation (2.157) may be written as follows:

$$\vec{I}(\beta, s_a; k) = u(-s_a) \int_{L_{23}} \vec{G}(s)\, e^{-jk(\beta s + s^3/3)}\, ds$$

$$+ \int_{P_m} \vec{G}(s)\, e^{-jk(\beta s + s^3/3)}\, ds\,, \tag{2.160}$$

$$m = \begin{cases} 2 \text{ if } s_a < 0 \\ 3 \text{ if } s_a > 0. \end{cases} \tag{2.161}$$

Next, it is assumed that the vector amplitude function, $\vec{G}(s)$, is regular and slowly varying along each of the paths of integration in Equations (2.158) and (2.160), and since the principal contribution from each integral would come from the neighborhood of either a saddle point or an endpoint, $\vec{G}(s)$ can be expanded in Taylor series near the pertinent critical point for each integral. Thus, using the definitions for the ordinary, Fock-type, and incomplete Airy functions in Appendices A and B, (2.158) and (2.160) may be written as follows:

$$\begin{aligned} \vec{I}(\beta, s_a; k) &\simeq j\sqrt{\pi}\, k^{-1/3}\, \vec{G}(s_2)\, \mathrm{W}_2(k^{2/3}\beta)\, u(s_2 - s_a) \\ &- j\sqrt{\pi}\, k^{-1/3}\, \vec{G}(s_1)\, \mathrm{W}_1(k^{2/3}\beta)\, u(s_1 - s_a) \\ &+ k^{-1/3}\, \vec{G}(s_a)\, \mathrm{g}_i^*(k^{2/3}\beta, k^{1/3}s_a) + O(k^{-1}) \text{ if } \beta < 0, \qquad (2.162) \\ i &= \begin{cases} 1 \text{ if } s_a > s_1 \\ 2 \text{ if } s_a < s_2 \\ 3 \text{ otherwise,} \end{cases} \\ \vec{I}(\beta, s_a; k) &\simeq 2\pi\, k^{-1/3}\, \vec{G}(s_2)\, \mathrm{Ai}(k^{2/3}\beta)\, u(-s_a) \\ &+ k^{-1/3}\, \vec{G}(s_a)\, \mathrm{g}_i^*(k^{2/3}\beta, k^{1/3}s_a) + O(k^{-1}) \text{ if } \beta > 0, \qquad (2.163) \\ i &= \begin{cases} 1 \text{ if } s_a > 0 \\ 2 \text{ if } s_a < 0, \end{cases} \end{aligned}$$

where

$$\vec{G}(s_{1,2}) = \vec{F}(\ell_{1,2})(-\beta)^{1/4} \sqrt{\frac{\pm 2}{\ddot{\phi}(\ell_{1,2})}}, \tag{2.164}$$

$$\vec{G}(s_a) = \frac{\vec{F}(\ell_a)}{\dot{\phi}(\ell_a)} (\beta + s_a^2), \tag{2.165}$$

$$\vec{F}(\ell_{1,2}) = \sqrt{\frac{jk}{2\pi}} \frac{\cos\theta_{1,2}^i \vec{A}(Q_{1,2}) \cdot \bar{\bar{R}}\,(Q_{1,2})}{\sqrt{s_{1,2}^i s_{1,2}^r}}, \tag{2.166}$$

$$\ddot{\phi}(\ell_{1,2}) = \cos^2\theta_{1,2}^i \left(\frac{1}{s_{1,2}^r} + \frac{1}{\rho_{1,2}^r} \right), \tag{2.167}$$

$$\frac{\vec{F}(\ell_a)}{\dot{\phi}(\ell_a)} = \frac{jk\vec{A}(Q_a) \cdot \bar{\bar{D}}_{nu}\,(Q_a)}{\sqrt{s_a^i s_a^d}}, \tag{2.168}$$

$\bar{\bar{R}}(Q_{1,2})$ is the dyadic GO reflection coefficient given in Equations (2.60) and (2.61), and $\bar{\bar{D}}_{nu}(Q_a)$ is the dyadic non-uniform PO diffraction coefficient given in (2.115) and (2.116). The first two terms in Equation (2.162) are the uniform contributions from the two real stationary phase points associated with the reflected field in the lit side of the caustic. The first term in (2.163) is the uniform contribution from the complex stationary phase point associated with the complex ray field in the dark side of the caustic. Finally, the third term in (2.162) and the second term in (2.163) are the uniform endpoint contributions associated with the edge diffracted field. The main advantage of (2.162) and (2.163) over the formulation of the previous section is that the expression for each term contributing to the integral is independent of the others, and also the correction to the non-uniform edge diffraction coefficient near the optical boundaries is multiplicative rather than additive. These very desirable features, however, come at the expense of a solution that does not contain the higher order terms involving the derivatives of the canonical functions. The derivative terms in the expressions of the previous section implicitly include slope scattering that occurs when the source pattern has a null in the direction corresponding to observation points near the caustic or the composite shadow boundary. It is believed, however, that when slope scattering effects are not important the higher order terms are not significant in terms of solution accuracy because they are only necessary for recovering the well known non-uniform expressions for observation points away from the transition regions. As will be shown later in this section, the UGO/EUTD expressions for the reflected, complex ray, and edge diffracted field also recover the non-uniform expressions outside the transition regions even though the derivative terms are absent. Furthermore, the results of Section 2.1 may be used to derive slope reflection and diffraction coefficients to be used in conjunction with the regular UGO/EUTD expressions.

2.2.1 UGO expression for the reflected field

The UGO expression for the reflected field is as follows:

$$\begin{aligned}\vec{E}^r(P_L) \;\sim\; & u_1 \vec{E}^i(Q_1)\cdot \bar{\bar{\mathcal{R}}}\,(Q_1)\sqrt{\frac{\rho_1^r}{\rho_1^r+s_1^r}}\,e^{-jks_1^r} \\ & + \; u_2 \vec{E}^i(Q_2)\cdot \bar{\bar{\mathcal{R}}}^*(Q_2)\sqrt{\frac{\rho_2^r}{\rho_2^r+s_2^r}}\,e^{-jks_2^r}, \end{aligned} \tag{2.169}$$

where $u_1 = 1$ in regions I and II of Figures 2.2 and 2.3 and zero elsewhere, and $u_2 = 1$ only in region I and zero elsewhere. The quantity $\bar{\bar{\mathcal{R}}}\,(Q_{1,2})$ is the dyadic UGO reflection coefficient and is given by

$$\bar{\bar{\mathcal{R}}}\,(Q_{1,2}) = \mathcal{R}_s(Q_{1,2})\,\hat{e}_\perp\hat{e}_\perp + \mathcal{R}_h(Q_{1,2})\,\hat{e}_\parallel^i\hat{e}_\parallel^r, \tag{2.170}$$

$$\mathcal{R}_{s,h}(Q_{1,2}) = R_{s,h}\,e^{-j\frac{\pi}{4}}\,\gamma_{1,2}^{1/4}\,e^{-j(2/3)\gamma_{1,2}^{3/2}}\,\mathrm{W}_1(-\gamma_{1,2}), \tag{2.171}$$

$$R_{s,h} = \mp 1, \quad \text{for a PEC boundary.} \tag{2.172}$$

A plot of the scalar UGO reflection coefficients, $\mathcal{R}_{s,h}$, appears in Figure 2.8. Equation (2.169) shows that the complex conjugate of the UGO reflection coefficient should be used when the spread factor $\rho^r/(\rho^r+s^r) < 0$. The parameter $\gamma_{1,2}$ depends on the relative phase distance between the reflection point and the point Q_0 associated with the smooth caustic and is given by

$$\gamma_{1,2} = \left[\frac{3}{2}k\left|(s_0^i + R_0) - \left(s_{1,2}^i + s_{1,2}^r\right)\right|\right]^{\frac{2}{3}}. \tag{2.173}$$

The caustic point Q_0 is found from the following relation:

$$\frac{\left[\hat{R}(Q_0) - \hat{s}^i(Q_0)\right]\cdot\hat{n}(Q_0)}{\rho_g(Q_0)} + \frac{[\hat{s}^i(Q_0)\cdot\hat{n}(Q_0)]^2}{s^i(Q_0)} + \frac{\left[\hat{R}(Q_0)\cdot\hat{n}(Q_0)\right]^2}{R(Q_0)} = 0 \tag{2.174}$$

which in general must be solved using a computer search procedure. Notice that in the case of plane wave incidence with the observer in the far-zone of the scattering boundary, Q_0 is simply an inflection or zero-curvature point.

When the observation point is in the deep lit side of the smooth caustic, $\gamma_{1,2} \gg 1$ and using the large negative argument form of the Fock-type Airy function, $\mathcal{R}_{s,h} \rightarrow R_{s,h} = \mp 1$ which is the usual GO reflection coefficient for a PEC boundary. When the observation point lies on the smooth caustic, the reflected ray spread factors in (2.169)

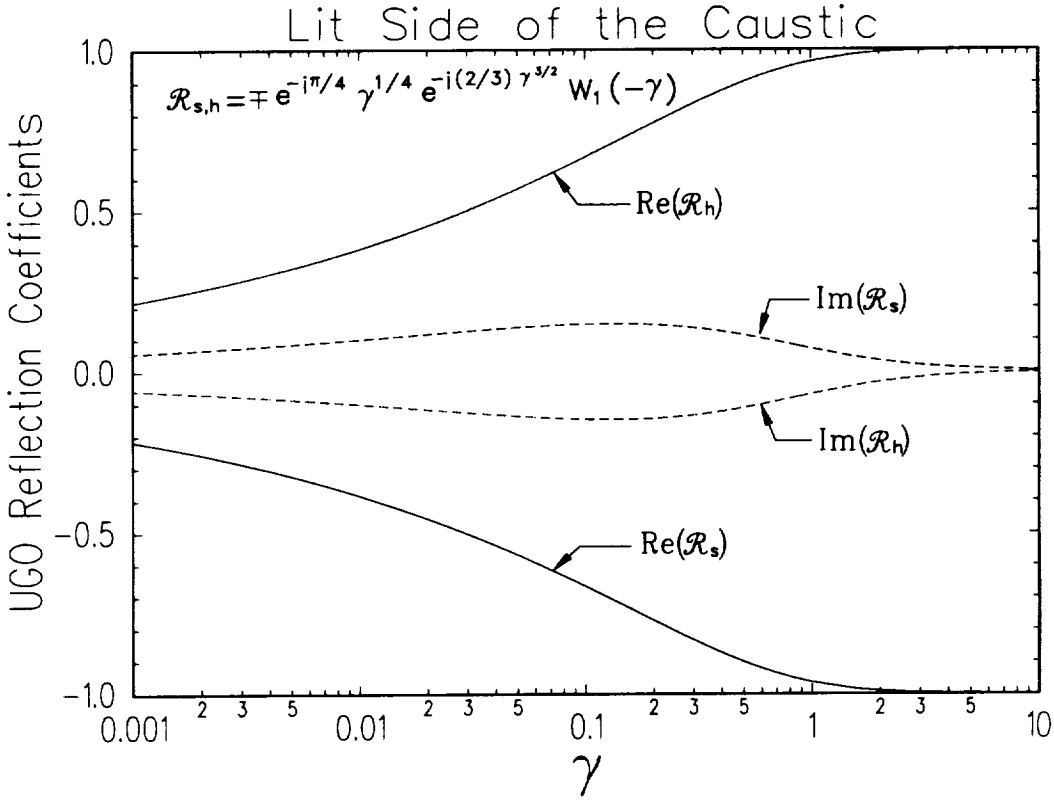

Figure 2.8: Plot of the scalar UGO real ray reflection coefficients.

become singular where the parameter $\gamma_{1,2} \to 0$ in (2.171), and using Equations (2.28), (2.31), and (2.36) $\mathcal{R}_{s,h}$ assumes the following form:

$$\mathcal{R}_{s,h}(Q_0) = k^{\frac{1}{6}} R_{s,h}\, e^{-j\frac{\pi}{4}} \mathrm{W}_1(0)\, |m_r(Q_0)|^{-\frac{1}{3}} \cos\theta_0^i \sqrt{\frac{\rho_0^r + s_0^r}{\rho_0^r}}\,, \tag{2.175}$$

$$\begin{aligned} m_r(Q_0) &= \cos\theta_0^i\, \kappa_g'(Q_0) - \frac{3\cos^2\theta_0^i \sin\theta_0^i}{2s_0^i}\left[\frac{1}{\rho_g(Q_0)\cos\theta_0^i} + \frac{1}{s_0^i}\right] \\ &\quad - \frac{3\cos^2\theta_0^r \sin\theta_0^r}{2s_0^r}\left[\frac{1}{\rho_g(Q_0)\cos\theta_0^r} + \frac{1}{s_0^r}\right]. \end{aligned} \tag{2.176}$$

Hence, the singular spread factors are cancelled and the total reflected field remains finite and agrees with the expression in (2.96) derived in the previous section.

2.2.2 UGO expression for the complex ray field

The UGO expression for the complex ray field in the dark side of the caustic designated as region IV of Figures 2.2 and 2.3 is as follows:

$$\vec{E}^c(P_S) \sim \vec{E}^i(Q_{1,2}^c) \cdot \bar{\bar{\mathcal{R}}}^c(Q_{1,2}^c) \sqrt{\frac{\rho_{1,2}^{rc}}{\rho_{1,2}^{rc} + s_{1,2}^{rc}}}\, e^{-jks_{1,2}^{rc}}\,;\ m(Q_0) \lesssim 0\,, \tag{2.177}$$

where $\rho_{1,2}^{rc}/(\rho_{1,2}^{rc} + s_{1,2}^{rc}) < 0$ in this case and $\bar{\bar{\mathcal{R}}}^c(Q_{1,2}^c)$ is the UGO dyadic complex ray reflection coefficient given by

$$\bar{\bar{\mathcal{R}}}^c(Q_{1,2}^c) = \mathcal{R}_s^c(Q_{1,2}^c)\,\hat{e}_\perp^{ic}\hat{e}_\perp^{rc} + \mathcal{R}_h^c(Q_{1,2}^c)\,\hat{e}_\parallel^{ic}\hat{e}_\parallel^{rc}\,, \tag{2.178}$$

$$\mathcal{R}_{s,h}^c(Q_{1,2}^c) = 2R_{s,h}^c\sqrt{\pi}\,\gamma_s^{1/4}\, e^{(2/3)\gamma_s^{3/2}}\,\mathrm{Ai}(\gamma_s)\,, \tag{2.179}$$

$$R_{s,h}^c = \mp 1\,, \quad \text{for a PEC boundary.} \tag{2.180}$$

A plot of the scalar UGO complex ray reflection coefficients, $\mathcal{R}_{s,h}^c$, appears in Figure 2.9. The parameter γ_s depends on the relative phase distance between the complex reflection point Q_1^c or Q_2^c and the point Q_0 associated with the smooth caustic and is given by

$$\gamma_s = \left[\frac{3}{2}k\left|(s_0^i + R_0) - \left(s_{1,2}^{ic} + s_{1,2}^{rc}\right)\right|\right]^{\frac{2}{3}}. \tag{2.181}$$

When the observation point is in the deep dark side of the smooth caustic, $\gamma_s \gg 1$ and using the large positive argument form of the ordinary Airy function, $\mathcal{R}_{s,h}^c \to R_{s,h}^c = \mp 1$ which is the complex GO reflection coefficient for a PEC boundary.

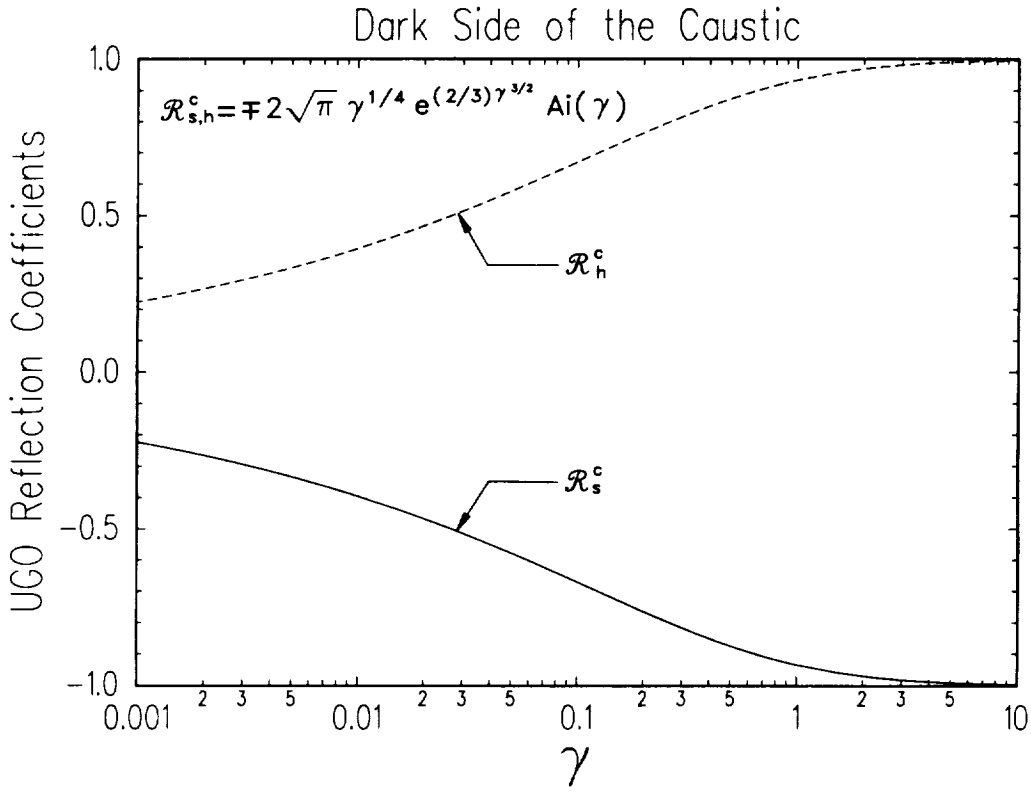

Figure 2.9: Plot of the scalar UGO complex ray reflection coefficients.

2.2.3 EUTD expression for the edge diffracted field

The EUTD expression for the edge diffracted field is as follows:

$$\vec{E}^d(P) \sim \vec{E}^i(Q_a) \cdot \bar{\bar{\mathcal{D}}}\,(Q_a) \frac{e^{-jks_a^d}}{\sqrt{s_a^d}}\,, \tag{2.182}$$

where $\bar{\bar{\mathcal{D}}}\,(Q_a)$ is the EUTD dyadic edge diffraction coefficient given by

$$\bar{\bar{\mathcal{D}}}\,(Q_a) = \mathcal{D}_s(\varphi_a', \varphi_a)\,\hat{e}_\perp \hat{e}_\perp + \mathcal{D}_h(\varphi_a', \varphi_a)\,\hat{e}_\parallel^i \hat{e}_\parallel^d\,, \tag{2.183}$$

$$\mathcal{D}_{s,h}(\varphi_a', \varphi_a) = \frac{-e^{-j\frac{\pi}{4}}}{2\sqrt{2\pi k}} \left[\frac{1}{\cos\left(\frac{\varphi_a' - \varphi_a}{2}\right)} \mp \frac{1}{\cos\left(\frac{\varphi_a' + \varphi_a}{2}\right)} \right] \mathcal{F}(\gamma_a, \zeta_a)\,. \tag{2.184}$$

$\mathcal{F}(\gamma_a, \zeta_a)$ is the EUTD transition function given by

$$\mathcal{F}(\gamma, \zeta) = j\,(\gamma + \zeta^2)\; \mathrm{g}_i^*(\gamma, \zeta)\, e^{j(\gamma\zeta + \zeta^3/3)}\,, \tag{2.185}$$

$$i = \left\{ \begin{array}{ll} 1 & \text{if } \zeta > (-\gamma)^{1/2} \\ 2 & \text{if } \zeta < -(-\gamma)^{1/2} \\ 3 & \text{otherwise} \end{array} \right\};\ \text{for } \gamma < 0, \text{ or}$$

$$i = \left\{ \begin{array}{ll} 1 & \text{if } \zeta > 0 \\ 2 & \text{if } \zeta < 0 \end{array} \right\};\ \text{for } \gamma > 0.$$

The parameters γ_a and ζ_a are given by the following expressions:

$$\gamma_a \approx -u_a\, k^{2/3} \frac{(\cos\varphi_0' + \cos\varphi_0)}{|L_d(\varphi_a', \varphi_a)|^{1/3}}\,, \tag{2.186}$$

$$u_a = \mathrm{sgn}[L_d(\varphi_a', \varphi_a)]\,, \tag{2.187}$$

$$\zeta_a \approx u_0 k^{1/3} \frac{\sqrt{|\cos\varphi_0' + \cos\varphi_0 - \cos\varphi_a' - \cos\varphi_a|}}{|L_d(\varphi_a', \varphi_a)|^{1/6}}\,, \tag{2.188}$$

$$u_0 = \left\{ \begin{array}{ll} +1 & \text{if } Q_0 \ni C \\ -1 & \text{if } Q_0 \in C, \end{array} \right. \tag{2.189}$$

where $L_d(\varphi_a', \varphi_a)$ is the EUTD distance parameter and is given by

$$\begin{aligned} L_d(\varphi_a', \varphi_a) = {} & \frac{1}{2}(\sin\varphi_a' + \sin\varphi_a)\kappa_g'(Q_a) + \frac{\cos\varphi_a' + \cos\varphi_a}{2\rho_g^2(Q_a)} \\ & + \frac{3\sin\varphi_a' \cos\varphi_a'}{2s_a^i} \left[\frac{1}{\rho_g(Q_a)} + \frac{\sin\varphi_a'}{s_a^i} \right] \\ & + \frac{3\sin\varphi_a \cos\varphi_a}{2s_a^d} \left[\frac{1}{\rho_g(Q_a)} + \frac{\sin\varphi_a}{s_a^d} \right]. \end{aligned} \tag{2.190}$$

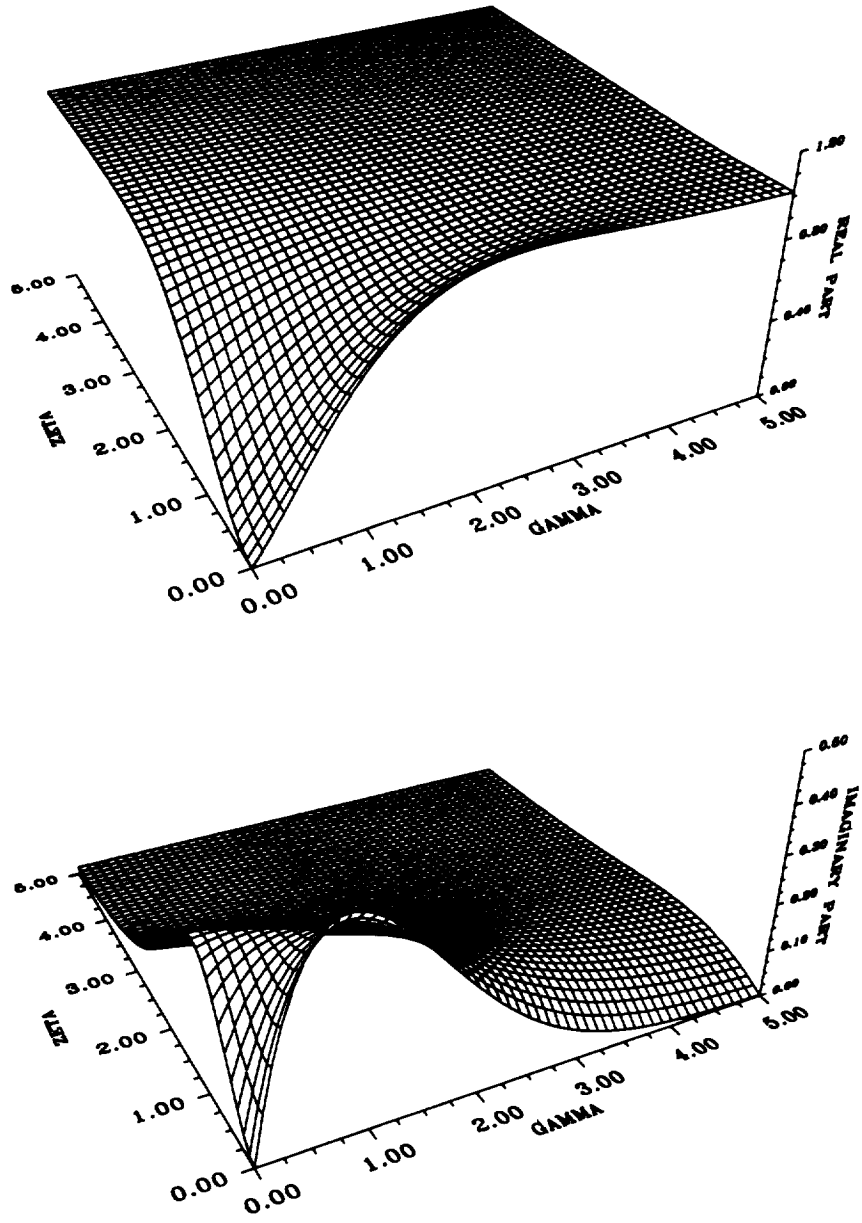

Figure 2.10: Plots of the real and imaginary parts of the EUTD transition function in the first quadrant of the $\gamma\zeta$–plane.

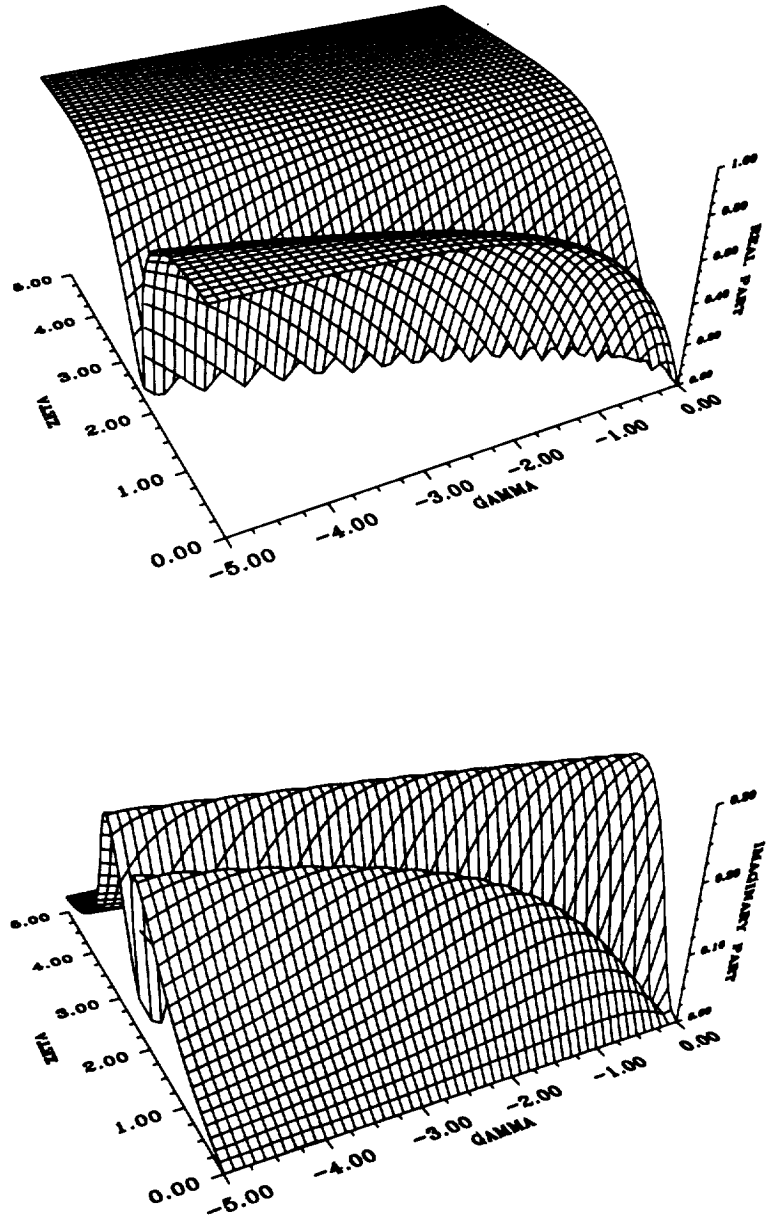

Figure 2.11: Plots of the real and imaginary parts of the EUTD transition function in the second quadrant of the $\gamma\zeta$–plane.

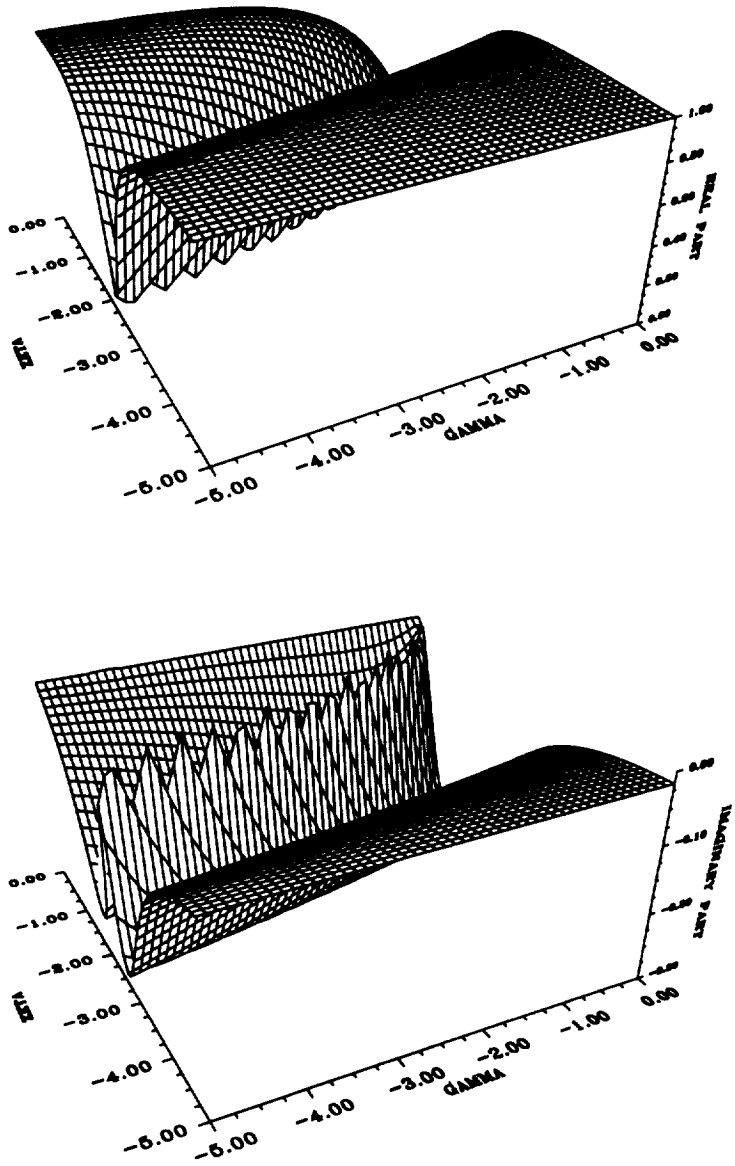

Figure 2.12: Plots of the real and imaginary parts of the EUTD transition function in the third quadrant of the $\gamma\zeta$–plane.

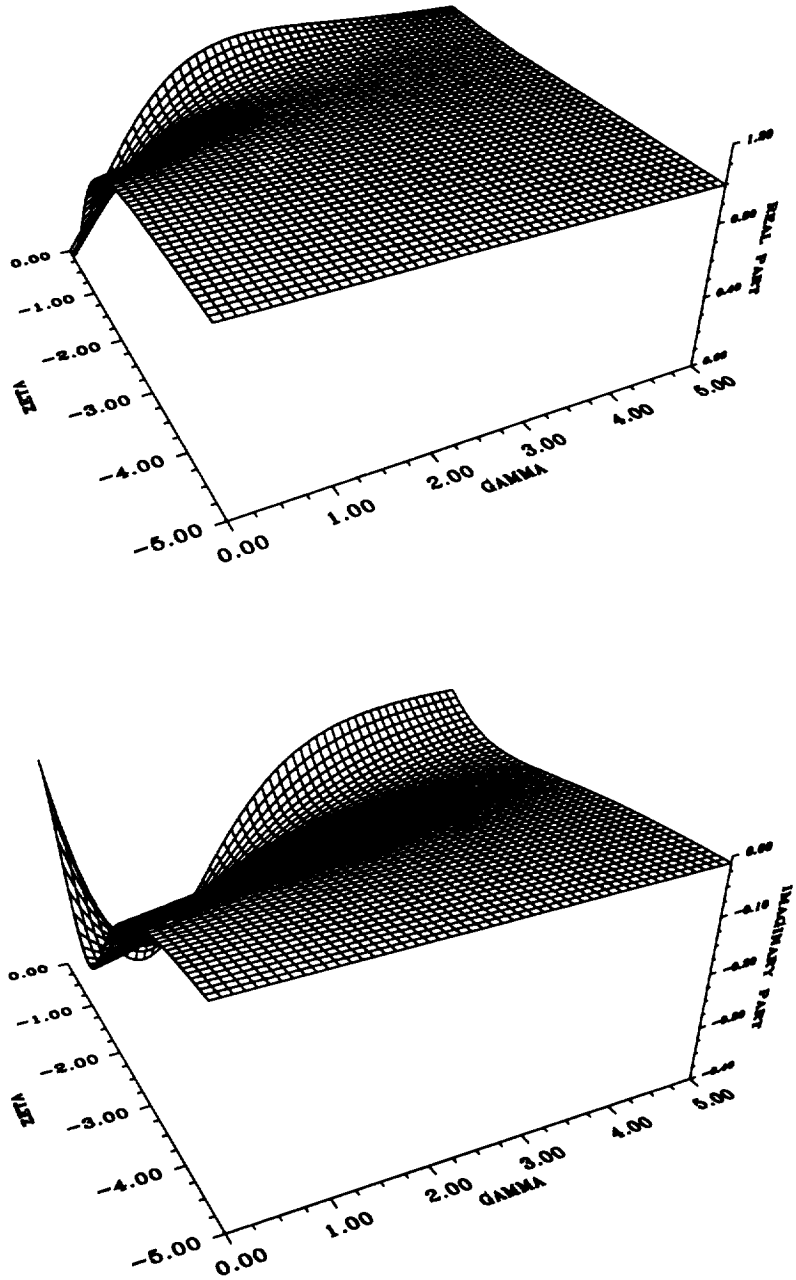

Figure 2.13: Plots of the real and imaginary parts of the EUTD transition function in the fourth quadrant of the $\gamma\zeta$–plane.

It is understood that when $L_a(\varphi_a', \varphi_a) < 0$, the EUTD transition function in (2.184) should be replaced by its complex conjugate version. Plots of the real and imaginary parts of the EUTD transition function in the four quadrants of the $\gamma\zeta$–plane appear in Figures 2.10- 2.13. One can observe that the EUTD transition function exhibits three lines of discontinuity. The first discontinuity occurs along the $\zeta = 0$ line which is the boundary between the first and fourth quadrants of the $\gamma\zeta$–plane, and physically corresponds to the CRSB. Figures 2.10 and 2.13 show that only the imaginary part of the transition function is discontinuous across the CRSB while the real part remains continuous. Also, as $\gamma \gg 1$ the discontinuity diminishes. This transition function behavior makes sense physically since $\gamma \gg 1$ corresponds to the deep dark side of the smooth caustic where the complex ray field becomes vanishingly small and accordingly its discontinuity across the CRSB should also diminish. The second discontinuity of the transition function occurs along the $\zeta = (-\gamma)^{1/2}$ line in the second quadrant of the $\gamma\zeta$–plane as shown in Figure 2.11. This line physically corresponds to the ISB. Finally, the third discontinuity of the transition function occurs along the $\zeta = -(-\gamma)^{1/2}$ line in the third quadrant of the $\gamma\zeta$–plane as shown in Figure 2.12. This line physically corresponds to the RSB.

Next, the behavior of the EUTD transition function for observation points in the deep lit side of the smooth caustic will be examined, so that a comparison between the EUTD edge diffraction coefficient and the original UTD expression [4] can be made. In this case the EUTD transition function assumes the following form:

$$\mathcal{F}(\gamma_a, \zeta_a) \sim (\gamma_a + \zeta_a^2)\left[\frac{F(\eta^2) - 1}{2\eta(-\gamma_a)^{1/4}}\right] + 1\,, \tag{2.191}$$

where the parameter η is given in Equation (2.122). When the observation point is away from the optical boundaries, $|\eta| \gg 1$, the UTD transition function $F(\eta^2) \to 1$, and $\mathcal{F}(\gamma_a, \zeta_a) \to 1$. Hence, the EUTD edge diffraction coefficient assumes the exact expression outside the transition regions associated with the optical boundaries. When the observation point is near an optical boundary, we have that $\gamma_a + \zeta_a^2 \approx 2\eta(-\gamma_a)^{1/4}$ and therefore $\mathcal{F}(\gamma_a, \zeta_a) \approx F(\eta^2)$, with η reducing to the following expres-

sion:

$$\eta \approx -\frac{1}{2}(\cos\varphi'_a + \cos\varphi_a)\sqrt{\frac{2k}{|\Psi(\varphi'_a,\varphi_a)|}}, \tag{2.192}$$

$$\Psi(\varphi'_a,\varphi_a) = \frac{\sin\varphi'_a + \sin\varphi_a}{\rho_g(Q_a)} + \frac{\sin^2\varphi'_a}{s^i_a} + \frac{\sin^2\varphi_a}{s^d_a}. \tag{2.193}$$

Near the RSB, $\varphi_a \approx \pi - \varphi'_a$ and thus

$$\Psi(\varphi'_a,\varphi_a) \approx \left(\frac{1}{\rho^r_a} + \frac{1}{s^d_a}\right)\cos^2\left(\frac{\varphi'_a - \varphi_a}{2}\right), \text{ and} \tag{2.194}$$

$$\eta^2 \approx 2k\left(\frac{\rho^r_a s^d_a}{\rho^r_a + s^d_a}\right)\cos^2\left(\frac{\varphi'_a + \varphi_a}{2}\right) = kL^r a(\varphi'_a + \varphi_a). \tag{2.195}$$

Near the ISB, $\varphi_a \approx \pi + \varphi'_a$ and thus

$$\Psi(\varphi'_a,\varphi_a) \approx \left(\frac{1}{s^i_a} + \frac{1}{s^d_a}\right)\cos^2\left(\frac{\varphi'_a + \varphi_a}{2}\right), \text{ and} \tag{2.196}$$

$$\eta^2 \approx 2k\left(\frac{s^i_a s^d_a}{s^i_a + s^d_a}\right)\cos^2\left(\frac{\varphi'_a - \varphi_a}{2}\right) = kL^i a(\varphi'_a - \varphi_a), \tag{2.197}$$

where $L^{i,r}$ are the UTD distance parameters. Both $L^{i,r}$ and $a(\varphi' \pm \varphi)$ are defined in [4]. The above results indeed show that near the optical boundaries the EUTD transition function is identical to the UTD transition function. Therefore the two diffraction coefficients should give equivalent results despite the fact that the correction near the optical boundaries is applied differently in the two methods. In the UTD case, two transition functions with different arguments are used, one for each of the two terms in the non-uniform diffraction coefficient. In the EUTD case, only one transition function is used and operates on the entire non-uniform diffraction coefficient.

Chapter 3

Near-Zone Uniform Asymptotic Analysis and UGO/EUTD Formulation for the Scattered Fields near a Three Dimensional Smooth Caustic and Composite Shadow Boundary

In this chapter, the behavior of near-zone high frequency scattered EM fields near a three dimensional smooth caustic and composite shadow boundary is investigated, and a UGO/EUTD solution is developed for the description of the scattering mechanisms. The analysis for the 3–D case is very similar to the 2–D case of Chapter 2. The three dimensional surfaces considered in this chapter are assumed to be rotationally symmetric or slowly varying in the transverse direction, with the 2–D boundaries of Figures 1.1 and 1.2 being the generator curves representing one of the principal coordinate curves of the 3–D surface.

In order to further simplify the asymptotic analysis, it is also assumed that the plane of incidence defined by the incident ray direction and the normal to the surface at a real reflection point coincides with one of the principal coordinate curves of the surface. Although this is a very special case in a general scattering problem, the derivation of key expressions in the asymptotic analysis such as the reflected ray spread factors will be kept as general as possible. Because of the highly local nature

of high-frequency fields, the results for this special case will remain valid for general 3–D boundaries that are not necessarily rotationally symmetric with the plane of incidence not necessarily coinciding with one of the principal coordinate curves of the surface.

The PO approximation is also employed for the 3–D case. The problem formulation and the derivation of a uniform asymptotic solution that remains valid near a three dimensional smooth caustic and a composite shadow boundary is derived in Section 3.1 using the Chester expansion for the asymptotic reduction of the PO radiation integral. In Section 3.2 the method of steepest descent is employed for the asymptotic reduction of the PO radiation integral and the UGO/EUTD expressions for the reflected, complex ray, and edge diffracted fields are derived.

3.1 Derivation of a uniform asymptotic solution using the Chester expansion

The electric field $\vec{E}^s$ which is scattered by a 3–D surface containing an edge illuminated by a ray optical field due to a point source at P' and observed at a point P exterior to the surface as shown in Figure 3.1 can be expressed in terms of the usual radiation integral over the induced current $\vec{J}$ on the surface S as follows:

$$\vec{E}^s(P) \approx \frac{jkZ_0}{4\pi} \iint_S \left[\hat{R} \times \hat{R} \times \vec{J}(Q')\right] \frac{e^{-jkR}}{R} ds', \tag{3.1}$$

where Q' is any point on S, $\vec{R} = \overline{Q'P}$, $R = |\vec{R}|$, $\hat{R} = \vec{R}/R$, and P cannot be too close to S for (3.1) to be valid. As in the 2–D case, the PO approximation to (3.1) is employed using the GO currents of Equation (2.2), where $\hat{n}'$ is the outward unit normal vector to S at Q'. The incident magnetic field at Q' due to the point source at P' is expressed ray optically as follows:

$$\vec{H}^i(Q') \sim Z_0^{-1}\left(\hat{s}^i \times \vec{A}\right) \frac{e^{-jks^i}}{s^i}; \ \hat{s}^i \cdot \vec{A} = 0, \tag{3.2}$$

$$= Z_0^{-1}\hat{s}^i \times \vec{E}^i(Q'), \tag{3.3}$$

$$\vec{E}^i(Q') = \vec{A}(Q')\frac{e^{-jks^i}}{s^i}, \tag{3.4}$$

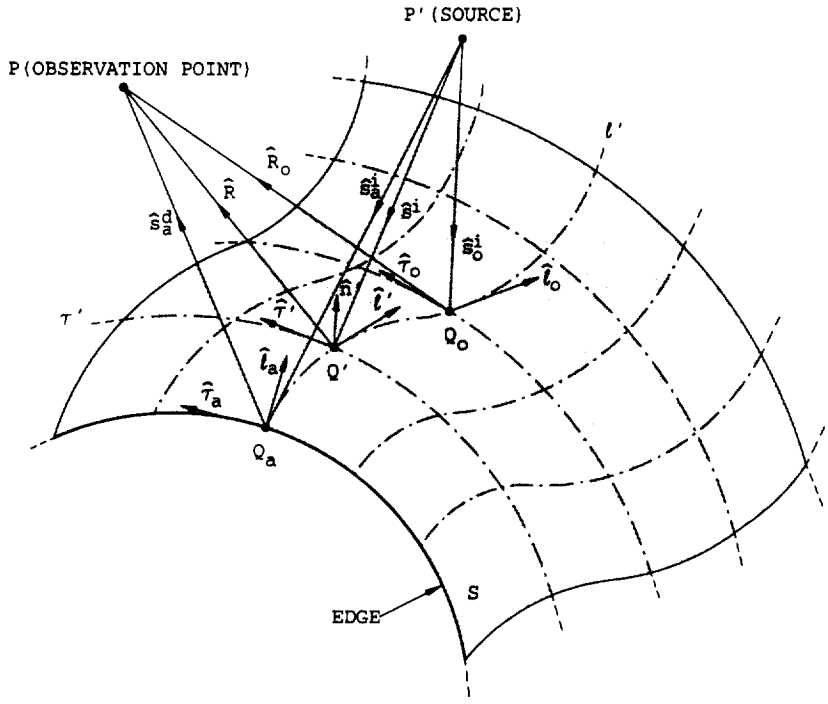

Figure 3.1: A smoothly indented three dimensional surface containing an edge.

where $\vec{A}$ is the vector source pattern, $\vec{s}^i = \overline{P'Q'}$, $s^i = |\vec{s}^i|$, and $\hat{s}^i = \vec{s}^i/s^i$. Thus, using the PO approximation Equation (3.1) is given by the following stationary phase integral:

$$\vec{E}^s(P) \approx \int_{\ell_a}^{\infty}\int_{-\infty}^{\infty} \vec{F}(\ell',\tau')\, e^{-jk\phi(\ell',\tau')}\, d\ell' d\tau' , \tag{3.5}$$

where

$$\vec{F}(\ell',\tau') = \frac{jk}{2\pi} \frac{\hat{R}\times\hat{R}\times\left[\hat{n}'\times\hat{s}^i\times\vec{A}(\ell',\tau')\right]}{s^i R} , \tag{3.6}$$

$$\phi(\ell',\tau') = s^i(\ell',\tau') + R(\ell',\tau') , \tag{3.7}$$

and ℓ', τ' are the principal coordinate curves of the 3–D surface S as shown in Figure 3.1. It is also assumed in (3.5) that the edge is located at (ℓ_a,τ'), and therefore it extends along the principal coordinate curve τ' which is always orthogonal to ℓ' and assumed to have a slowly varying radius of curvature. In order to simplify the analysis, it is further assumed that the plane of incidence defined by the incident ray direction and the normal to the surface at the reflection point coincides with the principal coordinate curve ℓ' on the surface. Although this situation occurs only in special cases, it is chosen because it greatly simplifies the asymptotic reduction of (3.5). Nevertheless, due to the highly local nature of high frequency fields, the results for this special case can also be applied to general 3–D boundaries that are not necessarily rotationally symmetric and the plane of incidence does not necessarily coincide with one of the principal coordinate curves of the surface.

The phase function in (3.7) contains two real or complex stationary phase points corresponding to real or complex reflection points Q_1 and Q_2 on S that are arbitrarily close together or to an edge diffraction point Q_a as in the 2–D case of Chapter 2. The stationary phase condition is given by

$$\hat{\ell}'\cdot\nabla\phi(\ell',\tau') = 0 \text{ and } \hat{\tau}'\cdot\nabla\phi(\ell',\tau') = 0 , \tag{3.8}$$

where $\hat{\ell}'$, $\hat{\tau}'$ are the principal surface directions, and both equations in (3.8) must be satisfied simultaneously at the stationary points. With the assumption that the plane of incidence coincides with the principal coordinate curve ℓ', Equation (3.8) yields stationary phase points for which $\tau' = \tau$, along with $\ell' = \ell_1$ for Q_1 and $\ell' = \ell_2$

for Q_2. Therefore, the coordinates of the stationary phase points are $Q_1 = (\ell_1, \tau_s)$ and $Q_2 = (\ell_2, \tau_s)$ with the edge diffraction point coordinate being $Q_a = (\ell_a, \tau_s)$. Then, using a local quadratic approximation, the phase function in (3.7) may be written as follows:

$$\phi(\ell', \tau') \simeq \phi(\ell', \tau_s) + (\tau' - \tau_s)\dot{\phi}_\tau(\ell', \tau_s) + \frac{1}{2}(\tau' - \tau_s)^2 \ddot{\phi}_{\tau\tau}(\ell', \tau_s)\,, \tag{3.9}$$

where the notation $\frac{\partial^2 \phi(x', y')}{\partial x' \partial y'} \triangleq \ddot{\phi}_{xy}(x', y')$ was used in (3.9). Upon inserting (3.9) in Equation (3.5) we get

$$\vec{E}^s(P) \approx \int_{\ell_a}^{\infty} d\ell'\, e^{-jk\psi(\ell', \tau_s)} \cdot \int_{-\infty}^{\infty} d\tau'\, \vec{F}(\ell', \tau')\, e^{-j\frac{k}{2}\ddot{\phi}_{\tau\tau}(\ell', \tau_s)[\tau' - \xi(\ell', \tau_s)]^2}\,, \tag{3.10}$$

where

$$\psi(\ell', \tau_s) = \phi(\ell', \tau_s) - \frac{\dot{\phi}_\tau^2(\ell', \tau_s)}{2\ddot{\phi}_{\tau\tau}(\ell', \tau_s)}\,, \tag{3.11}$$

$$\psi(\ell_{1,2}, \tau_s) = \phi(\ell_{1,2}, \tau_s)\,, \tag{3.12}$$

$$\xi(\ell', \tau_s) = \tau_s - \frac{\dot{\phi}_\tau(\ell', \tau_s)}{2\ddot{\phi}_{\tau\tau}(\ell', \tau_s)}\,. \tag{3.13}$$

When the plane of incidence coincides with the principal coordinate curve ℓ', $\dot{\phi}_\tau(\ell', \tau_s) = 0$, $\forall\ \ell'$, and thus $\psi(\ell', \tau_s) = \phi(\ell', \tau_s)$ and $\xi(\ell', \tau_s) = \tau_s$, $\forall\ \ell'$. However, we will keep all expressions as general as possible since we would like our results to remain valid for an arbitrary plane of incidence, in which case $\dot{\phi}_\tau(\ell', \tau_s) = 0$ only when $\ell' = \ell_{1,2}$ from the stationary phase condition. It is also assumed in (3.11) and (3.13) that $\ddot{\phi}_{\tau\tau}(\ell', \tau_s) \neq 0\ \forall\ \ell'$. An additional necessary condition is the matching of the phase function when one or both reflection points coincide with the edge diffraction point, that is

$$\psi(\ell_a, \tau_s) = \psi(\ell_{1,2}, \tau_s)\,. \tag{3.14}$$

From (3.11) Equation (3.14) is satisfied only if $\dot{\phi}_\tau(\ell_a, \tau_s) = 0$, and using (G.81) this edge condition can be expressed as follows:

$$(\hat{s}_a^d - \hat{s}_a^i) \cdot \hat{\tau}_a = 0\,, \tag{3.15}$$

where $\hat{\tau}_a$ is the unit edge tangent vector at Q_a. Equation (3.15) can be used to find Q_a and is recognized as Keller's *law of edge diffraction*. An additional consequence

of Equation (3.15) used in (3.13) is that

$$\xi(\ell_a, \tau_s) = \tau_s \,. \tag{3.16}$$

Next, the inner integral in (3.10) denoted as $\vec{I}_s(\ell', \tau_s)$ can be evaluated using the stationary phase method [8] which yields

$$\vec{I}_s(\ell', \tau_s) \sim \sqrt{\frac{2\pi}{jk}} \frac{\vec{F}(\ell', \xi)}{\sqrt{\left|\ddot{\phi}_{\tau\tau}(\ell', \tau_s)\right|}} \,. \tag{3.17}$$

Hence, employing (3.17) in (3.10) the 3–D analysis effectively reduces to a 2–D situation with $\vec{E}^s(P)$ given by

$$\vec{E}^s(P) \approx \int_{\ell_a}^{\infty} d\ell' \, \vec{G}(\ell', \tau_s) \, e^{-jk\psi(\ell', \tau_s)} \,, \tag{3.18}$$

where

$$\vec{G}(\ell', \tau_s) = \sqrt{\frac{jk}{2\pi}} \frac{\hat{R} \times \hat{R} \times \left[\hat{n}' \times \hat{s}^i \times \vec{A}(\ell', \xi)\right]}{s^i \, R \sqrt{\left|\ddot{\phi}_{\tau\tau}(\ell', \tau_s)\right|}} \,, \tag{3.19}$$

and the phase function $\psi(\ell', \tau_s)$ is given by Equation (3.11) and has stationary phase points at $\ell' = \ell_{1,2}$ corresponding to $Q_{1,2}$, that is $\dot{\psi}(\ell_{1,2}, \tau_s) = 0$. Therefore, the asymptotic reduction of the integral in (3.18) would follow the same steps as the asymptotic reduction of the integral in (2.7) for the 2–D case.

The phase function $\psi(\ell', \tau_s)$ is then expanded in a Taylor series around the point ℓ_0 which is a stationary point of the derivative of the phase function, that is $\ddot{\psi}(\ell_0, \tau_s) = 0$ and must necessarily lie between the two stationary phase points $\ell_{1,2}$. Thus, using a local cubic approximation, $\psi(\ell', \tau_s)$ may be written as follows:

$$\begin{aligned} \psi(\ell', \tau_s) \;\simeq\; & \psi(\ell_0, \tau_s) + (\ell' - \ell_0)\dot{\psi}(\ell_0, \tau_s) + \frac{(\ell' - \ell_0)^2}{2!}\ddot{\psi}(\ell_0, \tau_s) \\ & + \frac{(\ell' - \ell_0)^3}{3!} \dddot{\psi}\,(\ell_0, \tau_s) \,. \end{aligned} \tag{3.20}$$

A phase matching condition is also required at the caustic point Q_0 for the case when $\ell_{1,2} \to \ell_0$ corresponding to observation points at the smooth caustic; therefore we have

$$\psi(\ell_0, \tau_s) = \psi(\ell_{1,2}, \tau_s) \,, \tag{3.21}$$

which is satisfied only if $\dot{\phi}_\tau(\ell_0, \tau_s) = 0$ in Equation (3.11). Using Equation (G.19) this caustic condition can be expressed as follows:

$$\left(\hat{R}_0 - \hat{s}_0^i\right) \cdot \hat{\tau}_0 = 0\,. \tag{3.22}$$

Then, using Equations (3.11) and (3.22), $\psi(\ell_0, \tau_s)$ and its derivatives in (3.20) are given by:

$$\begin{aligned}
\psi(\ell_0, \tau_s) &= s_0^i + R_0\,, && (3.23)\\
\dot{\psi}(\ell_0, \tau_s) &= \phi_{10}(Q_0)\,, && (3.24)\\
\ddot{\psi}(\ell_0, \tau_s) &= \phi_{20}(Q_0) - \frac{\phi_{11}^2(Q_0)}{\phi_{02}(Q_0)} = 0\,, && (3.25)\\
\dddot{\psi}\,(\ell_0, \tau_s) &= \phi_{30}(Q_0) - \frac{\phi_{11}(Q_0)}{\phi_{02}(Q_0)}\left[3\phi_{21}(Q_0) - \frac{\phi_{11}(Q_0)\phi_{12}(Q_0)}{\phi_{02}(Q_0)}\right]\\
&= m(Q_0)\,, && (3.26)\\
\phi_{mn}(Q_0) &\triangleq \left.\frac{\partial^{m+n}\phi(\ell', \tau')}{\partial \ell'^m \partial \tau'^n}\right|_{(\ell_0, \tau_s)}\,. && (3.27)
\end{aligned}$$

Using (G.18), (G.19), (G.35)–(G.37), and (G.59)–(G.62) the derivative functions ϕ_{10}, ϕ_{20}, ϕ_{11}, ϕ_{02}, ϕ_{30}, ϕ_{21}, and ϕ_{12} at $Q_0 = (\ell_0, \tau_s)$ can be expressed in terms of the geometric parameters of the surface S at Q_0, that is

$$\begin{aligned}
\phi_{10}(Q_0) &= \left(\hat{s}_0^i - \hat{R}_0\right) \cdot \hat{\ell}_0\,, && (3.28)\\
\phi_{20}(Q_0) &= \kappa_1(Q_0)\left(\hat{R}_0 - \hat{s}_0^i\right) \cdot \hat{n}_0 + \frac{1 - \left(\hat{s}_0^i \cdot \hat{\ell}_0\right)^2}{s_0^i} + \frac{1 - \left(\hat{R}_0 \cdot \hat{\ell}_0\right)^2}{R_0}\,, && (3.29)\\
\phi_{11}(Q_0) &= -\frac{\left(\hat{s}_0^i \cdot \hat{\ell}_0\right)\left(\hat{s}_0^i \cdot \hat{\tau}_0\right)}{s_0^i} - \frac{\left(\hat{R}_0 \cdot \hat{\ell}_0\right)\left(\hat{R}_0 \cdot \hat{\tau}_0\right)}{R_0}\,, && (3.30)\\
\phi_{02}(Q_0) &= \kappa_2(Q_0)\left(\hat{R}_0 - \hat{s}_0^i\right) \cdot \hat{n}_0 + \frac{1 - \left(\hat{s}_0^i \cdot \hat{\tau}_0\right)^2}{s_0^i} + \frac{1 - \left(\hat{R}_0 \cdot \hat{\tau}_0\right)^2}{R_0}\,, && (3.31)\\
\phi_{30}(Q_0) &= \left(\hat{R}_0 - \hat{s}_0^i\right) \cdot \left\{\kappa_1^2(Q_0)\hat{\ell}_0 + \left[\hat{\ell}_0 \cdot \nabla\kappa_1(Q_0)\right]\hat{n}_0\right\}\\
&\quad + \frac{\hat{s}_0^i \cdot \hat{\ell}_0}{s_0^i}\left[3\kappa_1(Q_0)\left(\hat{s}_0^i \cdot \hat{n}_0\right) - \frac{1 - \left(\hat{s}_0^i \cdot \hat{\ell}_0\right)^2}{s_0^i}\right]\\
&\quad + \frac{\hat{R}_0 \cdot \hat{\ell}_0}{R_0}\left[3\kappa_1(Q_0)\left(\hat{R}_0 \cdot \hat{n}_0\right) + \frac{1 - \left(\hat{R}_0 \cdot \hat{\ell}_0\right)^2}{R_0}\right]\,, && (3.32)\\
\phi_{21}(Q_0) &= \frac{\hat{s}_0^i \cdot \hat{\tau}_0}{s_0^i}\left[\kappa_1(Q_0)\left(\hat{s}_0^i \cdot \hat{n}_0\right) - \frac{1 - 3\left(\hat{s}_0^i \cdot \hat{\ell}_0\right)^2}{s_0^i}\right]
\end{aligned}$$

$$+ \quad \frac{\hat{R}_0 \cdot \hat{\tau}_0}{R_0}\left[\kappa_1(Q_0)\left(\hat{R}_0 \cdot \hat{n}_0\right) + \frac{1-3\left(\hat{R}_0 \cdot \hat{\ell}_0\right)^2}{R_0}\right], \tag{3.33}$$

$$\phi_{12}(Q_0) = \frac{\hat{s}_0^i \cdot \hat{\ell}_0}{s_0^i}\left[\kappa_2(Q_0)\left(\hat{s}_0^i \cdot \hat{n}_0\right) - \frac{1-3\left(\hat{s}_0^i \cdot \hat{\tau}_0\right)^2}{s_0^i}\right]$$

$$+ \quad \frac{\hat{R}_0 \cdot \hat{\ell}_0}{R_0}\left[\kappa_2(Q_0)\left(\hat{R}_0 \cdot \hat{n}_0\right) + \frac{1-3\left(\hat{R}_0 \cdot \hat{\tau}_0\right)^2}{R_0}\right], \tag{3.34}$$

where $\hat{\ell}_0$, $\hat{\tau}_0$ are the principal surface directions at Q_0, $\hat{n}_0$ is the outward unit normal at Q_0, and $\kappa_{1,2}(Q_0) = 1/R_{1,2}(Q_0)$ are the principal surface curvatures at Q_0 along the $\hat{\ell}_0$ and $\hat{\tau}_0$ directions, respectively. The caustic point Q_0 is therefore found from Equations (3.25) and (3.29)–(3.31), that is

$$\phi_{20}(Q_0)\phi_{02}(Q_0) - \phi_{11}^2(Q_0) = 0\,, \tag{3.35}$$

and must satisfy the caustic condition in (3.22). Notice that in the case of plane wave incidence with observation in the far-zone of S, that is s_0^i, $R_0 \to \infty$, Q_0 is a stationary point on a zero curvature line and satisfies $\kappa_1(Q_0) = 0$ along with (3.22). Also worth noting is the fact that when the plane of incidence coincides with one of the principal surface directions, the cross-derivative functions $\phi_{11}(Q_0)$ and either $\phi_{21}(Q_0)$ or $\phi_{12}(Q_0)$ reduce to zero. This is also true for the plane wave far-zone scattering problem where all three cross-derivative functions reduce to zero for any arbitrary plane of incidence.

Next, making the usual linear transformation, the stationary phase integral of Equation (3.18) transforms to the following expression:

$$\vec{E}^s(P) \approx e^{-jk\alpha} \int_{s_a}^{\text{"}\infty\text{"}} \vec{\mathcal{G}}(s) e^{-jk(\beta s + s^3/3)}\, ds\,, \tag{3.36}$$

where

$$\alpha = s_0^i + R_0\,, \text{ or} \tag{3.37}$$

$$= \frac{1}{2}\left[\left(s_1^i + s_1^r\right) + \left(s_2^i + s_2^r\right)\right], \text{ or} \tag{3.38}$$

$$= s_{1,2}^i + s_{1,2}^r \pm \frac{2}{3}(-\beta)^{3/2}, \text{ or} \tag{3.39}$$

$$= s_a^i + s_a^d - \beta s_a - s_a^3/3\,, \tag{3.40}$$

$$\beta = \hat{\ell}_0 \cdot (\hat{s}_0^i - \hat{R}_0) \left[\frac{2}{m(Q_0)}\right]^{\frac{1}{3}}, \text{ or} \tag{3.41}$$

$$= -\left\{\frac{3}{4}\left[(s_2^i + s_2^r) - (s_1^i + s_1^r)\right]\right\}^{2/3}, \text{ or} \tag{3.42}$$

$$= -\left\{\frac{3}{2}\left[(s_0^i + R_0) - (s_{1,2}^i + s_{1,2}^r)\right]\right\}^{2/3}, \tag{3.43}$$

$$s_a = \pm\sqrt{\hat{\ell}_a \cdot (\hat{s}_a^i - \hat{s}_a^d) - \hat{\ell}_0 \cdot (\hat{s}_0^i - \hat{R}_0)} \left[\frac{2}{m(Q_0)}\right]^{\frac{1}{6}}; \begin{cases} + \text{ if } Q_0 \ni S \\ - \text{ if } Q_0 \in S, \end{cases} \tag{3.44}$$

$$\vec{G}(s) = \vec{G}(\ell', \tau_s)\frac{d\ell'}{ds}, \tag{3.45}$$

$$\frac{d\ell'}{ds} = \left[\frac{2}{m(Q_0)}\right]^{\frac{1}{3}}, \tag{3.46}$$

and the proper branches for β, s_a, and $d\ell'/ds$ depend on the sign of $m(Q_0)$ given in (3.26). Also, "∞" $= \infty \exp[-j\arg(d\ell'/ds)]$. The asymptotic evaluation of (3.36) is then carried out by employing Chester's expansion [7], and following the same steps as in the 2–D case of Chapter 2 the scattered electric field is given by

$$\vec{E}^s(P) \sim \frac{e^{-jk\alpha}}{\sqrt{k}}\left[\vec{a}_0 \overline{\mathrm{Ai}}^*(\gamma, \zeta_a) + j\vec{b}_0 \frac{\partial}{\partial\gamma}\overline{\mathrm{Ai}}^*(\gamma, \zeta_a)\right]$$
$$+ e^{-jk\psi(\ell_a, \tau_s)}\left[\frac{\vec{G}(\ell_a, \tau_s)}{jk\dot{\psi}(\ell_a, \tau_s)} + \frac{j\left(\vec{a}_0 + \zeta_a\vec{b}_0\right)}{\sqrt{k}\,(\gamma + \zeta_a^2)}\right] \text{ if } m(Q_0) > 0, \tag{3.47}$$

$$\vec{E}^s(P) \sim \frac{e^{-jk\alpha}}{\sqrt{k}}\left[\vec{a}_0 \overline{\mathrm{Ai}}(\gamma, \zeta_a) - j\vec{b}_0 \frac{\partial}{\partial\gamma}\overline{\mathrm{Ai}}(\gamma, \zeta_a)\right]$$
$$+ e^{-jk\psi(\ell_a, \tau_s)}\left[\frac{\vec{G}(\ell_a, \tau_s)}{jk\dot{\psi}(\ell_a, \tau_s)} - \frac{j\left(\vec{a}_0 + \zeta_a\vec{b}_0\right)}{\sqrt{k}\,(\gamma + \zeta_a^2)}\right] \text{ if } m(Q_0) < 0, \tag{3.48}$$

where $\overline{\mathrm{Ai}}(\gamma, \zeta_a)$ is the incomplete Airy integral defined in (2.48), $\gamma = k^{2/3}\beta$, $\zeta_a = k^{1/3}s_a$, and α, $\vec{a}_0$, and $\vec{b}_0$ are given by the following expressions:

$$\alpha = s_a^i + s_a^d - \delta k^{-1}\left(\gamma\zeta_a + \zeta_a^3/3\right), \text{ or} \tag{3.49}$$

$$= s_{1,2}^i + s_{1,2}^r \pm \delta k^{-1}\frac{2}{3}(-\gamma)^{3/2}, \tag{3.50}$$

$$\delta = \mathrm{sgn}[m(Q_0)], \tag{3.51}$$

$$\begin{Bmatrix} \vec{a}_0 \\ \vec{b}_0 \end{Bmatrix} = \frac{(-\gamma)^{\pm\frac{1}{4}}}{2}\left[\vec{G}(\ell_1, \tau_s)\sqrt{\frac{2}{|\ddot{\psi}(\ell_1, \tau_s)|}} \pm \vec{G}(\ell_2, \tau_s)\sqrt{\frac{2}{|\ddot{\psi}(\ell_2, \tau_s)|}}\right]. \tag{3.52}$$

From Equations (3.13) and (3.19), $\vec{G}(\ell_{1,2},\tau_s)$ may be written as follows:

$$\vec{G}(\ell_{1,2},\tau_s) = \sqrt{\frac{jk}{2\pi}}\,\frac{\cos\theta^i_{1,2}\,\vec{A}(Q_{1,2})\cdot\bar{\bar{R}}\,(Q_{1,2})}{s^i_{1,2}\,s^r_{1,2}\sqrt{\left|\ddot{\phi}_{\tau\tau}(\ell_{1,2},\tau_s)\right|}}\,, \tag{3.53}$$

where $\bar{\bar{R}}\,(Q_{1,2})$ is the dyadic GO reflection coefficient given by

$$\bar{\bar{R}}\,(Q_{1,2}) = R_s\hat{e}^i_\perp(Q_{1,2})\hat{e}^r_\perp(Q_{1,2}) + R_h\hat{e}^i_\parallel(Q_{1,2})\hat{e}^r_\parallel(Q_{1,2})\,, \tag{3.54}$$

$$R_{s,h} = \mp 1\,;\ \text{for a perfectly conducting boundary.} \tag{3.55}$$

From Equation (3.11), $\ddot{\psi}(\ell_{1,2},\tau_s)$ is given by

$$\ddot{\psi}(\ell_{1,2},\tau_s) = \frac{\ddot{\phi}_{\ell\ell}(\ell_{1,2},\tau_s)\ddot{\phi}_{\tau\tau}(\ell_{1,2},\tau_s) - \ddot{\phi}^2_{\ell\tau}(\ell_{1,2},\tau_s)}{\ddot{\phi}_{\tau\tau}(\ell_{1,2},\tau_s)}\,. \tag{3.56}$$

Using Equation (G.69), (3.56) can be written as follows:

$$\ddot{\psi}(\ell_{1,2},\tau_s) = \frac{\cos^2\theta^i_{1,2}}{\ddot{\phi}_{\tau\tau}(\ell_{1,2},\tau_s)}\left(\frac{1}{s^r_{1,2}}+\frac{1}{\rho^r_{\ell 1,\ell 2}}\right)\left(\frac{1}{s^r_{1,2}}+\frac{1}{\rho^r_{\tau 1,\tau 2}}\right)\,, \tag{3.57}$$

where $\rho^r_{\ell,\tau}$ are the radii of curvature of the reflected wavefront given in (G.70) or (G.71), and $\theta^i_{1,2}$ is the usual angle of incidence (between the incident ray and the outward normal of S at $Q_{1,2}$). Thus, using (3.53) and (3.57) $\vec{a}_0$ and $\vec{b}_0$ may be written as follows:

$$\begin{Bmatrix}\vec{a}_0\\ \vec{b}_0\end{Bmatrix} = \frac{\sqrt{k}\,e^{j\frac{\pi}{4}}(-\gamma)^{\pm\frac{1}{4}}}{2\sqrt{\pi}}\left[\frac{\vec{A}(Q_1)\cdot\bar{\bar{R}}\,(Q_1)}{s^i_1}\left|\sqrt{\frac{\rho^r_{\ell 1}\,\rho^r_{\tau 1}}{(\rho^r_{\ell 1}+s^r_1)(\rho^r_{\tau 1}+s^r_1)}}\right|\right.$$
$$\left. \pm\ \frac{\vec{A}(Q_2)\cdot\bar{\bar{R}}\,(Q_2)}{s^i_2}\left|\sqrt{\frac{\rho^r_{\ell 2}\,\rho^r_{\tau 2}}{(\rho^r_{\ell 2}+s^r_2)(\rho^r_{\tau 2}+s^r_2)}}\right|\right]\,. \tag{3.58}$$

Also, from Equations (3.11), (3.15), (3.16), (G.18), (G.20), (G.82), and (G.83) we have that

$$\psi(\ell_a,\tau_s) = s^i_a + s^d_a\,, \tag{3.59}$$

$$\dot{\psi}(\ell_a,\tau_s) = (\hat{s}^i_a - \hat{s}^d_a)\cdot\hat{\ell}_a = -\sin\vartheta_a\,(\cos\varphi'_a + \cos\varphi_a)\,, \tag{3.60}$$

$$\vec{G}(\ell_a,\tau_s) = \sqrt{\frac{jk}{2\pi}}\,\frac{\vec{A}(Q_a)\cdot\left[(\hat{n}_a\cdot\hat{s}^i_a)\hat{e}^i_\perp\hat{e}^d_\perp + (\hat{n}_a\cdot\hat{s}^d_a)\hat{e}^i_\parallel\hat{e}^d_\parallel\right]}{s^i_a\,s^d_a\sqrt{\left|\ddot{\phi}_{\tau\tau}(\ell_a,\tau_s)\right|}}\,, \tag{3.61}$$

$$\hat{n}_a\cdot\hat{s}^i_a = -\sin\vartheta_a\sin\varphi'_a\,, \tag{3.62}$$

$$\hat{n}_a \cdot \hat{s}_a^d = \sin\vartheta_a \sin\varphi_a , \tag{3.63}$$

$$\ddot{\phi}_{\tau\tau}(\ell_a, \tau_s) = \sin^2\vartheta_a \left(\frac{1}{s_a^d} + \frac{1}{\rho_a^d}\right) , \tag{3.64}$$

$$\frac{1}{\rho_a^d} = \frac{1}{s_a^i} + \frac{\hat{n}_a \cdot (\hat{s}_a^d - \hat{s}_a^i)}{R_a \sin^2\vartheta_a} , \tag{3.65}$$

where ϑ_a is the angle of diffraction as shown in Figure G.3, φ_a' and φ_a are the angles between $\hat{\ell}_a$ and the projected incident and diffracted ray directions in the plane perpendicular to $\hat{\tau}_a$ as shown in Figure G.4, $\hat{e}_\perp^{i,d}$ and $\hat{e}_\parallel^{i,d}$ are the unit vectors fixed in the incident and diffracted rays as shown in Figure G.3, ρ_a^d is the distance between the caustic at Q_a and the second caustic of the diffracted ray, and $R_a > 0$ is the radius of curvature of the edge at Q_a.

Finally, using (3.59)–(3.64) the scattered electric field is given by

$$\begin{aligned}
\vec{E}^s(P) \sim\ & \frac{e^{-jks}}{\sqrt{s}} \left[\vec{a}_0 \overline{\mathrm{Ai}}^*(\gamma, \zeta_a) + j\vec{b}_0 \frac{\partial}{\partial\gamma}\overline{\mathrm{Ai}}^*(\gamma, \zeta_a)\right] \\
&+ \left\{\vec{E}^i(Q_a) \cdot \bar{\bar{D}}_{nu}(Q_a) \sqrt{\frac{\rho_a^d}{s_a^d(\rho_a^d + s_a^d)}}\right. \\
&+ \left.\frac{j}{\sqrt{k}} e^{-jks_a^i} \left[\frac{\vec{a}_0 + \zeta_a \vec{b}_0}{\gamma + \zeta_a^2}\right]\right\} e^{-jks_a^d}, \quad \text{if } m(Q_0) > 0,
\end{aligned} \tag{3.66}$$

$$\begin{aligned}
\vec{E}^s(P) \sim\ & \frac{e^{-jks}}{\sqrt{s}} \left[\vec{a}_0 \overline{\mathrm{Ai}}(\gamma, \zeta_a) - j\vec{b}_0 \frac{\partial}{\partial\gamma}\overline{\mathrm{Ai}}(\gamma, \zeta_a)\right] \\
&+ \left\{\vec{E}^i(Q_a) \cdot \bar{\bar{D}}_{nu}(Q_a) \sqrt{\frac{\rho_a^d}{s_a^d(\rho_a^d + s_a^d)}}\right. \\
&- \left.\frac{j}{\sqrt{k}} e^{-jks_a^i} \left[\frac{\vec{a}_0 + \zeta_a \vec{b}_0}{\gamma + \zeta_a^2}\right]\right\} e^{-jks_a^d}, \quad \text{if } m(Q_0) < 0,
\end{aligned} \tag{3.67}$$

where $\bar{\bar{D}}_{nu}(Q_a)$ is the non-uniform PO dyadic edge diffraction coefficient for oblique incidence and is given by

$$\bar{\bar{D}}_{nu}(Q_a) = D_s(\varphi_a', \varphi_a; \vartheta_a)\, \hat{e}_\perp^i\, \hat{e}_\perp^d + D_h(\varphi_a', \varphi_a; \vartheta_a)\, \hat{e}_\parallel^i\, \hat{e}_\parallel^d , \tag{3.68}$$

$$D_{s,h}(\varphi_a', \varphi_a; \vartheta_a) = \pm \frac{e^{-j\frac{\pi}{4}}}{\sin\vartheta_a \sqrt{2\pi k}} \frac{\left\{\begin{array}{c}\sin\varphi_a' \\ \sin\varphi_a\end{array}\right\}}{(\cos\varphi_a' + \cos\varphi_a)} . \tag{3.69}$$

The reflected, complex ray, and edge diffracted field components in (3.66) and (3.67) can then be separated as usual using the properties and complex plane topology of the incomplete Airy integral in Appendix C.

3.1.1 Reflected field solution on the lit side of the caustic

From (3.66) and (3.67) and using the appropriate form of the incomplete Airy integral in Appendix C, the reflected field on the lit side of the caustic is given by

$$\begin{aligned}\vec{E}^r(P_L) \;\sim\; & \frac{e^{-j\frac{\pi}{4}}}{2}\Big\{u_1\, e^{-jka_1}\left[\vec{A}_\ell\,\gamma_\ell^{1/4}\,\mathrm{W}_1(-\gamma_\ell) - j\vec{B}_\ell\,\gamma_\ell^{-1/4}\,\mathrm{W}_1'(-\gamma_\ell)\right] \\ & - u_2\, e^{-jka_2}\left[\vec{A}_\ell\,\gamma_\ell^{1/4}\,\mathrm{W}_2(-\gamma_\ell) - j\vec{B}_\ell\,\gamma_\ell^{-1/4}\,\mathrm{W}_2'(-\gamma_\ell)\right]\Big\}\,, \qquad (3.70) \\ & \text{if}\quad m(Q_0) > 0\,, \\ \vec{E}^r(P_L) \;\sim\; & -\frac{e^{-j\frac{\pi}{4}}}{2}\Big\{u_1\, e^{-jka_1}\left[\vec{A}_\ell\,\gamma_\ell^{1/4}\,\mathrm{W}_1^*(-\gamma_\ell) + j\vec{B}_\ell\,\gamma_\ell^{-1/4}\,\mathrm{W}_1'^*(-\gamma_\ell)\right] \\ & - u_2\, e^{-jka_2}\left[\vec{A}_\ell\,\gamma_\ell^{1/4}\,\mathrm{W}_2^*(-\gamma_\ell) + j\vec{B}_\ell\,\gamma_\ell^{-1/4}\,\mathrm{W}_2'^*(-\gamma_\ell)\right]\Big\}\,, \qquad (3.71) \\ & \text{if}\quad m(Q_0) < 0\,,\end{aligned}$$

where $\mathrm{W}_{1,2}$ are the Fock-type Airy functions [16], $u_{1,2}$, γ_ℓ, and $\alpha_{1,2}$ are the same as in (2.84)–(2.86), and $\vec{A}_\ell$, $\vec{B}_\ell$ are given by

$$\begin{aligned}\left\{\begin{array}{c}\vec{A}_\ell \\ \vec{B}_\ell\end{array}\right\} \;=\; & \frac{\vec{A}(Q_1)\cdot\bar{\bar{R}}\,(Q_1)}{s_1^i}\left|\sqrt{\frac{\rho_{\ell 1}^r\,\rho_{\tau 1}^r}{(\rho_{\ell 1}^r+s_1^r)(\rho_{\tau 1}^r+s_1^r)}}\,\right| \\ & \pm\; \frac{\vec{A}(Q_2)\cdot\bar{\bar{R}}\,(Q_2)}{s_2^i}\left|\sqrt{\frac{\rho_{\ell 2}^r\,\rho_{\tau 2}^r}{(\rho_{\ell 2}^r+s_2^r)(\rho_{\tau 2}^r+s_2^r)}}\,\right|. \qquad (3.72)\end{aligned}$$

The first term in (3.70) and (3.71) is the uniform contribution from Q_1 where the second term in (3.70) and (3.71) is the uniform contribution from Q_2.

3.1.2 Complex ray field solution on the dark side of the caustic

From (3.66) and (3.67) and using the appropriate form of the incomplete Airy integral in Appendix C, the complex ray field on the dark side of the caustic is given by

$$\begin{aligned}\vec{E}^c(P_S) \;\sim\; & j\sqrt{\pi}\, e^{-jka_{1,2}^c}\left[\vec{A}_s\,\gamma_s^{1/4}\,\mathrm{Ai}(\gamma_s) \mp \vec{B}_s\,\gamma_s^{-1/4}\,\mathrm{Ai}'(\gamma_s)\right] u(-\zeta_a) \qquad (3.73) \\ & \text{for}\quad m(Q_0)\lesseqgtr 0\,,\end{aligned}$$

where $\mathrm{Ai}(\gamma_s)$ is the ordinary or Miller-type Airy function, γ_s and $\alpha_{1,2}^c$ are the same as in (2.98) and (2.99), and $\vec{A}_s$, $\vec{B}_s$ are given by

$$\left\{\begin{array}{c}\vec{A}_s \\ \vec{B}_s\end{array}\right\} \;=\; \frac{\vec{A}(Q_1^c)\cdot\bar{\bar{R}}\,(Q_1^c)}{s_1^{ic}}\left|\sqrt{\frac{\rho_{\ell 1}^{rc}\,\rho_{\tau 1}^{rc}}{(\rho_{\ell 1}^{rc}+s_1^{rc})(\rho_{\tau 1}^{rc}+s_1^{rc})}}\,\right|$$

$$\pm \frac{\vec{A}(Q_2^c)\cdot \bar{\bar{R}}\,(Q_2^c)}{s_2^{ic}} \left| \sqrt{\frac{\rho_{t2}^{rc}\,\rho_{\tau 2}^{rc}}{(\rho_{t2}^{rc}+s_2^{rc})(\rho_{\tau 2}^{rc}+s_2^{rc})}} \right| . \tag{3.74}$$

Although the values from both complex reflection points appear in (3.73), in the deep dark side of the caustic only the contribution from one of the complex reflection points is involved since the contribution from its complex conjugate counterpart violates the radiation condition and produces an unbounded result.

3.1.3 Edge diffracted field solution

The edge diffracted field is written as follows:

$$\vec{E}^d(P) = \vec{E}^d_{nu}(P) + \vec{E}^d_c(P)\,, \tag{3.75}$$

where $\vec{E}^d_{nu}(P)$ and $\vec{E}^d_c(P)$ are the non-uniform and curvature correction terms of the edge diffracted field, respectively. From (3.66) and (3.67) and using the appropriate expression for the incomplete Airy integral in Appendix C, they are given by the following expressions:

$$\vec{E}^d_{nu}(P) \sim \vec{E}^i(Q_a)\cdot \bar{\bar{D}}_{nu}\,(Q_a)\sqrt{\frac{\rho_a^d}{s_a^d(\rho_a^d+s_a^d)}}\, e^{-jks_a^d}\,, \tag{3.76}$$

$$\begin{aligned}\vec{E}^d_c(P) \sim\ & e^{-jk(s_a^i+s_a^d)}\left\{\vec{A}_d\left[e^{j(\gamma_a\zeta_a+\zeta_a^3/3)}\mathrm{g}_i^*(\gamma_a,\zeta_a)+\frac{j}{\gamma_a+\zeta_a^2}\right]\right.\\ &+\left. j\vec{B}_d\left[e^{j(\gamma_a\zeta_a+\zeta_a^3/3)}\frac{\partial}{\partial\gamma_a}\mathrm{g}_i^*(\gamma_a,\zeta_a)+\frac{\zeta_a}{\gamma_a+\zeta_a^2}\right]\right\}, \\ &\text{if}\quad m(Q_0)>0\,,\end{aligned} \tag{3.77}$$

$$\begin{aligned}\vec{E}^d_c(P) \sim\ & e^{-jk(s_a^i+s_a^d)}\left\{\vec{A}_d\left[e^{-j(\gamma_a\zeta_a+\zeta_a^3/3)}\mathrm{g}_i(\gamma_a,\zeta_a)-\frac{j}{\gamma_a+\zeta_a^2}\right]\right.\\ &-\left. j\vec{B}_d\left[e^{-j(\gamma_a\zeta_a+\zeta_a^3/3)}\frac{\partial}{\partial\gamma_a}\mathrm{g}_i(\gamma_a,\zeta_a)+\frac{\zeta_a}{\gamma_a+\zeta_a^2}\right]\right\}, \\ &\text{if}\quad m(Q_0)<0\,,\end{aligned} \tag{3.78}$$

$$i = \left\{\begin{array}{l} 1 \text{ if } \zeta_a > (-\gamma_a)^{1/2} \\ 2 \text{ if } \zeta_a < -(-\gamma_a)^{1/2} \\ 3 \text{ otherwise}\end{array}\right\} \text{ if } \gamma_a < 0, \text{ or} \tag{3.79}$$

$$i = \left\{\begin{array}{l} 1 \text{ if } \zeta_a > 0 \\ 2 \text{ if } \zeta_a < 0\end{array}\right\} \text{ if } \gamma_a > 0, \tag{3.80}$$

where γ_a, ζ_a, $\vec{A}_d$, and $\vec{B}_d$ are given by

$$\gamma_a = \delta k^{2/3} \hat{\ell}_0 \cdot \left(\hat{s}_0^i - \hat{R}_0 \right) \left| \frac{2}{m(Q_0)} \right|^{\frac{1}{3}}, \tag{3.81}$$

$$\zeta_a = u_0 k^{1/3} \left| \hat{\ell}_a \cdot (\hat{s}_a^i - \hat{s}_a^d) - \hat{\ell}_0 \cdot \left(\hat{s}_0^i - \hat{R}_0 \right) \right|^{1/2} \left| \frac{2}{m(Q_0)} \right|^{\frac{1}{6}}, \tag{3.82}$$

$$u_0 = \begin{cases} +1 & \text{if } Q_0 \ni S \\ -1 & \text{if } Q_0 \in S, \end{cases} \tag{3.83}$$

$$\begin{Bmatrix} \vec{A}_d \\ \vec{B}_d \end{Bmatrix} = \frac{e^{j\frac{\pi}{4}}}{2\sqrt{\pi}} \begin{Bmatrix} (-\gamma_a)^{1/4} \vec{A}_\ell \\ (-\gamma_a)^{-1/4} \vec{B}_\ell \end{Bmatrix} \quad \text{if } \gamma_a < 0, \tag{3.84}$$

$$= \frac{1}{2\sqrt{\pi}} \begin{Bmatrix} j\gamma_a^{1/4} \vec{A}_s \\ \gamma_a^{-1/4} \vec{B}_s \end{Bmatrix} \quad \text{if } \gamma_a > 0. \tag{3.85}$$

Notice that the curvature correction term of the edge diffracted field contains information about the reflection points through the vector quantities $\vec{A}_d$ and $\vec{B}_d$ given in (3.84) and (3.85) above. Also, $\bar{\bar{D}}_{nu}$ is given in (3.68) and (3.69), and James's correction factors [20] given in (2.117) and (2.118) can still be employed to improve the PO diffraction coefficient away from the optical boundaries.

3.2 Derivation of the UGO/EUTD solution using the method of steepest descent

In this section, the UGO/EUTD solution for the reflected, complex ray, and edge diffracted fields is formulated using the method of steepest descent for the asymptotic reduction of the PO radiation integral representation for the scattered field formulated in the previous section. We begin with the expression for the scattered field in (3.36), that is

$$\vec{E}^s(P) \approx e^{-jk\alpha} \vec{I}(\beta, s_a; k), \tag{3.86}$$

where α is given in (3.37)–(3.40) and $\vec{I}(\beta, s_a; k)$ is a stationary phase integral in the s–plane given by

$$\vec{I}(\beta, s_a; k) = \int_{s_a}^{\infty} \vec{\mathcal{G}}(s)\, e^{-jk(\beta s + s^3/3)}\, ds, \tag{3.87}$$

with β, s_a, and $\vec{\mathcal{G}}(s)$ given in (3.41)–(3.46). Only the case of $m(Q_0) > 0$ will be considered here since the results for $m(Q_0) < 0$ can be easily obtained by letting $\beta = \beta \exp(j2\pi/3)$ and $s_a = s_a \exp(j\pi/3)$ in (3.87). Then, using the same procedure as in section 2.2, that is deforming the original path of integration in (3.87) into the appropriate steepest descent paths through the endpoint s_a and the two real or complex saddle points $s_{1,2} = \pm(-\beta)^{1/2}$ as shown in Figures 2.6 and 2.7, and expanding the amplitude function $\vec{\mathcal{G}}(s)$ in Taylor series near each pertinent critical point, (3.87) may be written as follows:

$$\begin{aligned}
\vec{I}(\beta, s_a; k) &\simeq -j\sqrt{\pi}\, k^{-1/3}\, \vec{\mathcal{G}}(s_1)\, \mathrm{W}_1(k^{2/3}\beta)\, u(s_1 - s_a) \\
&+ j\sqrt{\pi}\, k^{-1/3}\, \vec{\mathcal{G}}(s_2)\, \mathrm{W}_2(k^{2/3}\beta)\, u(s_2 - s_a) \\
&+ k^{-1/3}\, \vec{\mathcal{G}}(s_a) \mathrm{g}_n^*(k^{2/3}\beta, k^{1/3}s_a) + O(k^{-1}) \quad \text{if } \beta < 0, \qquad (3.88)
\end{aligned}$$

$$n = \begin{cases} 1 \text{ if } s_a > s_1 \\ 2 \text{ if } s_a < s_2 \\ 3 \text{ if otherwise,} \end{cases} \qquad (3.89)$$

$$\begin{aligned}
\vec{I}(\beta, s_a; k) &\simeq 2\pi\, k^{-1/3}\, \vec{\mathcal{G}}(s_2)\, \mathrm{Ai}(k^{2/3}\beta)\, u(-s_a) \\
&+ k^{-1/3}\, \vec{\mathcal{G}}(s_a)\, \mathrm{g}_m^*(k^{2/3}\beta, k^{1/3}s_a) + O(k^{-1}) \quad \text{if } \beta > 0, \qquad (3.90)
\end{aligned}$$

$$m = \begin{cases} 1 \text{ if } s_a > 0 \\ 2 \text{ if } s_a < 0, \end{cases} \qquad (3.91)$$

where

$$\vec{\mathcal{G}}(s_{1,2}) = \vec{G}(\ell_{1,2}, \tau_s)(-\beta)^{1/4} \sqrt{\frac{\pm 2}{\ddot{\psi}(\ell_{1,2}, \tau_s)}}, \qquad (3.92)$$

$$\vec{\mathcal{G}}(s_a) = \frac{\vec{G}(\ell_a, \tau_s)}{\dot{\psi}(\ell_a, \tau_s)} (\beta + s_a^2), \qquad (3.93)$$

$$\vec{G}(\ell_{1,2}, \tau_s) = \sqrt{\frac{jk}{2\pi}} \frac{\cos\theta^i_{1,2} \vec{A}(Q_{1,2}) \cdot \bar{\bar{R}}\,(Q_{1,2})}{s^i_{1,2}\, s^r_{1,2} \sqrt{\ddot{\phi}_{\tau\tau}(\ell_{1,2}, \tau_s)}}, \qquad (3.94)$$

$$\ddot{\psi}(\ell_{1,2}, \tau_s) = \frac{\cos^2\theta^i_{1,2}}{\ddot{\phi}_{\tau\tau}(\ell_{1,2}, \tau_s)} \left(\frac{1}{s^r_{1,2}} + \frac{1}{\rho^r_{\ell 1, \ell 2}}\right) \left(\frac{1}{s^r_{1,2}} + \frac{1}{\rho^r_{\tau 1, \tau 2}}\right), \qquad (3.95)$$

$$\frac{\vec{G}(\ell_a, \tau_s)}{\dot{\psi}(\ell_a, \tau_s)} = \frac{jk\vec{A}(Q_a) \cdot \bar{\bar{D}}_{nu}\,(Q_a)}{s^i_a} \sqrt{\frac{\rho^d_a}{s^d_a\,(\rho^d_a + s^d_a)}}, \qquad (3.96)$$

with $\bar{\bar{D}}_{nu}(Q_a)$ given in (3.68) and (3.69). The first two terms in (3.88) are the uniform contributions from the real reflection points in the lit side of the smooth caustic, where the third term in (3.88) is the uniform edge diffracted field contribution in the lit side of the smooth caustic. The first term in (3.90) is the uniform contribution from the complex reflection point in the dark side of the smooth caustic, where the second term in (3.90) is the uniform edge diffracted field contribution in the dark side of the smooth caustic.

3.2.1 UGO expression for the reflected field

The UGO expression for the reflected field is as follows:

$$\begin{aligned}\vec{E}^r(P_L) \;\sim\; & u_1\,\vec{E}^i(Q_1)\cdot\bar{\bar{\mathcal{R}}}\,(Q_1)\sqrt{\frac{\rho^r_{\ell 1}\rho^r_{\tau 1}}{(\rho^r_{\ell 1}+s^r_1)(\rho^r_{\tau 1}+s^r_1)}}\,e^{-jks^r_1} \\ +\; & u_2\,\vec{E}^i(Q_2)\cdot\bar{\bar{\mathcal{R}}}^*(Q_2)\sqrt{\frac{\rho^r_{\ell 2}\rho^r_{\tau 2}}{(\rho^r_{\ell 2}+s^r_2)(\rho^r_{\tau 2}+s^r_2)}}\,e^{-jks^r_2}\,, \end{aligned} \tag{3.97}$$

where $u_1 = 1$ if $Q_1 \in S$ and zero otherwise, $u_2 = 1$ if $Q_2 \in S$ and zero otherwise, and $\rho^r_{\ell,\tau}$ are the radii of curvature of the reflected wavefront given in (G.70) or (G.71). The UGO dyadic reflection coefficient, $\bar{\bar{\mathcal{R}}}\,(Q_{1,2})$, is given by

$$\bar{\bar{\mathcal{R}}}\,(Q_{1,2}) = \mathcal{R}_s(Q_{1,2})\hat{e}^i_\perp\hat{e}^r_\perp + \mathcal{R}_h(Q_{1,2})\hat{e}^i_\parallel\hat{e}^r_\parallel\,, \tag{3.98}$$

where $\mathcal{R}_{s,h}(Q_{1,2})$ are given in (2.171)–(2.173). The caustic point Q_0 for the 3–D case is found from (3.22), (3.29)–(3.31) and (3.35), usually through a computer search procedure. In the case of plane wave incidence with the observer in the far-zone of S, Q_0 is simply an inflection or zero-curvature point satisfying $\kappa_1(Q_0) = 0$, where $\kappa_1(Q_0)$ is a principal surface curvature at Q_0. When the observer is in the deep lit side of the smooth caustic, $\mathcal{R}_{s,h} \to R_{s,h} = \mp 1$ and (3.97) becomes the usual GO expression for the reflected field. When the observation point lies on the smooth caustic, we have that $\rho^r_{\ell 1,\ell 2} = -s^r_{1,2}$ and the spread factors in (3.97) become singular. In this case the UGO scalar diffraction coefficients, $\mathcal{R}_{s,h}$, assume the following form:

$$\mathcal{R}_{s,h}(Q_{1,2}) = k^{\frac{1}{6}}R_{s,h}\,e^{-j\frac{\pi}{4}}\mathrm{W}_1(0)\;|m(Q_0)|^{-\frac{1}{3}}\sqrt{\frac{(\rho^r_{\ell 0}+s^r_0)(\rho^r_{\tau 0}+s^r_0)}{\rho^r_{\ell 0}\,\rho^r_{\tau 0}}}\,, \tag{3.99}$$

where $m(Q_0)$ is given in (3.26), and thus the singular spread factors are cancelled and the reflected field remains finite.

3.2.2 UGO expression for the complex ray field

The UGO expression for the complex ray field in the dark side of the caustic is as follows:

$$\vec{E}^c(P_S) \sim \vec{E}^i(Q^c_{1,2}) \cdot \bar{\bar{\mathcal{R}}}^c(Q^c_{1,2}) \sqrt{\frac{\rho^{rc}_{\ell 1,\ell 2}\, \rho^{rc}_{\tau 1,\tau 2}}{\left(\rho^{rc}_{\ell 1,\ell 2} + s^{rc}_{1,2}\right)\left(\rho^{rc}_{\tau 1,\tau 2} + s^{rc}_{1,2}\right)}}\, e^{-jks^{rc}_{1,2}}\,;\ m(Q_0) \lesseqgtr 0\,, \tag{3.100}$$

where $\rho^{rc}_{\ell,\tau}$ are the radii of curvature of the complex ray wavefront and are simply analytic continuations in complex space of the usual real ray wavefront radii of curvature, $\rho^{r}_{\ell,\tau}$, given in (G.70) or (G.71). The dyadic UGO complex ray reflection coefficient, $\bar{\bar{\mathcal{R}}}^c$ is given by

$$\bar{\bar{\mathcal{R}}}^c(Q^c_{1,2}) = \mathcal{R}^c_s\, \hat{e}^{ic}_{\perp} \hat{e}^{rc}_{\perp} + \mathcal{R}^c_h\, \hat{e}^{ic}_{\parallel} \hat{e}^{rc}_{\parallel}\,, \tag{3.101}$$

where $\mathcal{R}^c_{s,h}$ is given in (2.179)–(2.181). When the observer is in the deep dark side of the smooth caustic, $\mathcal{R}^c_{s,h}(Q^c_{1,2}) \to R^c_{s,h} = \mp 1$ and (3.100) reduces to the usual complex GO expression for the complex ray field.

3.2.3 EUTD expression for the edge diffracted field

The EUTD expression for the edge diffracted field is as follows:

$$\vec{E}^d(P) \sim \vec{E}^i(Q_a) \cdot \bar{\bar{\mathcal{D}}}\,(Q_a) \sqrt{\frac{\rho^d_a}{s^d_a\left(\rho^d_a + s^d_a\right)}}\, e^{-jks^d_a}, \tag{3.102}$$

where $\bar{\bar{\mathcal{D}}}\,(Q_a)$ is the EUTD dyadic edge diffraction coefficient given by

$$\bar{\bar{\mathcal{D}}}\,(Q_a) = \mathcal{D}_s(Q_a)\, \hat{e}^i_{\perp} \hat{e}^d_{\perp} + \mathcal{D}_h(Q_a)\, \hat{e}^i_{\parallel} \hat{e}^d_{\parallel}\,, \tag{3.103}$$

$$\mathcal{D}_{s,h}(Q_a) = \frac{-e^{-j\frac{\pi}{4}}}{2\sin\vartheta_a\sqrt{2\pi k}} \left[\frac{1}{\cos\left(\frac{\varphi'_a - \varphi_a}{2}\right)} \mp \frac{1}{\cos\left(\frac{\varphi'_a + \varphi_a}{2}\right)}\right] \mathcal{F}(\gamma_a, \zeta_a)\,. \tag{3.104}$$

$\mathcal{F}(\gamma_a, \zeta_a)$ is the EUTD transition function given in (2.185), φ'_a and φ_a are the angles between the projected incidence and observation directions on a plane perpendicular to $\hat{e}_a$ (unit tangent vector to the edge at Q_a) and $\hat{t}_a$ ($= \hat{e}_a \times \hat{n}_a$, $\hat{n}_a$ is the outward unit normal of S at Q_a), ϑ_a is the usual angle of diffraction, and ρ^d_a is the distance from the caustic at Q_a and the second caustic of the diffracted ray given by

$$\frac{1}{\rho^d_a} = \frac{1}{s^i_a} + \frac{\hat{n}_e \cdot \left(\hat{s}^d_a - \hat{s}^i_a\right)}{R_a \sin^2\vartheta_a}\,, \tag{3.105}$$

where $\hat{n}_e$ is the associated unit normal vector to the edge at Q_a directed away from the center of curvature (in general $\neq \hat{n}_a$), and $R_a > 0$ is the radius of curvature of the edge at Q_a. The parameters of the EUTD transition function γ_a and ζ_a for the 3–D case are given by the following expressions:

$$\gamma_a \approx -u_a\, k^{2/3}\, \frac{\sin\vartheta_0(\cos\varphi_0' + \cos\varphi_0)}{|L_d(\varphi_a', \varphi_a; \vartheta_a)|^{1/3}}, \tag{3.106}$$

$$u_a = \mathrm{sgn}[L_d(\varphi_a', \varphi_a; \vartheta_a)], \tag{3.107}$$

$$\zeta_a \approx u_0\, k^{1/3}\, \frac{|\sin\vartheta_0(\cos\varphi_0' + \cos\varphi_0) - \sin\vartheta_a(\cos\varphi_a' + \cos\varphi_a)|^{1/2}}{|L_d(\varphi_a', \varphi_a; \vartheta_a)|^{1/6}}, \tag{3.108}$$

$$u_0 = \begin{cases} +1 \text{ if } Q_0 \ni S \\ -1 \text{ if } Q_0 \in S, \end{cases} \tag{3.109}$$

where the angles ϑ_0, φ_0', and φ_0 associated with Q_0 are defined in the same manner as ϑ_a, φ_a', and φ_a associated with Q_a, and $L_d(\varphi_a', \varphi_a; \vartheta_a)$ is the EUTD distance parameter given by

$$\begin{aligned} L_d(\varphi_a', \varphi_a; \vartheta_a) &= \frac{1}{2m_e^2(Q_a)} \{m_{30}(Q_a)m_{02}^2(Q_a) - m_{11}(Q_a) \\ &\cdot [3m_{21}(Q_a)m_{02}(Q_a) - m_{12}(Q_a)m_{11}(Q_a)]\}, \end{aligned} \tag{3.110}$$

$$\begin{aligned} m_{20}(Q_a) &= \kappa_1(Q_a)\sin\vartheta_a(\sin\varphi_a' + \sin\varphi_a) + \frac{\sin^2\theta_{\ell a}'}{s_a^i} \\ &+ \frac{\sin^2\theta_{\ell a}}{s_a^d}, \end{aligned} \tag{3.111}$$

$$m_{11}(Q_a) = \frac{\cos\theta_{\ell a}'\cos\theta_{\tau a}'}{s_a^i} + \frac{\cos\theta_{\ell a}\cos\theta_{\tau a}}{s_a^d}, \tag{3.112}$$

$$\begin{aligned} m_{02}(Q_a) &= \kappa_2(Q_a)\sin\vartheta_a(\sin\varphi_a' + \sin\varphi_a) + \frac{\sin^2\theta_{\tau a}'}{s_a^i} \\ &+ \frac{\sin^2\theta_{\tau a}}{s_a^d}, \end{aligned} \tag{3.113}$$

$$\begin{aligned} m_{30}(Q_a) &= (\cos\theta_{\ell a} + \cos\theta_{\ell a}')\kappa_1^2(Q_a) \\ &+ \sin\vartheta_a(\sin\varphi_a' + \sin\varphi_a)\left[\hat{\ell}_a \cdot \nabla\kappa_1(Q_a)\right] \\ &+ \frac{\cos\theta_{\ell a}'}{s_a^i}\left[3\kappa_1(Q_a)\sin\vartheta_a\sin\varphi_a' + \frac{\sin^2\theta_{\ell a}'}{s_a^i}\right] \\ &+ \frac{\cos\theta_{\ell a}}{s_a^d}\left[3\kappa_1(Q_a)\sin\vartheta_a\sin\varphi_a + \frac{\sin^2\theta_{\ell a}}{s_a^d}\right], \end{aligned} \tag{3.114}$$

$$m_{21}(Q_a) = \frac{\cos\theta_{\tau a}'}{s_a^i}\left[\kappa_1(Q_a)\sin\vartheta_a\sin\varphi_a' + \frac{1 - 3\cos^2\theta_{\ell a}'}{s_a^i}\right]$$

$$+ \quad \frac{\cos\theta_{ra}}{s_a^d}\left[\kappa_1(Q_a)\sin\vartheta_a\sin\varphi_a + \frac{1-3\cos^2\theta_{la}}{s_a^d}\right], \qquad (3.115)$$

$$m_{12}(Q_a) = \frac{\cos\theta'_{la}}{s_a^i}\left[\kappa_2(Q_a)\sin\vartheta_a\sin\varphi'_a + \frac{1-3\cos^2\theta'_{ra}}{s_a^i}\right]$$

$$+ \quad \frac{\cos\theta_{la}}{s_a^d}\left[\kappa_2(Q_a)\sin\vartheta_a\sin\varphi_a + \frac{1-3\cos^2\theta_{ra}}{s_a^d}\right], \qquad (3.116)$$

$$m_e(Q_a) = \sin^2\vartheta_a\left(\frac{1}{s_a^d}+\frac{1}{\rho_a^d}\right), \qquad (3.117)$$

where $\theta'_{la,ra}$ are the angles between the incident ray direction at Q_a and $\hat{\ell}_a$, $\hat{\tau}_a$ (principal surface directions at Q_a), respectively, $\theta_{la,ra}$ are the angles between the diffracted ray direction at Q_a and $\hat{\ell}_a$, $\hat{\tau}_a$, respectively, and $\kappa_{1,2}(Q_a)$ are the principal surface curvatures at Q_a in the direction of $\hat{\ell}_a$, $\hat{\tau}_a$, respectively. It is also understood that when $L_d(\varphi'_a,\varphi_a;\vartheta_a) < 0$, the EUTD transition function in (3.104) should be replaced by its complex conjugate version.

In the derivation of the results for the 2–D case in Section 2.2.3, it was shown that when the observation point is on the deep lit side of the smooth caustic and near an optical boundary, the EUTD transition function assumes the following form:

$$\mathcal{F}(\gamma_a,\zeta_a) \approx F(\eta^2), \qquad (3.118)$$

where $F(x)$ is the UTD transition function and η is given by

$$\eta \approx \frac{\gamma_a+\zeta_a^2}{2(-\gamma_a)^{1/4}} = -\frac{k^{2/3}\sin\vartheta_a(\cos\varphi'_a+\cos\varphi_a)}{2(-\gamma_a)^{1/4}|L_d(\varphi'_a,\varphi_a;\vartheta_a)|^{1/3}}. \qquad (3.119)$$

From (3.106) and (3.110)-(3.117), near an optical boundary on the deep lit side of the smooth caustic, $L_d(\varphi'_a,\varphi_a;\vartheta_a)$ assumes the following form:

$$L_d(\varphi'_a,\varphi_a;\vartheta_a) = \frac{\sqrt{k}}{(-\gamma_a)^{3/4}}\left[\frac{m_{20}(Q_a)m_{02}(Q_a)-m_{11}^2(Q_a)}{2m_e(Q_a)}\right]^{3/2}. \qquad (3.120)$$

Near the RSB, $\varphi_a \approx \pi - \varphi'_a$ and using (G.69) we have

$$m_{20}(Q_a)m_{02}(Q_a)-m_{11}^2(Q_a) \approx \sin^2\vartheta_a\cos^2\left(\frac{\varphi'_a-\varphi_a}{2}\right)\left(\frac{1}{s_a^d}+\frac{1}{\rho_{la}^r}\right)$$

$$\cdot\left(\frac{1}{s_a^d}+\frac{1}{\rho_{ra}^r}\right). \qquad (3.121)$$

Also, near the RSB $m_e(Q_a)$ is given by

$$m_e(Q_a) \approx \sin^2\vartheta_a\left(\frac{1}{s_a^d}+\frac{1}{\rho_a^r}\right), \qquad (3.122)$$

where from (3.105)

$$\frac{1}{\rho_a^r} = \frac{1}{s_a^i} - \frac{2(\hat{n}_a \cdot \hat{n}_e)(\hat{s}_a^i \cdot \hat{n}_a)}{R_a \sin^2 \vartheta_a} . \tag{3.123}$$

Thus, using (3.119)–(3.122), η^2 near the RSB is given by

$$\eta^2 \approx 2k \cos^2\left(\frac{\varphi_a' + \varphi_a}{2}\right)\left[\frac{s_a^d(\rho_{ra}^r + s_a^d)\rho_{ta}^r \rho_{ra}^r \sin^2 \vartheta_a}{\rho_a^r(\rho_{ta}^r + s_a^d)(\rho_{ra}^r + s_a^d)}\right] = kL^r a(\varphi_a' + \varphi_a) . \tag{3.124}$$

Near the ISB, $\varphi_a \approx \pi + \varphi_a'$ and using (G.38)–(G.40) the quantity $m_{20}m_{02} - m_{11}^2$ at Q_a assumes the following form:

$$m_{20}(Q_a)m_{02}(Q_a) - m_{11}^2(Q_a) \approx \sin^2 \vartheta_a \cos^2\left(\frac{\varphi_a' + \varphi_a}{2}\right)\left(\frac{1}{s_a^d} + \frac{1}{s_a^i}\right)^2 . \tag{3.125}$$

Also, near the ISB $\rho_a^d = s_a^i$ from (3.105) and $m_e(Q_a)$ is given by

$$m_e(Q_a) \approx \sin^2 \vartheta_a \left(\frac{1}{s_a^d} + \frac{1}{s_a^i}\right) . \tag{3.126}$$

Thus, using (3.120), (3.125), and (3.126), η^2 near the ISB is given by

$$\eta^2 \approx 2k \cos^2\left(\frac{\varphi_a' - \varphi_a}{2}\right)\left(\frac{s_a^i s_a^d \sin^2 \vartheta_a}{s_a^i + s_a^d}\right) = kL^i a(\varphi_a' - \varphi_a) , \tag{3.127}$$

where $L^{i,r}$ are the UTD distance parameters for spherical wave incidence. Both $L^{i,r}$ and $a(\varphi_a' \pm \varphi_a)$ are defined in [4]. The results in (3.118), (3.124), and (3.127) demonstrate that near the optical boundaries in the deep lit side of the smooth caustic, both the EUTD transition function and its argument reduce to the conventional UTD formulations as expected.

Chapter 4

Plane Wave Scattering from Polynomial Surfaces

In this chapter, a UGO/EUTD solution for the plane wave scattering and diffraction from polynomial surfaces is developed. The derivation of the solution follows a similar procedure as the uniform asymptotic analysis in Chapters 2 and 3, with a generalized form of Chester's expansion being employed for the asymptotic reduction of the PO radiation integral. The observer is assumed to be in the Fraünhofer region of the scatterer, and due to the symmetry introduced by this assumption the alternative method of steepest descent employed in Chapters 2 and 3 yields the same expressions, except for the edge diffracted field solution where the resulting edge diffraction coefficients are slightly different.

The predominant scattering contribution from polynomial type surfaces would come from the neighborhood of the zero-curvature points on the boundary [22] which are associated with caustics of the GO reflected rays. In addition, the contributions from the complex stationary phase points in the PO integral are interpreted as diffraction from the zero-curvature points rather than complex ray contributions. This zero-curvature diffraction interpretation is indeed equivalent to the complex ray interpretation, yet it eliminates the need for a complex extension of the scattering boundary and the evaluation of geometric parameters in complex space.

The PO approximation is also employed in this chapter, thus, only the first order scattering mechanisms will be considered, namely reflection, zero-curvature diffraction, and first order edge diffraction. The canonical function involved in the expression

for the total scattered field from a polynomial surface is the generalized incomplete Airy integral [22]. In the special case of a cubic polynomial surface, this generalized integral reduces to the usual incomplete Airy integral and the expressions for the scattering mechanisms are in agreement with the results of Chapters 2 and 3 specialized for the case of plane wave incidence with observation in the far-zone. In the case of a fourth order polynomial surface, the generalized incomplete Airy integral reduces to a special case of the incomplete Pearcy integral. It should be understood that the results of the analysis employed in this chapter do not remain uniformly valid for observation points in the intermediate or near zone of the scatterer. In the near zone problem, the dominant contribution to the PO integral is no longer localized at the zero-curvature points and a more general treatment along the lines of Chapters 2 and 3 must be employed.

The outline of this chapter is as follows: The geometric properties of polynomial surfaces and their relation to the scattering mechanisms are discussed in Section 4.1. The UGO/EUTD expressions for the reflected, zero-curvature and edge diffracted field contributions from finite two and three dimensional polynomial surfaces are derived in Sections 4.2 and 4.3, respectively.

4.1 Polynomial surfaces and high-frequency scattering considerations

Let's consider a two dimensional polynomial surface. As a plane parametric curve it may be expressed as follows:

$$\vec{r}(u) = u\,\hat{x} + Y(u)\,\hat{y}\,, \quad a \leq u \leq b\,. \tag{4.1}$$

where $Y(u)$ is an nth order polynomial function given by

$$Y(u) = P_n(u) = a_0 + a_1 u + a_2 u^2 + \cdots + a_n u^n\,. \tag{4.2}$$

The distinguishing feature of polynomial defined surfaces are the existence of zero-curvature points which are real roots of the second derivative of the surface, that

is

$$Y''(u_m) = \bar{a}_2 + \bar{a}_3 u_m + \bar{a}_4 u_m^2 + \cdots + \bar{a}_n u_m^{n-2} = 0\,;\ \ m = 1, 2\cdots, n-2\,, \quad (4.3)$$

$$\bar{a}_n = n(n-1)a_n\,. \quad (4.4)$$

If $a \le u_m \le b$ is a first order real root of (4.3), then the surface near u_m is locally cubic, that is $Y'''(u_m) \neq 0$ and $Y(u)$ may be approximated as follows:

$$Y(u) \approx Y(u_m) + Y'(u_m)(u-u_m) + \frac{Y'''(u_m)}{3!}(u-u_m)^3\,. \quad (4.5)$$

In general, if u_m is an lth order real root of (4.3) or an lth order zero-curvature point with $1 \le l \le n-2$, we have that

$$Y^{(k)}(u_m) = 0\,;\ \ 2 \le k \le l+1 \quad (4.6)$$

$$Y^{(l+2)}(u_m) \neq 0\,, \quad (4.7)$$

and near u_m, $Y(u)$ may be approximated as follows:

$$Y(u) \approx Y(u_m) + Y'(u_m)(u-u_m) + \frac{Y^{(l+2)}(u_m)}{(l+2)!}(u-u_m)^{l+2}\,. \quad (4.8)$$

It should also be noted that near an odd order zero-curvature point ($l = 1, 3, 5, \cdots$) the polynomial surface is concave-convex, whereas near an even order zero-curvature point ($l = 2, 4, 6, \cdots$) the polynomial surface is strictly concave or convex. The unit tangent, normal, and surface curvature vectors for the polynomial boundary defined in (4.1) are as follows:

$$\hat{t}(u) = \frac{\vec{r}\,'(u)}{h(u)} = \frac{\hat{x} + Y'(u)\,\hat{y}}{h(u)}\,, \quad (4.9)$$

$$\hat{n}(u) = \hat{t}(u) \times \hat{z}\,, \quad (4.10)$$

$$\vec{\kappa}(u) = \frac{\vec{r}\,''(u)h(u) - \vec{r}\,'(u)h'(u)}{h^3(u)} = -\kappa(u)\,\hat{n}(u)\,, \quad (4.11)$$

$$\kappa(u) = |\vec{\kappa}(u)| = \frac{Y''(u)}{h^3(u)}\,, \quad (4.12)$$

$$h(u) = |\vec{r}\,'(u)| = \left\{1 + [Y'(u)]^2\right\}^{1/2} = \text{Jacobian.} \quad (4.13)$$

The results of Chapter 2 and specifically Equation (2.14) show that when both the source and the observer are in the far-zone of the scattering surface, the zero-curvature points are associated with caustics of the GO reflected rays. Figure 4.1

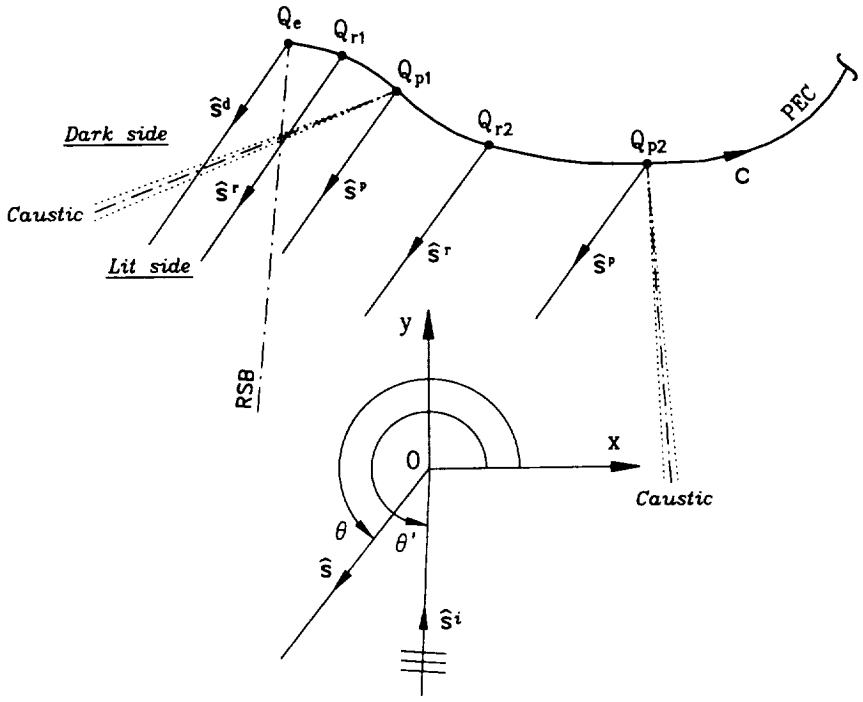

Figure 4.1: First order scattering mechanisms associated with a polynomial boundary illuminated by a plane wave.

illustrates a polynomial boundary illuminated by a plane wave. The boundary C contains an edge point, Q_e, and two zero-curvature points, $Q_{p1,p2}$, with their associated GO ray caustics. When the two zero-curvature points are sufficiently far apart, the high-frequency scattering from C can be effectively analyzed by treating each caustic separately.

The scattering mechanisms of interest in the analysis that follows are reflection that remains uniform as the reflection point $Q_r \rightarrow Q_p$, first order edge diffraction that remains uniform as $Q_e \rightarrow Q_p$, and zero-curvature diffraction or complex ray (evanescent) field contribution that compensates the discontinuity of the reflected field across the GO ray caustics. Although additional higher order mechanisms such as edge exited surface rays and whispering gallery modes may also exist and con-

tribute significantly to the scattered field in certain regions of the coordinate space surrounding a polynomial surface, they will not be considered in the present analysis.

4.2 Uniform asymptotic analysis (2–D case)

The canonical geometries for the uniform asymptotic analysis are shown in Figure 4.2. Figure 4.2a shows a semi-infinite perfectly conducting concave-convex polynomial surface that contains an odd order zero-curvature point. Figure 4.2b shows a semi-infinite perfectly conducting polynomial surface that contains an even order zero-curvature point. The electric field $\vec{E}^s$ scattered by the 2–D polynomial boundary C illuminated by a plane wave and observed at a point P in the far-zone of the boundary can then be expressed in terms of the usual radiation integral over the electric current $\vec{J}$ on C as follows:

$$\vec{E}^s(P) \approx \frac{kZ_0}{4} \int_C \left[\hat{s} \times \hat{s} \times \vec{J}(Q')\right] H_0^{(2)}(kR)\, d\ell' , \tag{4.14}$$

where

$$R = \left|\overline{Q'P}\right| \approx \rho - \vec{r}(Q') \cdot \hat{s}, \text{ (far-zone approximation)} \tag{4.15}$$

$$\hat{s} = \hat{x} \cos\theta + \hat{y} \sin\theta , \tag{4.16}$$

$$\vec{r}(Q') = x\,\hat{x} + Y(x)\,\hat{y} = \vec{r}(x);\ a \le x < \infty , \tag{4.17}$$

$Y(x)$ is a polynomial function, $\rho = \left|\overline{OP}\right|$, and $\hat{s}$ is the observation direction. As before, the PO approximation to (4.14) is employed using the GO currents in (2.2), where the incident magnetic field at Q' under the plane wave illumination assumption is given by

$$\vec{H}^i(Q') = Z_0^{-1} \left(\hat{s}^i \times \hat{p}\right) e^{-jk\vec{r}(Q')\cdot\hat{s}^i};\ \hat{s}^i \cdot \hat{p} = 0 , \tag{4.18}$$

$$= Z_0^{-1}\, \hat{s}^i \times \vec{E}^i(Q') , \tag{4.19}$$

$$\vec{E}^i(Q') = \hat{p}\, e^{-jk\vec{r}(Q')\cdot\hat{s}^i} , \tag{4.20}$$

$\hat{p}$ is the polarization vector of the incident plane wave, and $\hat{s}^i$ is the direction of incidence given by

$$\hat{s}^i = -\hat{x} \cos\theta' - \hat{y} \sin\theta' . \tag{4.21}$$

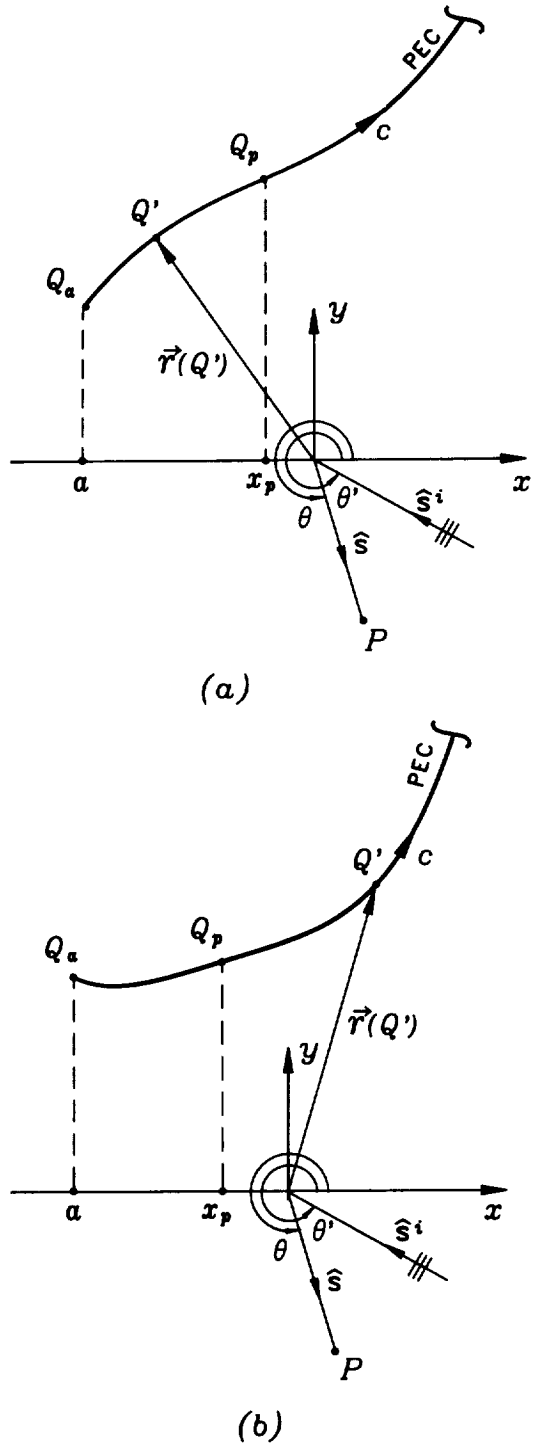

Figure 4.2: Canonical geometries for the uniform asymptotic analysis: (a) polynomial boundary containing an odd order zero-curvature point, (b) polynomial boundary containing an even order zero-curvature point.

Thus, using the PO approximation and the large argument form of the Hankel function given in (2.6) the far-zone scattered electric field is given by

$$\vec{E}^s(\theta',\theta;\rho) \approx \vec{e}(\theta',\theta)\,\frac{e^{-jk\rho}}{\sqrt{\rho}}\,, \tag{4.22}$$

where $R \approx \rho$ was used in the magnitude term of (2.6). The vector quantity $\vec{e}(\theta',\theta)$ is the angular field dependence and is given by the following stationary phase integral:

$$\vec{e}(\theta',\theta) = \int_{\ell_a}^{\infty} \vec{F}(\ell')\, e^{jk\phi(\ell')}\, d\ell'\,, \tag{4.23}$$

where

$$\vec{F}(\ell') = \sqrt{\frac{jk}{2\pi}}\left\{\hat{s}\times\hat{s}\times\left[\hat{n}(\ell')\times\hat{s}^i\times\hat{p}\right]\right\}\,, \tag{4.24}$$

$$\phi(\ell') = \vec{r}(\ell')\cdot\left(\hat{s}-\hat{s}^i\right)\,, \tag{4.25}$$

and $\hat{n}(\ell')$ is the outward unit normal to the surface at Q'. The next step in the procedure is the uniform asymptotic evaluation of $\vec{e}(\theta',\theta)$ using a generalized form of Chester's expansion [22].

4.2.1 Uniform asymptotic evaluation of $\vec{e}(\theta',\theta)$

First, the stationary phase integral in (4.23) must be transformed into a canonical form. This is done by using the surface approximation near the zero-curvature point given in (4.8), or alternatively by expanding the phase function in Taylor series around the zero-curvature point. Both methods give the same result, and if l is the order of the zero-curvature point, that is x_p is an lth order root of the equation $\vec{r}\,''(x) = 0$, the appropriate transformation is as follows:

$$\phi(\ell') = \tau(s) = \alpha + \beta s + \frac{s^\nu}{\nu}\,, \tag{4.26}$$

where $\nu = l + 2$,

$$\alpha = \tau(0) = \phi(\ell_p)\,, \tag{4.27}$$

$$\beta = \hat{t}_p\cdot\left(\hat{s}-\hat{s}^i\right)\left.\frac{d\ell'}{ds}\right|_{s=0}\,, \tag{4.28}$$

and $\hat{t}_p$ is the unit tangent vector at Q_p Hence, using (4.26) the stationary phase integral in (4.23) transforms to the following canonical form:

$$\vec{e}(\theta',\theta) = e^{jka} \int_{s_a}^{\text{"}\infty\text{"}} \vec{G}(s)\, e^{jk(\beta s + s^\nu/\nu)}\, ds\,, \tag{4.29}$$

where

$$s_a = u_a \left[\hat{t}_a \cdot \left(\hat{s} - \hat{s}^i\right) \left.\frac{d\ell'}{ds}\right|_{s=s_a} - \hat{t}_p \cdot \left(\hat{s} - \hat{s}^i\right) \left.\frac{d\ell'}{ds}\right|_{s=0} \right]^{\frac{1}{\nu-1}}, \tag{4.30}$$

$$u_a = \begin{cases} +1 & \text{if } Q_p \ni C \\ -1 & \text{if } Q_p \in C, \end{cases} \tag{4.31}$$

$$\vec{G}(s) = \vec{F}(\ell') \frac{d\ell'}{ds}\,, \tag{4.32}$$

$$\frac{d\ell'}{ds} = \frac{d\ell'}{dx}\frac{dx}{ds} = \left[\frac{(\nu-1)!}{m(x,\nu)}\right]^{\frac{1}{\nu}}, \tag{4.33}$$

$$m(x,\nu) = \frac{\vec{r}^{\,(\nu)}(x_p)\cdot\left(\hat{s}-\hat{s}^i\right)}{|\vec{r}\,'(x)|^\nu}, \tag{4.34}$$

$$\text{"}\infty\text{"} = \infty \exp\left[-j\arg\left(\frac{d\ell'}{ds}\right)\right], \tag{4.35}$$

and $\hat{t}_a$ is the unit tangent vector at Q_a. The proper branches for β, s_a and $d\ell'/ds$ depend on the sign of $m(x_p,\nu)$.

Next, we employ a generalized form of Chester's expansion [22] for the amplitude function in (4.29), that is

$$\begin{aligned} \vec{G}(s) &= \sum_{m=0}^{\infty} \left[\vec{a}_{m,0}\left(s^{\nu-1}+\beta\right)^m + \vec{a}_{m,1}\, s\left(s^{\nu-1}+\beta\right)^m \right. \\ &+ \left. \cdots + \vec{a}_{m,\nu-2}\, s^{\nu-2}\left(s^{\nu-1}+\beta\right)^m\right], \end{aligned} \tag{4.36}$$

and since only the leading terms in the asymptotic expansion of (4.29) will be retained, (4.36) may be written as follows:

$$\vec{G}(s) = \sum_{n=0}^{\nu-2} s^n \vec{a}_{0,n} + \left(s^{\nu-1}+\beta\right)\vec{g}\,(s)\,, \tag{4.37}$$

where

$$\begin{aligned} \vec{g}\,(s) &= \sum_{m=1}^{\infty} \left[\vec{a}_{m,0}\left(s^{\nu-1}+\beta\right)^{m-1} + \vec{a}_{m,1}\, s\left(s^{\nu-1}+\beta\right)^{m-1} \right. \\ &+ \left. \cdots + \vec{a}_{m,\nu-2}\, s^{\nu-2}\left(s^{\nu-1}+\beta\right)^{m-1}\right]. \end{aligned} \tag{4.38}$$

Due to the symmetry introduced by the plane wave far-zone observation assumption, only the vector coefficient $\vec{a}_{0,0}$ is non-zero in (4.37), that is

$$\vec{a}_{0,0} = \frac{1}{\nu-1}\sum_{k=1}^{\nu-1}\vec{G}(s_k), \text{ and} \tag{4.39}$$

$$\vec{a}_{0,n} = 0;\ n=1,\cdots,\nu-2, \tag{4.40}$$

where $\vec{G}(s_k)$ is given by

$$\vec{G}(s_k) = \vec{F}(\ell_k)\left.\frac{d\ell'}{ds}\right|_{s=s_k}, \tag{4.41}$$

$$\left.\frac{d\ell'}{ds}\right|_{s=s_k} = \left[\frac{(\nu-1)(-\beta)^{\frac{\nu-2}{\nu-1}}e^{j2(k-1)(\nu-2)\pi/(\nu-1)}}{\phi''(\ell_k)}\right]^{\frac{1}{2}}, \tag{4.42}$$

and s_k are the stationary phase points of $\tau(s)$, that is $\tau'(s_k)=0$, and are given by

$$s_k = (-\beta)^{\frac{1}{\nu-1}}\,e^{j2(k-1)\pi/(\nu-1)};\ k=1,2,\cdots,\nu-1. \tag{4.43}$$

Thus, using (4.37) along with integration by parts $\vec{e}(\theta',\theta)$ may be written as follows:

$$\vec{e}(\theta',\theta) \simeq e^{jk\alpha}\left[\vec{a}_{0,0}\int_{s_a}^{"\infty"} e^{jk(\beta s+s^\nu/\nu)}\,ds - \frac{1}{jk}\vec{g}(s_a)\,e^{jk(\beta s_a+s_a^\nu/\nu)}\right] + O(k^{-2}), \tag{4.44}$$

and using (4.26) and (4.37) we have that

$$\begin{aligned}\vec{e}(\theta',\theta) &\simeq e^{jk\alpha}\vec{a}_{0,0}\int_{s_a}^{"\infty"} e^{jk(\beta s+s^\nu/\nu)}\,ds \\ &+ e^{jk\tau(s_a)}\left[\frac{\vec{a}_{0,0}}{jk\left(\beta+s_a^{\nu-1}\right)} - \frac{\vec{G}(s_a)}{jk\tau'(s_a)}\right] + O(k^{-2}).\end{aligned} \tag{4.45}$$

We then let $s = tk^{-1/\nu}$, $\gamma = \beta k^{(\nu-1)/\nu}$, and $\zeta_a = s_a k^{1/\nu}$ in (4.45), thus

$$\begin{aligned}\vec{e}(\theta',\theta) &\simeq \frac{e^{jk\alpha}}{k^{1/\nu}}\vec{a}_{0,0}\int_{\zeta_a}^{"\infty"} e^{j(\gamma t+t^\nu/\nu)}\,dt \\ &+ e^{jk\tau(s_a)}\left[\frac{\vec{a}_{0,0}}{jk^{1/\nu}\left(\gamma+\zeta_a^{\nu-1}\right)} - \frac{\vec{G}(s_a)}{jk\tau'(s_a)}\right] + O(k^{-2}).\end{aligned} \tag{4.46}$$

Finally, depending on the sign of $m(x_p,\nu)$ the angular field dependence $\vec{e}(\theta',\theta)$ is given by

$$\vec{e}(\theta',\theta) \sim \frac{e^{jk\alpha}}{\sqrt{k}}\vec{\epsilon}_0\,\overline{K}_\omega(\gamma,\zeta_a,\nu) + e^{jk\phi(\ell_a)}\left[\frac{j\vec{F}(\ell_a)}{k\phi'(\ell_a)} + \frac{\vec{\epsilon}_0}{j\sqrt{k}\left(\gamma+\zeta_a^{\nu-1}\right)}\right] \tag{4.47}$$

$$\vec{e}(\theta',\theta) \sim \begin{cases} \text{if } m(x_p,\nu) > 0\,, \\ \dfrac{e^{jka}}{\sqrt{k}}\vec{\epsilon}_0\,\overline{K}_\omega^{\,\circ}(\gamma,\zeta_a,\nu) + e^{jk\phi(\ell_a)}\left[\dfrac{j\vec{F}(\ell_a)}{k\phi'(\ell_a)} - \dfrac{\vec{\epsilon}_0}{j\sqrt{k}\,(\gamma+\zeta_a^{\nu-1})}\right] \\ \text{if } m(x_p,\nu) < 0\,, \end{cases} \tag{4.48}$$

where the $O(k^{-2})$ terms were omitted, and the parameters γ, ζ_a, and $\vec{\epsilon}_0$ are given by the following expressions:

$$\gamma = u_p\, k^{(\nu-1)/\nu}\,\hat{t}_p\cdot\left(\hat{s}-\hat{s}^{\,i}\right) w(x_p,\nu)\,, \tag{4.49}$$

$$u_p = \mathrm{sgn}[m(x_p,\nu)]\,, \tag{4.50}$$

$$\zeta_a = u_a k^{1/\nu}\left|\hat{t}_a\cdot\left(\hat{s}-\hat{s}^{\,i}\right) w(a,\nu) - \hat{t}_p\cdot\left(\hat{s}-\hat{s}^{\,i}\right) w(x_p,\nu)\right|^{\frac{1}{\nu-1}}\,, \tag{4.51}$$

$$w(x,\nu) = \left|\frac{(\nu-1)!}{m(x,\nu)}\right|^{\frac{1}{\nu}}\,, \tag{4.52}$$

$$\vec{\epsilon}_0 = \frac{(-\gamma)^{\frac{\nu-2}{2(\nu-1)}}}{\nu-1}\sum_{k=1}^{\nu-1}\vec{F}(\ell_k)\sqrt{\frac{\nu-1}{|\phi''(\ell_k)|}}\,. \tag{4.53}$$

The function $\overline{K}_\omega(\gamma,\zeta,\nu)$ is the generalized incomplete Airy integral [22] defined as follows:

$$\overline{K}_\omega(\gamma,\zeta,\nu) \triangleq \int_\zeta^\infty e^{j(\gamma z + z^\nu/\nu)}\,dz\,;\quad \nu = 3,4,5,\cdots \tag{4.54}$$

The second term in both (4.47) and (4.48) is a purely edge diffraction contribution where the first term in (4.47) and (4.48) involving the generalized incomplete Airy integral contains all three scattering mechanisms, namely reflection, edge, and zero-curvature diffraction. These scattering contributions may be separated using the properties and complex plane topology of $\overline{K}_\omega(\gamma,\zeta,\nu)$ in Appendix C. Also, the parameters α, γ, ζ_a, and $\vec{\epsilon}_0$ can be expressed in terms of the local geometric parameters on the boundary relevant to each scattering mechanism.

4.2.2 Reflected field contribution

There exist two cases. The first case corresponds to a concave-convex polynomial boundary that contains an odd order zero-curvature point. In this case ν is odd in (4.54) and the reflected field consists of two specular contributions that only exist in the lit side of the caustic. The second case corresponds to a strictly concave or

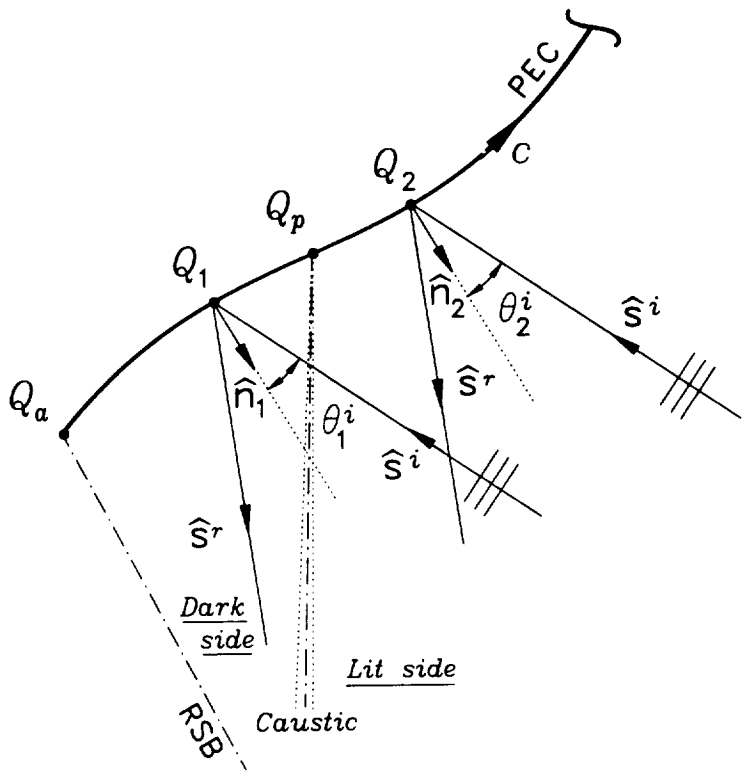

Figure 4.3: Reflection near an odd order zero-curvature point.

convex boundary that contains an even order zero-curvature point. In this case ν is even in (4.54) and the reflected field consists of a single specular contribution that exists on both sides of the caustic. The concave-convex case will be considered first.

A. Reflection from a concave-convex polynomial boundary

The geometry for the reflected field from a polynomial boundary that contains an odd order zero-curvature point is shown in Figure 4.3. Using (4.22), (4.47), (4.48), and the appropriate expression for $\overline{K}_\omega(\gamma,\zeta,\nu)$ for ν odd and $\gamma < 0$ in Appendix C, the reflected field in the lit side of the caustic is given by

$$\vec{E}^r(\theta',\theta;\rho) \sim \{u_1\, e^{jk\alpha_1}\, \vec{\epsilon}_1\, I_r(-\gamma_1,\nu) + u_2\, e^{jk\alpha_2}\, \vec{\epsilon}_2\, I_r^*(-\gamma_2,\nu)\}\, \frac{e^{-jk\rho}}{\sqrt{\rho}} \qquad (4.55)$$

$$\text{if} \quad m(x_p,\nu) < 0\,,$$

$$\vec{E}^r(\theta',\theta;\rho) \sim \{u_1\, e^{jk\alpha_1}\, \vec{\epsilon}_1\, I_r^*(-\gamma_1,\nu) + u_2\, e^{jk\alpha_2}\, \vec{\epsilon}_2\, I_r(-\gamma_2,\nu)\}\, \frac{e^{-jk\rho}}{\sqrt{\rho}} \qquad (4.56)$$

$$\text{if} \quad m(x_p,\nu) > 0\,,$$

where $u_{1,2} = 1$ if $Q_{1,2} \in C$ and zero otherwise, and the function $I_r(\gamma, \nu)$ is defined as follows:

$$I_r(\gamma,\nu) \triangleq \int_{\infty \exp(-j3\pi/2\nu)}^{\infty \exp(j\pi/2\nu)} e^{j(\gamma x + z^\nu/\nu)}\, dz\,; \quad \nu \text{ is odd.} \tag{4.57}$$

The sign of $m(x_p, \nu)$ designates which side of the boundary C is illuminated. For the situation depicted in Figure 4.3 $m(x_p, \nu) < 0$. From (4.24)–(4.26) and (4.53) the parameters $\alpha_{1,2}$, $\gamma_{1,2}$, and $\vec{\epsilon}_{1,2}$ may be written as follows:

$$\alpha_{1,2} = \vec{r}(Q_{1,2}) \cdot (\hat{s}^r - \hat{s}^i) \pm u_p\, k^{-1} \left(\frac{\nu-1}{\nu}\right) \gamma_{1,2}^{\frac{\nu}{\nu-1}}, \tag{4.58}$$

$$\gamma_{1,2} = \left\{ k \left(\frac{\nu}{\nu-1}\right) |[\vec{r}(Q_{1,2}) - \vec{r}(Q_p)] \cdot (\hat{s} - \hat{s}^i)| \right\}^{\frac{\nu-1}{\nu}}, \tag{4.59}$$

$$\vec{\epsilon}_{1,2} = e^{j\frac{\pi}{4}} \sqrt{\frac{\nu-1}{2\pi}}\, \gamma_{1,2}^{\frac{\nu-2}{2(\nu-1)}} \left[\hat{p} \cdot \bar{\bar{R}}\,(Q_{1,2})\right] \sqrt{\frac{1}{2}|\rho_g(Q_{1,2})| \cos\theta^i_{1,2}}, \tag{4.60}$$

where $\bar{\bar{R}}\,(Q_{1,2})$ is the GO dyadic reflection coefficient given in (2.60) and (2.61), and $\rho_g(Q_{1,2})$, $\theta^i_{1,2}$ are the surface radius of curvature and angle of incidence at $Q_{1,2}$, respectively. Thus, using (4.58)–(4.60) the reflected field from a concave-convex polynomial boundary for the case of $m(x_p, \nu) < 0$, that is $\rho_g(Q_1) < 0$ and $\rho_g(Q_2) > 0$, may be written as follows:

$$\begin{aligned} \vec{E}^r(\theta', \theta; \rho) \sim & \left[u_1\, \vec{E}^i(Q_1) \cdot \bar{\bar{\mathcal{R}}}^*(Q_1) \sqrt{\frac{1}{2}\rho_g(Q_1) \cos\theta^i_1}\, e^{jk\vec{r}(Q_1)\cdot\hat{s}^r} \right. \\ & \left. + \; u_2\, \vec{E}^i(Q_2) \cdot \bar{\bar{\mathcal{R}}}\,(Q_2) \sqrt{\frac{1}{2}\rho_g(Q_2) \cos\theta^i_2}\, e^{jk\vec{r}(Q_2)\cdot\hat{s}^r} \right] \frac{e^{-jk\rho}}{\sqrt{\rho}}, \end{aligned} \tag{4.61}$$

where $\vec{E}^i(Q_{1,2})$ is the incident plane wave at $Q_{1,2}$ given in (4.20), and $\bar{\bar{\mathcal{R}}}\,(Q_{1,2})$ is the UGO dyadic reflection coefficient and is given by

$$\bar{\bar{\mathcal{R}}}\,(Q_{1,2}) = \mathcal{R}_s(Q_{1,2})\, \hat{e}_\perp \hat{e}_\perp + \mathcal{R}_h(Q_{1,2})\, \hat{e}^i_\parallel \hat{e}^r_\parallel, \tag{4.62}$$

$$\mathcal{R}_{s,h}(Q_{1,2}) = R_{s,h}\, e^{j\frac{\pi}{4}} \sqrt{\frac{\nu-1}{2\pi}}\, \gamma_{1,2}^{\frac{\nu-2}{2(\nu-1)}}\, e^{-j\left(\frac{\nu-1}{\nu}\right)\gamma_{1,2}^{\frac{\nu}{\nu-1}}}\, I_r^*(-\gamma_{1,2}, \nu), \tag{4.63}$$

$$R_{s,h} = \mp 1, \text{ for a perfectly conducting boundary.} \tag{4.64}$$

Equation (4.61) shows that the complex conjugate version of the UGO reflection coefficient should be used when $\rho_g(Q_{1,2}) < 0$. When $\nu = 3$, (4.63) reduces to the UGO reflection coefficients derived in Chapter 2 and given in (2.171).

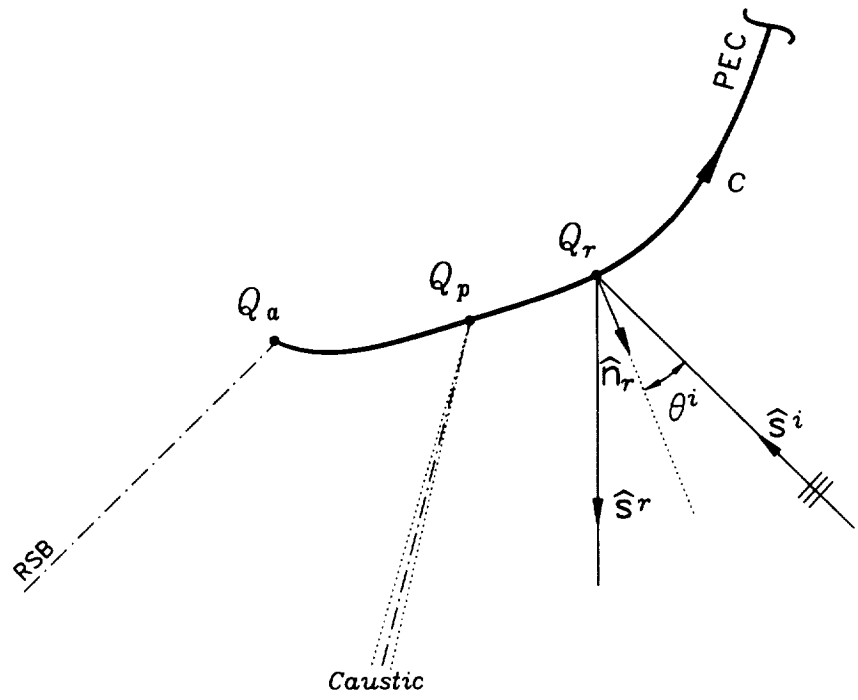

Figure 4.4: Reflection near an even order zero-curvature point.

B. Reflection from strictly concave or convex polynomial boundary

The geometry for the reflected field from a polynomial boundary that contains an even order zero-curvature point is shown in Figure 4.4. Using (4.22), (4.47), (4.48), and the appropriate expression for $\overline{K}_\omega(\gamma,\zeta,\nu)$ for ν even in Appendix C, the reflected field on either side of the caustic is given by

$$\vec{E}^r(\theta',\theta;\rho) \sim u_r\, e^{jk\alpha_r}\, \vec{\epsilon}_r\, I_r^*(-\gamma_r,\nu)\, \frac{e^{-jk\rho}}{\sqrt{\rho}}\,;\ \text{if } m(x_p,\nu) < 0, \tag{4.65}$$

$$\vec{E}^r(\theta',\theta;\rho) \sim u_r\, e^{jk\alpha_r}\, \vec{\epsilon}_r\, I_r(-\gamma_r,\nu)\, \frac{e^{-jk\rho}}{\sqrt{\rho}}\,;\ \text{if } m(x_p,\nu) > 0, \tag{4.66}$$

where $u_r = 1$ if $Q_r \in C$ and zero otherwise, $I_r(\gamma,\nu)$ is the same as in (4.57) with ν even , and the parameters α_r, γ_r, and $\vec{\epsilon}_r$ are given by

$$\alpha_r = \vec{r}(Q_r)\cdot(\hat{s}^r - \hat{s}^i) \pm u_p\, k^{-1}\left(\frac{\nu-1}{\nu}\right)\gamma_r^{\frac{-\nu}{\nu-1}}, \tag{4.67}$$

$$\gamma_r = \left\{k\left(\frac{\nu}{\nu-1}\right)\left|[\vec{r}(Q_r)-\vec{r}(Q_p)]\cdot(\hat{s}-\hat{s}^i)\right|\right\}^{\frac{\nu-1}{\nu}}, \tag{4.68}$$

$$\vec{\epsilon}_r \;=\; e^{j\frac{\pi}{4}}\sqrt{\frac{\nu-1}{2\pi}}\,\gamma_r^{\frac{\nu-2}{2(\nu-1)}}\left[\hat{p}\cdot\,\overline{\overline{R}}\,(Q_r)\right]\sqrt{\frac{1}{2}|\rho_g(Q_r)|\cos\theta^i}\,. \tag{4.69}$$

Thus, using (4.67)–(4.69) the reflected field from a strictly concave or convex polynomial boundary for the case of $m(x_p,\nu) < 0$ or $\rho_g(Q_r) > 0$ depicted in Figure 4.4 may be written as follows:

$$\vec{E}^r(\theta',\theta;\rho) \sim u_r\,\vec{E}^i(Q_r)\cdot\,\overline{\overline{\mathcal{R}}}\,(Q_r)\sqrt{\frac{1}{2}\rho_g(Q_r)\cos\theta^i}\,e^{jk\vec{r}(Q_r)\cdot\hat{s}^r}\,\frac{e^{-jk\rho}}{\sqrt{\rho}}\,, \tag{4.70}$$

where $\vec{E}^i(Q_r)$ is the incident plane wave at Q_r given in (4.20) and $\overline{\overline{\mathcal{R}}}\,(Q_r)$ is the UGO dyadic reflection coefficient and is the same as in (4.62)–(4.64) with ν even. Again, when $\rho_g(Q_r) < 0$ the complex conjugate version of $\overline{\overline{\mathcal{R}}}\,(Q_r)$ should be used.

4.2.3 Zero-curvature diffracted field contribution

As in the case of the reflected field, we also have two cases for the zero-curvature diffracted field. The first case involves diffraction from a an odd order zero-curvature point associated with with a concave-convex polynomial boundary. Since the reflected field is discontinuous across the caustic in this case, the zero curvature diffracted field has to compensate this discontinuity. The second case involves diffraction from an even order zero-curvature point associated with a strictly concave or convex polynomial boundary. In the latter case the reflected field is continuous across the caustic, thus the zero-curvature diffracted field only accounts for higher order surface discontinuities.

A. Diffraction from an odd order zero-curvature point

The geometry for the diffracted field from an odd order zero-curvature point is shown in Figure 4.5. Using (4.22), (4.47), (4.48), and the appropriate expression for $\overline{K}_\omega(\gamma,\zeta,\nu)$ for ν odd and $\zeta < 0$ in Appendix C, the odd order zero-curvature diffracted field is given by

$$\vec{E}^p(\theta',\theta;\rho) \;\sim\; u_0\,e^{jk\alpha_p}\,\vec{\epsilon}_p\,I_{pl}(-\gamma_p,\nu)\,\frac{e^{-jk\rho}}{\sqrt{\rho}}\,,\quad\text{(lit side)} \tag{4.71}$$

$$\vec{E}^p(\theta',\theta;\rho) \;\sim\; u_0\,e^{jk\alpha_p}\,\vec{\epsilon}_p\,I_{pd}(\gamma_p,\nu)\,\frac{e^{-jk\rho}}{\sqrt{\rho}}\,,\quad\text{(dark side)} \tag{4.72}$$

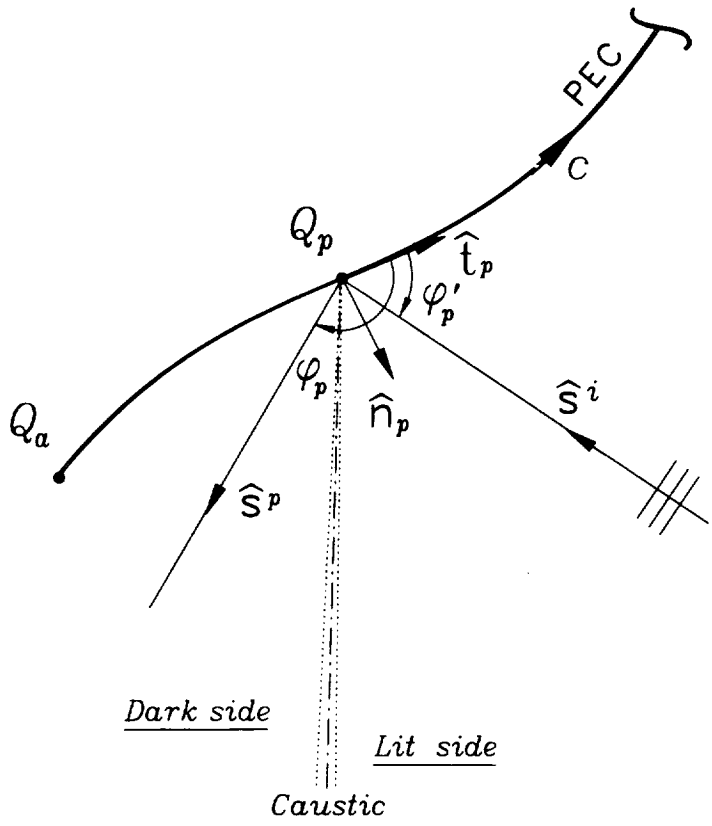

Figure 4.5: Diffraction from an odd order zero-curvature point.

where $u_0 = 1$ if $Q_p \in C$ and zero otherwise, and the functions $I_{p\ell}(\gamma,\nu)$, $I_{pd}(\gamma,\nu)$ are defined as follows:

$$I_{p\ell}(\gamma,\nu) \triangleq \int_{\infty\exp[j(-\pi+3\pi/2\nu)]}^{\infty\exp(-j3\pi/2\nu)} e^{j(\gamma z+z^\nu/\nu)}\,dz\,;\ \ \nu \text{ is odd,} \tag{4.73}$$

$$I_{pd}(\gamma,\nu) \triangleq \int_{\infty\exp[j(\pi-\pi/2\nu)]}^{\infty\exp(j\pi/2\nu)} e^{j(\gamma z+z^\nu/\nu)}\,dz\,;\ \ \nu \text{ is odd.} \tag{4.74}$$

From (4.24), (4.25), (4.27), (4.28), and (4.53) along with some algebraic manipulations, the parameters α_p, γ_p, and $\vec{\epsilon}_p$ are given by

$$\alpha_p = \vec{r}(Q_p)\cdot(\hat{s}^p - \hat{s}^i)\,, \tag{4.75}$$

$$\gamma_p = k^{(\nu-1)/\nu}\,|\cos\varphi_p' + \cos\varphi_p|\,\tilde{w}(Q_p,\nu)\,, \tag{4.76}$$

$$\vec{\epsilon}_p = \frac{e^{j\frac{\pi}{4}}k^{\frac{\nu-2}{2\nu}}}{\sqrt{2\pi}}\,L_p(\varphi_p',\varphi_p;\nu)\left[\hat{p}\cdot\left(-\hat{e}_\perp\hat{e}_\perp + \hat{e}_\parallel^i\hat{e}_\parallel^p\right)\right]\,, \tag{4.77}$$

where

$$\tilde{w}(Q_p,\nu) = \left|\frac{(\nu-1)!}{\widetilde{m}(Q_p,\nu)}\right|^{\frac{1}{\nu}}\,, \tag{4.78}$$

$$\widetilde{m}(Q_p,\nu) = -\kappa^{(\nu-2)}(Q_p)\,\hat{n}_p\cdot(\hat{s}-\hat{s}^i)\,,\ \text{ and} \tag{4.79}$$

$$L_p(\varphi_p',\varphi_p;\nu) = \tilde{w}(Q_p,\nu)\cos\left(\frac{\varphi_p'-\varphi_p}{2}\right)\,. \tag{4.80}$$

The angles φ_p' and φ_p are defined in Figure 4.5, $\kappa^{(\nu-2)}(Q_p)$ is the $\nu-2$th derivative of the surface curvature at Q_p, and $\hat{n}_p$ is the outward unit normal at Q_p. Thus, using (4.75)–(4.77) the zero-curvature diffracted field from a concave-convex polynomial boundary may be written as follows:

$$\vec{E}^p(\theta',\theta;\rho) \sim u_0\,\vec{E}^i(Q_p)\cdot\bar{\bar{D}}^{co}(Q_p)\,e^{jk\hat{s}^p(Q_p)\cdot\hat{s}^p}\,\frac{e^{-jk\rho}}{\sqrt{\rho}}\,, \tag{4.81}$$

where $\vec{E}^i(Q_p)$ is the incident plane wave at Q_p given in (4.20), and $\bar{\bar{D}}^{co}(Q_p)$ is the EUTD dyadic odd order zero-curvature diffraction coefficient given by

$$\bar{\bar{D}}^{co}(Q_p) = \mathcal{D}_s^{co}(\varphi_p',\varphi_p;\nu)\,\hat{e}_\perp\hat{e}_\perp + \mathcal{D}_h^{co}(\varphi_p',\varphi_p;\nu)\,\hat{e}_\parallel^i\hat{e}_\parallel^p\,, \tag{4.82}$$

$$\mathcal{D}_{s,h}^{co}(\varphi_p',\varphi_p;\nu) = \mp\frac{e^{j\frac{\pi}{4}}k^{\frac{\nu-2}{2\nu}}}{\sqrt{2\pi}}\,L_p(\varphi_p',\varphi_p;\nu)\begin{cases} I_{p\ell}(-\gamma_p,\nu)\,, & \text{(lit side)} \\ I_{pd}(\gamma_p,\nu)\,. & \text{(dark side)} \end{cases} \tag{4.83}$$

Notice that when $\nu = 3$, $I_{p\ell}(-\gamma_p,3) = 0$ and the EUTD expression for the zero-curvature diffracted field is equivalent to the complex ray field solution derived in

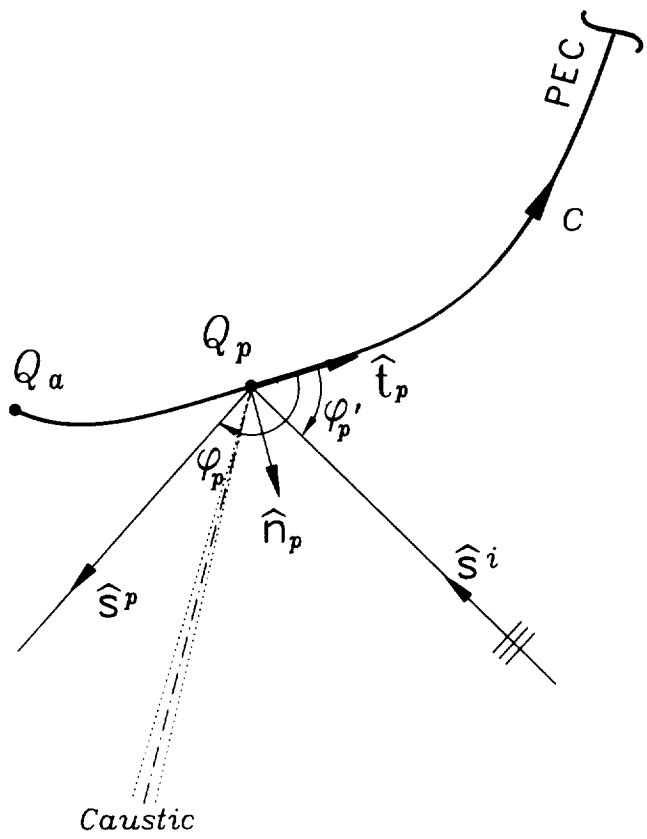

Figure 4.6: Diffraction from an even order zero-curvature point.

Chapter 2 specialized for the case of plane wave incidence with the observer in the far-zone.

B. Diffraction from an even order zero-curvature point

The geometry for the diffracted field from an even order zero-curvature point is shown in Figure 4.6. Using Equations (4.22), (4.47), (4.48), and the appropriate expression for $\overline{K}_{\omega}(\gamma, \zeta, \nu)$ for ν even and $\zeta < 0$ in Appendix C, the even order zero-curvature diffracted field on either side of the caustic is given by

$$\vec{E}^p(\theta', \theta; \rho) \sim u_0 \, e^{jka_p} \, \vec{\epsilon}_p \, J_p^*(\gamma_p, \nu) \, \frac{e^{-jk\rho}}{\sqrt{\rho}}; \text{ if } m(x_p, \nu) < 0, \tag{4.84}$$

$$\vec{E}^p(\theta', \theta; \rho) \sim u_0 \, e^{jka_p} \, \vec{\epsilon}_p \, J_p(\gamma_p, \nu) \, \frac{e^{-jk\rho}}{\sqrt{\rho}}; \text{ if } m(x_p, \nu) > 0. \tag{4.85}$$

Again, the sign of $m(x_p, \nu)$ depends on which side of the polynomial boundary is illuminated, with $m(x_p, \nu) < 0$ corresponding to the situation depicted in Figure 4.6.

The parameters u_0, α_p, γ_p, and $\vec{\epsilon}_p$ are the same as in the odd order zero-curvature diffraction case. The function $J_p(\gamma,\nu)$ is defined as follows:

$$J_p(\gamma,\nu) \triangleq \int_{\infty\exp[j(\pi-3\pi/2\nu)]}^{\infty\exp(j\pi/2\nu)} e^{j(\gamma z+z^\nu/\nu)}\,dz\,;\quad \nu \text{ is even.} \tag{4.86}$$

Thus, using (4.75)–(4.77) the even order zero-curvature diffracted field may be written as follows:

$$\vec{E}^p(\theta',\theta;\rho) \sim u_0\,\vec{E}^i(Q_p)\cdot\bar{\bar{\mathcal{D}}}^{ce}(Q_p)\,e^{jk\hat{\rho}(Q_p)\cdot\hat{s}^p}\,\frac{e^{-jk\rho}}{\sqrt{\rho}}\,, \tag{4.87}$$

where $\vec{E}^i(Q_p)$ is the incident plane wave at Q_p given in (4.20), and $\bar{\bar{\mathcal{D}}}^{ce}(Q_p)$ is the EUTD dyadic even order zero-curvature diffraction coefficient given by

$$\bar{\bar{\mathcal{D}}}^{ce}(Q_p) = \mathcal{D}_s^{ce}(\varphi_p',\varphi_p;\nu)\,\hat{e}_\perp\hat{e}_\perp + \mathcal{D}_h^{ce}(\varphi_p',\varphi_p;\nu)\,\hat{e}_\parallel^i\hat{e}_\parallel^p\,, \tag{4.88}$$

$$\mathcal{D}_{s,h}^{ce}(\varphi_p',\varphi_p;\nu) = \mp\frac{e^{j\frac{\pi}{4}}k^{\frac{\nu-2}{2\nu}}}{\sqrt{2\pi}}\,L_p(\varphi_p',\varphi_p;\nu)\begin{cases} J_p^*(\gamma_p,\nu) & \text{if } m(x_p,\nu)<0,\\ J_p(\gamma_p,\nu) & \text{if } m(x_p,\nu)>0.\end{cases} \tag{4.89}$$

4.2.4 Edge diffracted field contribution

The geometry for the edge diffracted field from a polynomial boundary is shown in Figures 4.7a and 4.7b. Unlike the reflected and zero-curvature diffracted fields, the two methods of analysis employed in Chapter 2, namely Chester's expansion and the method of steepest descent, result in two different expressions for the edge diffracted field. However, the resulting diffraction coefficients make use of the same transition function and are in agreement to the first order term for observation points near the RSB. They also reduce to the exact expression for the half-plane diffraction coefficient outside the transition regions. When $\nu = 3$, the general transition function reduces to the EUTD transition function derived in Chapter 2. The results obtained using Chester's expansion method will be considered first.

A. Chester's expansion formulation for the edge diffracted field

Using (4.22), (4.47), (4.48), and the appropriate expression for $\overline{K}_\omega(\gamma,\zeta,\nu)$ in Appendix C, the edge diffracted field may be written as follows:

$$\vec{E}_1^d(\theta',\theta;\rho) \sim \{e^{jka_a}\,\vec{\epsilon}_a\,I_a(\gamma_a,\zeta_a,\nu)$$

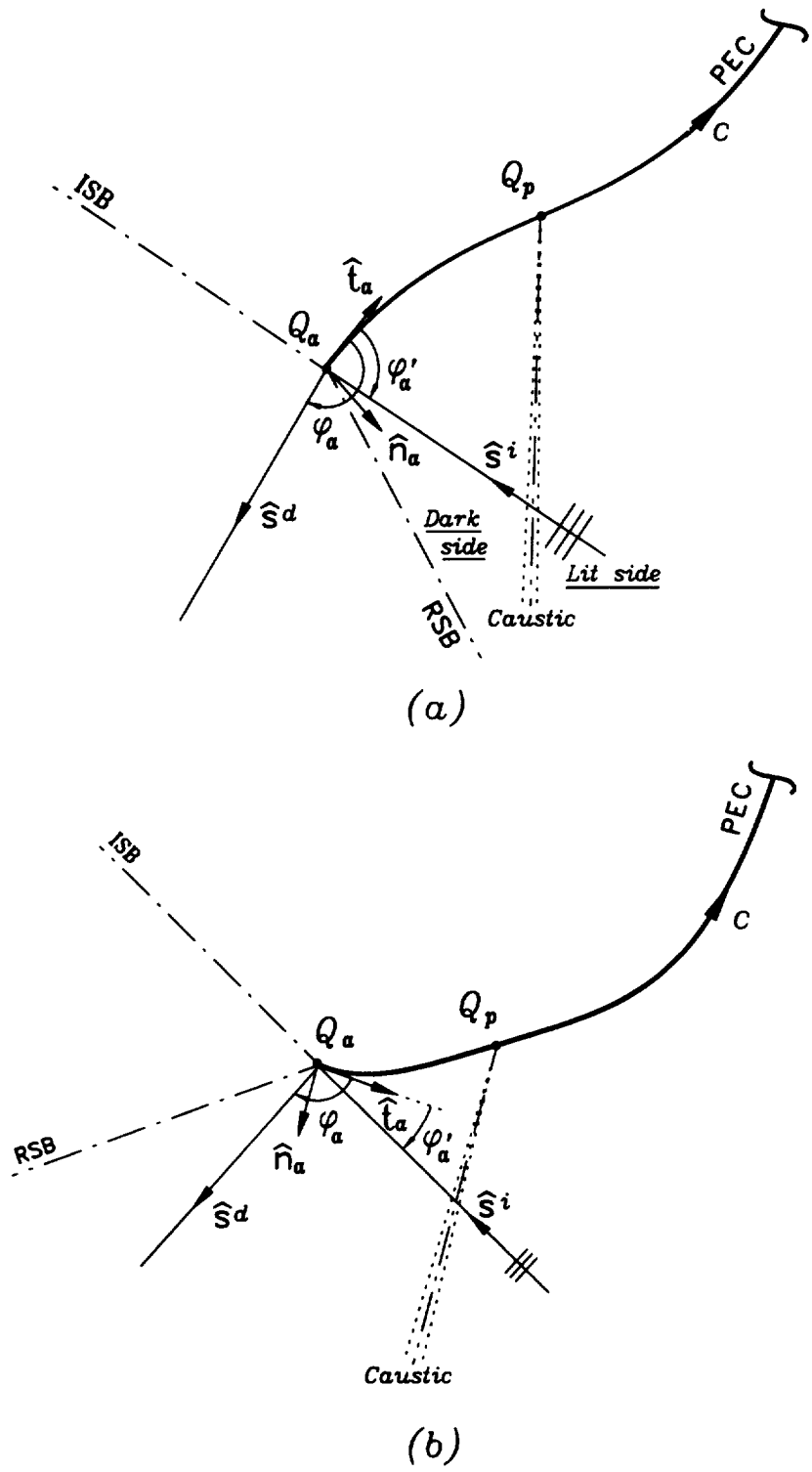

Figure 4.7: Diffraction from an edge in a polynomial boundary: (a) concave-convex case, (b) strictly concave or convex case.

$$+ \quad e^{jk\phi(\ell_a)} \left[\frac{j\vec{F}(\ell_a)}{k\phi'(\ell_a)} + \frac{\vec{\epsilon}_a}{j\,(\gamma + \zeta_a^{\nu-1})} \right] \Bigg\} \frac{e^{-jk\rho}}{\sqrt{\rho}}\,; \ \text{if } m(x_p,\nu) > 0, \quad (4.90)$$

$$\vec{E}_1^d(\theta',\theta;\rho) \ \sim \ \{ e^{jk\alpha_a}\, \vec{\epsilon}_a\, I_a^*(\gamma_a,\zeta_a,\nu)$$
$$+ \quad e^{jk\phi(\ell_a)} \left[\frac{j\vec{F}(\ell_a)}{k\phi'(\ell_a)} - \frac{\vec{\epsilon}_a}{j\,(\gamma + \zeta_a^{\nu-1})} \right] \Bigg\} \frac{e^{-jk\rho}}{\sqrt{\rho}}\,; \ \text{if } m(x_p,\nu) < 0. \quad (4.91)$$

From (4.24)–(4.26) and (4.49)–(4.53) along with some algebraic manipulations, the parameters α_a, γ_a, ζ_a, and $\vec{\epsilon}_a$ are given by

$$\alpha_a \ = \ \vec{r}(Q_a)\cdot(\hat{s}^d - \hat{s}^i) - u_p k^{-1}\,(\gamma_a\zeta_a + \zeta_a^\nu/\nu)\,, \quad (4.92)$$

$$\gamma_a \ = \ u_p\, k^{(\nu-1)/\nu}\,(\cos\varphi_p' + \cos\varphi_p)\, w(x_p,\nu)\,, \quad (4.93)$$

$$\zeta_a \ = \ u_a\, k^{1/\nu} \left| (\cos\varphi_a' + \cos\varphi_a)\, w(a,\nu) - (\cos\varphi_p' + \cos\varphi_p)\, w(x_p,\nu) \right|^{\frac{1}{\nu-1}}\,, \quad (4.94)$$

$$\vec{\epsilon}_a \ \approx \ u_p\,(\gamma_a + \zeta_a^{\nu-1})\, \frac{\vec{f}(\ell_a)}{k\phi'(\ell_a)}\,, \quad (4.95)$$

where u_p and $w(x,\nu)$ are given in (4.50) and (4.52), respectively, and

$$\vec{f}(\ell_a) = \sqrt{\frac{jk}{2\pi}} \left[\hat{p}\cdot\left(-\hat{e}_\perp\hat{e}_\perp + \hat{e}_\parallel^i\hat{e}_\parallel^d \right) \right] \cos\left(\frac{\varphi_a' - \varphi_a}{2} \right)\,. \quad (4.96)$$

The function $I_a(\gamma,\zeta,\nu)$ is defined as follows:

$$I_a(\gamma,\zeta,\nu) \ \triangleq \ \int_\zeta^{\infty\, \exp[j\psi_0(\nu)]} e^{j(\gamma z + z^\nu/\nu)}\, dz\,; \ \zeta > 0\,, \quad (4.97)$$

$$I_a(\gamma,\zeta,\nu) \ = \ \left\{ \begin{array}{ll} -I_a^*(\gamma,-\zeta) & \text{if } \nu \text{ is odd} \\ -I_a(-\gamma,-\zeta) & \text{if } \nu \text{ is even,} \end{array} \right\} \ \text{if } \zeta < 0, \quad (4.98)$$

$$\psi_0(\nu) \ = \ \left\{ \begin{array}{ll} \pi/2\nu & \text{if } [\mathrm{sgn}(\zeta)]^{\nu-1}\,(\gamma + \zeta^{\nu-1}) > 0 \\ -3\pi/2\nu & \text{otherwise.} \end{array} \right. \quad (4.99)$$

Also, from (4.24) and (4.25) we have that

$$\vec{F}(\ell_a) \ = \ \sqrt{\frac{jk}{2\pi}} \left[\hat{p}\cdot\left(-\sin\varphi_a'\,\hat{e}_\perp\hat{e}_\perp + \sin\varphi_a\,\hat{e}_\parallel^i\hat{e}_\parallel^d \right) \right]\,, \quad (4.100)$$

$$\phi'(\ell_a) \ = \ \cos\varphi_a' + \cos\varphi_a\,. \quad (4.101)$$

Thus, using (4.92), (4.95), (4.96), (4.97)–(4.101) and the PO correction factors in (2.117) and (2.118), the edge diffracted field may be written as follows:

$$\vec{E}_1^d(\theta',\theta;\rho) \ \sim \ \vec{E}^i(Q_a)\cdot\bar{\bar{D}}_1^e(Q_a)\, e^{jk\hat{r}(Q_a)\cdot\hat{s}^d}\, \frac{e^{-jk\rho}}{\sqrt{\rho}}\,, \quad (4.102)$$

$$\bar{\bar{\mathcal{D}}}_i^e(Q_a) = \mathcal{D}_s^{e1}(\varphi_a', \varphi_a)\,\hat{e}_\perp\hat{e}_\perp + \mathcal{D}_h^{e1}(\varphi_a', \varphi_a)\,\hat{e}_\parallel^i\hat{e}_\parallel^d, \tag{4.103}$$

$$\mathcal{D}_{s,h}^{e1}(\varphi_a', \varphi_a) = \frac{-e^{-j\frac{\pi}{4}}}{2\sqrt{2\pi k}}\left[\frac{1}{\cos\left(\frac{\varphi_a'-\varphi_a}{2}\right)} \mp \frac{\mathcal{F}(\gamma_d, \zeta_d, \nu)}{\cos\left(\frac{\varphi_a'+\varphi_a}{2}\right)}\right], \tag{4.104}$$

$$\gamma_d = \begin{cases} \gamma_a & \text{if } \nu \text{ is odd} \\ \mathrm{sgn}(\zeta_a)\gamma_a & \text{if } \nu \text{ is even,} \end{cases} \tag{4.105}$$

$$\zeta_d = |\zeta_a|\,. \tag{4.106}$$

The EUTD transition function $\mathcal{F}(\gamma, \zeta, \nu)$ is defined as follows:

$$\mathcal{F}(\gamma, \zeta, \nu) \triangleq j\,(\gamma + \zeta^{\nu-1})\; I_a^*(\gamma, \zeta, \nu)\, e^{j(\gamma\zeta + \zeta^\nu/\nu)}, \tag{4.107}$$

and when $\nu = 3$, it reduces to the expression derived in Chapter 2 and given in (2.185). It is also understood that when $\rho_g(Q_a) < 0$, the complex conjugate version of $\mathcal{F}(\gamma, \zeta, \nu)$ should be used in (4.104).

When the observation direction is near an optical boundary and far removed from the caustic, that is $\gamma_d + \zeta_a^{\nu-1} \approx 0$ with $\gamma_d \ll -1$, $I_a(\gamma, \zeta, \nu)$ can be expressed in terms of the Fresnel integral and the transition function $\mathcal{F}(\gamma, \zeta, \nu)$ reduces to the UTD transition function $F(x)$ as was shown in Chapter 2 for the $\nu = 3$ case. Therefore, near the optical boundaries and away from composite shadow boundaries the EUTD diffraction coefficient in (4.104) is in agreement with the regular UTD diffraction coefficient. In addition, away from transition regions, that is $\gamma_d + \zeta_d^{\nu-1} \gg 1$, it can be easily shown by employing integration by parts in (4.97) that $\mathcal{F}(\gamma, \zeta, \nu) \to 1$ and (4.104) reduces to the exact expression for the half-plane diffraction coefficient.

B. Steepest descent formulation for the edge diffracted field

For the steepest descent analysis we begin with the expression for the scattered field in (4.22) and (4.23), that is

$$\vec{E}^s(\theta', \theta; \rho) \approx e^{jk\alpha}\,\vec{I}_s(\beta, s_a, \nu; k)\,\frac{e^{-jk\rho}}{\sqrt{\rho}}, \tag{4.108}$$

where α, β, and s_a are given in (4.27), (4.28), and (4.30), respectively, and $m(x_p, \nu)$ given in (4.34) is taken as positive in the analysis that follows. $\vec{I}_s(\beta, s_a, \nu; k)$ is a

stationary phase integral in the complex s–plane and is given by

$$\vec{I}_s(\beta, s_a, \nu; k) = \int_{s_a}^{\infty} \vec{G}(s)\, e^{jk(\beta s + s^\nu/\nu)}\, ds\,. \tag{4.109}$$

$\vec{I}_s(\beta, s_a, \nu; k)$ has the same complex plane topology as the generalized incomplete Airy integral in Appendix C. Thus, by deforming the original path of integration in (4.109) into the appropriate steepest descent paths through the integration endpoint as shown in Figures C.1–C.3, the edge diffracted field contribution in (4.108) may be written as follows:

$$\vec{E}_2^d(\theta', \theta; \rho) \approx e^{jk\alpha}\, \vec{I}_d(\beta, s_a, \nu; k)\, \frac{e^{-jk\rho}}{\sqrt{\rho}}\,, \tag{4.110}$$

where

$$\vec{I}_d(\beta, s_a, \nu; k) = \int_{s_a}^{\infty \exp[j\psi_d(\nu)]} \vec{G}(s)\, e^{jk(\beta s + s^\nu/\nu)}\, ds\,, \tag{4.111}$$

$$\psi_d(\nu) = \left\{ \begin{array}{ll} \pi/2\nu & \text{if } \beta + s_a^{\nu-1} > 0 \\ -3\pi/2\nu & \text{otherwise} \end{array} \right\};\ \text{for } s_a > 0, \tag{4.112}$$

$$= \left\{ \begin{array}{ll} \pi - \pi/2\nu & \text{if } \beta + s_a^{\nu-1} > 0 \\ -\pi + 3\pi/2\nu & \text{otherwise} \end{array} \right\};\ \text{for } s_a < 0 \text{ and } \nu \text{ odd}, \tag{4.113}$$

$$= \left\{ \begin{array}{ll} -\pi + \pi/2\nu & \text{if } \beta + s_a^{\nu-1} < 0 \\ \pi - 3\pi/2\nu & \text{otherwise} \end{array} \right\};\ \text{for } s_a < 0 \text{ and } \nu \text{ even}. \tag{4.114}$$

Next, it is assumed that $\vec{G}(s)$ is regular and slowly varying along the path of integration in (4.111) and thus, for large k the principal contribution to the integral would come from the neighborhood of the integration endpoint. Upon expanding $\vec{G}(s)$ in Taylor series around s_a and making the substitution $s = tk^{-1/\nu}$, the edge diffracted field may be written as follows:

$$\vec{E}_2^d(\theta', \theta; \rho) \sim e^{jk\alpha_a} \frac{\vec{F}(\ell_a)}{k\phi'(\ell_a)}\, (\gamma_a + \zeta_a^{\nu-1})\, I_a(\gamma_a, \zeta_a, \nu)\, \frac{e^{-jk\rho}}{\sqrt{\rho}} \tag{4.115}$$

$$\text{if} \quad m(x_p, \nu) > 0\,,$$

$$\vec{E}_2^d(\theta', \theta; \rho) \sim -e^{jk\alpha_a} \frac{\vec{F}(\ell_a)}{k\phi'(\ell_a)}\, (\gamma_a + \zeta_a^{\nu-1})\, I_a^*(\gamma_a, \zeta_a, \nu)\, \frac{e^{-jk\rho}}{\sqrt{\rho}} \tag{4.116}$$

$$\text{if} \quad m(x_p, \nu) < 0\,,$$

where α_a, γ_a, ζ_a are the same as in (4.92)–(4.94) and $I_a(\gamma,\zeta,\nu)$ is defined in (4.97)–(4.99). Finally, using (4.100), (4.101) and the PO correction factors in (2.117) and (2.118) the steepest descent formulation for the edge diffracted field for the case of $\rho_g(Q_a) > 0$ is given by

$$\vec{E}_2^d(\theta',\theta;\rho) \sim \vec{E}^i(Q_a)\cdot\bar{\bar{D}}_2^e(Q_a)\, e^{jk\hat{s}^i(Q_a)\cdot\hat{s}^d}\,\frac{e^{-jk\rho}}{\sqrt{\rho}}, \tag{4.117}$$

$$\bar{\bar{D}}_2^e(Q_a) = \mathcal{D}_s^{e2}(\varphi_a',\varphi_a)\,\hat{e}_\perp\hat{e}_\perp + \mathcal{D}_h^{e2}(\varphi_a',\varphi_a)\,\hat{e}_\parallel^i\hat{e}_\parallel^d, \tag{4.118}$$

$$\mathcal{D}_{s,h}^{e2}(\varphi_a',\varphi_a) = \frac{-e^{-j\frac{\pi}{4}}}{2\sqrt{2\pi k}}\left[\frac{1}{\cos\left(\frac{\varphi_a'-\varphi_a}{2}\right)} \mp \frac{1}{\cos\left(\frac{\varphi_a'+\varphi_a}{2}\right)}\right]\mathcal{F}(\gamma_d,\zeta_d,\nu), \tag{4.119}$$

where γ_d, ζ_d, and $\mathcal{F}(\gamma,\zeta,\nu)$ are the same as in (4.105)–(4.107). When $\rho_g(Q_a) < 0$ the complex conjugate of $\mathcal{F}(\gamma,\zeta,\nu)$ should be used in (4.119).

The major difference between the steepest descent diffraction coefficient in (4.119) and the diffraction coefficient in (4.104) derived using Chester's expansion method is that in (4.119) the transition function operates on the entire non-uniform coefficient as opposed to the Chester expansion formulation in (4.104) where the transition function operates only on the reflection term of the non-uniform coefficient. Thus, near the RSB and away from the caustic, (4.119) would be in agreement with the UTD diffraction coefficient only to the first order term. Away from transition regions, however, it reduces to the exact expression for the half-plane diffraction coefficient as well.

4.3 Uniform asymptotic analysis (3–D case)

The surfaces considered for the 3–D analysis are assumed to be rotationally symmetric or slowly varying in the transverse direction, with the 2–D polynomial boundaries of Figure 4.2 in the previous section being the generator curves representing one of the principal coordinate curves of the 3–D surface. The general procedure employed in this section is very similar to the one employed in Chapter 3 for the near-zone problem. Hence, some of the details will be omitted.

As usual, the electric field $\vec{E}^s$ scattered from a 3–D polynomial surface containing an edge illuminated by a plane wave and observed at a point P in the far-zone of the

surface is expressed in terms of the radiation integral over the electric current $\vec{J}$ on S, that is

$$\vec{E}^s(P) \approx \frac{jkZ_0}{4\pi} \iint_S \left[\hat{s} \times \hat{s} \times \vec{J}(Q')\right] \frac{e^{-jkR}}{R}\, ds', \tag{4.120}$$

where

$$R = \left|\overline{Q'P}\right| \approx r_o - \vec{r}(Q') \cdot \hat{s}, \text{ (far-zone approximation)} \tag{4.121}$$

$$\hat{s} = \hat{x} \sin\theta_o \cos\varphi_o + \hat{y} \sin\theta_o \sin\varphi_o + \hat{z} \cos\theta_o, \tag{4.122}$$

$$\hat{s}^i = -\hat{x} \sin\theta'_o \cos\varphi'_o - \hat{y} \sin\theta'_o \sin\varphi'_o - \hat{z} \cos\theta'_o, \tag{4.123}$$

Q' is any point on S, $r_o = \left|\overline{OP}\right|$ is the distance between the origin of the reference coordinate system and the observation point, $\vec{r}(Q') = \overline{OQ'}$ is the surface vector, and $\hat{s}^i$, $\hat{s}$ are the directions of incidence and observation, respectively. The PO approximation to (4.120) is employed once again using the GO currents in (2.2) with the incident magnetic field under the plane wave assumption given in (4.18). Thus, the far-zone scattered electric field may be written as follows:

$$\vec{E}^s(\theta'_o, \varphi'_o, \theta_o, \varphi_o; r_o) \approx \vec{e}(\theta'_o, \varphi'_o, \theta_o, \varphi_o) \frac{e^{-jkr_o}}{r_o}, \tag{4.124}$$

where $R \approx r_o$ was used for the magnitude term in (4.120). The vector quantity $\vec{e}(\theta'_o, \varphi'_o, \theta_o, \varphi_o)$ is the angular field dependence and is given by the following stationary phase integral:

$$\vec{e}(\theta'_o, \varphi'_o, \theta_o, \varphi_o) \approx \int_{\ell_a}^{\infty} \int_{-\infty}^{\infty} \vec{F}(\ell', \tau')\, e^{jk\phi(\ell', \tau')}\, d\ell' d\tau', \tag{4.125}$$

where

$$\vec{F}(\ell', \tau') = \frac{jk}{2\pi} \left\{\hat{s} \times \hat{s} \times [\hat{n}(\ell', \tau') \times \hat{s}^i \times \hat{p}]\right\}, \tag{4.126}$$

$$\phi(\ell', \tau') = \vec{r}(\ell', \tau') \cdot (\hat{s} - \hat{s}^i), \tag{4.127}$$

$\hat{n}(\ell', \tau')$ is the outward unit normal to the surface at Q', and ℓ', τ' are the principal coordinate curves of the 3–D polynomial surface S. The edge is located at (ℓ_a, τ') and therefore extends along the principal coordinate curve τ' which is assumed to have a slowly varying curvature. The next step in the procedure is the uniform asymptotic evaluation of $\vec{e}(\theta'_o, \varphi'_o, \theta_o, \varphi_o)$.

4.3.1 Uniform asymptotic evaluation of $\vec{e}(\theta_o', \varphi_o', \theta_o, \varphi_o)$

First, it is assumed that the 3–D polynomial surface contains an isolated zero-curvature line that satisfies the following relation:

$$c(\tau') = \ddot{\vec{r}}_{\ell\ell}(\ell', \tau')\Big|_{\ell'=\ell_p} = 0\,, \tag{4.128}$$

and is arbitrarily close to the edge. Also, the phase function in (4.127) contains at least one real and a number of complex stationary phase points that are situated near the zero curvature line and satisfy the stationary phase condition given in (3.8). The corresponding zero-curvature diffraction point is a stationary point along the zero-curvature line, it has coordinates $Q_p = (\ell_p, \tau_s)$ and it can be arbitrarily close to the edge diffraction point with coordinates $Q_a = (\ell_a, \tau_s)$. The zero-curvature diffraction point satisfies the following phase condition:

$$\ddot{\phi}_{\ell\ell}(\ell', \tau') = \ddot{\vec{r}}_{\ell\ell}(\ell_p, \tau_s) = 0 \text{ and } \dot{\phi}_{\tau}(\ell', \tau') = \hat{\tau}_p \cdot (\hat{s} - \hat{s}^i) = 0\,, \tag{4.129}$$

where $\hat{\tau}_p$ is the unit tangent along the zero-curvature line at Q_p. The second condition in (4.129) is analogous to the law of edge diffraction, and both conditions in (4.129) must be satisfied simultaneously at the zero curvature point. If l is the order of the zero curvature point, that is $Q_p = (\ell_p, \tau_s)$ is an lth order root of $\ddot{\vec{r}}_{\ell\ell}(\ell', \tau_s) = 0$, we have that

$$\frac{\partial^n}{\partial \ell'^n}\vec{r}(\ell', \tau')\Big|_{(\ell_p, \tau_s)} = 0\,;\ \ 2 \le n \le l+1\,, \tag{4.130}$$

and $\phi(\ell', \tau')$ contains $l+1$ stationary phase points. When l is even, the surface near the zero-curvature point along the ℓ' principal coordinate is strictly concave or convex, and one of the stationary phase points is real and corresponds to a single specular reflection point. When l is odd, the surface near the zero-curvature point along the ℓ' principal coordinate is concave-convex, and two of the stationary phase points are real and correspond to a pair of specular reflection points for observation directions in the lit side of the caustic. In the dark side of the caustic all stationary phase points are complex.

The 3–D analysis can be effectively reduced to a 2–D situation using the same procedure employed in Chapter 3, that is a local quadratic approximation is initially

used for the phase function and the integral along the τ' principal coordinate is evaluated using the stationary phase method. Thus, $\vec{e}(\theta'_o, \varphi'_o, \theta_o, \varphi_o)$ is given by the following expression:

$$\vec{e}(\theta'_o, \varphi'_o, \theta_o, \varphi_o) \approx \int_{\ell_a}^{\infty} \vec{G}(\ell', \tau_s)\, e^{jk\psi(\ell', \tau_s)}\, d\ell' \,, \tag{4.131}$$

where

$$\vec{G}(\ell', \tau_s) = \sqrt{\frac{jk}{2\pi}}\, \frac{\hat{s} \times \hat{s} \times [\hat{n}(\ell', \xi_s) \times \hat{s}^i \times \hat{p}]}{\sqrt{|\ddot{\phi}_{\tau\tau}(\ell', \tau_s)|}} \,, \tag{4.132}$$

$$\psi(\ell', \tau_s) = \phi(\ell', \tau_s) - \frac{\dot{\phi}_\tau^2(\ell', \tau_s)}{2\ddot{\phi}_{\tau\tau}(\ell', \tau_s)} \,, \tag{4.133}$$

$$\xi_s = \tau_s - \frac{\dot{\phi}_\tau(\ell', \tau_s)}{2\ddot{\phi}_{\tau\tau}(\ell', \tau_s)} \,, \text{ and} \tag{4.134}$$

$$\ddot{\phi}_{\tau\tau}(\ell', \tau_s) \neq 0 \;\forall\, \ell' \,. \tag{4.135}$$

The asymptotic reduction of the integral in (4.131) would follow the same steps as the asymptotic reduction of the integral in (4.23). Therefore, the following transformation is introduced in (4.131):

$$\psi(\ell', \tau_s) = \tilde{\psi}(t) = \alpha + \beta t + \frac{t^\nu}{\nu} \,, \tag{4.136}$$

where $\nu = l + 2$, and

$$\alpha = \phi(\ell_p, \tau_s) = \vec{r}(Q_p) \cdot \left(\hat{s} - \hat{s}^i\right) \tag{4.137}$$

$$\beta = \hat{\ell}_p \cdot \left(\hat{s} - \hat{s}^i\right) \left.\frac{d\ell'}{dt}\right|_{t=0} \,, \tag{4.138}$$

and $\hat{\ell}_p$ is the principal unit tangent at Q_p along the ℓ' surface coordinate. Hence, using (4.136) the field angular dependance is given by

$$\vec{e}(\theta'_o, \varphi'_o, \theta_o, \varphi_o) \approx e^{jk\alpha} \int_{t_a}^{\text{"}\infty\text{"}} \vec{\mathcal{G}}(t)\, e^{jk(\beta t + t^\nu/\nu)}\, dt \,, \tag{4.139}$$

where

$$t_a = u_a \left[\hat{\ell}_a \cdot (\hat{s} - \hat{s}^i) \left.\frac{d\ell'}{dt}\right|_{t=t_a} - \hat{\ell}_p \cdot (\hat{s} - \hat{s}^i) \left.\frac{d\ell'}{dt}\right|_{t=0}\right]^{\frac{1}{\nu-1}} \,, \tag{4.140}$$

$$u_a = \begin{cases} +1 & \text{if } Q_p \ni S \\ -1 & \text{if } Q_p \in S, \end{cases} \tag{4.141}$$

$$\vec{\mathcal{G}}(t) = \vec{G}(\ell', \tau_s)\frac{d\ell'}{dt}, \tag{4.142}$$

$$\frac{d\ell'}{dt} = \frac{d\ell'}{dv}\frac{dv}{dt} = \left[\frac{(\nu-1)!}{m(v,\nu)}\right]^{\frac{1}{\nu}}, \tag{4.143}$$

$$m(v,\nu) = \frac{\vec{r}^{(\nu)}(v_p)\cdot(\hat{s}-\hat{s}^i)}{|\vec{r}'(v)|^{\nu}}, \tag{4.144}$$

and $\vec{r}(v)$ is the parametric generator polynomial boundary of the 3–D surface, or a parametric representation of the ℓ' principal coordinate curve. The proper branches for β, t_a and $d\ell'/dt$ depend on the sign of $m(v_p,\nu)$ and as usual "∞" $= \infty\exp(-j\arg(d\ell'/dt))$. The asymptotic evaluation of (4.139) is then carried out by employing the generalized Chester expansion [22], and in exactly the same manner as was done for the 2–D case in the previous section. Without any further details, the field angular dependence is given by the following expression:

$$\vec{e}(\theta_o',\varphi_o',\theta_o,\varphi_o) \sim \frac{e^{jk\alpha}}{\sqrt{k}}\vec{\epsilon}_0\,\overline{K}_\omega(\gamma,\zeta_a,\nu) + e^{jk\psi(\ell_a,\tau_s)}\left[\frac{j\vec{G}(\ell_a,\tau_s)}{k\dot{\psi}(\ell_a,\tau_s)} + \frac{\vec{\epsilon}_0}{j\sqrt{k}\,(\gamma+\zeta_a)^{\nu-1}}\right];\ \text{if } m(v_p,\nu)>0, \tag{4.145}$$

$$\vec{e}(\theta_o',\varphi_o',\theta_o,\varphi_o) \sim \frac{e^{jk\alpha}}{\sqrt{k}}\vec{\epsilon}_0\,\overline{K}^*_\omega(\gamma,\zeta_a,\nu) + e^{jk\psi(\ell_a,\tau_s)}\left[\frac{j\vec{G}(\ell_a,\tau_s)}{k\dot{\psi}(\ell_a,\tau_s)} - \frac{\vec{\epsilon}_0}{j\sqrt{k}\,(\gamma+\zeta_a)^{\nu-1}}\right];\ \text{if } m(v_p,\nu)<0, \tag{4.146}$$

where $\overline{K}_\omega(\gamma,\zeta,\nu)$ is the generalized incomplete Airy integral [22] defined in (4.54). The parameters γ, ζ_a, and $\vec{\epsilon}_0$ are given by the following expressions:

$$\gamma = u_p k^{(\nu-1)/\nu}\hat{\ell}_p\cdot\left(\hat{s}-\hat{s}^i\right)w(v_p,\nu), \tag{4.147}$$

$$u_p = \text{sgn}[m(v_p,\nu)], \tag{4.148}$$

$$\zeta_a = u_a k^{1/\nu}\left|\hat{\ell}_a\cdot\left(\hat{s}-\hat{s}^i\right)w(v_a,\nu) - \hat{\ell}_p\cdot\left(\hat{s}-\hat{s}^i\right)w(v_p,\nu)\right|^{\frac{1}{\nu-1}}, \tag{4.149}$$

$$w(v,\nu) = \left|\frac{(\nu-1)!}{m(v_p,\nu)}\right|^{\frac{1}{\nu}}, \tag{4.150}$$

$$\vec{\epsilon}_0 = \frac{(-\gamma)^{\frac{\nu-2}{2(\nu-1)}}}{\nu-1}\sum_{k=1}^{\nu-1}\vec{G}(\ell_k,\tau_s)\sqrt{\frac{\nu-1}{|\ddot{\psi}(\ell_k,\tau_s)|}}, \tag{4.151}$$

where (ℓ_k, τ_s), $k = 1, 2, \cdots, \nu - 1$ are the stationary phase points of $\psi(\ell', \tau_s)$. Also, using (4.127) and (4.132)–(4.134) we have the following relationships:

$$\psi(\ell_a, \tau_s) = \phi(\ell_a, \tau_s) = \vec{r}(Q_a) \cdot (\hat{s}^d - \hat{s}^i) \,, \tag{4.152}$$

$$\ddot{\psi}(\ell_k, \tau_s) = \ddot{\phi}(\ell_k, \tau_s) = -2\,\kappa_1(Q_k)\,\cos\theta_k^i \,, \tag{4.153}$$

$$\vec{G}(\ell_k, \tau_s) = \sqrt{\frac{jk}{2\pi}}\,\frac{\cos\theta_k^i\,\hat{p}\cdot\bar{\bar{R}}\,(Q_k)}{\sqrt{|\ddot{\phi}_{\tau\tau}(\ell_k, \tau_s)|}} \,, \tag{4.154}$$

$$\ddot{\phi}_{\tau\tau}(\ell_k, \tau_s) = -2\,\kappa_2(Q_k)\,\cos\theta_k^i \,, \tag{4.155}$$

$$\frac{\vec{G}(\ell_a, \tau_s)}{\dot{\psi}(\ell_a, \tau_s)} = jk\,\hat{p}\cdot\bar{\bar{D}}_{nu}\,(Q_a)\sqrt{\rho_a^d} \,, \tag{4.156}$$

$$\rho_a^d = \frac{R_a\,\sin^2\vartheta_a}{\hat{n}_e\cdot(\hat{s}^d - \hat{s}^i)} \,, \tag{4.157}$$

where $\bar{\bar{D}}_{nu}\,(Q_a)$ is non-uniform PO dyadic edge diffraction coefficient given in (3.68) and (3.69), ρ_a^d is the distance between the caustic at Q_a and the second caustic of the edge diffracted ray, $R_a > 0$ is the edge radius of curvature, ϑ_a is the usual angle of diffraction, and $\hat{n}_e$ is the unit edge normal.

Next, the scattering mechanisms in (4.145) and (4.146) are separated using the properties and complex plane topology of $\overline{K}_\omega(\gamma, \zeta, \nu)$ in Appendix C.

4.3.2 Reflected field contribution

There exist two cases for the reflection from a three dimensional polynomial surface as well. For the first case we consider a polynomial surface that contains an odd order zero-curvature line with ν odd in (4.145) and (4.146). The reflected field consists of two specular contributions in this case, that only exist on the lit side of the caustic. For the second case we consider a polynomial surface that contains an even order zero-curvature line with ν even in (4.145) and (4.146). The reflected field in this case consists of a single specular contribution that exists on both sides of the caustic.

A. Reflection near an odd order zero-curvature line

Using (4.124), (4.145), (4.146) and the appropriate expression for $\overline{K}_\omega(\gamma, \zeta, \nu)$ with ν odd and $\gamma < 0$ in Appendix C, the reflected field on the lit side of the caustic is given

by

$$\vec{E}^r(\theta_o', \varphi_o', \theta_o, \varphi_o; r_o) \sim \{u_1 e^{jk\alpha_1} \vec{\epsilon}_1 I_r(-\gamma_1, \nu) + u_2 e^{jk\alpha_2} \vec{\epsilon}_2 I_r^*(-\gamma_2, \nu)\} \frac{e^{-jkr_o}}{r_o}; \text{ if } m(v_p, \nu) < 0, \quad (4.158)$$

$$\vec{E}^r(\theta_o', \varphi_o', \theta_o, \varphi_o; r_o) \sim \{u_1 e^{jk\alpha_1} \vec{\epsilon}_1 I_r^*(-\gamma_1, \nu) + u_2 e^{jk\alpha_2} \vec{\epsilon}_2 I_r(-\gamma_2, \nu)\} \frac{e^{-jkr_o}}{r_o}; \text{ if } m(v_p, \nu) > 0, \quad (4.159)$$

where $u_{1,2} = 1$ if $Q_{1,2} \in S$ and zero otherwise, the function $I_r(\gamma, \nu)$ is defined in (4.57), $\alpha_{1,2}$, $\gamma_{1,2}$ are the same as in (4.58) and (4.59), and $\vec{\epsilon}_{1,2}$ for the 3-D case is given by

$$\vec{\epsilon}_{1,2} = e^{j\frac{\pi}{4}} \sqrt{\frac{\nu-1}{2\pi}} \gamma_{1,2}^{\frac{\nu-2}{2(\nu-1)}} \left[\hat{p} \cdot \bar{\bar{R}}(Q_{1,2})\right] \frac{1}{2} \sqrt{|R_1(Q_{1,2}) R_2(Q_{1,2})|}, \quad (4.160)$$

where $\bar{\bar{R}}(Q_{1,2})$ is the GO dyadic reflection coefficient given in (3.54) and (3.55), and $R_{1,2}(Q_{1,2})$ are the principal surface radii of curvature at $Q_{1,2}$. Thus, using (4.58) and (4.160) the reflected field from a polynomial surface that contains an odd order zero-curvature line for the case of $R_1(Q_1) < 0$, and $R_1(Q_2) > 0$ may be written as follows:

$$\vec{E}^r(\theta_o', \varphi_o', \theta_o, \varphi_o; r_o) \sim \left[\frac{u_1}{2} \vec{E}^i(Q_1) \cdot \bar{\bar{\mathcal{R}}}^*(Q_1) \sqrt{R_1(Q_1) R_2(Q_1)}\, e^{jk\hat{r}(Q_1)\cdot\hat{s}^r} + \frac{u_2}{2} \vec{E}^i(Q_2) \cdot \bar{\bar{\mathcal{R}}}(Q_2) \sqrt{R_1(Q_2) R_2(Q_2)}\, e^{jk\hat{r}(Q_2)\cdot\hat{s}^r}\right] \frac{e^{-jkr_o}}{r_o}, \quad (4.161)$$

where $\vec{E}^i(Q_{1,2})$ is the incident plane wave at $Q_{1,2}$ given in (4.20), $\bar{\bar{\mathcal{R}}}(Q_{1,2})$ is the UGO dyadic reflection coefficient given by

$$\bar{\bar{\mathcal{R}}}(Q_{1,2}) = \mathcal{R}_s(Q_{1,2})\, \hat{e}_\perp^i \hat{e}_\perp^r + \mathcal{R}_h(Q_{1,2})\, \hat{e}_\parallel^i \hat{e}_\parallel^r, \quad (4.162)$$

and $\mathcal{R}_{s,h}(Q_{1,2})$ are the same as in (4.63) and (4.64). It is also understood in (4.161) that if $R_1(Q_{1,2}) R_2(Q_{1,2}) < 0$, $\sqrt{R_1(Q_{1,2}) R_2(Q_{1,2})} = j\sqrt{|R_1(Q_{1,2}) R_2(Q_{1,2})|}$.

B. Reflection near an even order zero-curvature line

Using (4.124), (4.145), (4.146) and the appropriate expression for $\overline{K}_\omega(\gamma, \zeta, \nu)$ with ν even in Appendix C, the reflected field on either side of the caustic is given by

$$\vec{E}^r(\theta_o', \varphi_o', \theta_o, \varphi_o; r_o) \sim u_r e^{jk\alpha_r} \vec{\epsilon}_r I_r^*(-\gamma_r, \nu) \frac{e^{-jkr_o}}{r_o}; \text{ if } m(Q_p) < 0, \quad (4.163)$$

$$\vec{E}^r(\theta_o', \varphi_o', \theta_o, \varphi_o; r_o) \sim u_r e^{jk\alpha_r} \vec{\epsilon}_r I_r(-\gamma_r, \nu) \frac{e^{-jkr_o}}{r_o}; \text{ if } m(Q_p) > 0, \quad (4.164)$$

and $\vec{\epsilon}_p$ for the 3–D case are given by

$$\gamma_p = k^{(\nu-1)/\nu}\,\tilde{w}(Q_p,\nu)\,\sin\vartheta_p\,|\cos\varphi_p' + \cos\varphi_p|\,, \tag{4.169}$$

$$\vec{\epsilon}_p \approx \frac{e^{j\frac{\pi}{4}}k^{\frac{\nu-2}{2\nu}}}{\sin\vartheta_p\sqrt{2\pi}}\,L_p(\varphi_p',\varphi_p,\vartheta_p;\nu)\left[\hat{p}\cdot\left(-\hat{e}_\perp^{\,i}\hat{e}_\perp^{\,p}+\hat{e}_\parallel^{\,i}\hat{e}_\parallel^{\,p}\right)\right]\sqrt{\rho_p^d}\,, \tag{4.170}$$

where

$$\tilde{w}(Q_p,\nu) = \left|\frac{(\nu-1)!}{\widetilde{m}(Q_p,\nu)}\right|^{\frac{1}{\nu}}, \tag{4.171}$$

$$\widetilde{m}(Q_p,\nu) = -\kappa_1^{(\nu-2)}(Q_p)\hat{n}_p\cdot(\hat{s}-\hat{s}^{\,i})\,, \tag{4.172}$$

$$L_p(\varphi_p',\varphi_p,\vartheta_p,\nu) = \tilde{w}(Q_p,\nu)\,\sin\vartheta_p\cos\left(\frac{\varphi_p'-\varphi_p}{2}\right), \tag{4.173}$$

$$\rho_p^d = \frac{R_p\,\sin^2\vartheta_p}{\hat{n}_p\cdot(\hat{s}^{\,p}-\hat{s}^{\,i})}\,, \tag{4.174}$$

$\hat{n}_p$ is the outward unit normal at Q_p, ϑ_p is the angle between the tangent along the zero-curvature line at Q_p and the direction of incidence (analogous to the angle of diffraction,) φ_p', φ_p are the angles of incidence and observation, respectively, projected on the plane perpendicular to the tangent along the zero-curvature line at Q_p, ρ_p^d is the distance between the caustic at Q_p and the second caustic of the zero-curvature diffracted ray, $R_p > 0$ is the radius of curvature of the zero-curvature line, and $\hat{n}_p$ is the unit normal of the zero-curvature line at Q_p. Also, the $\nu-2$th derivative of the surface curvature in (4.172) is along the the ℓ' principal coordinate line. Thus, using (4.75), (4.169), and (4.170) the odd order zero-curvature diffracted field from a polynomial surface may be written as follows:

$$\vec{E}^{\,p}(\theta_o',\varphi_o',\theta_o,\varphi_o;r_o) \sim u_0\,\vec{E}^{\,i}(Q_p)\cdot\bar{\bar{\mathcal{D}}}^{\,co}(Q_p)\sqrt{\rho_p^d}\,e^{jk\vec{r}(Q_p)\cdot\hat{s}^p}\,\frac{e^{-jkr_o}}{r_o}\,, \tag{4.175}$$

where $\vec{E}^{\,i}(Q_p)$ is the incident plane wave at Q_p given in (4.20), and $\bar{\bar{\mathcal{D}}}^{\,co}(Q_p)$ is the EUTD dyadic odd order zero-curvature diffraction coefficient for oblique incidence given by

$$\bar{\bar{\mathcal{D}}}^{\,co}(Q_p) = \mathcal{D}_s^{co}(\varphi_p',\varphi_p,\vartheta_p;\nu)\,\hat{e}_\perp^{\,i}\hat{e}_\perp^{\,p} + \mathcal{D}_h^{co}(\varphi_p',\varphi_p,\vartheta_p;\nu)\,\hat{e}_\parallel^{\,i}\hat{e}_\parallel^{\,p}\,, \tag{4.176}$$

$$\mathcal{D}_{s,h}^{co}(\varphi_p',\varphi_p,\vartheta_p;\nu) = \mp\frac{e^{j\frac{\pi}{4}}k^{\frac{\nu-2}{2\nu}}}{\sin\vartheta_p\sqrt{2\pi}}\,L_p(\varphi_p',\varphi_p,\vartheta_p,\nu)\begin{cases} I_{p\ell}(-\gamma_p,\nu)\,, & \text{(lit side)} \\ I_{pd}(\gamma_p,\nu)\,. & \text{(dark side)} \end{cases} \tag{4.177}$$

where $u_r = 1$ if $Q_r \in S$ and zero otherwise, $I_r(\gamma,\nu)$ is the same as in (4.57) with ν even, α_r, γ_r are the same as in (4.67) and (4.68) and $\vec{\epsilon}_r$ for the 3–D case is given by

$$\vec{\epsilon}_r = e^{j\frac{\pi}{4}}\sqrt{\frac{\nu-1}{2\pi}}\,\gamma_r^{\frac{\nu-2}{2(\nu-1)}}\left[\hat{p}\cdot\bar{\bar{R}}\,(Q_r)\right]\frac{1}{2}\sqrt{|R_1(Q_r)R_2(Q_r)|}\,. \tag{4.165}$$

Thus, using (4.67) and (4.165) the reflected field from a polynomial surface containing an even order zero-curvature line for the case of $R_1(Q_r) > 0$ may be written as follows:

$$\vec{E}^r(\theta_o',\varphi_o',\theta_o,\varphi_o;r_o) \sim \frac{u_r}{2}\,\vec{E}^i(Q_r)\cdot\bar{\bar{\mathcal{R}}}\,(Q_r)\sqrt{R_1(Q_r)R_2(Q_r)}\,e^{jk\hat{r}(Q_r)\cdot\hat{s}^r}\,\frac{e^{-jkr_o}}{r_o}\,, \tag{4.166}$$

where $\vec{E}^i(Q_r)$ is the incident plane wave at Q_r given in (4.20) and $\bar{\bar{\mathcal{R}}}\,(Q_r)$ is the UGO dyadic reflection coefficient and is the same as in (4.162), (4.63) and (4.64) with ν even. When $R_1(Q_r) < 0$ the complex conjugate version of $\bar{\bar{\mathcal{R}}}\,(Q_r)$ should be used.

4.3.3 Zero-curvature diffracted field contribution

As in the case of the reflected field, we also have two cases for the zero-curvature diffracted field. The first case involves diffraction from a zero-curvature point associated with an odd order zero-curvature line in a polynomial surface. The reflected field is discontinuous across the caustic in this case, therefore the zero-curvature diffracted field has to compensate this discontinuity. The second case involves diffraction from a zero-curvature point associated with an even order zero-curvature line in a polynomial surface. In the latter case no discontinuities have to be compensated by the zero-curvature diffracted field since the reflected field is continuous across the caustic.

A. Diffraction from an odd order zero-curvature point

Using (4.124), (4.145), (4.146), and the appropriate expression for $\overline{K}_\omega(\gamma,\zeta,\nu)$ for ν odd and $\zeta < 0$ in Appendix C, the odd order zero-curvature diffracted field is given by

$$\vec{E}^p(\theta_o',\varphi_o',\theta_o,\varphi_o;r_o) \sim u_0\,e^{jk\alpha_p}\,\vec{\epsilon}_p\,I_{p\ell}(-\gamma_p,\nu)\,\frac{e^{-jkr_o}}{r_o}\,, \text{ (lit side)} \tag{4.167}$$

$$\vec{E}^p(\theta_o',\varphi_o',\theta_o,\varphi_o;r_o) \sim u_0\,e^{jk\alpha_p}\,\vec{\epsilon}_p\,I_{pd}(\gamma_p,\nu)\,\frac{e^{-jkr_o}}{r_o}\,, \text{ (dark side)} \tag{4.168}$$

where $u_0 = 1$ if $Q_p \in S$ and zero otherwise, the functions $I_{p\ell}(\gamma,\nu)$, $I_{pd}(\gamma,\nu)$ are defined in (4.73) and (4.74), respectively, α_p is the same as in (4.75), and the parameters γ_p

Notice that when $\nu = 3$, $I_{p\ell}(-\gamma_p, 3) = 0$ and the EUTD expression for the zero-curvature diffracted field is equivalent to the complex ray field solution derived in Chapter 3 specialized for the case of plane wave incidence with the observer in the far-zone.

B. Diffraction from an even order zero-curvature point

Using (4.124), (4.145), (4.146), and the appropriate expression for $\overline{K}_\omega(\gamma, \zeta, \nu)$ for ν even and $\zeta < 0$ in Appendix C, the even order zero-curvature diffracted field on either side of the caustic is given by

$$\vec{E}^p(\theta_o', \varphi_o', \theta_o, \varphi_o; r_o) \sim u_0\, e^{jk\alpha_p}\, \vec{\epsilon}_p\, J_p^*(\gamma_p, \nu)\, \frac{e^{-jkr_o}}{r_o}; \text{ if } \widetilde{m}(Q_p, \nu) < 0, \tag{4.178}$$

$$\vec{E}^p(\theta_o', \varphi_o', \theta_o, \varphi_o; r_o) \sim u_0\, e^{jk\alpha_p}\, \vec{\epsilon}_p\, J_p(\gamma_p, \nu)\, \frac{e^{-jkr_o}}{r_o}; \text{ if } \widetilde{m}(Q_p, \nu) > 0. \tag{4.179}$$

The parameters u_0, α_p, γ_p, and $\vec{\epsilon}_p$ are the same as in the odd order zero-curvature diffraction case, and the function $J_p(\gamma, \nu)$ is defined in (4.86). Thus, using (4.75), (4.169), and (4.170) the even order zero-curvature diffracted field may be written as follows:

$$\vec{E}^p(\theta_o', \varphi_o', \theta_o, \varphi_o; r_o) \sim u_0\, \vec{E}^i(Q_p) \cdot \overline{\overline{\mathcal{D}}}^{ce}(Q_p) \sqrt{\rho_p^d}\, e^{jk\hat{r}(Q_p)\cdot \hat{s}^p}\, \frac{e^{-jkr_o}}{r_o}, \tag{4.180}$$

where $\vec{E}^i(Q_p)$ is the incident plane wave at Q_p given in (4.20), and $\overline{\overline{\mathcal{D}}}^{ce}(Q_p)$ is the EUTD dyadic even order zero-curvature diffraction coefficient for oblique incidence given by

$$\overline{\overline{\mathcal{D}}}^{ce}(Q_p) = \mathcal{D}_s^{ce}(\varphi_p', \varphi_p, \vartheta_p; \nu)\, \hat{e}_\perp^i \hat{e}_\perp^p + \mathcal{D}_h^{ce}(\varphi_p', \varphi_p, \vartheta_p; \nu)\, \hat{e}_\parallel^i \hat{e}_\parallel^p, \tag{4.181}$$

$$\mathcal{D}_{s,h}^{ce}(\varphi_p', \varphi_p, \vartheta_p; \nu) = \mp \frac{e^{j\frac{\pi}{4}} k^{\frac{\nu-2}{2\nu}}}{\sin\vartheta_p \sqrt{2\pi}}\, L_p(\varphi_p', \varphi_p, \vartheta_p; \nu) \begin{cases} J_p^*(\gamma_p, \nu), & \widetilde{m}(Q_p, \nu) < 0 \\ J_p(\gamma_p, \nu), & \widetilde{m}(Q_p, \nu) > 0\,. \end{cases} \tag{4.182}$$

4.3.4 Edge diffracted field contribution

As in the 2–D case of the previous section, the two methods of analysis employed in Chapter 3, namely Chester's expansion and the method of steepest descent, result in

two different expressions for the edge diffraction coefficient that are in agreement to the first order term, however, for observation points near the RSB. They also reduce to the exact expression for the half-plane diffraction coefficient for oblique incidence outside the transition regions. Let's consider Chester's expansion method first.

A. Chester's expansion formulation for the edge diffracted field

Using (4.124), (4.145), (4.146), and the appropriate expression for $\overline{K}_a(\gamma,\zeta,\nu)$ for in Appendix C, the edge diffracted field may be written as follows:

$$\vec{E}_1^d(\theta_o',\varphi_o',\theta_o,\varphi_o;r_o) \sim \left\{ e^{jk\alpha_a}\,\vec{\epsilon}_a\,I_a(\gamma_a,\zeta_a,\nu) + e^{jk\psi(\ell_a,\tau_s)}\left[\frac{j\vec{G}(\ell_a,\tau_s)}{k\dot{\psi}(\ell_a,\tau_s)} + \frac{\vec{\epsilon}_a}{j\,(\gamma+\zeta_a^{\nu-1})}\right]\right\}\frac{e^{-jkr_o}}{r_o};\ \text{if } m(v_p,\nu)>0, \tag{4.183}$$

$$\vec{E}_1^d(\theta_o',\varphi_o',\theta_o,\varphi_o;r_o) \sim \left\{ e^{jk\alpha_a}\,\vec{\epsilon}_a\,I_a^*(\gamma_a,\zeta_a,\nu) + e^{jk\psi(\ell_a,\tau_s)}\left[\frac{j\vec{G}(\ell_a,\tau_s)}{k\dot{\psi}(\ell_a,\tau_s)} - \frac{\vec{\epsilon}_a}{j\,(\gamma+\zeta_a^{\nu-1})}\right]\right\}\frac{e^{-jkr_o}}{r_o};\ \text{if } m(v_p,\nu)<0, \tag{4.184}$$

where α_a is the same as in (4.92). From (4.147)–(4.151), along with some algebraic manipulations, the parameters γ_a, ζ_a, and $\vec{\epsilon}_a$ for the 3–D case are given by

$$\gamma_a = u_p\,k^{(\nu-1)/\nu}\,\sin\vartheta_p(\cos\varphi_p'+\cos\varphi_p)\,w(v_p,\nu)\,, \tag{4.185}$$

$$\zeta_a = u_a\,k^{1/\nu}\,\left|\sin\vartheta_a(\cos\varphi_a'+\cos\varphi_a)w(v_a,\nu) - \sin\vartheta_p(\cos\varphi_p'+\cos\varphi_p)w(v_p,\nu)\right|^{\frac{1}{\nu-1}}\,, \tag{4.186}$$

$$\vec{\epsilon}_a \approx u_p\,(\gamma_a+\zeta_a^{\nu-1})\,\frac{\vec{f}(\ell_a,\tau_s)}{k\dot{\psi}(\ell_a,\tau_s)}\,, \tag{4.187}$$

where u_p and $w(v,\nu)$ are given in (4.148) and (4.150), respectively,

$$\vec{f}(\ell_a,\tau_s) \approx \sqrt{\frac{jk}{2\pi}}\left[\hat{p}\cdot\left(-\hat{e}_\perp^{\,i}\hat{e}_\perp^{\,d}+\hat{e}_\parallel^{\,i}\hat{e}_\parallel^{\,d}\right)\right]\sqrt{\rho_a^d}\,\cos\left(\frac{\varphi_a'-\varphi_a}{2}\right)\,, \tag{4.188}$$

and the function $I_a(\gamma,\zeta,\nu)$ is defined in (4.97)–(4.99). Thus, using (4.152), (4.156), (4.157), (4.92), (4.187), (4.188), and the PO correction factors in (2.117) and (2.118), the edge diffracted field may be written as follows:

$$\vec{E}_1^d(\theta_o',\varphi_o',\theta_o,\varphi_o;r_o) \sim \vec{E}^i(Q_a)\cdot\overline{\overline{D}}_1^e(Q_a)\sqrt{\rho_a^d}\,e^{jk\hat{r}(Q_a)\cdot\hat{s}^d}\,\frac{e^{-jkr_o}}{r_o}\,, \tag{4.189}$$

where $\bar{\bar{\mathcal{D}}}_1^e(Q_a)$ is the EUTD dyadic edge diffraction coefficient for oblique incidence derived using the Chester expansion method and is given by

$$\bar{\bar{\mathcal{D}}}_1^e(Q_a) = \mathcal{D}_s^{e1}(\varphi_a', \varphi_a; \vartheta_a)\,\hat{e}_\perp^i \hat{e}_\perp^d + \mathcal{D}_h^{e1}(\varphi_a', \varphi_a; \vartheta_a)\,\hat{e}_\parallel^i \hat{e}_\parallel^d, \tag{4.190}$$

$$\mathcal{D}_{s,h}^{e1}(\varphi_a', \varphi_a; \vartheta_a) = \frac{-e^{-j\frac{\pi}{4}}}{2\sin\vartheta_a\sqrt{2\pi k}}\left[\frac{1}{\cos\left(\frac{\varphi_a'-\varphi_a}{2}\right)} \mp \frac{\mathcal{F}(\gamma_d, \zeta_d, \nu)}{\cos\left(\frac{\varphi_a'+\varphi_a}{2}\right)}\right], \tag{4.191}$$

γ_d, ζ_d are the same as in (4.105), (4.106), and $\mathcal{F}(\gamma, \zeta, \nu)$ is defined in (4.107). It is understood that when $R_1(Q_a) < 0$, the complex conjugate version of $\mathcal{F}(\gamma, \zeta, \nu)$ should be used in (4.191).

B. Steepest descent formulation for the edge diffracted field

For the steepest descent analysis one begins with the expression for the scattered field in (4.124) and (4.139), that is

$$\vec{E}^s(\theta_o', \varphi_o', \theta_o, \varphi_o; r_o) \approx e^{jk\alpha}\,\vec{I}_s(\beta, t_a, \nu; k)\,\frac{e^{-jkr_o}}{r_o}, \tag{4.192}$$

where α, β, and t_a are given in (4.137), (4.138), and (4.140), respectively, and $\vec{I}_s(\beta, t_a, \nu; k)$ is a stationary phase integral in the complex t–plane given by

$$\vec{I}_s(\beta, t_a, \nu; k) = \int_{t_a}^{\infty} \vec{G}(t)\, e^{jk(\beta t + t^\nu/\nu)}\, ds\,. \tag{4.193}$$

$\vec{I}_s(\beta, t_a, \nu; k)$ has the same complex plane topology as the stationary phase integral in (4.109) for the 2–D case. Therefore, the edge diffracted field contribution in (4.192) is identified in the same fashion as in the 2–D case, and without further details it may be written as follows:

$$\vec{E}_2^d(\theta_o', \varphi_o', \theta_o, \varphi_o; r_o) \sim e^{jk\alpha_a}\,\frac{\vec{G}(\ell_a, \tau_s)}{k\dot{\psi}(\ell_a, \tau_s)}\,(\gamma_a + \zeta_a^{\nu-1})\,I_a(\gamma_a, \zeta_a, \nu)\,\frac{e^{-jkr_o}}{r_o} \tag{4.194}$$

$$\text{if} \quad m(v_p, \nu) > 0\,,$$

$$\vec{E}_2^d(\theta_o', \varphi_o', \theta_o, \varphi_o; r_o) \sim -e^{jk\alpha_a}\,\frac{\vec{G}(\ell_a, \tau_s)}{k\dot{\psi}(\ell_a, \tau_s)}\,(\gamma_a + \zeta_a^{\nu-1})\,I_a^*(\gamma_a, \zeta_a, \nu)\,\frac{e^{-jkr_o}}{r_o} \tag{4.195}$$

$$\text{if} \quad m(v_p, \nu) < 0\,,$$

where α_a is given in (4.92), γ_a, ζ_a are the same as in (4.185) and (4.186), and $I_a(\gamma, \zeta, \nu)$ is defined in (4.97)–(4.99). Finally, using (4.156) and the PO correction factors

in (2.117) and (2.118), the steepest descent formulation for the edge diffracted field for the case of $R_1(Q_a) > 0$ is given by

$$\vec{E}_2^d(\theta_o', \varphi_o', \theta_o, \varphi_o; r_o) \sim \vec{E}^i(Q_a) \cdot \bar{\bar{D}}_2^e(Q_a) \sqrt{\rho_a^d}\, e^{jk\hat{r}(Q_a)\cdot\hat{s}^d} \frac{e^{-jkr_o}}{r_o}, \tag{4.196}$$

where ρ_a^d is given in (4.157), and $\bar{\bar{D}}_2^e(Q_a)$ is the EUTD dyadic edge diffraction coefficient for oblique incidence derived using the method of steepest descent and is given by

$$\bar{\bar{D}}_2^e(Q_a) = \mathcal{D}_s^{e2}(\varphi_a', \varphi_a; \vartheta_a)\, \hat{e}_\perp^i \hat{e}_\perp^d + \mathcal{D}_h^{e2}(\varphi_a', \varphi_a; \vartheta_a)\, \hat{e}_\parallel^i \hat{e}_\parallel^d, \tag{4.197}$$

$$\mathcal{D}_{s,h}^{e2}(\varphi_a', \varphi_a; \vartheta_a) = \frac{-e^{-j\frac{\pi}{4}}}{2\sin\vartheta_a\sqrt{2\pi k}} \left[\frac{1}{\cos\left(\frac{\varphi_a' - \varphi_a}{2}\right)} \mp \frac{1}{\cos\left(\frac{\varphi_a' + \varphi_a}{2}\right)} \right] \mathcal{F}(\gamma_d, \zeta_d, \nu), \tag{4.198}$$

where γ_d, ζ_d, and $\mathcal{F}(\gamma, \zeta, \nu)$ are the same as in (4.105)–(4.107). When $R_1(Q_a) < 0$ the complex conjugate of $\mathcal{F}(\gamma, \zeta, \nu)$ should be used in (4.198).

Chapter 5

Numerical Results and Discussion

In this chapter, numerical results for the scattered fields from cubic and fourth order polynomial strips illuminated by a plane wave are presented and discussed. The accuracy and limitations of the UGO/EUTD solution derived in this report are assessed by comparison with an independent method of moments (MM) solution. Results obtained using the classic GO/UTD solution are also shown to illustrate its failure near caustics and composite shadow boundaries and the need for the new solution. The total scattered field is plotted in terms of echo width which is defined as follows:

$$L_e(\theta,\theta') \equiv \lim_{\rho\to\infty}\left(2\pi\rho\left|\frac{E^s}{E^i}\right|^2\right) . \tag{5.1}$$

Both monostatic and bistatic results for the plane wave scattering from cubic and fourth order polynomial strips are presented and discussed in Sections 5.1 and 5.2, respectively.

5.1 Scattering results for cubic polynomial strips

In this section, results for the plane wave scattering from cubic polynomial strips are presented and discussed. The method denoted as UGO/EUTD1 in the results that follow uses the edge diffraction coefficient in (4.104) derived using the Chester expansion. The method denoted as UGO/EUTD2 uses the edge diffraction coefficient in (4.119) derived using the method of steepest descent. The scattering geometry and the relevant parameters are illustrated in in Figure 5.1. Before proceeding with the results for the total scattered field, the various field mechanisms are examined and

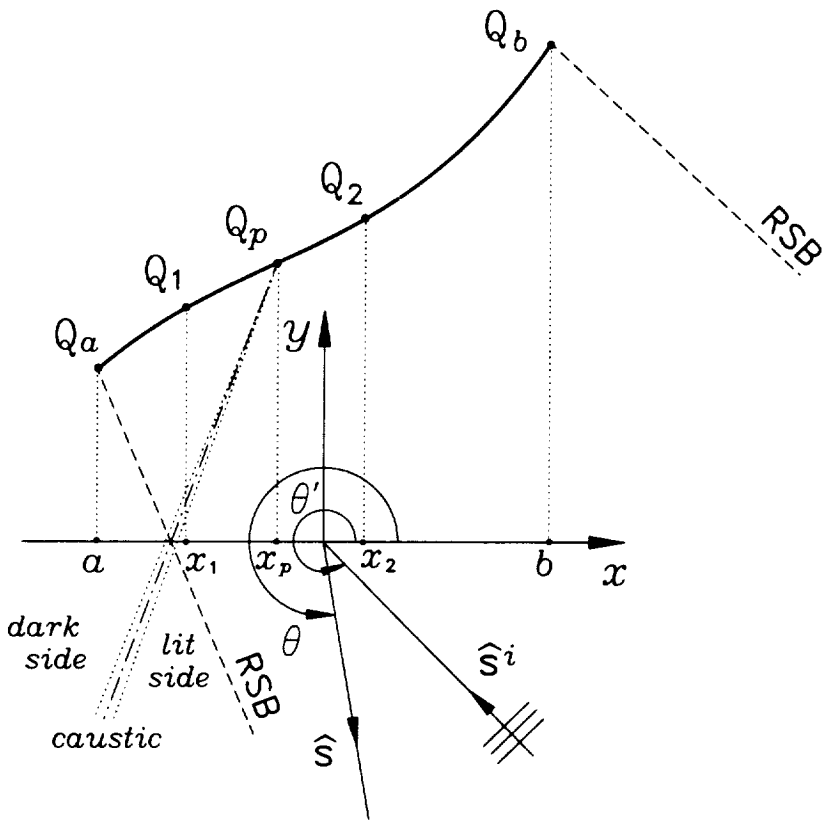

Figure 5.1: Geometry and relevant parameters for the scattering from a cubic polynomial strip.

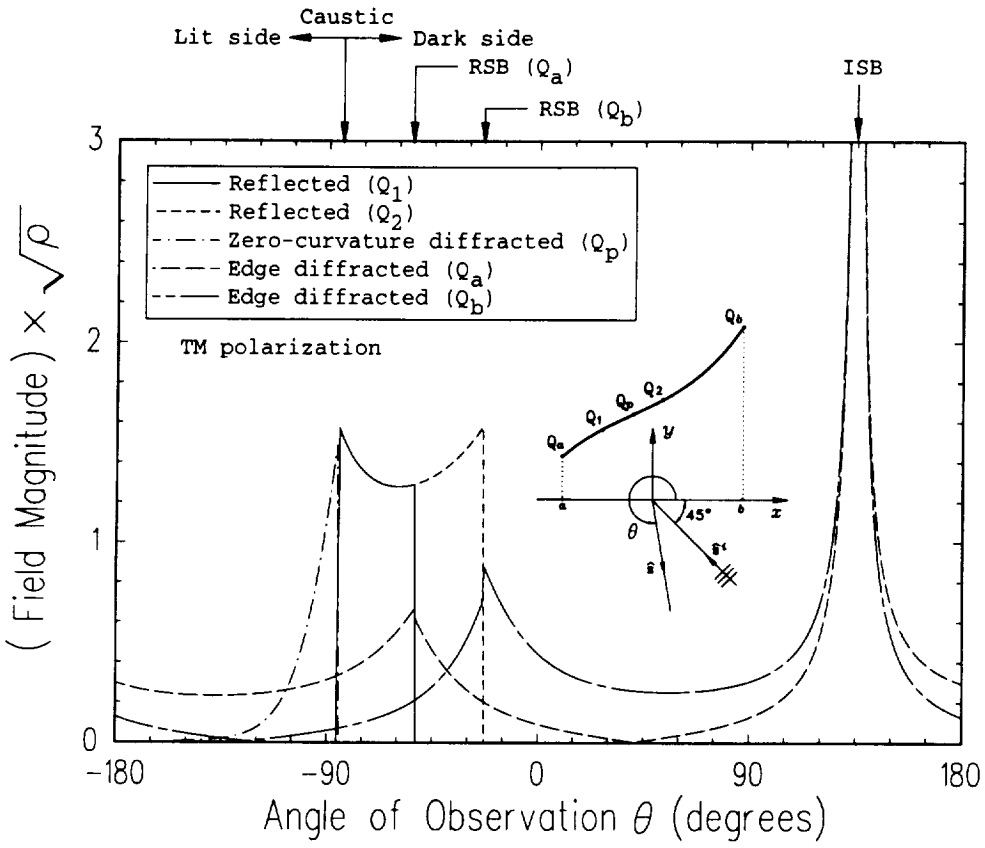

Figure 5.2: Scattered field contributions (TM case) from a cubic polynomial strip with $a_0 = 2.0\lambda$, $a_1 = 0.5$, $a_2 = 0.1\lambda^{-1}$, $a_3 = 0.1\lambda^{-2}$, $a = -1.5\lambda$, $b = 1.5\lambda$, and angle of incidence $\theta' = -45°$.

the EUTD1, EUTD2, and UTD edge diffraction coefficients are compared. The first example considered is a cubic polynomial strip with $a_0 = 2.0\lambda$, $a_1 = 0.5$, $a_2 = 0.1\lambda^{-1}$, $a_3 = 0.1\lambda^{-2}$, $a = -1.5\lambda$, and $b = 1.5\lambda$. In this case both edges are far removed from the zero-curvature point, and thus the two RSBs and the caustic of the reflected rays are clearly distinct. Figure 5.2 shows a plot of the magnitude of the various field contributions to the total scattered field due to a TM polarized plane wave incident at an angle $\theta' = -45°$, computed using the UGO/EUTD1 method. Notice that the two reflected field components exhibit a combined total of three discontinuities. The first discontinuity occurs across the caustic of the reflected rays ($\theta \approx -85°$) and is compensated by the zero-curvature diffracted field that only exists in the dark side of the caustic. The second discontinuity occurs at the RSB associated with the edge at Q_a ($\theta \approx -52°$) and is compensated by the edge diffracted field

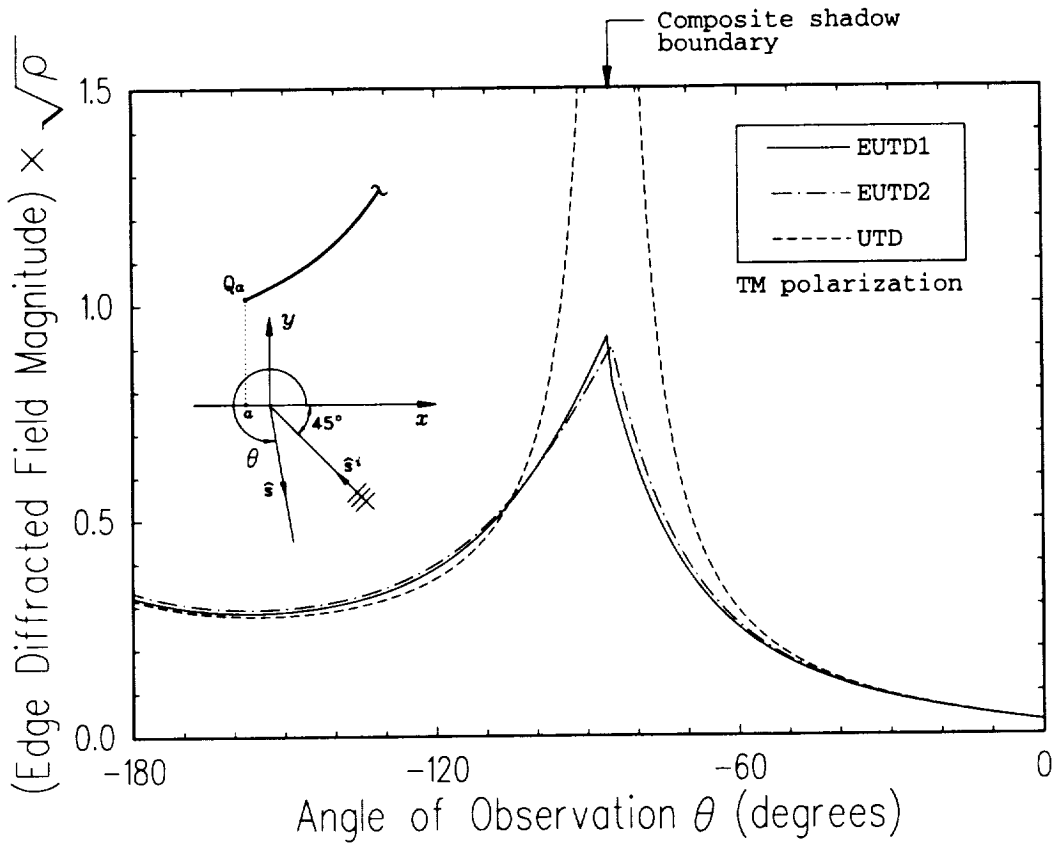

Figure 5.3: Edge diffracted field magnitude (TM case) from a semi-infinite cubic polynomial boundary with $a_0 = 2.0\lambda$, $a_1 = 0.5$, $a_2 = 0.1\lambda^{-1}$, $a_3 = 0.1\lambda^{-2}$, $a = -0.33\lambda$, and angle of incidence $\theta' = -45°$.

from Q_a. Similarly the third discontinuity occurs at the RSB associated with the edge Q_b ($\theta \approx -23°$) and is compensated by the edge diffracted field from Q_b. Also notice that the two edge diffraction terms become singular near the ISB ($\theta = 135°$); however, they combine to give a finite result. The second example considered is semi-infinite cubic polynomial boundary with $a_0 = 2.0\lambda$, $a_1 = 0.5$, $a_2 = 0.1\lambda^{-1}$, $a_3 = 0.1\lambda^{-2}$, $a = -0.33\lambda$. In this case the edge at Q_a coincides with the zero-curvature point, and thus a composite shadow boundary is formed. Figure 5.3 shows a plot of the magnitude of the edge diffracted field due to a TM polarized plane wave incident at an angle $\theta' = -45°$, computed using the EUTD1, EUTD2, and UTD diffraction coefficients. Notice that UTD produces a singular result near the composite shadow boundary. The EUTD1 and EUTD2 results are not in complete agreement near the composite shadow boundary, however they both remain finite. All

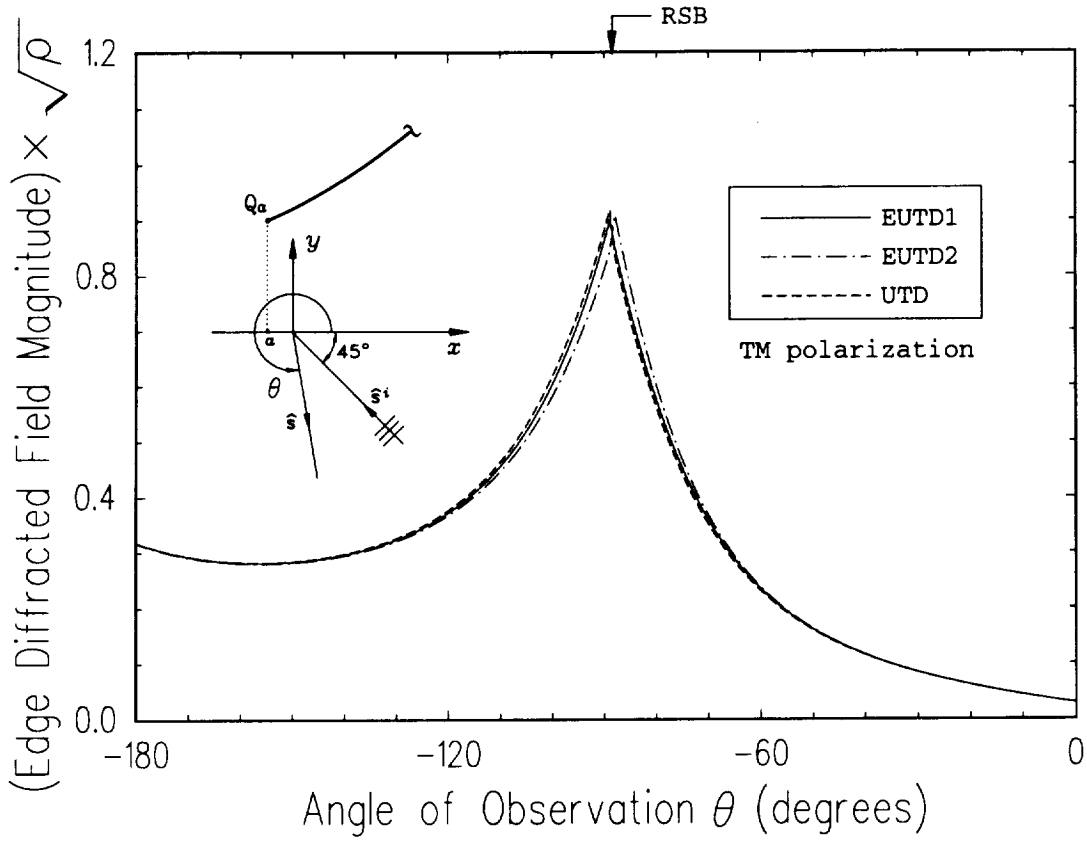

Figure 5.4: Edge diffracted field magnitude (TM case) from a semi-infinite cubic polynomial boundary with $a_0 = 2.0\lambda$, $a_1 = 0.5$, $a_2 = 0.1\lambda^{-1}$, $a_3 = 0.0\lambda^{-2}$, $a = -0.33\lambda$, and angle of incidence $\theta' = -45°$.

three diffraction coefficients seem to be in good agreement away from the composite shadow boundary. The third example considered is semi-infinite parabolic boundary which is a special case of a cubic polynomial boundary with $a_0 = 2.0\lambda$, $a_1 = 0.5$, $a_2 = 0.1\lambda^{-1}$, $a_3 = 0.0\lambda^{-2}$, $a = -0.33\lambda$. In this case no caustic or composite shadow boundary exists and UTD is expected to give accurate results for the edge diffracted field. Figure 5.4 shows a plot of the magnitude of the edge diffracted field due to a TM polarized plane wave incident at an angle $\theta' = -45°$ computed using the EUTD1, EUTD2, and UTD diffraction coefficients. All three diffraction coefficients are in good agreement, however, the EUTD1 diffraction coefficient seems to be in better agreement with UTD near the RSB. Figure 5.5 shows the bistatic echo width of a cubic polynomial strip with $a_0 = 2.0\lambda$, $a_1 = 0.5$, $a_2 = 0.1\lambda^{-1}$, $a_3 = 0.1\lambda^{-2}$, $a = -0.33\lambda$, and $b = 1.5\lambda$ illuminated by a TM polarized plane wave incident at an

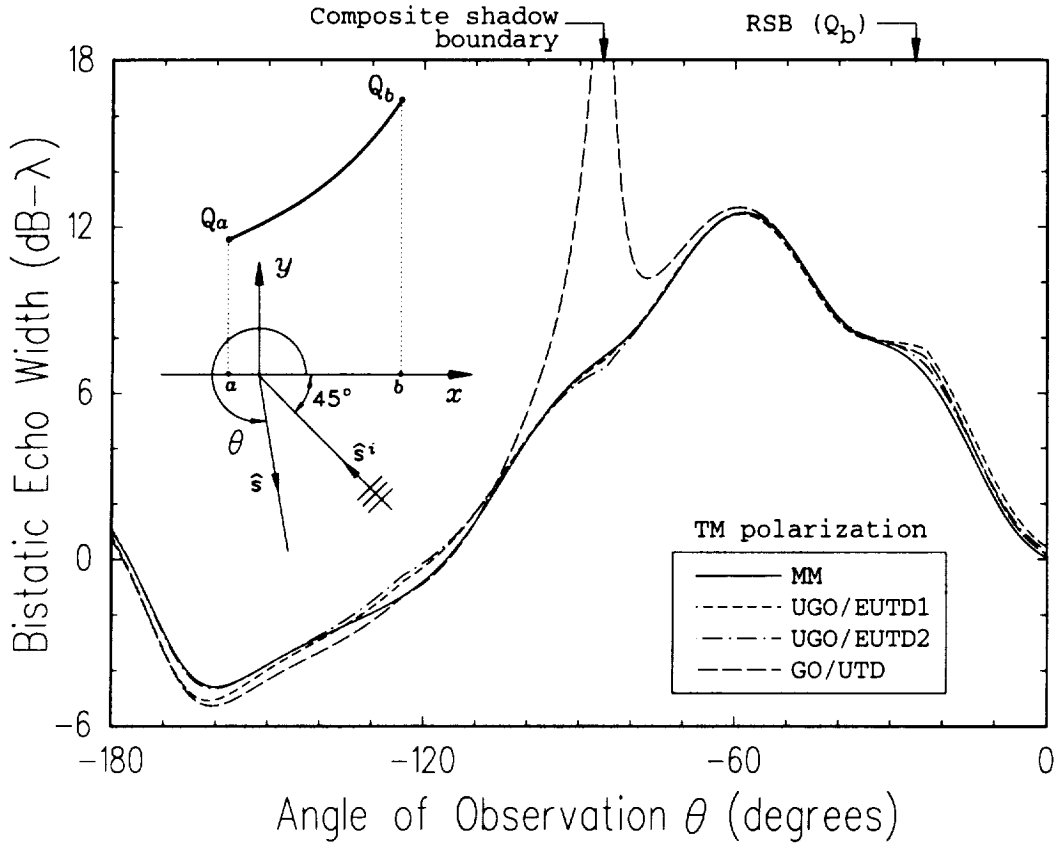

Figure 5.5: Bistatic echo width (TM case) of a cubic polynomial strip with $a_0 = 2.0\lambda$, $a_1 = 0.5$, $a_2 = 0.1\lambda^{-1}$, $a_3 = 0.1\lambda^{-2}$, $a = -0.33\lambda$, $b = 1.5\lambda$, and angle of incidence $\theta' = -45°$.

angle $\theta' = -45°$. The classic GO/UTD solution produces a singular result near the composite shadow boundary whereas the UGO/EUTD1 and UGO/EUTD2 remain finite. Notice that the UGO/EUTD1 solution is in better agreement with MM near the composite shadow boundary whereas the UGO/EUTD2 solution seems to be more accurate away from the composite shadow boundary. The differences, however, are quite minor (< 1 dB–λ) and therefore the two EUTD diffraction coefficients should be considered equivalent for all practical purposes. For the subsequent results only the UGO/EUTD1 results will be shown.

Figures 5.6 and 5.7 show plots of the bistatic echo width of a cubic polynomial strip with $a_0 = 2.0\lambda$, $a_1 = 0.5$, $a_2 = 0.1\lambda^{-1}$, $a_3 = 0.1\lambda^{-2}$, $a = -1.5\lambda$, $b = 1.5\lambda$, and angle of incidence $\theta' = -45°$, for the TM and TE polarization cases, respectively. The UGO/EUTD result shows excellent agreement with MM for the TM polarization

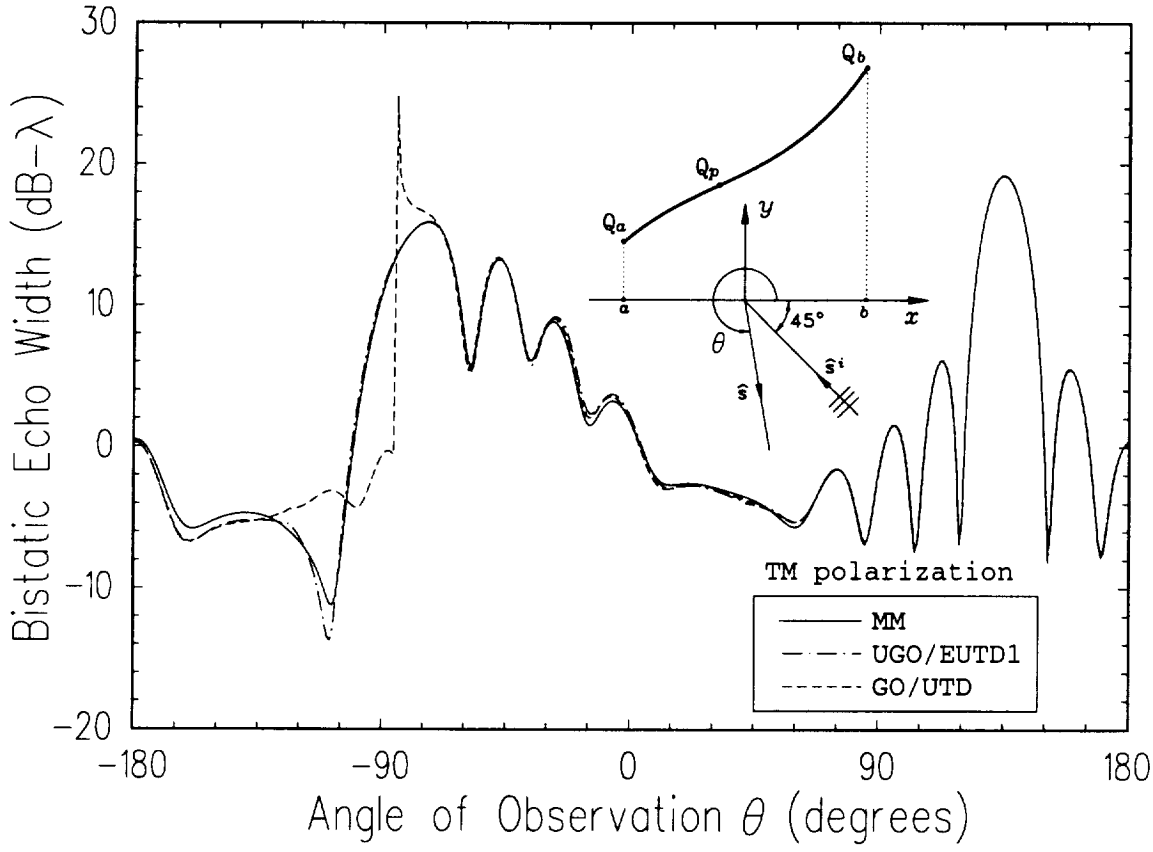

Figure 5.6: Bistatic echo width (TM case) of a cubic polynomial strip with $a_0 = 2.0\lambda$, $a_1 = 0.5$, $a_2 = 0.1\lambda^{-1}$, $a_3 = 0.1\lambda^{-2}$, $a = -1.5\lambda$, $b = 1.5\lambda$, and angle of incidence $\theta' = -45°$.

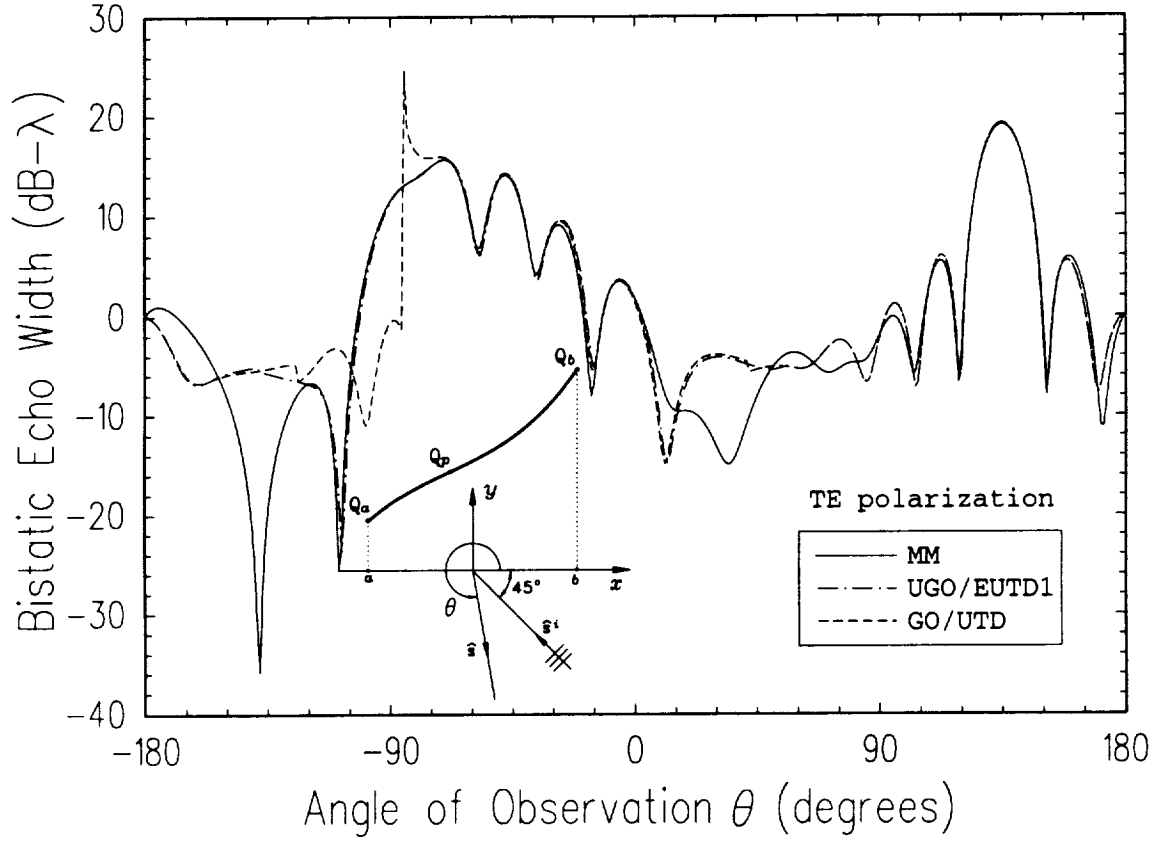

Figure 5.7: Bistatic echo width (TE case) of a cubic polynomial strip with $a_0 = 2.0\lambda$, $a_1 = 0.5$, $a_2 = 0.1\lambda^{-1}$, $a_3 = 0.1\lambda^{-2}$, $a = -1.5\lambda$, $b = 1.5\lambda$, and angle of incidence $\theta' = -45°$.

case. For the TE polarization case, the higher order mechanisms which are not included in the UGO/EUTD solution are quite significant and therefore the agreement is reasonable only near the specular and forward directions where the first order mechanisms are dominant. For observation directions near grazing the higher order mechanisms such as edge excited creeping waves and whispering gallery modes excited in the concave part of the cubic strip must be included to obtain accurate results for the TE polarization case. The classic GO/UTD solution gives an erroneous result near the caustic ($\theta \approx -85°$), and on both its lit and dark sides. This is expected since the classic UTD solution does not include zero-curvature diffraction information, and the GO expression for the reflected field gives singular results near caustics. Away from the caustic, the UGO/EUTD and GO/UTD results are in good agreement for both polarizations. Figures 5.8 and 5.9 show plots of the monostatic echo width of the same cubic polynomial strip for the TM and TE polarization cases, respectively. The monostatic UGO/EUTD result shows excellent agreement with MM for the TM polarization case. For the TE polarization case, the agreement is good only near broadside where the first order mechanisms are dominant. The classic GO/UTD solution gives an erroneous result near the caustics ($\theta \approx -67°$ and $\theta \approx 113°$), and on both the lit and dark sides. Away from the caustics, the UGO/EUTD and GO/UTD results are in good agreement for both polarizations.

Figure 5.10 shows a plot of the bistatic echo width of a cubic polynomial strip with $a_0 = 2.0\lambda$, $a_1 = 0.5$, $a_2 = 0.1\lambda^{-1}$, $a_3 = 0.1\lambda^{-2}$, $a = -0.33\lambda$, $b = 1.5\lambda$, and angle of incidence $\theta' = -45°$, for the TM polarization case. For this geometry, the edge at Q_a coincides with the zero-curvature point, thus the RSB and the caustic coalesce to form a composite shadow boundary. The GO/UTD result exhibits a singularity at the RSB associated with the edge at Q_a ($\theta \approx -85°$), whereas the UGO/EUTD result remains finite and is in excellent agreement with MM. Figure 5.11 shows a plot of the monostatic echo width of the same geometry. Again, the non-uniformity of the GO/UTD solution is clearly evident, whereas the UGO/EUTD solution remains valid across the composite shadow boundary and uniformly reduces to the the GO/UTD result away from the transition region.

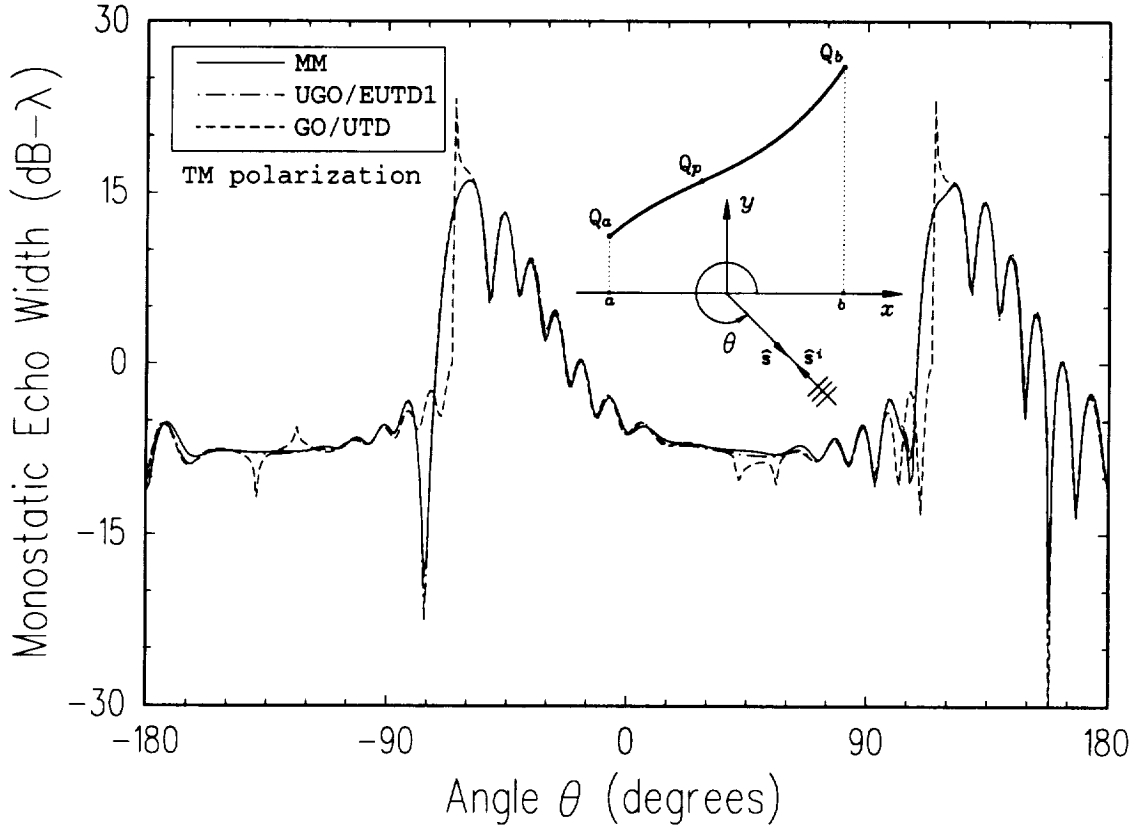

Figure 5.8: Monostatic echo width (TM case) of a cubic polynomial strip with $a_0 = 2.0\lambda$, $a_1 = 0.5$, $a_2 = 0.1\lambda^{-1}$, $a_3 = 0.1\lambda^{-2}$, $a = -1.5\lambda$, and $b = 1.5\lambda$.

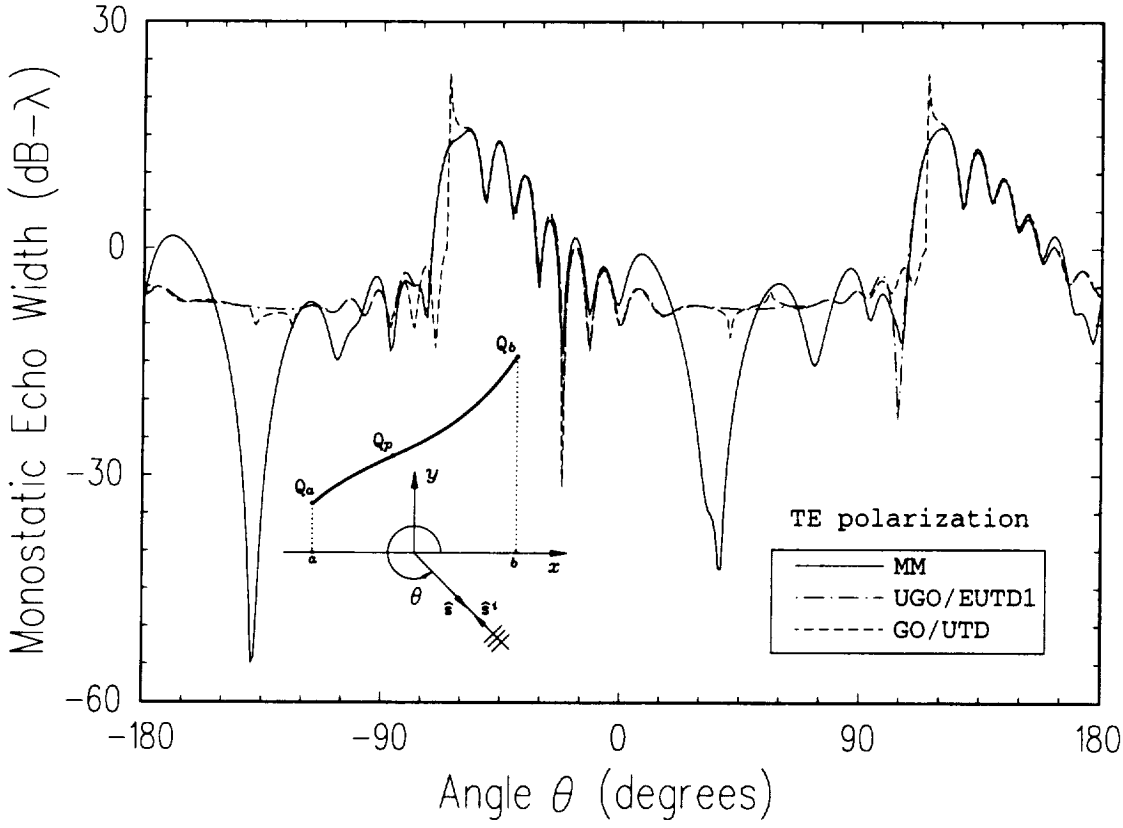

Figure 5.9: Monostatic echo width (TE case) of a cubic polynomial strip with $a_0 = 2.0\lambda$, $a_1 = 0.5$, $a_2 = 0.1\lambda^{-1}$, $a_3 = 0.1\lambda^{-2}$, $a = -1.5\lambda$, and $b = 1.5\lambda$.

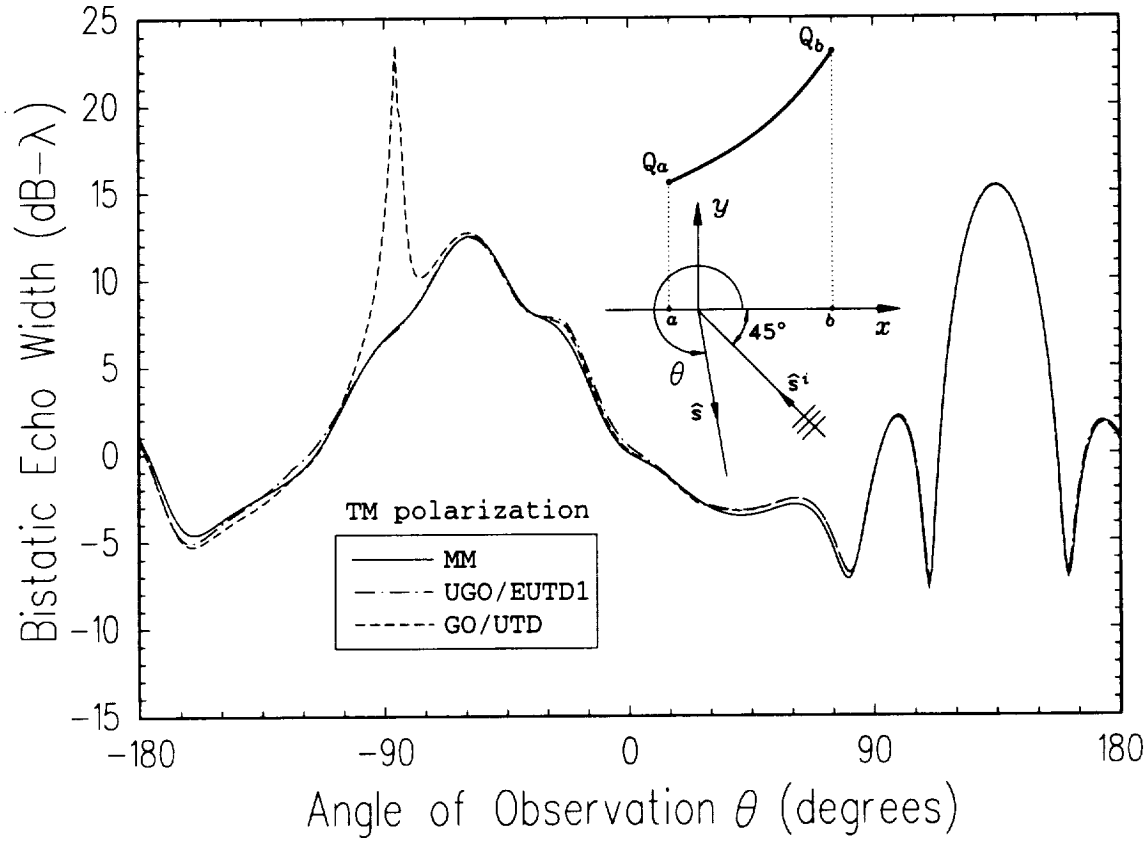

Figure 5.10: Bistatic echo width (TM case) of a cubic polynomial strip with $a_0 = 2.0\lambda$, $a_1 = 0.5$, $a_2 = 0.1\lambda^{-1}$, $a_3 = 0.1\lambda^{-2}$, $a = -0.33\lambda$, $b = 1.5\lambda$, and angle of incidence $\theta' = -45°$.

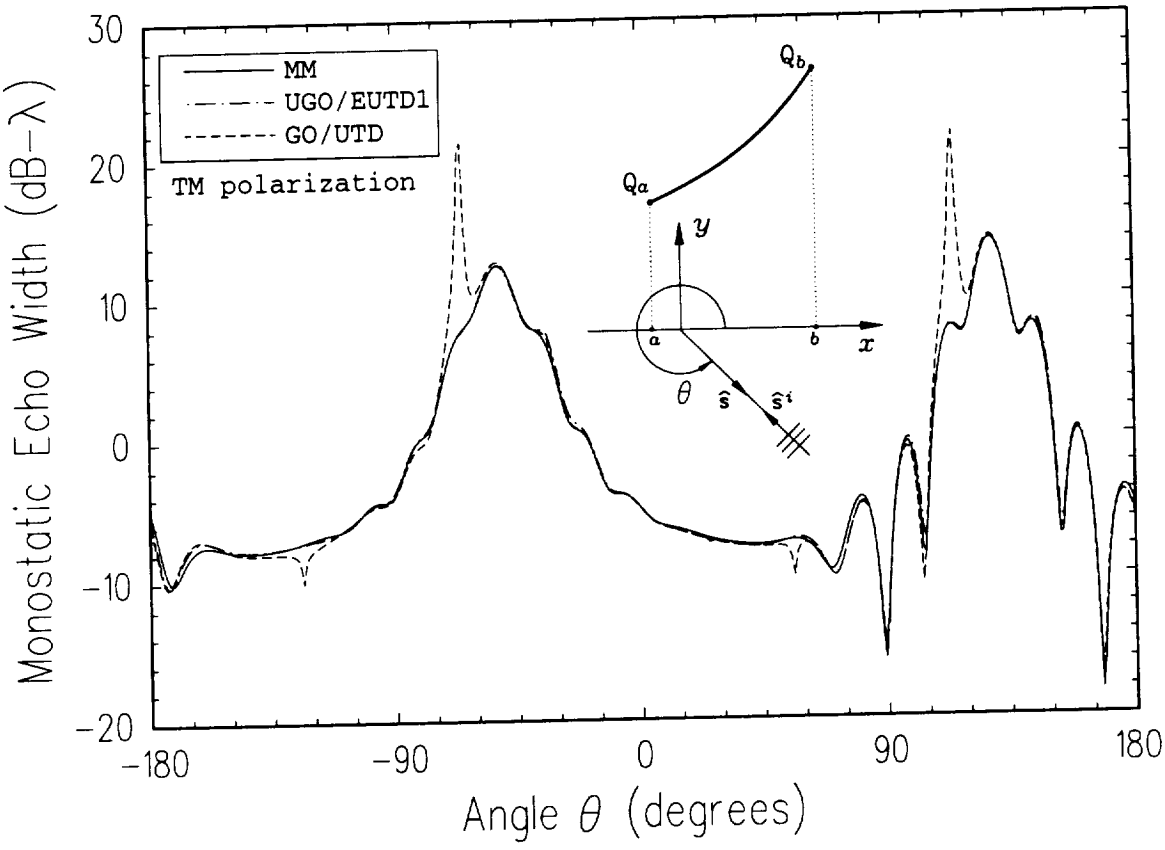

Figure 5.11: Monostatic echo width (TM case) of a cubic polynomial strip with $a_0 = 2.0\lambda$, $a_1 = 0.5$, $a_2 = 0.1\lambda^{-1}$, $a_3 = 0.1\lambda^{-2}$, $a = -0.33\lambda$ and $b = 1.5\lambda$.

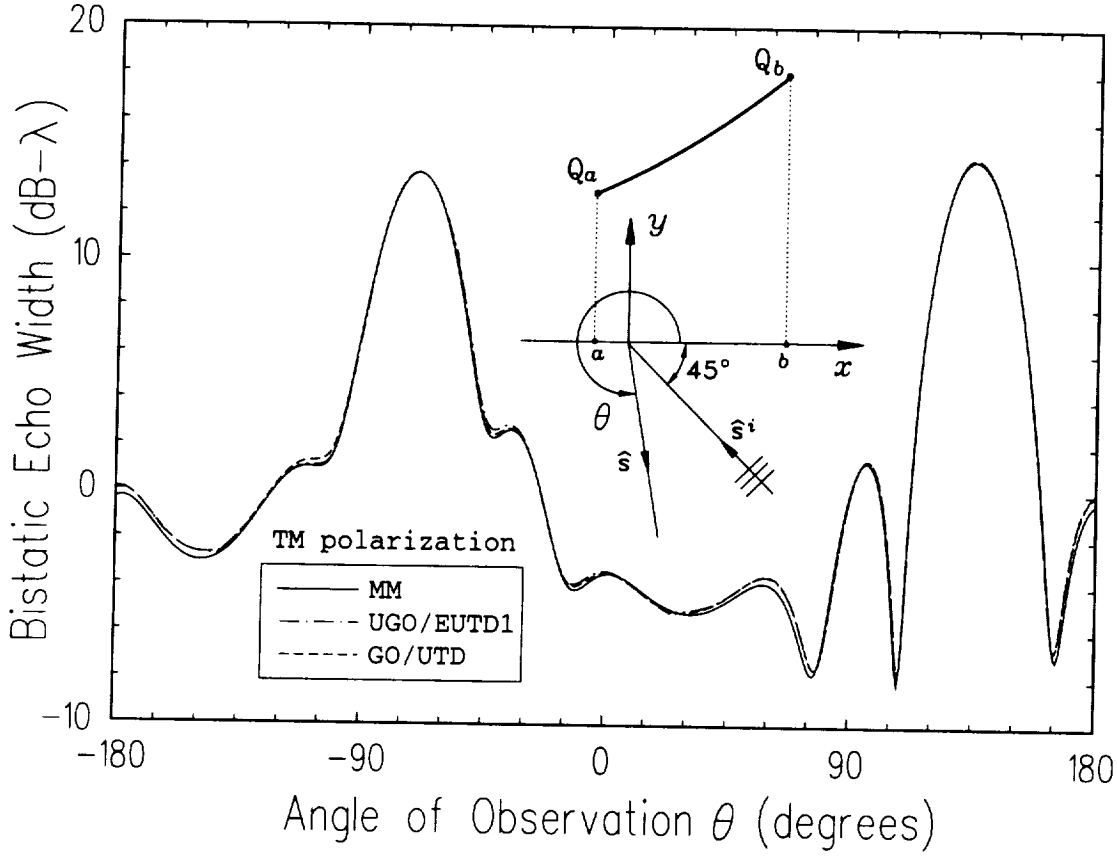

Figure 5.12: Bistatic echo width (TM case) of a cubic polynomial strip with $a_0 = 2.0\lambda$, $a_1 = 0.5$, $a_2 = 0.1\lambda^{-1}$, $a_3 = 0.0\lambda^{-2}$, $a = -0.33\lambda$, $b = 1.5\lambda$ and angle of incidence $\theta' = -45°$.

The remaining four results in this section illustrate the flexibility and universal nature of the UGO/EUTD solution. Figures 5.12 and 5.13 show plots of the bistatic and monostatic echo width, respectively, of a cubic polynomial strip with $a_0 = 2.0\lambda$, $a_1 = 0.5$, $a_2 = 0.1\lambda^{-1}$, $a_3 = 0.0\lambda^{-2}$, $a = -0.33\lambda$ and $b = 1.5\lambda$. This geometry of course corresponds to parabolic screen and the zero-curvature point theoretically moves to negative infinity. It is well known that the classic GO/UTD solution gives accurate results for these type of geometries. The UGO/EUTD solution remains valid and is in excellent agreement with both GO/UTD and MM.

Figures 5.14 and 5.15 show plots of the bistatic and monostatic echo width, respectively, of a cubic polynomial strip with $a_0 = 2.0\lambda$, $a_1 = 0.5$, $a_2 = 0.0\lambda^{-1}$, $a_3 = 0.0\lambda^{-2}$, $a = -0.33\lambda$ and $b = 1.5\lambda$. This case corresponds to a flat strip since both the cubic and quadratic coefficients are set equal to zero. The UGO/EUTD solution remains

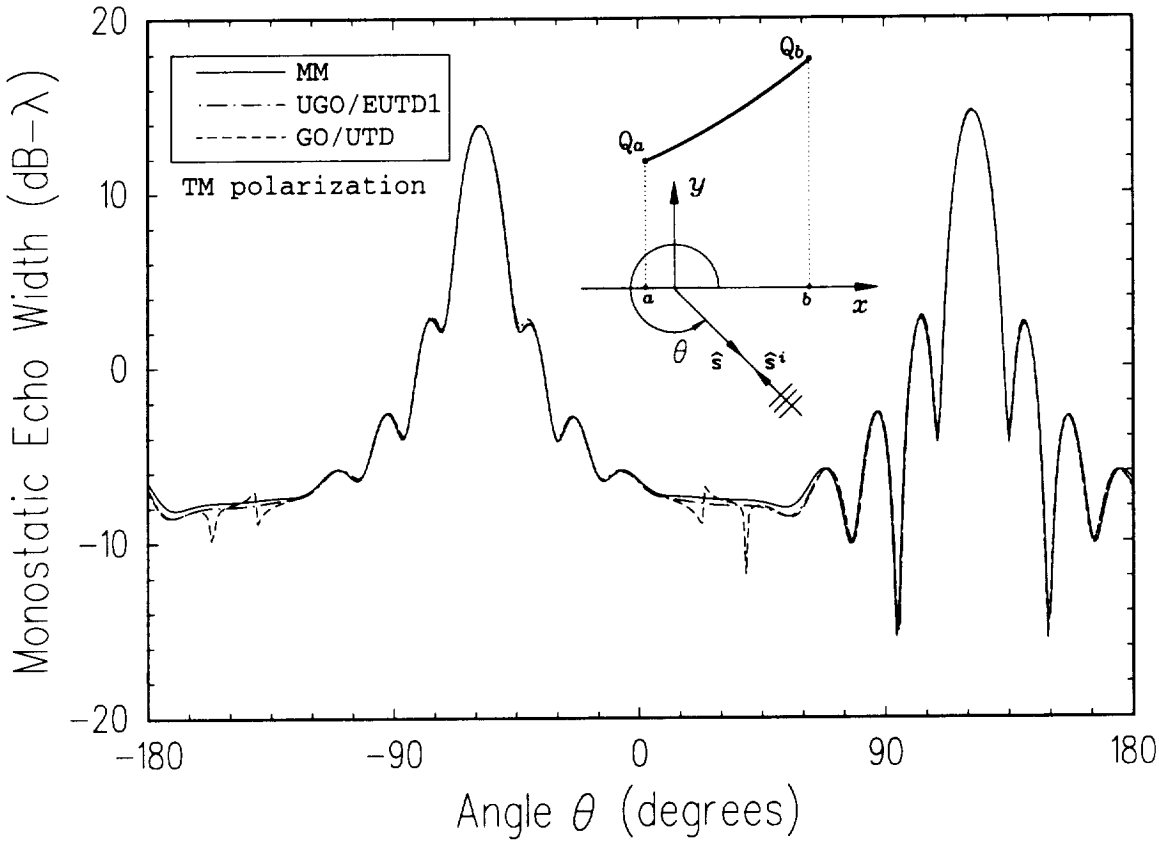

Figure 5.13: Monostatic echo width (TM case) of a cubic polynomial strip with $a_0 = 2.0\lambda$, $a_1 = 0.5$, $a_2 = 0.1\lambda^{-1}$, $a_3 = 0.0\lambda^{-2}$, $a = -0.33\lambda$ and $b = 1.5\lambda$.

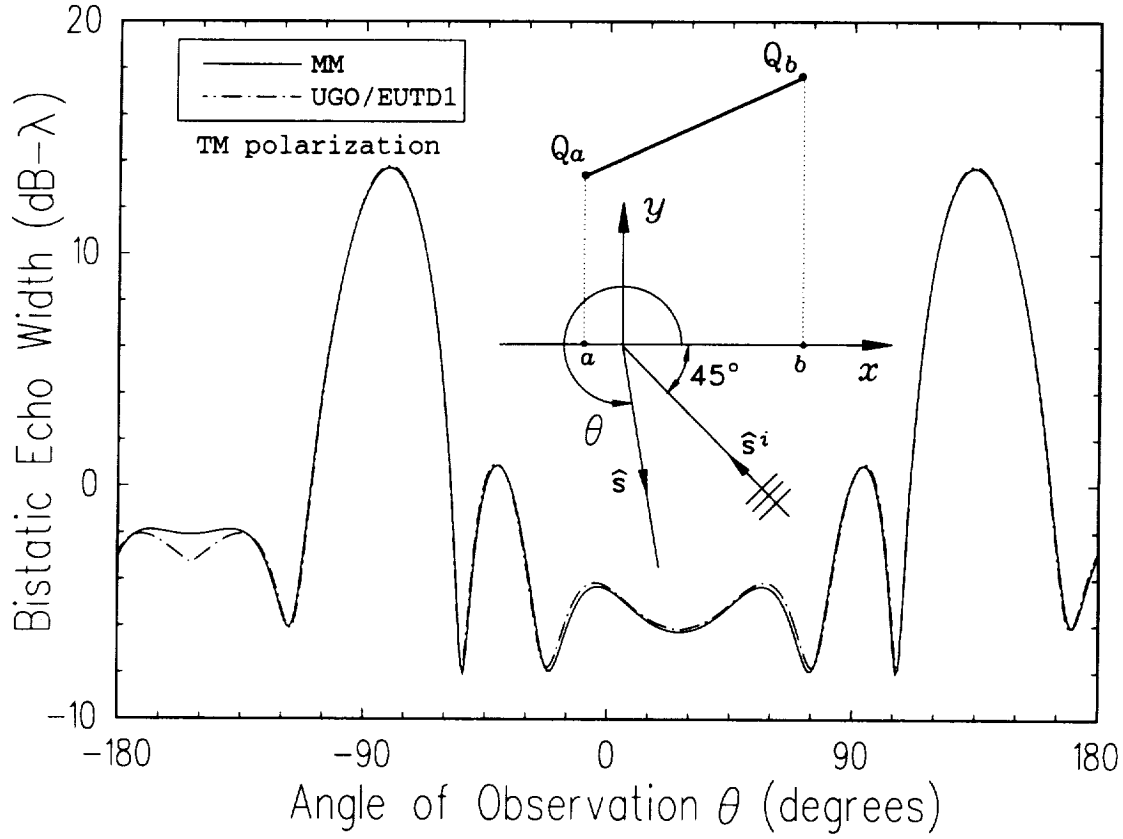

Figure 5.14: Bistatic echo width (TM case) of a cubic polynomial strip with $a_0 = 2.0\lambda$, $a_1 = 0.5$, $a_2 = 0.0\lambda^{-1}$, $a_3 = 0.0\lambda^{-2}$, $a = -0.33\lambda$, $b = 1.5\lambda$ and angle of incidence $\theta' = -45°$.

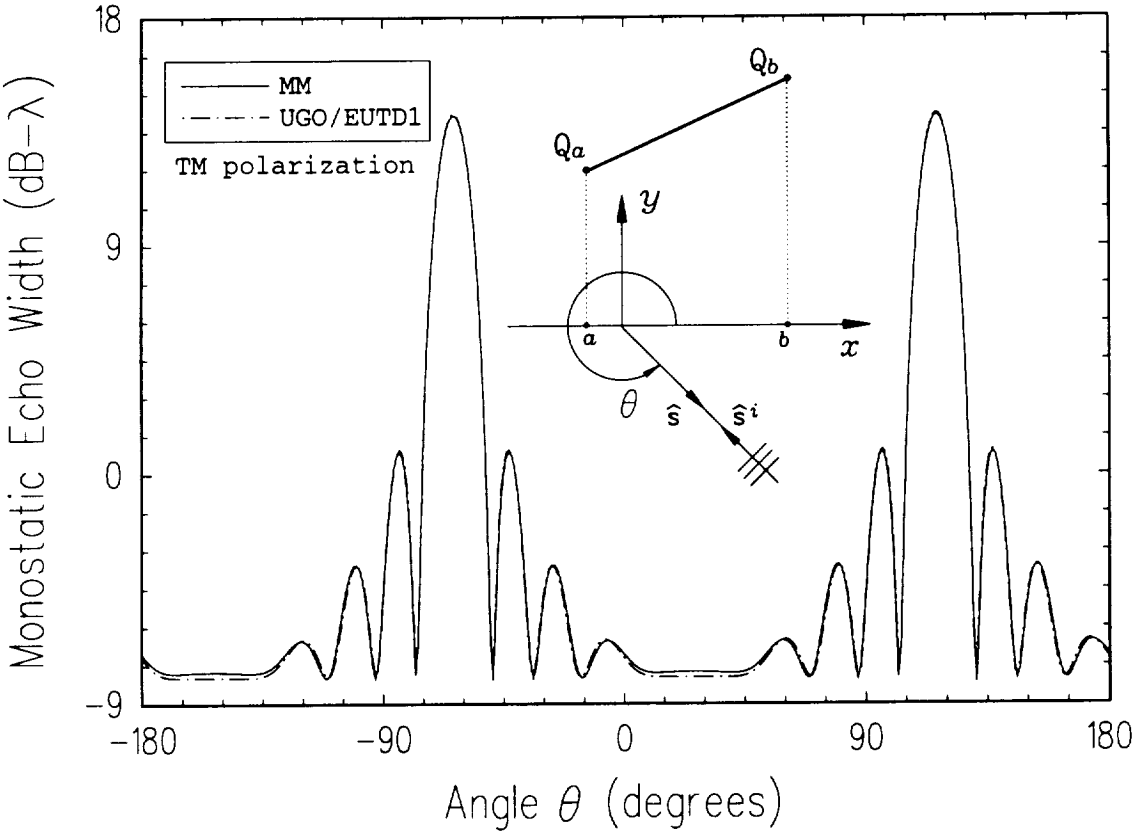

Figure 5.15: Monostatic echo width (TM case) of a cubic polynomial strip with $a_0 = 2.0\lambda$, $a_1 = 0.5$, $a_2 = 0.0\lambda^{-1}$, $a_3 = 0.0\lambda^{-2}$, $a = -0.33\lambda$ and $b = 1.5\lambda$.

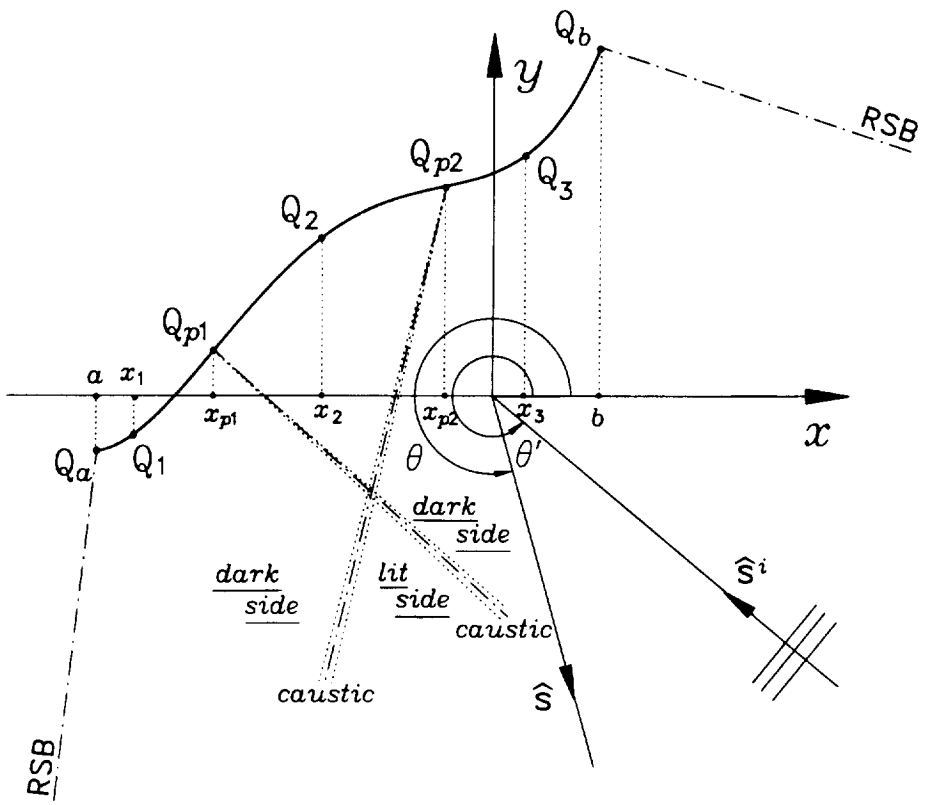

Figure 5.16: Geometry and relevant parameters for the scattering from a fourth order polynomial strip.

valid for this special case also, a fact that demonstrates its flexibility for treating general surfaces that are highly curved, slightly curved, or completely flat.

5.2 Scattering results for fourth order polynomial strips

In this section, results for the plane wave scattering from fourth order polynomial strips are presented and discussed. The scattering geometry and the relevant parameters are illustrated in Figure 5.16. The results in this section will be limited for the case where the two first order zero-curvature points, Q_{p1} and Q_{p2}, are sufficiently far apart. When Q_{p1} and Q_{p2} are close together, the two caustics form a cusp and the UGO/EUTD solution would fail. The UGO/EUTD solution does apply when Q_{p1}

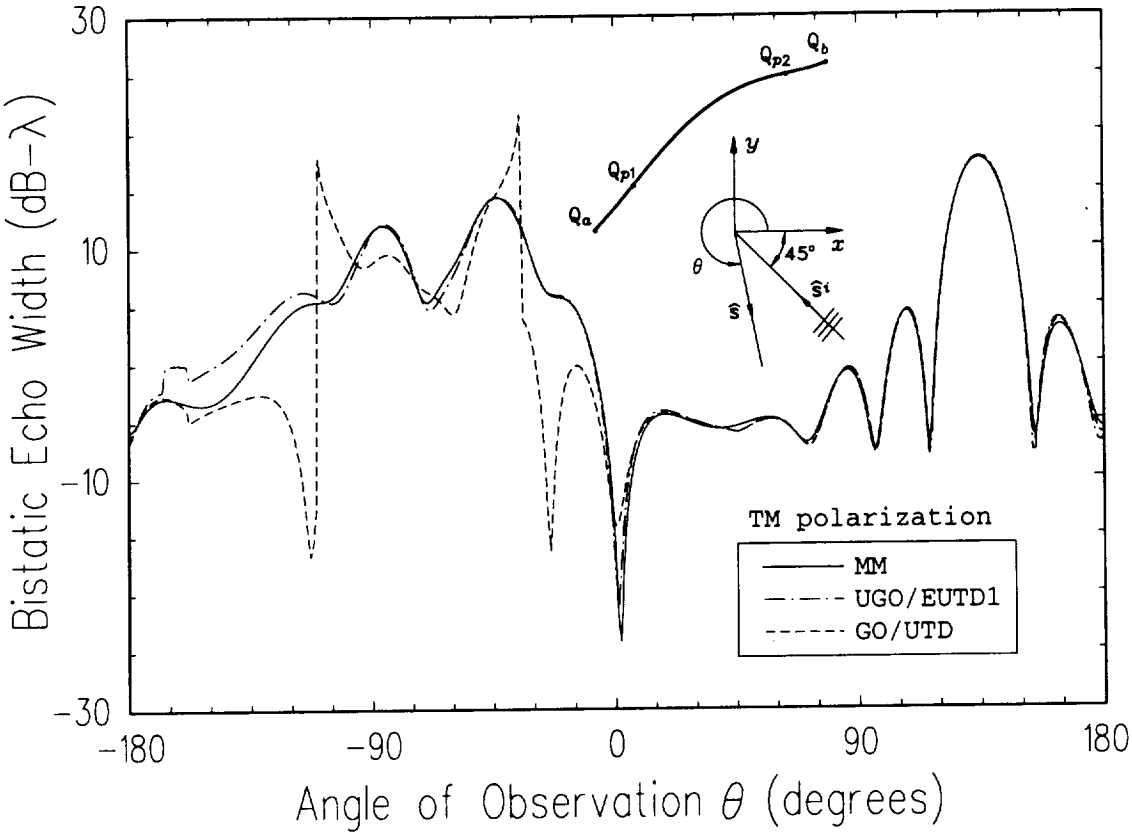

Figure 5.17: Bistatic echo width (TM Case) of a fourth order polynomial strip with $a_0 = 1.0\lambda$, $a_1 = 0.5$, $a_2 = -0.4\lambda^{-1}$, $a_3 = 0.1\lambda^{-2}$, $a_4 = 0.1\lambda^{-3}$, $a = -1.5\lambda$, $b = 1.0\lambda$, and angle of incidence $\theta' = -45°$.

and Q_{p2} coalesce to form a second order zero-curvature point, however, no results for this case are available at this time.

Figures 5.17 and 5.18 show plots for the bistatic echo width of a fourth order polynomial strip with $a_0 = 1.0\lambda$, $a_1 = 0.5$, $a_2 = -0.4\lambda^{-1}$, $a_3 = 0.1\lambda^{-2}$, $a_4 = 0.1\lambda^{-3}$, $a = -1.5\lambda$, and $b = 1.0\lambda$, illuminated by a TM and TE polarized plane wave, respectively, incident at an angle $\theta' = -45°$. The UGO/EUTD result shows good agreement with MM for the TM polarization case. For the TE polarization case, the agreement is good only near the specular and forward directions where the first order mechanisms are dominant. The classic GO/UTD solution fails dramatically near the caustics ($\theta \approx -112°$ and $\theta \approx -35°$). Figures 5.19 and 5.20 show plots for the monostatic echo width of the same geometry for the TM and TE polarization, respectively. Again, the UGO/EUTD result shows good agreement with MM for the TM polarization case,

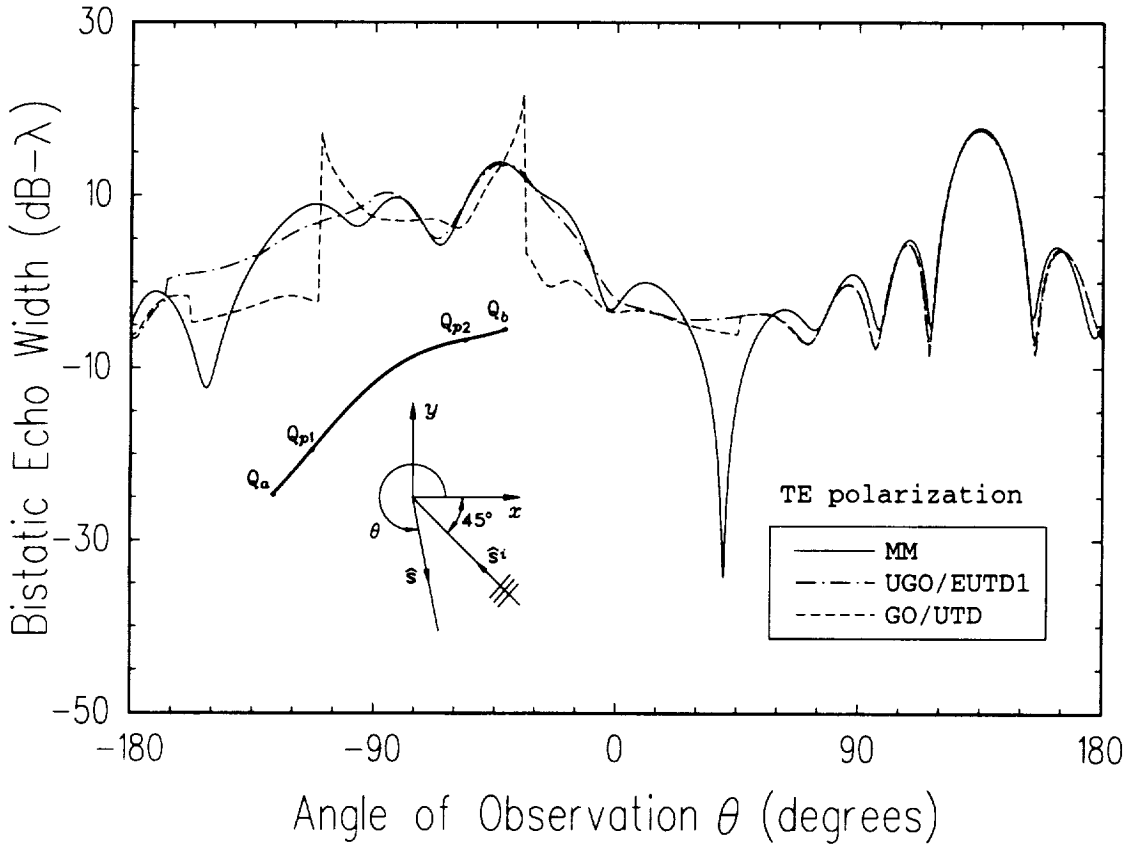

Figure 5.18: Bistatic echo width (TE Case) of a fourth order polynomial strip with $a_0 = 1.0\lambda$, $a_1 = 0.5$, $a_2 = -0.4\lambda^{-1}$, $a_3 = 0.1\lambda^{-2}$, $a_4 = 0.1\lambda^{-3}$, $a = -1.5\lambda$, $b = 1.0\lambda$, and angle of incidence $\theta' = -45°$.

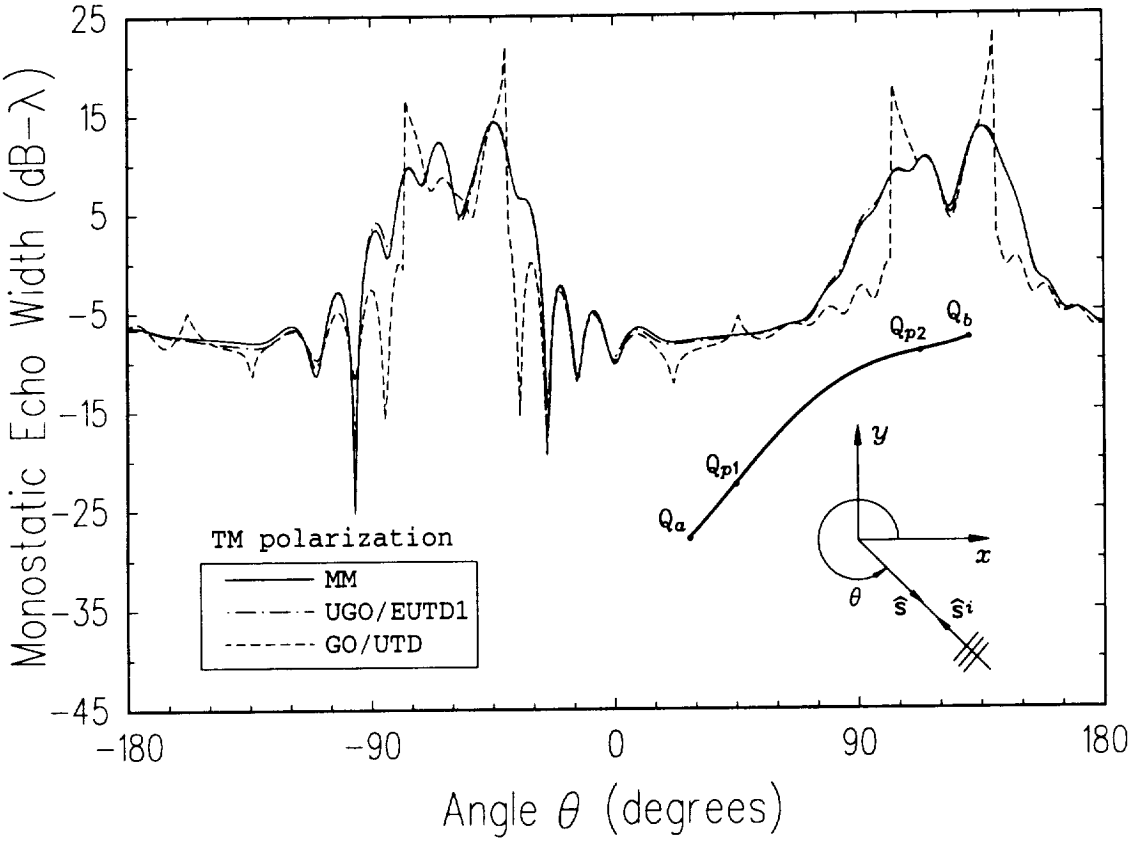

Figure 5.19: Monostatic echo width (TM Case) of a fourth order polynomial strip with $a_0 = 1.0\lambda$, $a_1 = 0.5$, $a_2 = -0.4\lambda^{-1}$, $a_3 = 0.1\lambda^{-2}$, $a_4 = 0.1\lambda^{-3}$, $a = -1.5\lambda$, $b = 1.0\lambda$.

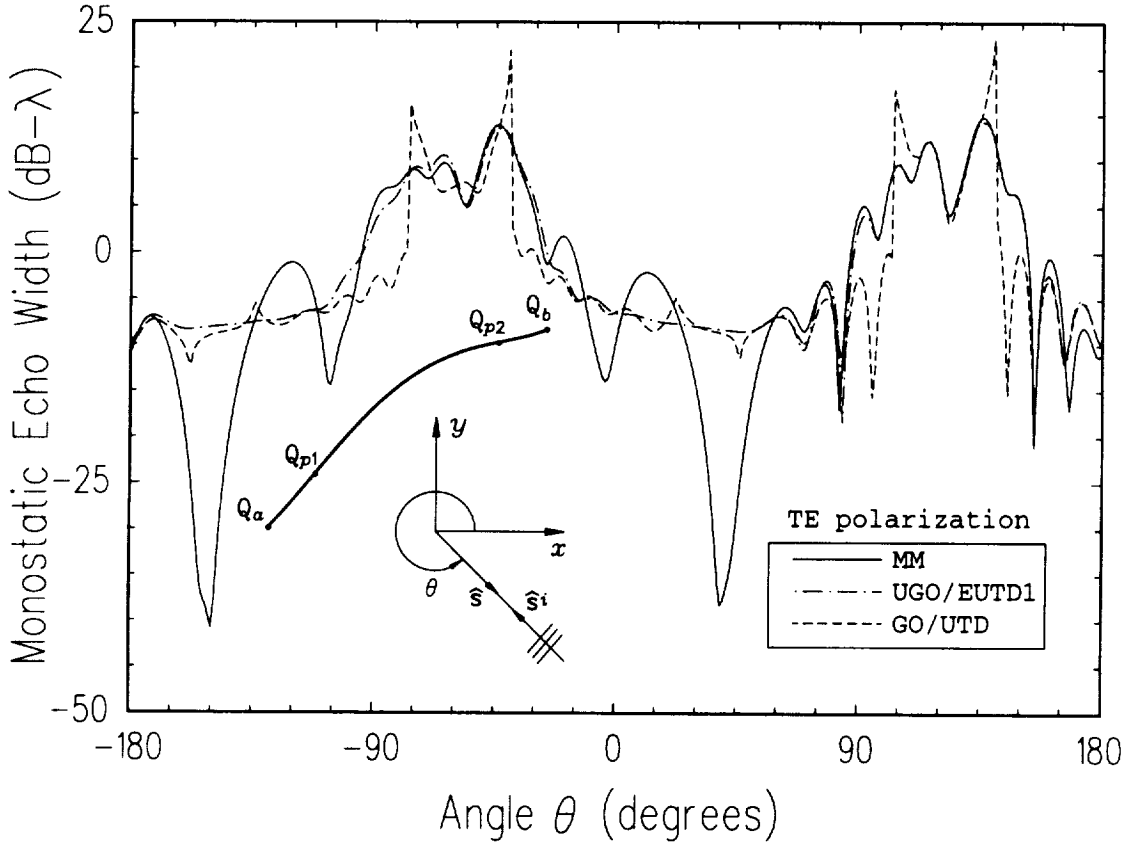

Figure 5.20: Monostatic echo width (TE Case) of a fourth order polynomial strip with $a_0 = 1.0\lambda$, $a_1 = 0.5$, $a_2 = -0.4\lambda^{-1}$, $a_3 = 0.1\lambda^{-2}$, $a_4 = 0.1\lambda^{-3}$, $a = -1.5\lambda$, and $b = 1.0\lambda$.

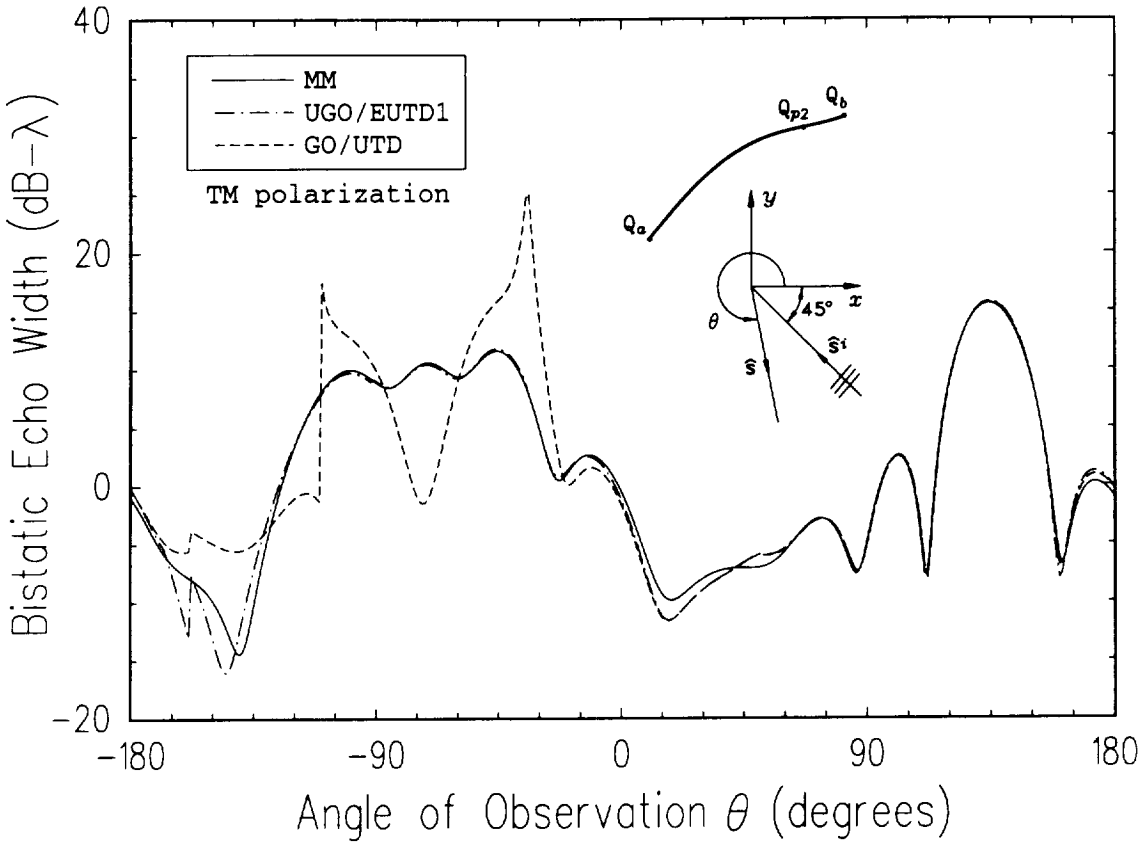

Figure 5.21: Bistatic echo width (TM Case) of a fourth order polynomial strip with $a_0 = 1.0\lambda$, $a_1 = 0.5$, $a_2 = -0.4\lambda^{-1}$, $a_3 = 0.1\lambda^{-2}$, $a_4 = 0.1\lambda^{-3}$, $a = -1.1\lambda$, $b = 1.0\lambda$, and angle of incidence $\theta' = -45°$.

whereas the agreement is only good near broadside for the TE case. Also, notice that when the concave part of the strip is illuminated and whispering gallery modes are excited, the agreement is worse than the case where the convex part of the strip is illuminated.

Figures 5.21 and 5.22 show plots for the bistatic and monostatic echo width, respectively, of a fourth order polynomial strip with $a_0 = 1.0\lambda$, $a_1 = 0.5$, $a_2 = -0.4\lambda^{-1}$, $a_3 = 0.1\lambda^{-2}$, $a_4 = 0.1\lambda^{-3}$, $a = -1.1\lambda$, and $b = 1.0\lambda$. For this geometry, the edge at Q_a coincides with the zero-curvature point, Q_{p1}, forming a composite shadow boundary. The UGO/EUTD solution shows good agreement with MM, whereas the GO/UTD solution fails both near the composite shadow boundary and the caustic associated with Q_{p2}.

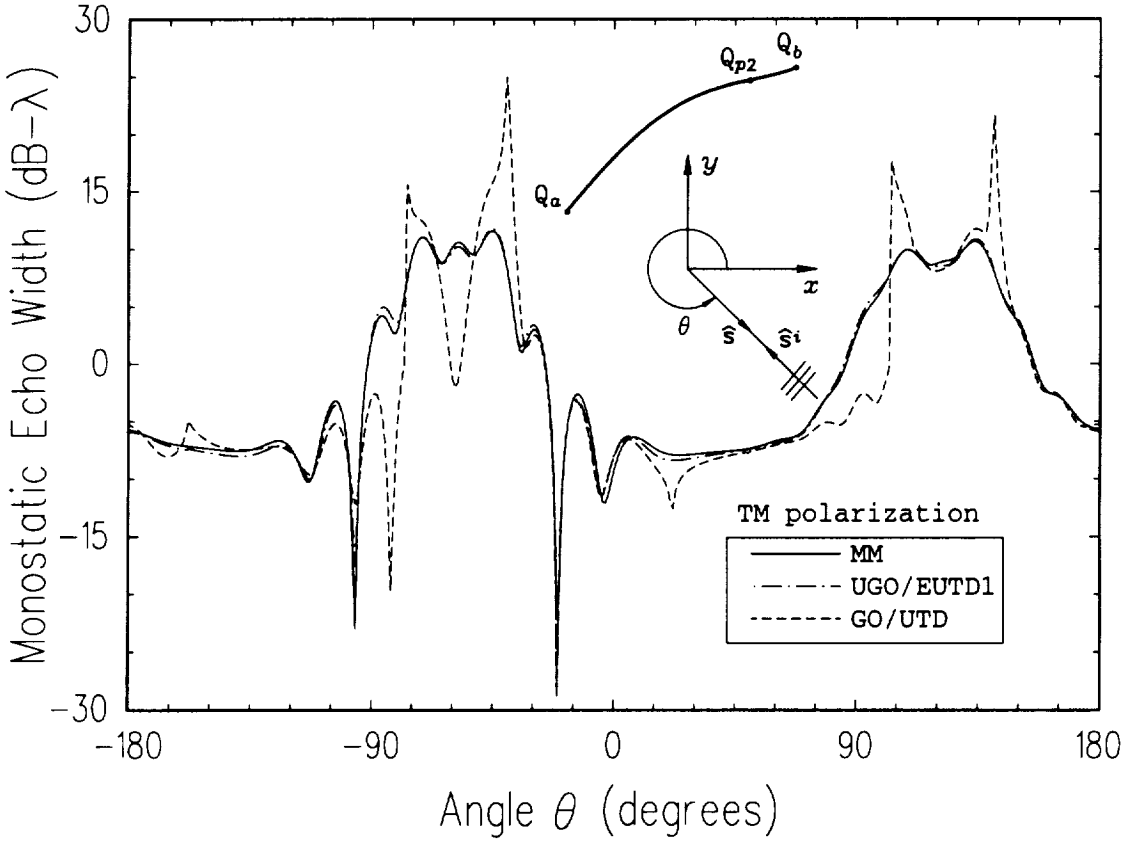

Figure 5.22: Monostatic echo width (TM Case) of a fourth order polynomial strip with $a_0 = 1.0\lambda$, $a_1 = 0.5$, $a_2 = -0.4\lambda^{-1}$, $a_3 = 0.1\lambda^{-2}$, $a_4 = 0.1\lambda^{-3}$, $a = -1.1\lambda$, $b = 1.0\lambda$.

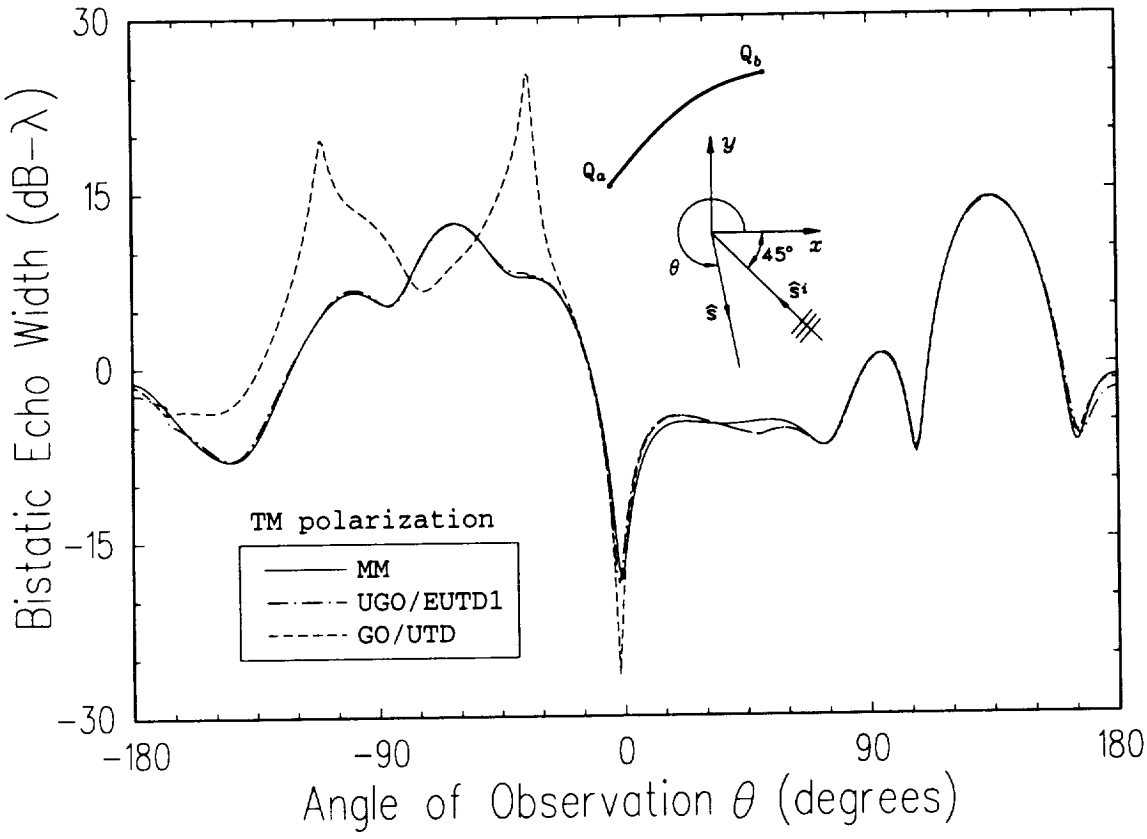

Figure 5.23: Bistatic echo width (TM Case) of a fourth order polynomial strip with $a_0 = 1.0\lambda$, $a_1 = 0.5$, $a_2 = -0.4\lambda^{-1}$, $a_3 = 0.1\lambda^{-2}$, $a_4 = 0.1\lambda^{-3}$, $a = -1.1\lambda$, $b = 0.6\lambda$, and angle of incidence $\theta' = -45°$.

Finally, Figures 5.23 and 5.24 show plots for the bistatic and monostatic echo width, respectively, of a fourth order polynomial strip with $a_0 = 1.0\lambda$, $a_1 = 0.5$, $a_2 = -0.4\lambda^{-1}$, $a_3 = 0.1\lambda^{-2}$, $a_4 = 0.1\lambda^{-3}$, $a = -1.1\lambda$, and $b = 0.6\lambda$. In this case, both edges coincide with the zero-curvature points forming a pair of composite shadow boundaries. The UGO/EUTD solution remains uniform across both composite shadow boundaries and shows good agreement with MM.

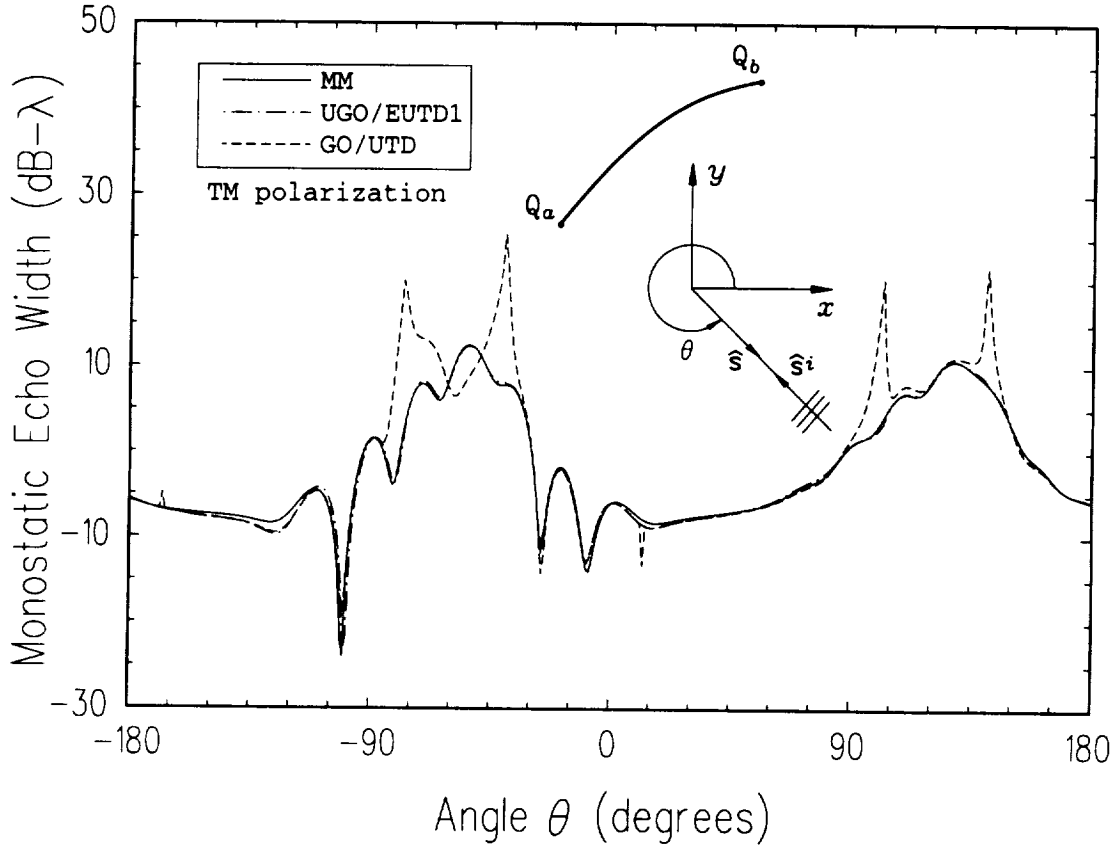

Figure 5.24: Monostatic echo width (TM Case) of a fourth order polynomial strip with $a_0 = 1.0\lambda$, $a_1 = 0.5$, $a_2 = -0.4\lambda^{-1}$, $a_3 = 0.1\lambda^{-2}$, $a_4 = 0.1\lambda^{-3}$, $a = -1.1\lambda$, $b = 0.6\lambda$.

Chapter 6

Summary and Conclusions

A uniform geometrical optics (UGO) and an extended uniform geometrical theory of diffraction (EUTD) were developed in this report for evaluating high frequency electromagnetic (EM) fields within transition regions associated with a two and three dimensional smooth caustic of reflected rays and a composite shadow boundary formed by the caustic termination or the confluence of the caustic with the reflection shadow boundary (RSB).

The UGO is a uniform version of the classic GO. It retains the simple ray optical expressions of classic GO and employs a new set of uniform reflection coefficients involving the Fock type Airy functions that provide for a finite reflected field near a smooth caustic on the lit side. Table 6.1 summarizes the UGO reflection coefficients for the lit side of a smooth caustic. The UGO also encompasses a uniform version of the complex GO ray field that exists on the dark side of the smooth caustic. The UGO complex ray reflection coefficients are summarized in Table 6.2 and involve the ordinary Airy function. They provide for a finite field near the smooth caustic on the dark side. The EUTD is an extension of the classic uniform geometrical theory of diffraction (UTD) and accounts for the non-ray optical behavior of the UGO reflected field near caustics by using a two-variable transition function involving the incomplete Airy functions in the expressions for the edge diffraction coefficients. It also uniformly recovers the classic UTD behavior of the edge diffracted field outside the composite shadow boundary transition region. The EUTD edge diffraction coefficients are summarized in Table 6.3. The UGO/EUTD expressions derived in this

Table 6.1: UGO reflection coefficients for the lit side of a smooth caustic (near-zone, arbitrary source illumination).

Reflection Coefficients	$\mathcal{R}_{s,h} = \mp e^{-j\frac{\pi}{4}}\,\gamma_\ell^{1/4}\,e^{-j(2/3)\gamma_\ell^{3/2}}\,\mathrm{W}_1(-\gamma_\ell)$ $\mp$ for a $\left\{\begin{array}{c}\text{soft}\\ \text{hard}\end{array}\right\}$ acoustic surface or $\left\{\begin{array}{c}\text{TM}\\ \text{TE}\end{array}\right\}$ polarization for a PEC surface.
Parameter	$\gamma_\ell = \left[\frac{3}{2}k\,\lvert(s_0^i + R_0) - (s^i + s^r)\rvert\right]^{2/3}$
Canonical Function	$\mathrm{W}_1(\gamma) \equiv \frac{j}{\sqrt{\pi}}\int_{L_{23}} e^{j(\gamma z + z^3/3)}dz$ Fock-type Airy function [16]
Notes	$\mathcal{R}^*_{s,h}$ should be used when $\rho_\ell^r/(\rho_\ell^r + s^r) < 0$.

Table 6.2: UGO complex ray reflection coefficients for the dark side of a smooth caustic (near-zone, arbitrary source illumination).

Reflection Coefficients	$\mathcal{R}_{s,h} = \mp 2\sqrt{\pi}\,\gamma_s^{1/4}\,e^{(2/3)\gamma_s^{3/2}}\,\mathrm{Ai}(\gamma_s)$ $\mp$ for a $\left\{\begin{array}{c}\text{soft}\\ \text{hard}\end{array}\right\}$ acoustic surface or $\left\{\begin{array}{c}\text{TM}\\ \text{TE}\end{array}\right\}$ polarization for a PEC surface.
Parameter	$\gamma_s = \left[\frac{3}{2}k\,\lvert(s_0^i + R_0) - (s^{ic} + s^{rc})\rvert\right]^{2/3}$
Canonical Function	$\mathrm{Ai}(\gamma) \equiv \frac{1}{2\pi}\int_{L_{21}} e^{j(\gamma z + z^3/3)}dz$ Ordinary (Miller-type) Airy function [17]

Table 6.3: EUTD edge diffraction coefficients valid near a composite shadow boundary (near-zone, oblique incidence, arbitrary source illumination).

Diffraction Coefficients	$\mathcal{D}_{s,h} = \frac{-e^{-j\frac{\pi}{4}}}{2\sin\vartheta_a\sqrt{2\pi k}}\left[\frac{1}{\cos\left(\frac{\varphi_a'-\varphi_a}{2}\right)} \mp \frac{1}{\cos\left(\frac{\varphi_a'+\varphi_a}{2}\right)}\right]\mathcal{F}(\gamma_a,\zeta_a)$ $\mp$ for a $\left\{\begin{array}{c}\text{soft}\\ \text{hard}\end{array}\right\}$ acoustic surface or $\left\{\begin{array}{c}\text{TM}\\ \text{TE}\end{array}\right\}$ polarization for a PEC surface.
Transition Function	$\mathcal{F}(\gamma,\zeta) = j(\gamma+\zeta^2)\mathrm{g}_i^*(\gamma,\zeta)e^{j(\gamma\zeta+\zeta^3/3)}$ $\mathrm{g}_i(\gamma,\zeta)$, $i=1,2,3$ are the incomplete Airy functions [9] $i = \left\{\begin{array}{ll}1 & \text{if } \zeta > (-\gamma)^{1/2}\\ 2 & \text{if } \zeta < -(-\gamma)^{1/2}\\ 3 & \text{otherwise}\end{array}\right\}$ for $\gamma < 0$, or $i = \left\{\begin{array}{ll}1 & \text{if } \zeta > 0\\ 2 & \text{if } \zeta < 0\end{array}\right\}$ for $\gamma > 0$
Arguments	$\gamma_a = -\mathrm{sgn}(L_d)k^{2/3}\frac{\sin\vartheta_0(\cos\varphi_0'+\cos\varphi_0)}{\lvert L_d(\varphi_a',\varphi_a;\vartheta_a)\rvert^{1/3}}$ $\zeta_a = u_a k^{1/3}\frac{\lvert\sin\vartheta_0(\cos\varphi_0'+\cos\varphi_0)-\sin\vartheta_a(\cos\varphi_a'+\cos\varphi_a)\rvert^{1/2}}{\lvert L_d(\varphi_a',\varphi_a;\vartheta_a)\rvert^{1/6}}$ $u_a = \left\{\begin{array}{ll}+1 & \text{if } Q_0 \ni S\\ -1 & \text{if } Q_0 \in S\end{array}\right.$
Notes	L_d is the EUTD distance parameter given in (3.110)-(3.117) $\mathcal{F}^*(\gamma_a,\zeta_a)$ should be used when $L_d < 0$

Table 6.4: UGO reflection coefficients (far-zone, plane wave illumination).

Reflection Coefficients	$\mathcal{R}_{s,h} = \mp e^{j\frac{\pi}{4}} \sqrt{\frac{\nu-1}{2\pi}} \gamma_r^{\frac{\nu-2}{2(\nu-1)}} e^{-jl[(\nu-1)/\nu]\gamma_r^{\frac{\nu}{\nu-1}}} I_r^*(-\gamma_r, \nu)$ $\mp$ for a $\left\{ \begin{array}{c} \text{soft} \\ \text{hard} \end{array} \right\}$ acoustic surface or $\left\{ \begin{array}{c} \text{TM} \\ \text{TE} \end{array} \right\}$ polarization for a PEC surface.
Parameters	$\gamma_r = \left\{ k \left(\frac{\nu}{\nu-1} \right) \left\| [\vec{r}(Q_r) - \vec{r}(Q_p)] \cdot (\hat{s} - \hat{s}^i) \right\| \right\}^{\frac{\nu-1}{\nu}}$ $\nu = l + 2$, l is the order of the z-c point, Q_p
Canonical Function	$I_r(\gamma, \nu) \equiv \int_{\infty \exp(-j3\pi/2\nu)}^{\infty \exp(j\pi/2\nu)} e^{j(\gamma z + z^\nu/\nu)} dz$
Notes	$\mathcal{R}_{s,h}^*$ should be used when $\rho_g(Q_r) < 0$.

report are approximate ones because the surface current used in the spatial domain radiation integral representation for the fields was found using the PO approximation. Therefore, the UGO/EUTD expressions account for only first order mechanisms and remain valid within regions where grazing fields do not exist.

The UGO/EUTD analysis was employed to investigate the far-zone RCS problem of plane wave scattering from two and three dimensional polynomial defined surfaces, and uniform reflection, zero-curvature, and edge diffraction coefficients were derived. These new UGO/EUTD coefficients involve a generalized form of the complete and incomplete Airy integrals that serve as canonical functions. The UGO reflection coefficients and the EUTD zero-curvature and edge diffraction coefficients for far-zone observation and plane wave illumination are summarized in Tables 6.4, 6.5, and 6.6, respectively.

Numerical results for the scattering and diffraction from cubic and fourth order polynomial strips were also shown and the UGO/EUTD solution was validated by comparison to an independent MM solution. The UGO/EUTD solution was also compared with the classic GO/UTD solution. The failure of the classic techniques near caustics and composite shadow boundaries was clearly demonstrated and it was

Table 6.5: EUTD zero-curvature diffraction coefficients (far-zone, plane wave illumination, oblique incidence).

Diffraction Coefficients	$\mathcal{D}^{co}_{s,h} = \mp \frac{e^{j\frac{\pi}{4}} k^{\frac{\nu-2}{2\nu}}}{\sin\vartheta_p\sqrt{2\pi}} L_p(\varphi'_p, \varphi_p, \vartheta_p, \nu) \begin{cases} I_{pl}(-\gamma_p, \nu), & \text{(lit side)} \\ I_{pd}(-\gamma_p, \nu), & \text{(dark side)} \end{cases}$ $\mathcal{D}^{ce}_{s,h} = \mp \frac{e^{j\frac{\pi}{4}} k^{\frac{\nu-2}{2\nu}}}{\sin\vartheta_p\sqrt{2\pi}} L_p(\varphi'_p, \varphi_p, \vartheta_p, \nu) J_p(\gamma_p, \nu)$ $\mp$ for a $\left\{ \begin{array}{c} \text{soft} \\ \text{hard} \end{array} \right\}$ acoustic surface or $\left\{ \begin{array}{c} \text{TM} \\ \text{TE} \end{array} \right\}$ polarization for a PEC surface.
Parameters	$\gamma_p = k^{\frac{\nu-1}{\nu}} \tilde{\omega}(Q_p, \nu) \sin\vartheta_p \lvert \cos\varphi'_p + \cos\varphi_p \rvert$ $L_p = \tilde{w}(Q_p, \nu) \sin\vartheta_p \cos\left(\frac{\varphi'_p - \varphi_p}{2}\right)$ $\tilde{w}(Q_p, \nu) = \left\lvert \frac{(\nu-1)!}{\widetilde{m}(Q_p,\nu)} \right\rvert^{\frac{1}{\nu}}$ $\widetilde{m}(Q_p, \nu) = -\kappa_1^{(\nu-2)}(Q_p)(\sin\varphi'_p + \sin\varphi_p)$ $\nu = l + 2$, l is the order of the z-c point, Q_p
Canonical Functions	$I_{pl}(\gamma, \nu) \equiv \int_{\infty \exp[j(-\pi+3\pi/2\nu)]}^{\infty \exp(-j3\pi/2\nu)} e^{j(\gamma z + z^\nu/\nu)} dz$; (ν odd) $I_{pd}(\gamma, \nu) \equiv \int_{\infty \exp[j(\pi-\pi/2\nu)]}^{\infty \exp(j\pi/2\nu)} e^{j(\gamma z + z^\nu/\nu)} dz$; (ν odd) $J_p(\gamma, \nu) \equiv \int_{\infty \exp[j(\pi-3\pi/2\nu)]}^{\infty \exp(j\pi/2\nu)} e^{j(\gamma z + z^\nu/\nu)} dz$; (ν even)
Notes	$J_p^*(\gamma_p, \nu)$ should be used when $\widetilde{m}(Q_p, \nu) < 0$.

Table 6.6: EUTD edge diffraction coefficients (far-zone, plane wave illumination, oblique incidence).

Diffraction Coefficients	$\mathcal{D}^{e}_{s,h} = \frac{-e^{-j\frac{\pi}{4}}}{2\sin\vartheta_a\sqrt{2\pi k}}\left[\frac{1}{\cos\left(\frac{\varphi'_a-\varphi_a}{2}\right)} \mp \frac{\mathcal{F}(\gamma_d,\zeta_d,\nu)}{\cos\left(\frac{\varphi'_a+\varphi_a}{2}\right)}\right]$ $\mp$ for a $\left\{\begin{array}{c}\text{soft}\\ \text{hard}\end{array}\right\}$ acoustic surface or $\left\{\begin{array}{c}\text{TM}\\ \text{TE}\end{array}\right\}$ polarization for a PEC surface.
Transition Function	$\mathcal{F}(\gamma,\zeta,\nu) = j(\gamma+\zeta^{\nu-1})I^{*}_{a}(\gamma,\zeta,\nu)e^{j(\gamma\zeta+\zeta^{\nu}/\nu)}$ $I_a(\gamma,\zeta,\nu) \equiv \int_{\zeta}^{\infty\exp[j\psi_0(\nu)]} e^{j(\gamma z+z^{\nu}/\nu)}dz$ $\psi_0(\nu) = \left\{\begin{array}{ll}\pi/2\nu & \text{if } [\text{sgn}(\zeta)]^{\nu-1}(\gamma+\zeta^{\nu-1})>0\\ -3\pi/2\nu & \text{otherwise}\end{array}\right.$
Arguments	$\gamma_d = \left\{\begin{array}{ll}\gamma_a & \text{if } \nu \text{ is odd}\\ \text{sgn}(\zeta_a) & \text{if } \nu \text{ is even,}\end{array}\right.$ $\zeta_d = \lvert\zeta_a\rvert$ $\gamma_a = \text{sgn}[m(v_p,\nu)]k^{\frac{\nu-1}{\nu}}\sin\vartheta_p(\cos\varphi'_p+\cos\varphi_p)\omega(v_p,\nu)$ $\zeta_a = u_a k^{1/\nu}\lvert\sin\vartheta_p(\cos\varphi'_p+\cos\varphi_p)\omega(v_p,\nu)$ $-\sin\vartheta_a(\cos\varphi'_a+\cos\varphi_a)\omega(v_a,\nu)\rvert^{\frac{1}{\nu-1}}$ $u_a = \left\{\begin{array}{ll}+1 & \text{if } Q_0 \ni S\\ -1 & \text{if } Q_0 \in S\end{array}\right.$ $w(v,\nu) = \left\lvert\frac{(\nu-1)!}{m(v_p,\nu)}\right\rvert^{\frac{1}{\nu}}$, $m(v,\nu) = \frac{\vec{r}^{(\nu)}(v_p)\cdot\left(\hat{s}-\hat{s}^{i}\right)}{\lvert\vec{r}'(v)\rvert^{\nu}}$ $\nu = l+2$, l is the order of the z-c point, Q_p
Notes	$\mathcal{F}^{*}(\gamma_d,\zeta_d,\nu)$ should be used when $R_1(Q_a)<0$

shown that the UGO/EUTD results remained valid and uniformly reduced to the classic results away from the transition regions.

It is believed that the work accomplished in this report is an important and timely first step in the development of a useful engineering solution for the interaction of high frequency electromagnetic waves with CAD generated surface components. Such components are often designed using polynomial or spline surface patches that are then put together to create the desired models for complex structures. It is therefore advantageous to use the CAD geometry information directly for RCS or antenna analysis. Topics for future research include the extension of the EUTD edge diffraction coefficients to handle wedge type geometries, and also the development of a diffraction coefficient for a vertex in a polynomial or spline surface patch.

Appendix A

The Ordinary and Fock-Type Airy Functions

Both the ordinary (Miller-type) and Fock-type Airy functions satisfy Airy's differential Equation [23], that is

$$y''(\sigma) - \sigma y(\sigma) \equiv 0\,. \tag{A.1}$$

The ordinary Airy functions $\mathrm{Ai}(\sigma)$ and $\mathrm{Bi}(\sigma)$ are two independent solutions of (A.1), and in integral form they are defined as follows:

$$\mathrm{Ai}(\sigma) \triangleq \frac{1}{2\pi}\int_{L_{21}} e^{j(\sigma z + z^3/3)}\,dz\,, \tag{A.2}$$

$$\mathrm{Bi}(\sigma) \triangleq \frac{j}{2\pi}\int_{L_{23}+L_{13}} e^{j(\sigma z + z^3/3)}\,dz\,, \tag{A.3}$$

where the contours of integration L_{21}, L_{23} and L_{31} are shown in Figure A.1.

Their power series form which may be used for small argument approximations is given by [21]

$$\mathrm{Ai}(\sigma) = c_1 f(\sigma) - c_2 g(\sigma)\,, \tag{A.4}$$

$$\mathrm{Bi}(\sigma) = \sqrt{3}\,[c_1 f(\sigma) + c_2 g(\sigma)]\,, \tag{A.5}$$

where

$$f(\sigma) = 1 + \frac{1}{3!}\sigma^3 + \frac{1\cdot 4}{6!}\sigma^6 + \frac{1\cdot 4\cdot 7}{9!}\sigma^9 + \cdots\,, \tag{A.6}$$

$$g(\sigma) = \sigma + \frac{2}{4!}\sigma^4 + \frac{2\cdot 5}{7!}\sigma^7 + \frac{2\cdot 5\cdot 8}{10!}\sigma^{10} + \cdots\,, \tag{A.7}$$

$$c_1 = \mathrm{Ai}(0) = \mathrm{Bi}(0)/\sqrt{3} = 3^{-2/3}/\Gamma(2/3)\,, \tag{A.8}$$

$$c_2 = -\mathrm{Ai}'(0) = \mathrm{Bi}'(0)/\sqrt{3} = 3^{-1/3}/\Gamma(1/3)\,. \tag{A.9}$$

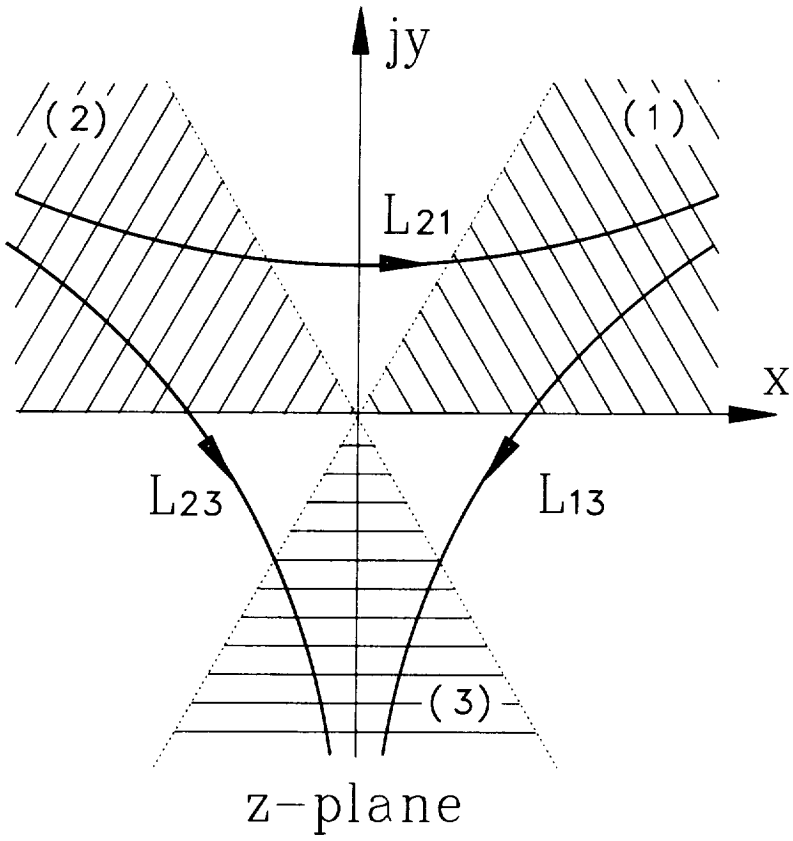

Figure A.1: Contours of integration for the ordinary Airy functions.

The asymptotic forms of the ordinary Airy functions and their derivatives are as follows:

1. $\sigma \gg 1$:

$$\mathrm{Ai}(\sigma) \sim \frac{\sigma^{-1/4}}{2\sqrt{\pi}} e^{-(2/3)\sigma^{3/2}}, \tag{A.10}$$

$$\mathrm{Ai}'(\sigma) \sim -\frac{\sigma^{1/4}}{2\sqrt{\pi}} e^{-(2/3)\sigma^{3/2}}, \tag{A.11}$$

$$\mathrm{Bi}(\sigma) \sim \frac{\sigma^{-1/4}}{\sqrt{\pi}} e^{(2/3)\sigma^{3/2}}, \tag{A.12}$$

$$\mathrm{Bi}'(\sigma) \sim \frac{\sigma^{1/4}}{\sqrt{\pi}} e^{(2/3)\sigma^{3/2}}, \tag{A.13}$$

2. $\sigma \ll -1$:

$$\mathrm{Ai}(-\sigma) \sim \frac{\sigma^{-1/4}}{\sqrt{\pi}} \sin\left(\frac{2}{3}\sigma^{3/2} + \frac{\pi}{4}\right), \tag{A.14}$$

$$\mathrm{Ai}'(-\sigma) \sim -\frac{\sigma^{1/4}}{\sqrt{\pi}} \cos\left(\frac{2}{3}\sigma^{3/2} + \frac{\pi}{4}\right), \tag{A.15}$$

$$\mathrm{Bi}(-\sigma) \sim \frac{\sigma^{-1/4}}{\sqrt{\pi}} \cos\left(\frac{2}{3}\sigma^{3/2} + \frac{\pi}{4}\right), \tag{A.16}$$

$$\mathrm{Bi}'(-\sigma) \sim \frac{\sigma^{1/4}}{\sqrt{\pi}} \sin\left(\frac{2}{3}\sigma^{3/2} + \frac{\pi}{4}\right). \tag{A.17}$$

Complete asymptotic expansions for the ordinary Airy functions may be found in [21].

The Fock-type Airy functions $\mathrm{W}_{1,2}(\sigma)$ [16] are also independent solutions of (A.1), and in integral form they are defined as follows:

$$\mathrm{W}_1(\sigma) \triangleq \frac{j}{\sqrt{\pi}} \int_{L_{23}} e^{j(\sigma z + z^3/3)}\, dz, \tag{A.18}$$

$$\mathrm{W}_2(\sigma) \triangleq \frac{j}{\sqrt{\pi}} \int_{L_{13}} e^{j(\sigma z + z^3/3)}\, dz = \mathrm{W}_1^*(\sigma). \tag{A.19}$$

In terms of the ordinary Airy functions they are given by

$$\mathrm{W}_{1,2}(\sigma) = \sqrt{\pi}\,[\mathrm{Bi}(\sigma) \pm j\mathrm{Ai}(\sigma)]. \tag{A.20}$$

Of particular interest are the asymptotic forms of $\mathrm{W}_{1,2}$ and their derivatives for $\sigma \ll -1$. Using (A.14)-(A.17) and (A.20) they are given by

$$\mathrm{W}_1(-\sigma) \sim e^{j\frac{\pi}{4}} \sigma^{-1/4}\, e^{j(2/3)\sigma^{3/2}}, \tag{A.21}$$

$$W_1'(-\sigma) \sim -e^{-j\frac{\pi}{4}}\sigma^{1/4}\, e^{j(2/3)\sigma^{3/2}}, \tag{A.22}$$

$$W_2(-\sigma) \sim e^{-j\frac{\pi}{4}}\sigma^{-1/4}\, e^{-j(2/3)\sigma^{3/2}}, \tag{A.23}$$

$$W_2'(-\sigma) \sim -e^{j\frac{\pi}{4}}\sigma^{1/4}\, e^{-j(2/3)\sigma^{3/2}}. \tag{A.24}$$

Appendix B

Numerical Evaluation of the Incomplete Airy Functions

In this appendix, a method for the accurate and efficient evaluation of the incomplete Airy functions is developed. The incomplete Airy functions are functions of two variables and they satisfy the parabolic partial differential equation applied by Fock [24] to the study of fields near the surface of a smooth convex scattering body, that is

$$\left[\frac{\partial^2}{\partial\beta^2} - \beta - j\frac{\partial}{\partial\xi}\right] \mathrm{g}_i(\beta,\xi) \equiv 0 \;\; ; \quad i = 1,2,3\,. \tag{B.1}$$

In integral form, the solutions of (B.1) are defined as follows:

$$\mathrm{g}_i(\beta,\xi) \triangleq \int_{\xi_i}^{\infty \exp(j\psi_i)} e^{j(\beta z + z^3/3)}\, dz \;\; ; \quad i = 1,2,3, \tag{B.2}$$

where the upper limit lies within one of the three sectors of the complex z–plane in which the integral converges, that is

$$2(i-1)\frac{\pi}{3} \;\leq\; \psi_i \;\leq\; (2i-1)\frac{\pi}{3} \;\; ; \quad i = 1,2,3\,. \tag{B.3}$$

The contours of integration for the incomplete Airy functions are shown in Figure B.1.

Only the function $\mathrm{g}_1(\beta,\xi)$ will be considered in this appendix since the other two functions, namely g_2 and g_3, can be obtained from g_1 and the ordinary and Fock-type Airy functions, that is

$$\mathrm{g}_2(\beta,\xi) = \mathrm{g}_1(\beta,\xi) - 2\pi\,\mathrm{Ai}(\beta)\,, \tag{B.4}$$

and

$$\mathrm{g}_3(\beta,\xi) = \mathrm{g}_1(\beta,\xi) - j\sqrt{\pi}\,\mathrm{W}_2(\beta)\,. \tag{B.5}$$

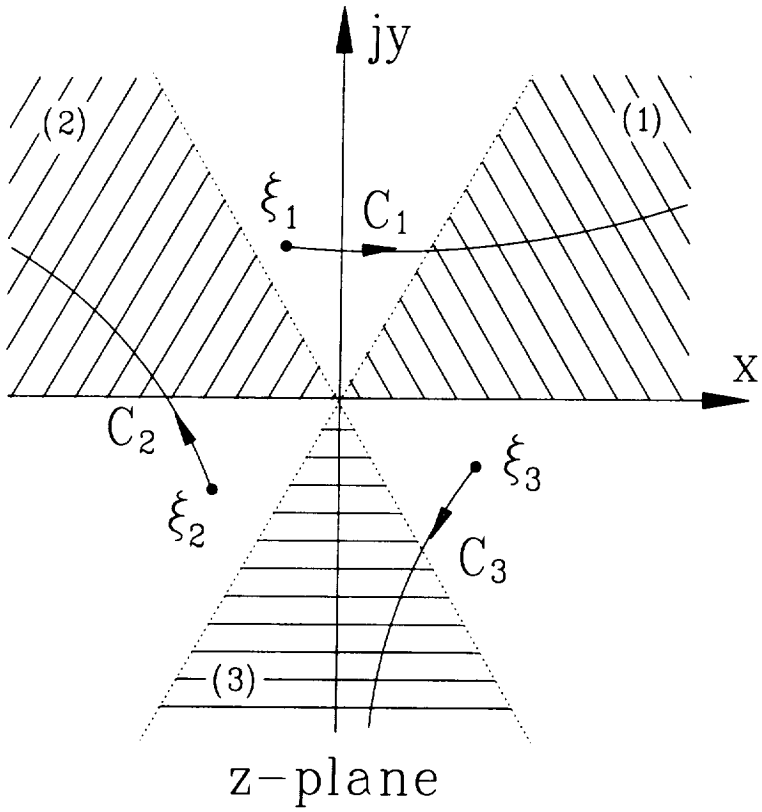

Figure B.1: Contours of integration for the incomplete Airy functions.

The arguments β and ξ will be taken as real, since in most practical applications real β and ξ are of primary interest. However, this is not a requirement for the analysis that follows and the resulting formulae are valid for arbitrary values of β and ξ. In addition, ξ will be restricted to positive values since for negative values of ξ, g_1 may be obtained using the following expression:

$$g_1(\beta, -\xi) = 2\pi \, \mathrm{Ai}(\beta) - g_1^*(\beta, \xi), \tag{B.6}$$

with $(*)$ denoting the complex conjugate operation.

B.1 Derivation of the series solution

In order to obtain a series solution for $g_1(\beta, \xi)$, we begin with the parabolic differential equation in (B.1) and assume two independent solutions of the form

$$y_1(\beta, \xi) = \sum_{n=0}^{\infty} a_n(\xi)\beta^n, \tag{B.7}$$

$$\text{and} \quad y_2(\beta, \xi) = \sum_{n=0}^{\infty} b_n(\xi)\beta^n. \tag{B.8}$$

Substituting (B.7) and (B.8) in (B.1) we obtain the following expressions:

$$\sum_{n=2}^{\infty} n(n-1)a_n(\xi)\beta^{n-2} - \sum_{n=0}^{\infty} a_n(\xi)\beta^{n+1} - j\sum_{n=0}^{\infty} a_n'(\xi)\beta^n \equiv 0, \tag{B.9}$$

$$\text{and} \quad \sum_{n=2}^{\infty} n(n-1)b_n(\xi)\beta^{n-2} - \sum_{n=0}^{\infty} b_n(\xi)\beta^{n+1} - j\sum_{n=0}^{\infty} b_n'(\xi)\beta^n \equiv 0. \tag{B.10}$$

For Equations (B.9) and (B.10) to be satisfied, the sum of coefficients of like powers of β must be zero for any value of ξ. To obtain the first independent solution, y_1, we let $a_1(\xi) \equiv 0$, and setting the sum of coefficients of like powers in (B.9) equal to zero we obtain

$$a_1(\xi) = 0, \quad \forall\, \xi, \tag{B.11}$$

$$a_2(\xi) = \frac{j}{2}a_0'(\xi), \tag{B.12}$$

$$\text{and} \quad a_n(\xi) = \frac{a_{n-3}(\xi) + j a_{n-2}'(\xi)}{n(n-1)}, \quad n \geq 3. \tag{B.13}$$

Similarly, for the second independent solution, y_2, we let $b_0(\xi) \equiv 0$ and setting the sum of coefficients of like powers in (B.10) equal to zero we obtain

$$b_0(\xi) = 0, \quad \forall\, \xi, \tag{B.14}$$

$$b_2(\xi) = 0, \quad \forall\, \xi, \tag{B.15}$$

$$\text{and} \quad b_n(\xi) = \frac{b_{n-3}(\xi) + j b'_{n-2}(\xi)}{n(n-1)}, \quad n \geq 3. \tag{B.16}$$

Thus, y_1 and y_2 are given by:

$$y_1(\beta,\xi) = a_0(\xi) + \sum_{n=2}^{\infty} a_n(\xi)\beta^n, \tag{B.17}$$

$$\text{and} \quad y_2(\beta,\xi) = b_1(\xi)\beta + \sum_{n=2}^{\infty} b_n(\xi)\beta^n, \tag{B.18}$$

where $a_n(\xi)$ and $b_n(\xi)$ for $n \geq 2$ can be expressed in terms of $a_0(\xi)$, $b_1(\xi)$ and their derivatives, respectively, via Equations (B.11)-(B.16). Now, $g_1(\beta,\xi)$ must be equal to the sum of the two independent solutions, that is

$$g_1(\beta,\xi) = a_0(\xi) + b_1(\xi)\beta + \sum_{n=2}^{\infty} [a_n(\xi) + b_n(\xi)]\beta^n, \tag{B.19}$$

$$\text{and} \quad \frac{\partial}{\partial\beta} g_1(\beta,\xi) = b_1(\xi) + \sum_{n=2}^{\infty} n[a_n(\xi) + b_n(\xi)]\beta^{n-1}. \tag{B.20}$$

Although the coefficients $a_n(\xi)$ and $b_n(\xi)$ can be combined into a single coefficient, keeping them separate greatly simplifies their evaluation in a computer code.

Finally, it remains to find expressions for $a_0(\xi)$ and $b_1(\xi)$ in order to complete the solution. This can be accomplished by applying the proper boundary conditions at $\beta = 0$ using the integral form of $g_1(\beta,\xi)$ given in (B.2), that is

$$a_0(\xi) = g_1(\beta,\xi)|_{\beta=0} = \int_{\xi}^{\infty} e^{jz^3/3}\, dz, \tag{B.21}$$

and

$$b_1(\xi) = \frac{\partial}{\partial\beta} g_1(\beta,\xi)\bigg|_{\beta=0} = \int_{\xi}^{\infty} jz\, e^{jz^3/3}\, dz. \tag{B.22}$$

The functions $a_0(\xi)$ and $b_1(\xi)$ can be expressed in terms of the incomplete Gamma function [21] as follows:

$$a_0(\xi) = e^{j\pi/6}\, 3^{-2/3}\, \Gamma(1/3, -j\xi^3/3), \tag{B.23}$$

$$b_1(\xi) = -e^{-j\pi/6}\, 3^{-1/3}\, \Gamma(2/3, -j\xi^3/3), \tag{B.24}$$

where

$$\Gamma(x,y) = \int_{y}^{\infty} t^{x-1}\, e^{-t}\, dt\,, \quad \Re(x) > 0\,. \tag{B.25}$$

Using the series solution of the incomplete Gamma function [21], $a_0(\xi)$ and $b_1(\xi)$ are computed using the following expressions:

$$a_0(\xi) \approx e^{j\pi/6}\, 3^{-2/3}\, \Gamma(1/3) - \xi \sum_{n=0}^{N(\xi)} \frac{(j\xi^3/3)^n}{(3n+1)n!}\,, \tag{B.26}$$

$$\text{and } b_1(\xi) \approx -e^{-j\pi/6}\, 3^{-1/3}\, \Gamma(2/3) - j\xi^2 \sum_{n=0}^{N(\xi)} \frac{(j\xi^3/3)^n}{(3n+2)n!}\,. \tag{B.27}$$

The number of terms in the series, $N(\xi)$, is given by the empirical formula:

$$N(\xi) = 2 + 4\xi^2\,, \tag{B.28}$$

and results in a truncation error of less than 10^{-6}. The derivatives of $a_0(\xi)$ and $b_1(\xi)$ are given by:

$$a_0^{(k)}(\xi) = j d_k a_0^{(k-3)}(\xi) + e_k a_0^{(k-2)}(\xi) + j\xi^2 a_0^{(k-1)}(\xi)\,, \quad n \geq 3\,, \tag{B.29}$$

$$b_1^{(k)}(\xi) = j(k-1) a_0^{(k-1)}(\xi) + j\xi a_0^{(k)}(\xi)\,, \quad n \geq 1\,, \tag{B.30}$$

where

$$a_0^{(1)}(\xi) = -e^{j\xi^3/3}\,, \tag{B.31}$$

$$\text{and } a_0^{(2)}(\xi) = -j\xi^2 e^{j\xi^3/3}\,. \tag{B.32}$$

The constants d_k and e_k are obtained using the following recursive relationships:

$$d_k = d_{k-1} + e_{k-1}\,, \tag{B.33}$$

$$\text{and } e_k = e_{k-1} + 2\,, \quad k \geq 3\,, \tag{B.34}$$

with $d_2 = e_2 = 0$.

When $\xi \to -\infty$, our solution should reduce to the series solution for the ordinary Airy function, $\mathrm{Ai}(\beta)$, given in Appendix A. In this case we have

$$a_0(\xi \to -\infty) = 2\pi\, \mathrm{Ai}(0) = 2.23070703\,, \tag{B.35}$$

$$b_1(\xi \to -\infty) = 2\pi\, \mathrm{Ai}'(0) = -1.62621025\,, \tag{B.36}$$

and using (B.11)–(B.18) we obtain

$$\begin{aligned} \mathrm{g}_1(\beta,\xi\to-\infty) &= 2\pi\,\mathrm{Ai}(0)\left(1+\frac{1}{3!}\beta^3+\frac{1\cdot4}{6!}\beta^6+\frac{1\cdot4\cdot7}{9!}\beta^9+\cdots\right) \\ &+ 2\pi\,\mathrm{Ai}'(0)\left(\beta+\frac{2}{4!}\beta^4+\frac{2\cdot5}{7!}\beta^7+\frac{2\cdot5\cdot8}{10!}\beta^{10}+\cdots\right) \\ &= 2\pi\,\mathrm{Ai}(\beta)\,, \end{aligned} \tag{B.37}$$

which is a necessary condition for the validity of (B.19).

B.2 Derivation of asymptotic formulae

In this section, three asymptotic formulae for the incomplete Airy function, $g_1(\beta,\xi)$, involving several terms are derived and serve as large argument forms. We begin by introducing the large parameter Ω in the integral form of $\mathrm{g}_1(\beta,\xi)$, and examine the following integral:

$$I_0(\sigma,\gamma;\Omega)=\int_\gamma^\infty e^{j\Omega(\sigma z+z^3/3)}\,dz\,. \tag{B.38}$$

The objective is to obtain asymptotic expansions for I_0 as $\Omega\to\infty$ for various dispositions of the saddle points and endpoint. Then, the asymptotic formulae for $g_1(\beta,\xi)$ may be obtained using the following expression:

$$g_1(\beta,\xi)=\Omega^{1/3}I_0(\sigma=\beta\Omega^{-2/3},\gamma=\xi\Omega^{-1/3};\Omega)\,. \tag{B.39}$$

Since we are interested in real β and ξ with $\xi\geq0$, the analysis that follows will be restricted to real σ and γ, with $\gamma\geq0$.

Asymptotic Formula for $\beta+\xi^2\gg1$

This case corresponds to the endpoint being far removed from the possibly neighboring saddle points of the integrand in (B.38), or $\gamma\gg|\sigma|^{1/2}$. Although the sign of σ is irrelevant in this case, the saddle points $z_{1,2}=\pm(-\sigma)^{1/2}$ are taken as real for simplicity. Also, the original integration path P_0 in Figure B.2 is deformed into the steepest descent path, P_{sdp}, leading away from the endpoint at $z=\gamma$ and into the sector $0\leq\arg(z)\leq\pi/3$ of the complex z–plane. The asymptotic evaluation of I_0 can then be performed by means of Watson's lemma or alternatively by repeated integration by parts as follows:

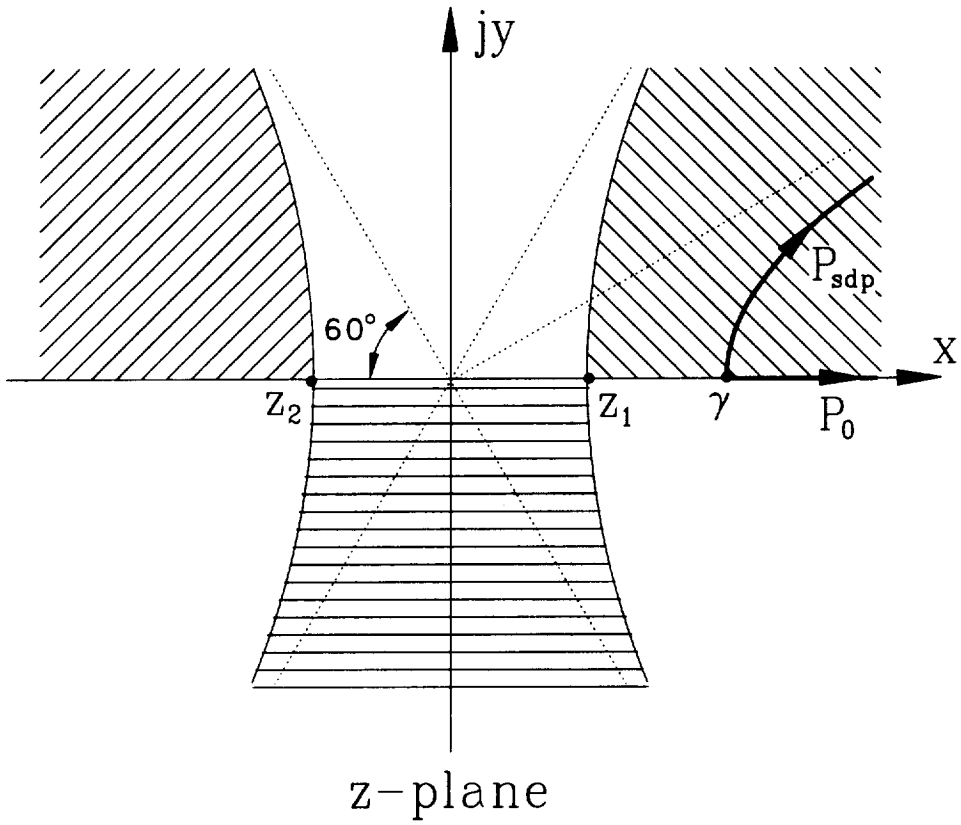

Figure B.2: Contour deformation of the incomplete Airy integral when $\gamma \gg (-\sigma)^{1/2}$.

$$I_0(\sigma,\gamma;\Omega) = \int_\gamma^\infty \frac{1}{j\Omega(\sigma+z^2)}\frac{d}{dz}e^{j\Omega(\sigma z+z^3/3)}dz = \frac{j}{\Omega(\sigma+\gamma^2)}e^{j\Omega(\sigma\gamma+\gamma^3/3)} + \int_\gamma^\infty \frac{2z}{j\Omega(\sigma+z^2)^2}e^{j\Omega(\sigma z+z^3/3)}dz\,. \tag{B.40}$$

Integration by parts can then be applied to the second integral in (B.40), and repeating the same procedure a few more times yields the following expression for $I_0(\sigma,\gamma;\Omega)$:

$$I_0(\sigma,\gamma;\Omega) \simeq e^{j\Omega(\sigma\gamma+\gamma^3/3)}\left\{\frac{1}{\Omega}\left[\frac{j}{\sigma+\gamma^2}\right]+\frac{1}{\Omega^2}\left[\frac{2\gamma}{(\sigma+\gamma^2)^3}\right] + \frac{1}{\Omega^3}\left[\frac{2j}{(\sigma+\gamma^2)^4}-\frac{12j\gamma^2}{(\sigma+\gamma^2)^5}\right]+\frac{1}{\Omega^4}\left[\frac{40\gamma}{(\sigma+\gamma^2)^6}-\frac{120\gamma^3}{(\sigma+\gamma^2)^7}\right] + \frac{1}{\Omega^5}\left[\frac{-40j}{(\sigma+\gamma^2)^7}-\frac{840j\gamma^2}{(\sigma+\gamma^2)^8}+\frac{1680j\gamma^4}{(\sigma+\gamma^2)^9}\right]\right\}+O(\Omega^{-6})\,. \tag{B.41}$$

Now, using Equations (B.39) and (B.41), the asymptotic formula for $\mathrm{g}_1(\beta,\xi)$ when $\xi \gg |\beta|^{1/2}$ is given by

$$\mathrm{g}_1(\beta,\xi) \sim e^{j(\beta\xi+\xi^3/3)}\left[\frac{j}{\beta+\xi^2}+\frac{2\xi}{(\beta+\xi^2)^3}+\frac{2j}{(\beta+\xi^2)^4}-\frac{12j\xi^2}{(\beta+\xi^2)^5} + \frac{40\xi}{(\beta+\xi^2)^6}-\frac{120\xi^3-40j}{(\beta+\xi^2)^7}-\frac{840j\xi^2}{(\beta+\xi^2)^8}+\frac{1680j\xi^4}{(\beta+\xi^2)^9}\right]. \tag{B.42}$$

The derivative of $\mathrm{g}_1(\beta,\xi)$ is given by

$$\frac{\partial}{\partial\beta}\mathrm{g}_1(\beta,\xi) \sim e^{j(\beta\xi+\xi^3/3)}\left[\frac{-\xi}{\beta+\xi^2}-\frac{j}{(\beta+\xi^2)^2}+\frac{2j\xi^2}{(\beta+\xi^2)^3}-\frac{8\xi}{(\beta+\xi^2)^4} - \frac{8j-12\xi^3}{(\beta+\xi^2)^5}+\frac{100j\xi^2}{(\beta+\xi^2)^6}-\frac{280\xi+120j\xi^4}{(\beta+\xi^2)^7} + \frac{1680\xi^3-280j}{(\beta+\xi^2)^8}+\frac{6720j\xi^2-1680\xi^5}{(\beta+\xi^2)^9}-\frac{15120j\xi^4}{(\beta+\xi^2)^{10}}\right]. \tag{B.43}$$

Asymptotic formula for $\beta \ll -1$

This case corresponds to real and widely separated saddle points ($\sigma \ll -1$) in the integrand of Equation (B.38), with the endpoint γ arbitrarily close to the saddle point $z_1 = (-\sigma)^{1/2}$, as shown in Figure B.3. For an asymptotic evaluation of (B.38) that holds uniformly as the endpoint γ approaches the saddle point z_1, we make the following transformation [9]:

$$q(z) = \sigma z + z^3/3 = q(z_1) + s^2 = -\frac{2}{3}(-\sigma)^{3/2} + s^2 = \tau(s)\,, \tag{B.44}$$

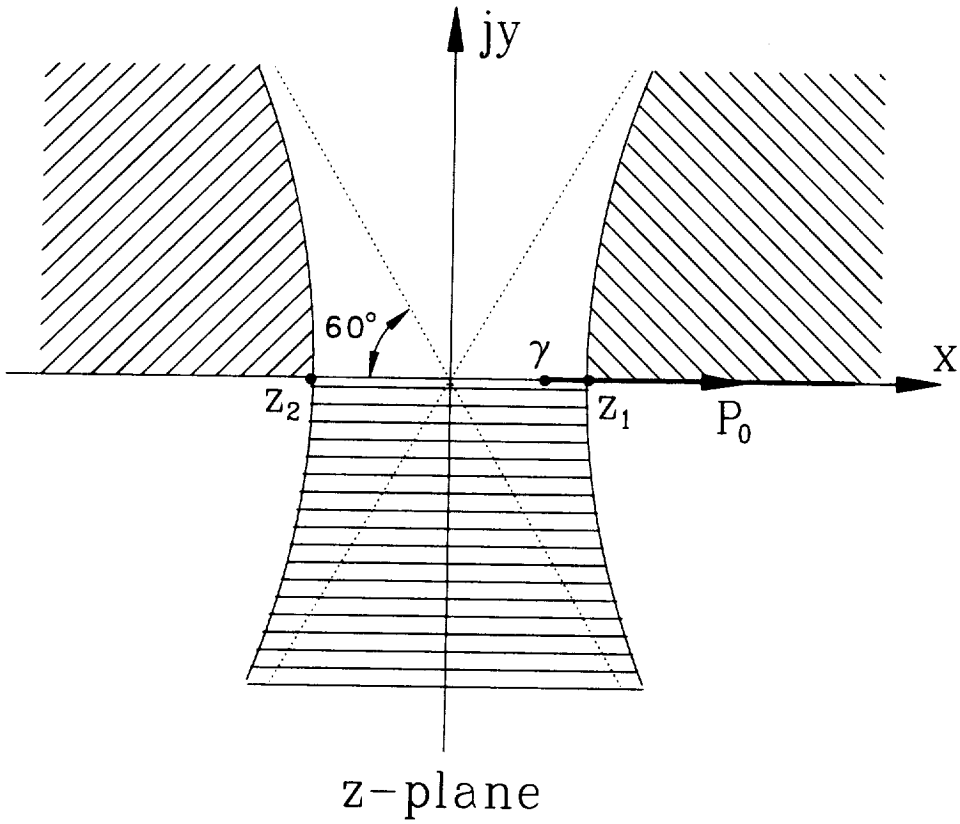

Figure B.3: Contour of integration of the incomplete Airy integral when $\sigma \ll -1$ and $\gamma \approx (-\sigma)^{1/2}$.

with $\arg(s)$ restricted so that $I_0(\sigma,\gamma;\Omega)$ converges as $s \to \infty$. Hence, employing (B.44) in (B.38) we have

$$I_0(\sigma,\gamma;\Omega) = e^{-j\frac{2}{3}\Omega(-\sigma)^{3/2}} \int_{\zeta}^{\infty} f(s) e^{j\Omega s^2}\, ds\,, \tag{B.45}$$

with the upper limit taken in the sector $0 \le \arg(s) \le \pi/2$ of the complex s-plane. The quantities ζ and $f(s)$ are given by

$$\zeta = \pm\left[\sigma\gamma + \gamma^3/3 + \frac{2}{3}(-\sigma)^{3/2}\right]^{1/2} \quad ; \quad \gamma \gtrless (-\sigma)^{1/2}\,, \tag{B.46}$$

and

$$f(s) = \frac{dz}{ds} = \frac{\tau'(s)}{q'(z)} = \frac{2s}{\sigma + z^2}\,. \tag{B.47}$$

Equation (B.45) can be written as follows [25]:

$$I_0(\sigma,\gamma;\Omega) = e^{-j\frac{2}{3}\Omega(-\sigma)^{3/2}} \left\{ f(0) \int_{\zeta}^{\infty} e^{j\Omega s^2}\, ds + \frac{1}{2j\Omega} \int_{\zeta}^{\infty} \left[\frac{f(s) - f(0)}{s}\right] \frac{d}{ds} e^{j\Omega s^2}\, ds \right\}, \tag{B.48}$$

and using integration by parts in the second integral we get

$$\begin{aligned} I_0(\sigma,\gamma;\Omega) \;=\; & e^{-j\frac{2}{3}\Omega(-\sigma)^{3/2}} \left\{ f(0) \int_{\zeta}^{\infty} e^{j\Omega s^2}\, ds - \frac{1}{2j\Omega} \left[\frac{f(\zeta) - f(0)}{\zeta}\right] e^{j\Omega\zeta^2} \right. \\ & \left. - \;\frac{1}{2j\Omega} \int_{\zeta}^{\infty} g(s) e^{j\Omega s^2}\, ds \right\}, \end{aligned} \tag{B.49}$$

where

$$g(s) = \frac{s f'(s) - f(s) + f(0)}{s^2}\,. \tag{B.50}$$

In a similar way, the second integral in Equation (B.49) can be written as follows:

$$\begin{aligned} \int_{\zeta}^{\infty} g(s) e^{j\Omega s^2}\, ds \;=\; & g(0) \int_{\zeta}^{\infty} e^{j\Omega s^2}\, ds - \frac{1}{2j\Omega} \left[\frac{g(\zeta) - g(0)}{\zeta}\right] e^{j\Omega\zeta^2} \\ & - \;\frac{1}{2j\Omega} \int_{\zeta}^{\infty} h(s) e^{j\Omega s^2}\, ds\,, \end{aligned} \tag{B.51}$$

where

$$h(s) = \frac{s g'(s) - g(s) + g(0)}{s^2}\,. \tag{B.52}$$

Thus, using (B.51), Equation (B.49) becomes

$$\begin{aligned} I_0(\sigma,\gamma;\Omega) &= e^{-j\frac{2}{3}\Omega(-\sigma)^{3/2}}\left[f(0)-\frac{1}{2j\Omega}g(0)\right]\int_\zeta^\infty e^{j\Omega s^2}\,ds \\ &+ e^{j\Omega(\sigma\gamma+\gamma^3/3)}\left\{-\frac{1}{2j\Omega}\left[\frac{f(\zeta)-f(0)}{\zeta}\right]+\frac{1}{(2j\Omega)^2}\left[\frac{g(\zeta)-g(0)}{\zeta}\right]\right\} \\ &+ e^{-j\frac{2}{3}\Omega(-\sigma)^{3/2}}\left[\frac{1}{(2j\Omega)^2}\int_\zeta^\infty h(s)e^{j\Omega s^2}\,ds\right]. \end{aligned} \tag{B.53}$$

The same procedure is repeated once more for the last integral in (B.53), that is

$$\begin{aligned} \int_\zeta^\infty h(s)e^{j\Omega s^2}\,ds &\simeq \left[h(0)-\frac{1}{2j\Omega}k(0)\right]\int_\zeta^\infty e^{j\Omega s^2}\,ds + e^{j\Omega\zeta^2}\left\{-\frac{1}{2j\Omega}\left[\frac{h(\zeta)-h(0)}{\zeta}\right]\right. \\ &+ \left.\frac{1}{(2j\Omega)^2}\left[\frac{k(\zeta)-k(0)}{\zeta}\right]\right\}+O(\Omega^{-3}), \end{aligned} \tag{B.54}$$

where

$$k(s)=\frac{sh'(s)-h(s)+h(0)}{s^2}, \tag{B.55}$$

and finally combining (B.53) and (B.54), the asymptotic expansion of $I_0(\sigma,\gamma;\Omega)$ when $\sigma \ll -1$ is given by

$$\begin{aligned} I_0(\sigma,\gamma;\Omega) &\simeq e^{-j\frac{2}{3}(-\sigma)^{3/2}}\left[f(0)-\frac{1}{2j\Omega}g(0)+\frac{1}{(2j\Omega)^2}h(0)\right. \\ &- \left.\frac{1}{(2j\Omega)^3}k(0)\right]\int_\zeta^\infty e^{j\Omega s^2}\,ds + e^{j\Omega(\sigma\gamma+\gamma^3/3)}\left\{-\frac{1}{2j\Omega}\left[\frac{f(\zeta)-f(0)}{\zeta}\right]\right. \\ &+ \frac{1}{(2j\Omega)^2}\left[\frac{g(\zeta)-g(0)}{\zeta}\right]-\frac{1}{(2j\Omega)^3}\left[\frac{h(\zeta)-h(0)}{\zeta}\right] \\ &+ \left.\frac{1}{(2j\Omega)^4}\left[\frac{k(\zeta)-k(0)}{\zeta}\right]\right\}+O(\Omega^{-5}). \end{aligned} \tag{B.56}$$

In order to express the functions f, g, h, and k in (B.56) in terms of σ and γ, we need to derive an expression for $f(s)$ and its derivatives when $s \approx 0$. Since $f(s)$ is regular near $s=0$, it can be expanded in a Taylor series around $s=0$ by means of Lagrange's theorem. This is done using a procedure introduced by Erdélyi [26] that yields

$$f(s) = \frac{1}{(-\sigma)^{1/4}}\sum_{n=1}^\infty \frac{\Gamma(3n/2-1)(-1)^{n-1}}{(n-1)!\Gamma(n/2)\left[3(-\sigma)^{3/4}\right]^{n-1}}\,s^{n-1}, \tag{B.57}$$

$$\frac{d^k}{ds^k}f(s) = \frac{1}{(-\sigma)^{1/4}}\sum_{n=k+1}^\infty \frac{\Gamma(3n/2-1)(-1)^{n-1}}{(n-k-1)!\Gamma(n/2)\left[3(-\sigma)^{3/4}\right]^{n-1}}\,s^{n-k-1}. \tag{B.58}$$

Hence, using (B.47), (B.50), (B.52), (B.55), (B.57), and (B.58) we have

$$f(\zeta) = \frac{2\zeta}{\sigma+\gamma^2}, \tag{B.59}$$

$$g(\zeta) = \frac{-8\gamma\zeta}{(\sigma+\gamma^2)^3} + \frac{1}{\zeta^2(-\sigma)^{1/4}}, \tag{B.60}$$

$$h(\zeta) = \frac{-16\zeta}{(\sigma+\gamma^2)^4} + \frac{96\gamma^2}{(\sigma+\gamma^2)^5} - \frac{3}{\zeta^4(-\sigma)^{1/4}} + \frac{5}{24\zeta^2(-\sigma)^{7/4}}, \tag{B.61}$$

$$k(\zeta) = \frac{640\gamma}{(\sigma+\gamma^2)^6} - \frac{1920\gamma^3}{(\sigma+\gamma^2)^7} + \frac{15}{\zeta^6(-\sigma)^{1/4}} - \frac{5}{8\zeta^4(-\sigma)^{7/4}} + \frac{77}{3456\zeta^3(-\sigma)^{13/4}}, \tag{B.62}$$

$$f(0) = \frac{1}{(-\sigma)^{1/4}}, \tag{B.63}$$

$$f'(0) = \frac{-1}{3(-\sigma)}, \tag{B.64}$$

$$g(0) = \frac{f''(0)}{2} = \frac{5}{24(-\sigma)^{7/4}}, \tag{B.65}$$

$$g'(0) = \frac{f'''(0)}{3} = \frac{-8}{27(-\sigma)^{5/2}}, \tag{B.66}$$

$$h(0) = \frac{f^{(4)}(0)}{8} = \frac{77}{3456(-\sigma)^{13/4}}, \tag{B.67}$$

$$h'(0) = \frac{f^{(5)}(0)}{15} = \frac{-56}{81(-\sigma)^4}, \tag{B.68}$$

$$k(0) = \frac{f^{(6)}(0)}{48} = \frac{12155}{82944(-\sigma)^{19/4}}, \text{ and} \tag{B.69}$$

$$k'(0) = \frac{f^{(7)}(0)}{105} = \frac{-640}{243(-\sigma)^{11/2}}. \tag{B.70}$$

Also, the Fresnel integral in (B.56) may be expressed in terms of the UTD transition function $F(x)$ [4], that is

$$\int_{\zeta}^{\infty} e^{j\Omega s^2}\, ds = \Omega^{-1/2}\left[\sqrt{\pi}\, e^{j\pi/4}\, u(-\eta) - \frac{F^*(\eta^2)}{2j\eta} e^{j\eta^2}\right] = \Omega^{-1/2}\Lambda(\eta), \tag{B.71}$$

where $\eta = \Omega^{1/2}\zeta$. The general properties of the UTD transition function and details on its computation are provided in Appendix D. Now, using (B.59)–(B.71), the asymptotic expansion of $I_0(\sigma,\gamma;\Omega)$ when $\sigma \ll -1$ is given by

$$I_0(\sigma,\gamma;\Omega) \simeq \frac{e^{-j\frac{2}{3}\Omega(-\sigma)^{3/2}}}{\Omega^{1/2}(-\sigma)^{1/4}} S(\sigma;\Omega)\,\Lambda(\eta) + e^{j\Omega(\sigma\gamma+\gamma^3/3)} E(\sigma,\gamma,\eta;\Omega) + O(\Omega^{-5}), \tag{B.72}$$

where

$$S(\sigma;\Omega) = 1 - \frac{s_1}{2j\Omega(-\sigma)^{3/2}} + \frac{s_2}{(2j\Omega)^2(-\sigma)^3} - \frac{s_3}{(2j\Omega)^3(-\sigma)^{9/2}}, \tag{B.73}$$

$$\begin{aligned} E(\sigma,\gamma,\eta;\Omega) &= -\frac{1}{2j\Omega}\left[\frac{2}{\sigma+\gamma^2} - \frac{\Omega^{1/2}}{\eta(-\sigma)^{1/4}}\right] \\ &+ \frac{1}{(2j\Omega)^2}\left[\frac{-8\gamma}{(\sigma+\gamma^2)^3} + \frac{\Omega^{3/2}}{\eta^3(-\sigma)^{1/4}} - \frac{\Omega^{1/2}s_1}{\eta(-\sigma)^{7/4}}\right] \\ &- \frac{1}{(2j\Omega)^3}\left[\frac{-16}{(\sigma+\gamma^2)^4} + \frac{96\gamma^2}{(\sigma+\gamma^2)^5} - \frac{3\Omega^{5/2}}{\eta^5(-\sigma)^{1/4}}\right. \\ &+ \left.\frac{\Omega^{3/2}s_1}{\eta^3(-\sigma)^{7/4}} - \frac{\Omega^{1/2}s_2}{\eta(-\sigma)^{13/4}}\right] + \frac{1}{(2j\Omega)^4}\left[\frac{640\gamma}{(\sigma+\gamma^2)^6}\right. \\ &- \frac{1920\gamma^3}{(\sigma+\gamma^2)^7} + \frac{15\Omega^{7/2}}{\eta^7(-\sigma)^{1/4}} - \frac{3\Omega^{5/2}s_1}{\eta^5(-\sigma)^{7/4}} + \frac{\Omega^{3/2}s_2}{\eta^3(-\sigma)^{13/4}} \\ &- \left.\frac{\Omega^{1/2}s_3}{\eta(-\sigma)^{19/4}}\right], \end{aligned} \tag{B.74}$$

with $s_1 = 0.20833333$, $s_2 = 0.33420139$, and $s_3 = 1.02581260$.

The asymptotic formulae for $\mathrm{g}_1(\beta,\xi)$ and its derivative when $\beta \ll -1$ are then obtained using (B.39)) and (B.72)-(B.74), that is

$$\mathrm{g}_1(\beta,\xi) \sim \frac{e^{-j\frac{2}{3}(-\beta)^{3/2}}}{(-\beta)^{1/4}} S(\beta)\,\Lambda(\eta) + e^{j(\beta\xi+\xi^3/3)} E(\beta,\xi,\eta), \tag{B.75}$$

$$\begin{aligned} \frac{\partial}{\partial\beta}\mathrm{g}_1(\beta,\xi) &\sim \frac{e^{-j\frac{2}{3}(-\beta)^{3/2}}}{(-\beta)^{1/4}}\left\{\left[j(-\beta)^{1/2} + \frac{1}{4(-\beta)}\right] S(\beta)\Lambda(\eta)\right. \\ &+ \left.\Lambda(\eta)\frac{d}{d\beta}S(\beta) + S(\beta)\frac{d}{d\beta}\Lambda(\eta)\right\} + e^{j(\beta\xi+\xi^3/3)}\left[j\xi E(\beta,\xi,\eta)\right. \\ &+ \left.\frac{\partial}{\partial\beta}E(\beta,\xi,\eta)\right], \end{aligned} \tag{B.76}$$

where

$$S(\beta) = 1 - \frac{s_1}{2j(-\beta)^{3/2}} + \frac{s_2}{(2j)^2(-\beta)^3} - \frac{s_3}{(2j)^3(-\beta)^{9/2}}, \tag{B.77}$$

$$\frac{d}{d\beta}S(\beta) = -\frac{1.5s_1}{2j(-\beta)^{5/2}} + \frac{3s_2}{(2j)^2(-\beta)^4} - \frac{4.5s_3}{(2j)^3(-\beta)^{11/2}}, \tag{B.78}$$

$$\begin{aligned} E(\beta,\xi,\eta) &= -\frac{1}{2j}\left[\frac{2}{\beta+\xi^2} - \frac{1}{\eta(-\beta)^{1/4}}\right] \\ &+ \frac{1}{(2j)^2}\left[\frac{-8\xi}{(\beta+\xi^2)^3} + \frac{1}{\eta^3(-\beta)^{1/4}} - \frac{s_1}{\eta(-\beta)^{7/4}}\right] \end{aligned}$$

$$
\begin{aligned}
&- \frac{1}{(2j)^3}\left[\frac{-16}{(\beta+\xi^2)^4}+\frac{96\xi^2}{(\beta+\xi^2)^5}-\frac{3}{\eta^5(-\beta)^{1/4}}+\frac{s_1}{\eta^3(-\beta)^{7/4}}\right.\\
&\left.- \frac{s_2}{\eta(-\beta)^{13/4}}\right]+\frac{1}{(2j)^4}\left[\frac{640\xi}{(\beta+\xi^2)^6}-\frac{1920\xi^3}{(\beta+\xi^2)^7}+\frac{15}{\eta^7(-\beta)^{1/4}}\right.\\
&\left.- \frac{3s_1}{\eta^5(-\beta)^{7/4}}+\frac{s_2}{\eta^3(-\beta)^{13/4}}-\frac{s_3}{\eta(-\beta)^{19/4}}\right], \qquad \text{(B.79)}
\end{aligned}
$$

$$
\begin{aligned}
\frac{\partial}{\partial\beta}E(\beta,\xi,\eta) &= -\frac{1}{2j}\left[\frac{-2}{(\beta+\xi^2)^2}-\frac{1}{4\eta(-\beta)^{5/4}}+\frac{\xi-(-\beta)^{1/2}}{2\eta^3(-\beta)^{1/4}}\right]\\
&+ \frac{1}{(2j)^2}\left\{\frac{24\xi}{(\beta+\xi^2)^4}+\frac{1}{4\eta^3(-\beta)^{5/4}}-\frac{3\left[\xi-(-\beta)^{1/2}\right]}{2\eta^5(-\beta)^{1/4}}\right.\\
&\left.- \frac{7s_1}{4\eta(-\beta)^{11/4}}+\frac{s_1\left[\xi-(-\beta)^{1/2}\right]}{2\eta^3(-\beta)^{7/4}}\right\}-\frac{1}{(2j)^3}\left\{\frac{64}{(\beta+\xi^2)^5}\right.\\
&- \frac{480\xi^2}{(\beta+\xi^2)^6}-\frac{3}{4\eta^5(-\beta)^{5/4}}+\frac{15\left[\xi-(-\beta)^{1/2}\right]}{2\eta^7(-\beta)^{1/4}}\\
&+ \frac{7s_1}{4\eta^3(-\beta)^{11/4}}-\frac{3s_1\left[\xi-(-\beta)^{1/2}\right]}{2\eta^5(-\beta)^{7/4}}-\frac{13s_2}{4\eta(-\beta)^{17/4}}\\
&\left.+ \frac{s_2\left[\xi-(-\beta)^{1/2}\right]}{2\eta^3(-\beta)^{13/4}}\right\}+\frac{1}{(2j)^4}\left\{\frac{-3840\xi}{(\beta+\xi^2)^7}+\frac{13440\xi^3}{(\beta+\xi^2)^8}\right.\\
&+ \frac{15}{4\eta^7(-\beta)^{5/4}}-\frac{105\left[\xi-(-\beta)^{1/2}\right]}{2\eta^9(-\beta)^{1/4}}-\frac{21s_1}{4\eta^5(-\beta)^{11/4}}\\
&+ \frac{15s_1\left[\xi-(-\beta)^{1/2}\right]}{2\eta^7(-\beta)^{7/4}}+\frac{13s_2}{4\eta^3(-\beta)^{17/4}}-\frac{3s_2\left[\xi-(-\beta)^{1/2}\right]}{2\eta^5(-\beta)^{13/4}}\\
&\left.- \frac{19s_3}{4\eta(-\beta)^{23/4}}+\frac{s_3\left[\xi-(-\beta)^{1/2}\right]}{2\eta^3(-\beta)^{19/4}}\right\}, \qquad \text{(B.80)}
\end{aligned}
$$

$$
\frac{d}{d\beta}\Lambda(\eta) = -\frac{\partial\eta}{\partial\beta}e^{j\eta^2} = -\left[\frac{\xi-(-\beta)^{1/2}}{2\eta}\right]e^{j\eta^2}, \qquad \text{(B.81)}
$$

and

$$
\eta = \pm\left[\beta\xi+\xi^3/3+\frac{2}{3}(-\beta)^{3/2}\right]^{1/2}; \quad \xi \gtrless (-\beta)^{1/2}. \qquad \text{(B.82)}
$$

It can be easily shown using the large argument form of the UTD transition function (see Appendix D) that when $\xi \gg (-\beta)^{1/2}$ or $\eta \gg 1$, Equation (B.75) appropriately reduces to the first six terms in (B.42). Also, (B.79) and (B.80) remain finite near the caustic when $\xi \to (-\beta)^{1/2}$ and $\eta \to 0$, however, they become numerically unstable and an alternative formulation should be used. Applying L'Hospital's rule in (B.56), and then using (B.39) and (B.57)-(B.70) we have

$$
E(\beta,\xi,\eta\approx 0) \approx \frac{f_0}{2j(-\beta)}\left[1-\frac{f_1\eta}{(-\beta)^{3/4}}+\frac{f_2\eta^2}{(-\beta)^{3/2}}\right]
$$

$$
\begin{aligned}
&- \frac{g_0}{(2j)^2(-\beta)^{5/2}}\left[1-\frac{g_1\eta}{(-\beta)^{3/4}}+\frac{g_2\eta^2}{(-\beta)^{3/2}}\right] \\
&+ \frac{h_0}{(2j)^3(-\beta)^4}\left[1-\frac{h_1\eta}{(-\beta)^{3/4}}+\frac{h_2\eta^2}{(-\beta)^{3/2}}\right] \\
&- \frac{k_0}{(2j)^4(-\beta)^{11/2}}\left[1-\frac{k_1\eta}{(-\beta)^{3/4}}+\frac{k_2\eta^2}{(-\beta)^{3/2}}\right], \qquad \text{(B.83)}
\end{aligned}
$$

and

$$
\begin{aligned}
\frac{\partial}{\partial\beta}E(\beta,\xi,\eta\approx 0) \;\approx\; & \frac{f_0}{2j(-\beta)^2}\left\{1-\frac{7f_1\eta}{4(-\beta)^{3/4}}-\frac{f_1}{2}+\frac{5f_2\eta^2}{2(-\beta)^{3/2}}\right. \\
&+ \left.\frac{f_2\left[\xi-(-\beta)^{1/2}\right]}{(-\beta)^{1/2}}\right\}-\frac{g_0}{(2j)^2(-\beta)^{7/2}}\left\{1-\frac{13g_1\eta}{4(-\beta)^{3/4}}\right. \\
&- \left.\frac{g_1}{2}+\frac{4g_2\eta^2}{(-\beta)^{3/2}}+\frac{g_2\left[\xi-(-\beta)^{1/2}\right]}{(-\beta)^{1/2}}\right\} \\
&+ \frac{h_0}{(2j)^3(-\beta)^5}\left\{1-\frac{19h_1\eta}{4(-\beta)^{3/4}}-\frac{h_1}{2}+\frac{11h_2\eta^2}{2(-\beta)^{3/2}}\right. \\
&+ \left.\frac{h_2\left[\xi-(-\beta)^{1/2}\right]}{(-\beta)^{1/2}}\right\}-\frac{k_0}{(2j)^4(-\beta)^{13/2}}\left\{1-\frac{25k_1\eta}{4(-\beta)^{3/4}}\right. \\
&- \left.\frac{k_1}{2}+\frac{7k_2\eta^2}{(-\beta)^{3/2}}+\frac{k_2\left[\xi-(-\beta)^{1/2}\right]}{(-\beta)^{1/2}}\right\}, \qquad \text{(B.84)}
\end{aligned}
$$

where

$f_0 = 1/3,\ f_1 = 1.25,\ f_2 = 4/3,$

$g_0 = 0.29629630,\ g_1 = 3.00781250,\ g_2 = 5.83333333,$

$h_0 = 0.69135802,\ h_1 = 4.74804688,\ h_2 = 13.3333333,$

$k_0 = 2.63374486,\ k_1 = 6.48405151,\ k_2 = 23.8333333.$

Also, $\Lambda(\eta)$ and its derivative near the caustic are given by

$$
\Lambda(\eta\approx 0) \;\simeq\; \frac{\sqrt{\pi}}{2}e^{j\pi/4}-\eta-\frac{j\eta^3}{3}, \qquad \text{(B.85)}
$$

$$
\text{and}\quad \frac{d}{d\beta}\Lambda(\eta\approx 0) \;=\; \frac{-e^{j\eta^2}}{2(-\beta)^{1/4}\left[1+\frac{\xi-(-\beta)^{1/2}}{3(-\beta)^{1/2}}\right]^{1/2}}. \qquad \text{(B.86)}
$$

Asymptotic formula for $\beta \gg 1$

This case corresponds to imaginary and widely separated saddle points ($\sigma \gg 1$) in the integrand of Equation (B.38), with the endpoint γ arbitrarily close to the saddle point $z_1 = j\sigma^{1/2}$, as shown in Figure B.4. For an asymptotic evaluation of (B.38) that

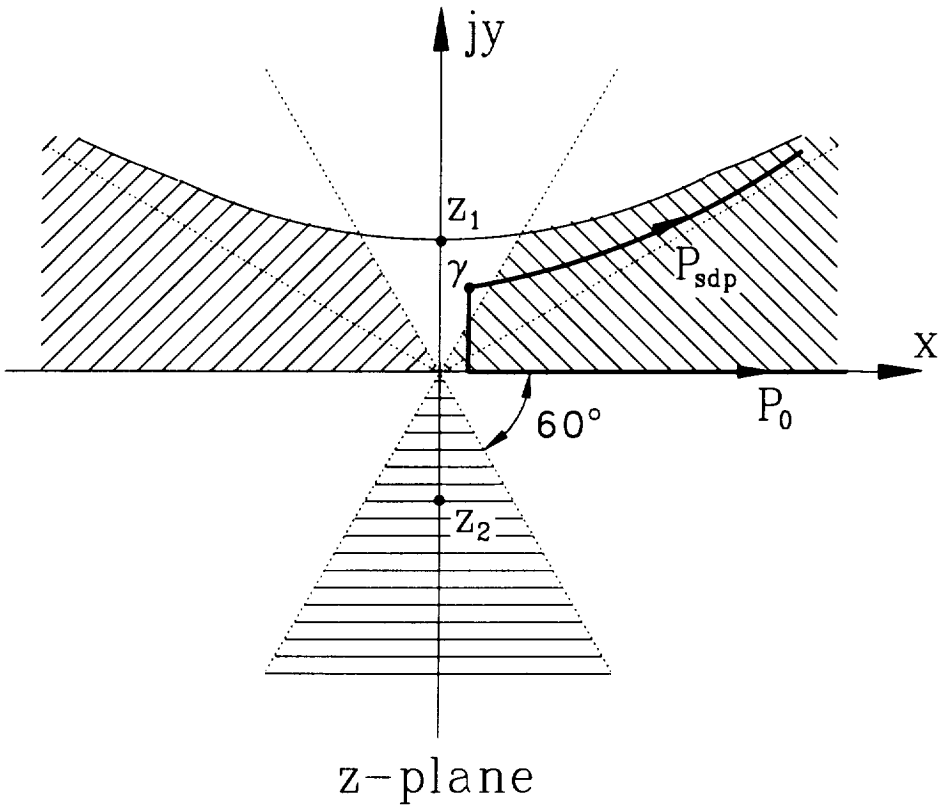

Figure B.4: Contour of integration of the incomplete Airy integral when $\sigma \gg 1$ and $\gamma \approx j\sigma^{1/2}$.

holds uniformly as the endpoint γ approaches the saddle point z_1, we make the same transformation as in (B.44), that is

$$q(z) = \sigma z + z^3/3 = q(z_1) + s^2 = j\frac{2}{3}\sigma^{3/2} + s^2 = \tilde{\tau}(s)\,, \tag{B.87}$$

with $\arg(s)$ restricted so that $I_0(\sigma, \gamma; \Omega)$ converges as $s \to \infty$. Hence, employing (B.87) in (B.38) we have

$$I_0(\sigma, \gamma; \Omega) = e^{-\frac{2}{3}\Omega\sigma^{3/2}} \int_{\tilde{\zeta}}^{\infty} f(s) e^{j\Omega s^2}\, ds\,, \tag{B.88}$$

with the upper limit taken in the sector $0 \leq \arg(s) \leq \pi/2$ of the complex s–plane. The quantity $\tilde{\zeta}$ is given by

$$\tilde{\zeta} = \pm\left[\sigma\gamma + \gamma^3/3 - j\frac{2}{3}\sigma^{3/2}\right]^{1/2} \;;\; \Re(\gamma) \gtrless 0\,, \tag{B.89}$$

and $f(s)$ is the same as in (B.47). Then using the same procedure as in the case of $\sigma \ll -1$, $I_0(\sigma,\gamma;\Omega)$ when $\sigma \gg 1$ is given by

$$\begin{aligned} I_0(\sigma,\gamma;\Omega) &\simeq \frac{e^{-\frac{2}{3}\Omega\sigma^{3/2}-j\pi/4}}{\Omega^{1/2}\sigma^{1/4}}\,\tilde{S}(\sigma;\Omega)\,\tilde{\Lambda}(\chi) \\ &+ e^{j\Omega(\sigma\gamma+\gamma^3/3)}\tilde{E}(\sigma,\gamma,\chi;\Omega)+O(\Omega^{-5}), \end{aligned} \tag{B.90}$$

where

$$\tilde{\Lambda}(\chi)=\left[\frac{\tilde{F}(\chi)}{2j\chi}\,e^{-j\chi^2}\right]^* \;;\; \chi=\Omega^{1/2}\tilde{\zeta}, \tag{B.91}$$

$\tilde{F}(\chi)$ is the Fresnel transition function of complex argument (see Appendix E), and

$$\tilde{S}(\sigma;\Omega)=1-\frac{js_1}{(2j\Omega)\sigma^{3/2}}-\frac{s_2}{(2j\Omega)^2\sigma^3}+\frac{js_3}{(2j\Omega)^3\sigma^{9/2}}, \tag{B.92}$$

$$\begin{aligned} \tilde{E}(\sigma,\gamma,\chi;\Omega) &= -\frac{1}{2j\Omega}\left[\frac{2}{\sigma+\gamma^2}-\frac{e^{-j\frac{\pi}{4}}\Omega^{1/2}}{\chi\sigma^{1/4}}\right] \\ &+ \frac{1}{(2j\Omega)^2}\left[\frac{-8\gamma}{(\sigma+\gamma^2)^3}+\frac{e^{-j\frac{\pi}{4}}\Omega^{3/2}}{\chi^3\sigma^{1/4}}-\frac{e^{j\frac{\pi}{4}}\Omega^{1/2}s_1}{\chi\sigma^{7/4}}\right] \\ &- \frac{1}{(2j\Omega)^3}\left[\frac{-16}{(\sigma+\gamma^2)^4}+\frac{96\gamma^2}{(\sigma+\gamma^2)^5}-\frac{3e^{-j\frac{\pi}{4}}\Omega^{5/2}}{\chi^5\sigma^{1/4}}\right. \\ &+ \left.\frac{e^{j\frac{\pi}{4}}\Omega^{3/2}s_1}{\chi^3\sigma^{7/4}}+\frac{e^{-j\frac{\pi}{4}}\Omega^{1/2}s_2}{\chi\sigma^{13/4}}\right]+\frac{1}{(2j\Omega)^4}\left[\frac{640\gamma}{(\sigma+\gamma^2)^6}\right. \\ &- \frac{1920\gamma^3}{(\sigma+\gamma^2)^7}+\frac{15e^{-j\frac{\pi}{4}}\Omega^{7/2}}{\chi^7\sigma^{1/4}}-\frac{3e^{j\frac{\pi}{4}}\Omega^{5/2}s_1}{\chi^5\sigma^{7/4}}-\frac{e^{-j\frac{\pi}{4}}\Omega^{3/2}s_2}{\chi^3\sigma^{13/4}} \\ &+ \left.\frac{e^{j\frac{\pi}{4}}\Omega^{1/2}s_3}{\chi(-\sigma)^{19/4}}\right]. \end{aligned} \tag{B.93}$$

The asymptotic formulae for $g_1(\beta,\xi)$ and its derivative when $\beta \ll -1$ are then obtained using (B.39) and (B.90)–(B.93), that is

$$g_1(\beta,\xi) \sim \frac{e^{-\frac{2}{3}\beta^{3/2}-j\pi/4}}{\beta^{1/4}}\,\tilde{S}(\beta)\,\tilde{\Lambda}(\chi)+e^{j(\beta\xi+\xi^3/3)}\tilde{E}(\beta,\xi,\chi), \tag{B.94}$$

$$\begin{aligned} \frac{\partial}{\partial\beta}g_1(\beta,\xi) &\sim -\frac{e^{-\frac{2}{3}\beta^{3/2}-j\pi/4}}{\beta^{1/4}}\left[\left(\beta^{1/2}+\frac{1}{4\beta}\right)\tilde{S}(\beta)\tilde{\Lambda}(\chi)\right. \\ &+ \left.\tilde{\Lambda}(\chi)\frac{d}{d\beta}\tilde{S}(\beta)+\tilde{S}(\beta)\frac{d}{d\beta}\tilde{\Lambda}(\chi)\right]+e^{j(\beta\xi+\xi^3/3)}\left[j\xi\tilde{E}(\beta,\xi,\chi)\right. \\ &+ \left.\frac{\partial}{\partial\beta}\tilde{E}(\beta,\xi,\chi)\right], \end{aligned} \tag{B.95}$$

where

$$\tilde{S}(\beta) = 1 - \frac{js_1}{(2j)\beta^{3/2}} - \frac{s_2}{(2j)^2\beta^3} + \frac{js_3}{(2j)^3\beta^{9/2}}, \tag{B.96}$$

$$\frac{d}{d\beta}\tilde{S}(\beta) = \frac{1.5js_1}{2j\beta^{5/2}} + \frac{3s_2}{(2j)^2\beta^4} - \frac{4.5js_3}{(2j)^3\beta^{11/2}}, \tag{B.97}$$

$$\begin{aligned}\tilde{E}(\beta,\xi,\chi) &= -\frac{1}{2j}\left[\frac{2}{\beta+\xi^2} - \frac{e^{-j\frac{\pi}{4}}}{\chi\beta^{1/4}}\right] \\ &+ \frac{1}{(2j)^2}\left[\frac{-8\xi}{(\beta+\xi^2)^3} + \frac{e^{-j\frac{\pi}{4}}}{\chi^3\beta^{1/4}} - \frac{e^{j\frac{\pi}{4}}s_1}{\chi\beta^{7/4}}\right] \\ &- \frac{1}{(2j)^3}\left[\frac{-16}{(\beta+\xi^2)^4} + \frac{96\xi^2}{(\beta+\xi^2)^5} - \frac{3e^{-j\frac{\pi}{4}}}{\chi^5\beta^{1/4}} + \frac{e^{j\frac{\pi}{4}}s_1}{\chi^3\beta^{7/4}}\right. \\ &+ \left.\frac{e^{-j\frac{\pi}{4}}s_2}{\chi\beta^{13/4}}\right] + \frac{1}{(2j)^4}\left[\frac{640\xi}{(\beta+\xi^2)^6} - \frac{1920\xi^3}{(\beta+\xi^2)^7} + \frac{15e^{-j\frac{\pi}{4}}}{\chi^7\beta^{1/4}}\right. \\ &- \left.\frac{3e^{j\frac{\pi}{4}}s_1}{\chi^5\beta^{7/4}} - \frac{e^{-j\frac{\pi}{4}}s_2}{\chi^3\beta^{13/4}} + \frac{e^{j\frac{\pi}{4}}s_3}{\chi\beta^{19/4}}\right],\end{aligned} \tag{B.98}$$

$$\begin{aligned}\frac{\partial}{\partial\beta}\tilde{E}(\beta,\xi,\chi) &= -\frac{1}{2j}\left[\frac{-2}{(\beta+\xi^2)^2} + \frac{e^{-j\frac{\pi}{4}}}{4\chi\beta^{5/4}} + \frac{e^{-j\frac{\pi}{4}}(\xi-j\beta^{1/2})}{2\chi^3\beta^{1/4}}\right] \\ &+ \frac{1}{(2j)^2}\left[\frac{24\xi}{(\beta+\xi^2)^4} - \frac{e^{-j\frac{\pi}{4}}}{4\chi^3\beta^{5/4}} - \frac{3e^{-j\frac{\pi}{4}}(\xi-j\beta^{1/2})}{2\chi^5\beta^{1/4}}\right. \\ &+ \left.\frac{7e^{j\frac{\pi}{4}}s_1}{4\chi\beta^{11/4}} + \frac{e^{-j\frac{\pi}{4}}s_1(\xi-j\beta^{1/2})}{2\chi^3\beta^{7/4}}\right] - \frac{1}{(2j)^3}\left[\frac{64}{(\beta+\xi^2)^5}\right. \\ &- \frac{480\xi^2}{(\beta+\xi^2)^6} + \frac{3e^{-j\frac{\pi}{4}}}{4\chi^5\beta^{5/4}} + \frac{15e^{-j\frac{\pi}{4}}(\xi-j\beta^{1/2})}{2\chi^7\beta^{1/4}} \\ &- \frac{7e^{j\frac{\pi}{4}}s_1}{4\chi^3\beta^{11/4}} + \frac{3e^{j\frac{\pi}{4}}s_1(\xi-j\beta^{1/2})}{2\chi^5\beta^{7/4}} - \frac{13e^{-j\frac{\pi}{4}}s_2}{4\chi\beta^{17/4}} \\ &- \left.\frac{e^{-j\frac{\pi}{4}}s_2(\xi-j\beta^{1/2})}{2\chi^3\beta^{13/4}}\right] + \frac{1}{(2j)^4}\left[\frac{-3840\xi}{(\beta+\xi^2)^7} + \frac{13440\xi^3}{(\beta+\xi^2)^8}\right. \\ &- \frac{15e^{-j\frac{\pi}{4}}}{4\chi^7\beta^{5/4}} - \frac{105e^{-j\frac{\pi}{4}}(\xi-j\beta^{1/2})}{2\chi^9\beta^{1/4}} + \frac{21e^{j\frac{\pi}{4}}s_1}{4\chi^5\beta^{11/4}} \\ &+ \frac{15e^{j\frac{\pi}{4}}s_1(\xi-j\beta^{1/2})}{2\chi^7\beta^{7/4}} + \frac{13e^{-j\frac{\pi}{4}}s_2}{4\chi^3\beta^{17/4}} + \frac{3e^{-j\frac{\pi}{4}}s_2(\xi-j\beta^{1/2})}{2\chi^5\beta^{13/4}} \\ &- \left.\frac{19e^{j\frac{\pi}{4}}s_3}{4\chi\beta^{23/4}} - \frac{e^{j\frac{\pi}{4}}s_3(\xi-j\beta^{1/2})}{2\chi^3\beta^{19/4}}\right],\end{aligned} \tag{B.99}$$

$$\frac{d}{d\beta}\tilde{\Lambda}(\chi) = -\frac{\partial\chi}{\partial\beta}e^{j\chi^2} = -\left[\frac{\xi-j\beta^{1/2}}{2\chi}\right]e^{j\chi^2}, \tag{B.100}$$

and

$$\chi = \pm\left[\beta\xi + \xi^3/3 - j\frac{2}{3}\beta^{3/2}\right]^{1/2}; \quad \Re(\xi) \gtrless 0. \tag{B.101}$$

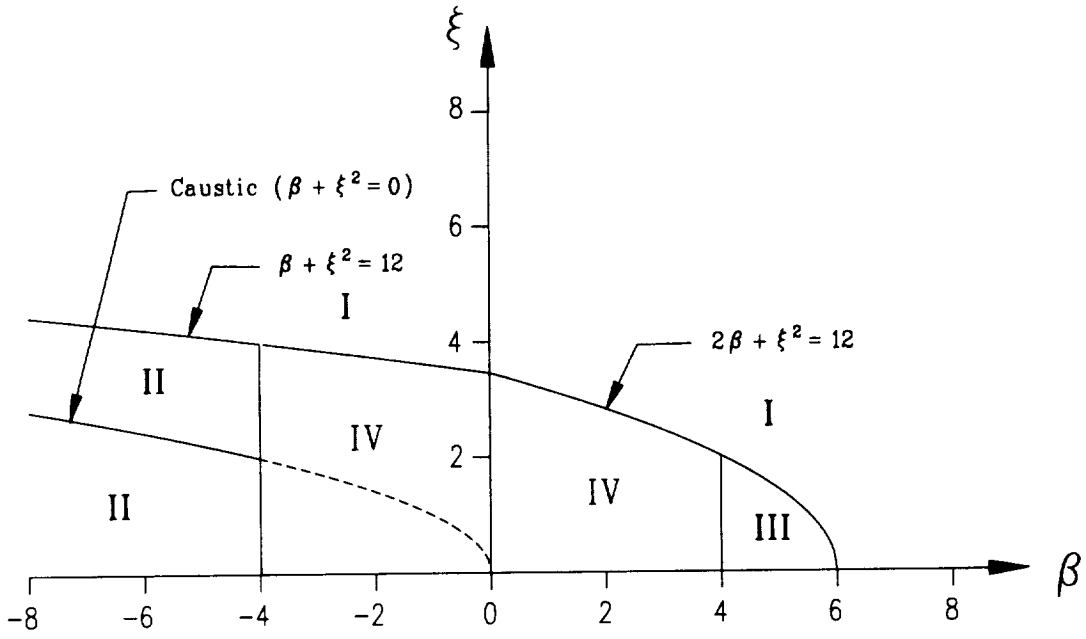

Figure B.5: Four different sets of formulae are used for the computation of the incomplete Airy function, one for each region in the Figure, and a fifth set that is used in the immediate vicinity of the caustic.

Using the large argument form of the Fresnel transition function given in Appendix E, it can be easily shown that when $\beta+\xi^2 \gg 1$ Equation (B.94) appropriately reduces to the first six terms in (B.42).

B.3 Computational aspects and error assessment

For an efficient and accurate computation of the incomplete Airy function $g_1(\beta,\xi)$ and its derivative, the argument space is divided into four regions as shown in Figure B.5. Four different sets of formulae are used, one for each region in Figure B.5, and a fifth set of formulae that is used in the immediate vicinity of the caustic ($\beta + \xi^2 \approx 0$. In region I, Equations (B.42) and (B.43) are used, in region II, Equations (B.75)–(B.82) are used, in region III Equations (B.94)–(B.101) are used, and in region IV, the series solution given in (B.19) and (B.20) is used. In the immediate vicinity of the caustic and specifically when $\eta < 0.1$ in (B.82), Equations (B.75)–(B.78) and (B.82)–(B.86) are used.

An empirical expression for the number of terms used in the series solution is given by:

$$N(\beta,\xi) = 8|\beta| + 4, \quad \text{when } \xi < 2.0, \tag{B.102}$$

$$= 8|\beta| + 4 + 3|\beta|(\xi - 2.0), \quad \text{when } \xi \geq 2.0, \tag{B.103}$$

and results in a truncation error of less than 10^{-6}.

Figure B.6 shows the percent amplitude error of the first asymptotic result ($\beta + \xi^2 \gg 1$) relative to the series solution along the boundary between regions I and IV. The results are plotted vs. the parameter β, with $\xi = (12 - 2\beta)^{1/2}$. The asymptotic result shows excellent agreement with the series solution, exhibiting a maximum error of 0.12%. Figure B.7 shows the percent amplitude error of the second asymptotic result ($\beta \ll -1$) relative to the series solution along the boundary between regions II and IV. The results for this case are plotted vs. the parameter ξ, with $\beta = -4$. Again the asymptotic result shows excellent agreement with the series solution, exhibiting a maximum error of only 0.075%.

Figures B.8 and B.9 show plots of the incomplete Airy function $g_1(\beta,\xi)$ in the first and second quadrants of the $\beta\xi$–plane, respectively. Figures B.10 and B.11 show plots of the derivative of the incomplete Airy function with respect to β in the first and second quadrants of the $\beta\xi$–plane, respectively.

A FORTRAN code for the computation of the incomplete Airy functions based on the formulae derived in this appendix is available from the author.

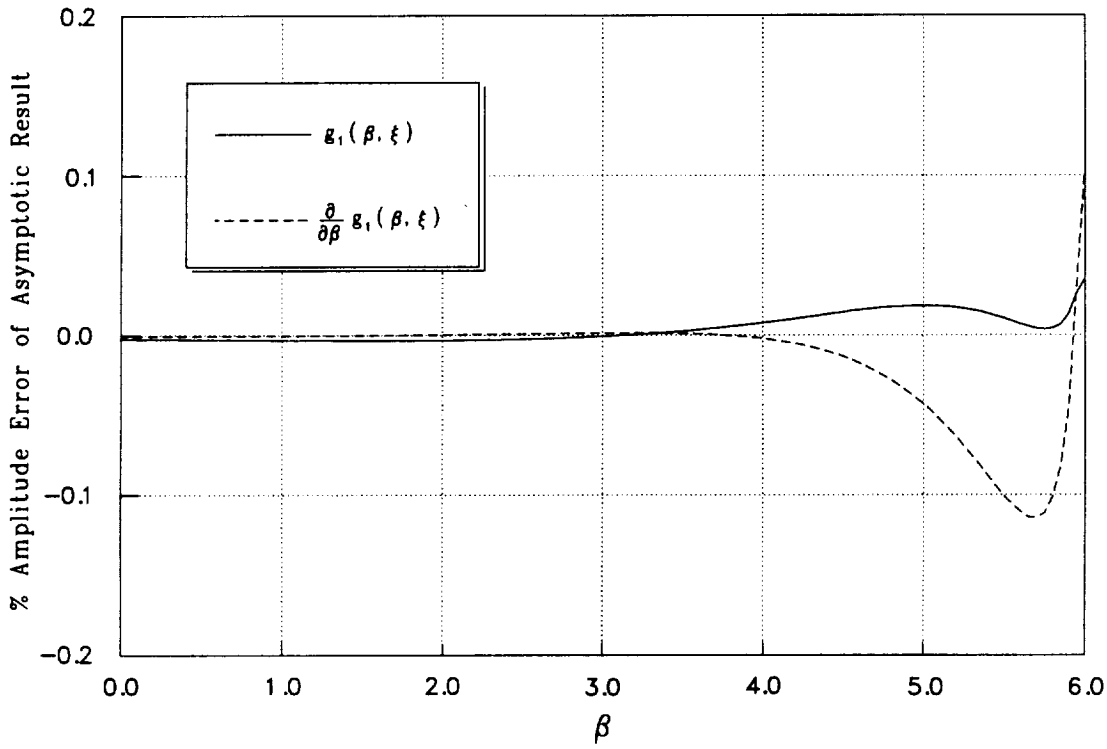

Figure B.6: Percent amplitude error of the first asymptotic result ($\beta + \xi^2$) for the incomplete Airy function (solid line) and its derivative (broken line) along the boundary between regions I and IV. Results are plotted vs. the parameter β with $\xi = (12 - 2\beta)^{1/2}$.

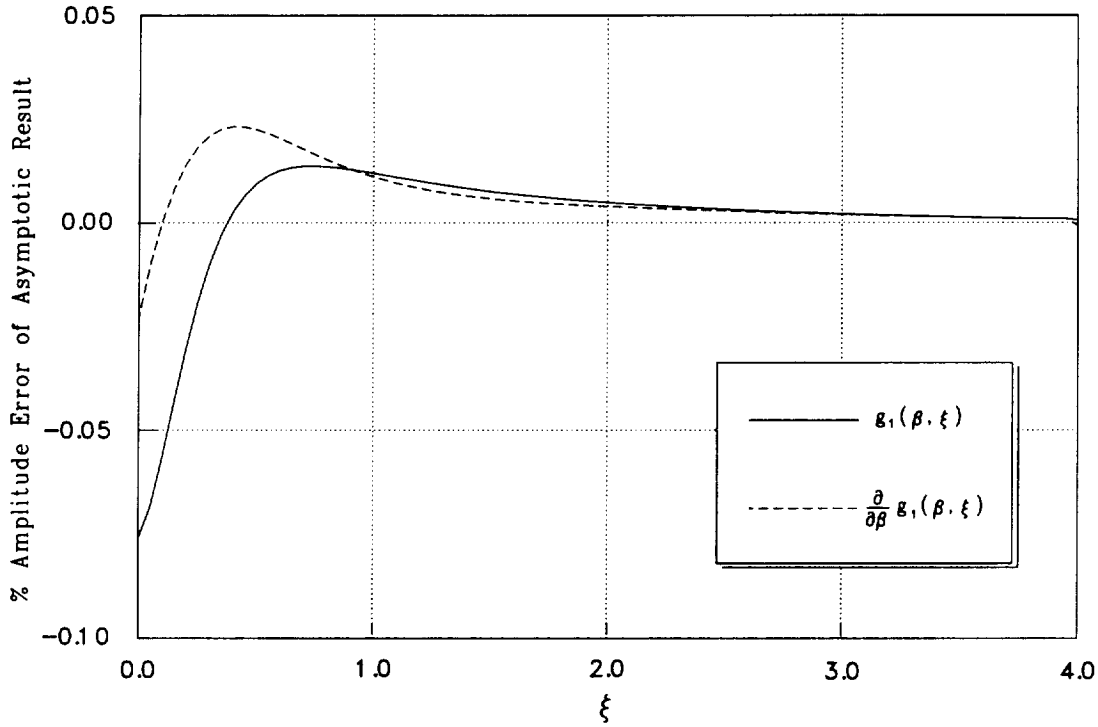

Figure B.7: Percent amplitude error of the second asymptotic result ($\beta \ll -1$) for the incomplete Airy function (solid line) and its derivative (broken line) along the boundary between regions II and IV. Results are plotted vs. the parameter ξ with $\beta = -4.0$.

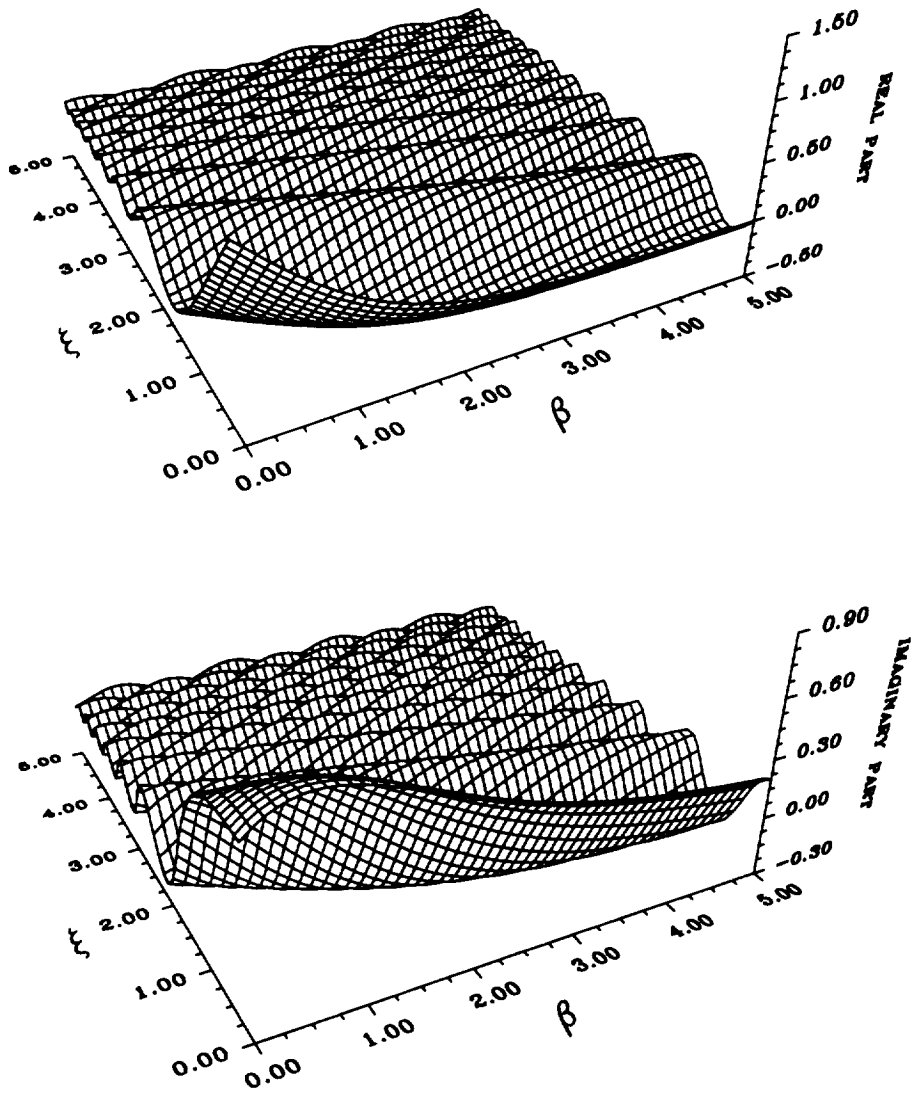

Figure B.8: Plots of the real and imaginary parts of the incomplete Airy function, $g_1(\beta, \xi)$, in the first quadrant of the $\beta\xi$–plane.

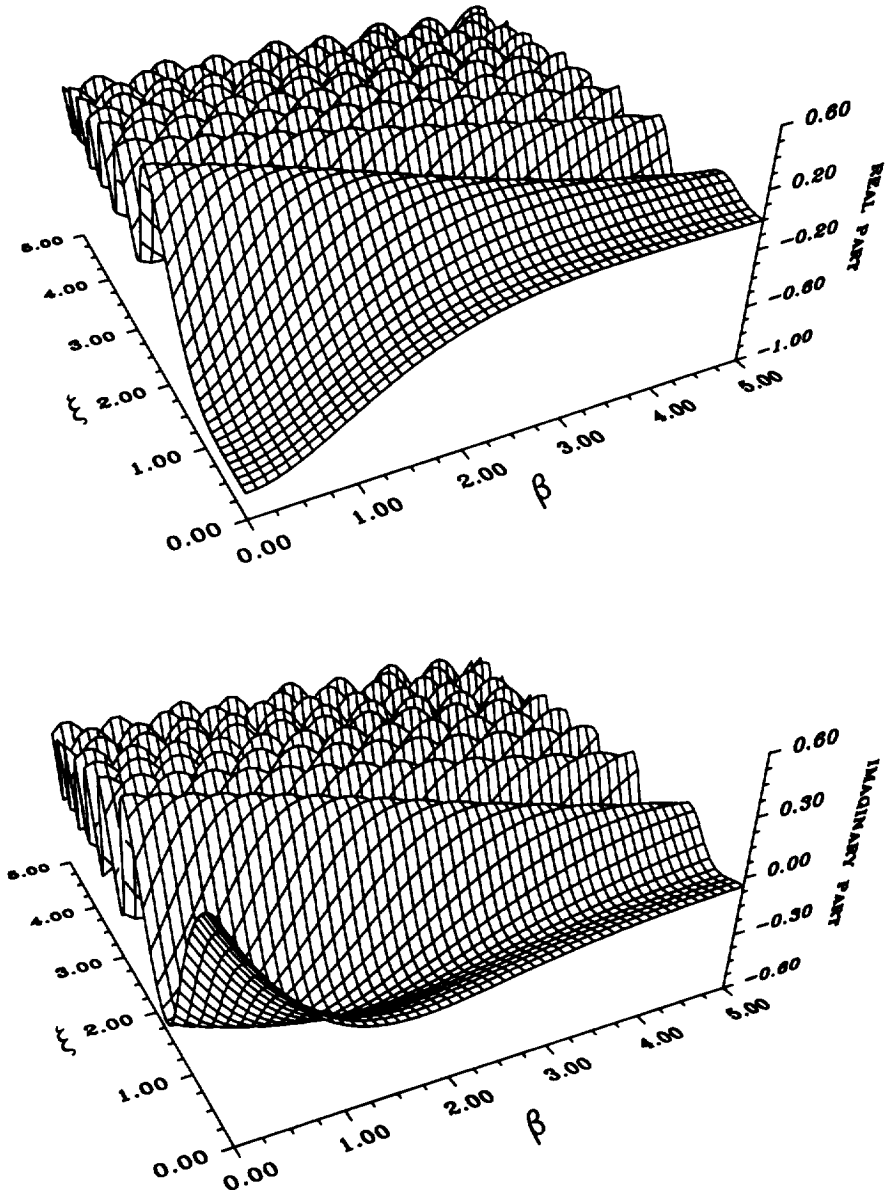

Figure B.9: Plots of the real and imaginary parts of the derivative with respect to β of the incomplete Airy function, $g_1(\beta, \xi)$, in the first quadrant of the $\beta\xi$–plane.

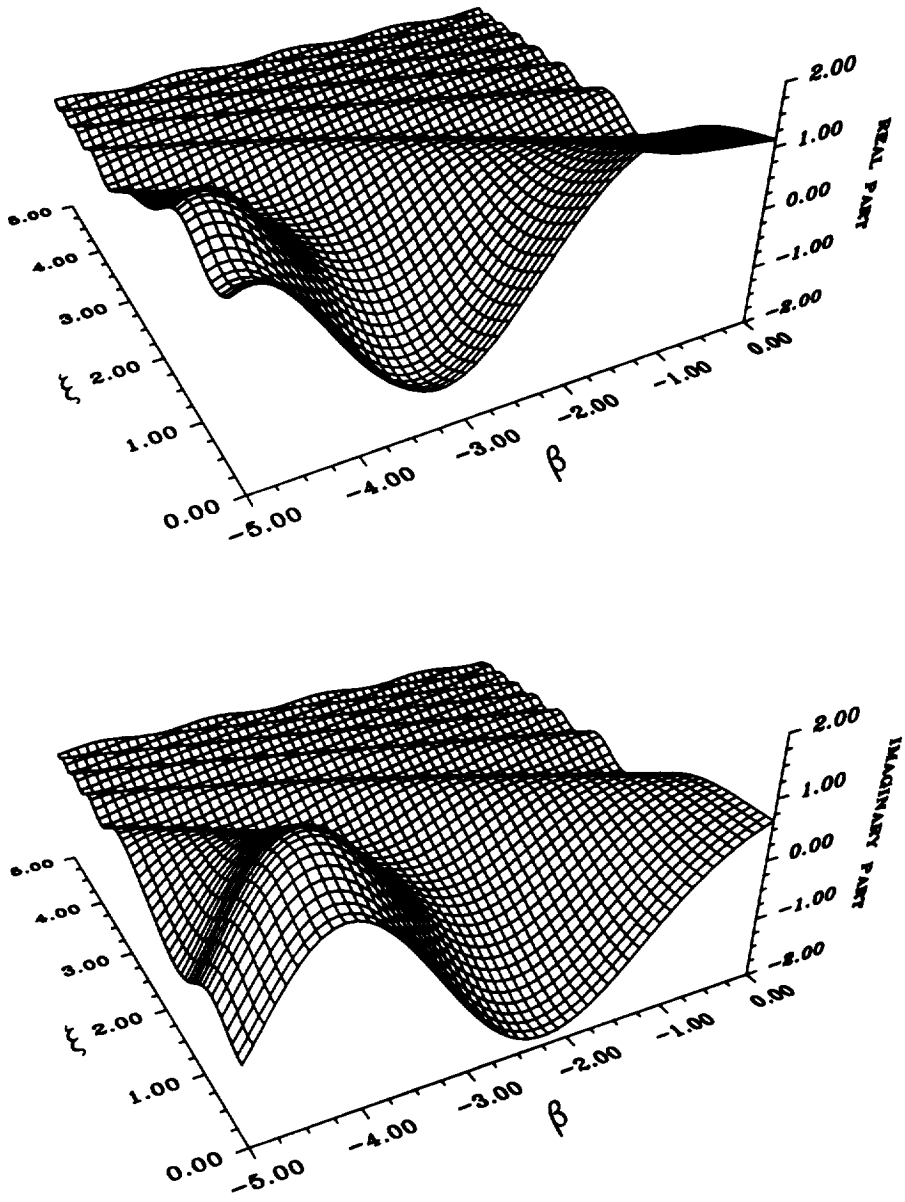

Figure B.10: Plots of the real and imaginary parts of the incomplete Airy function, $g_1(\beta, \xi)$, in the second quadrant of the $\beta\xi$-plane.

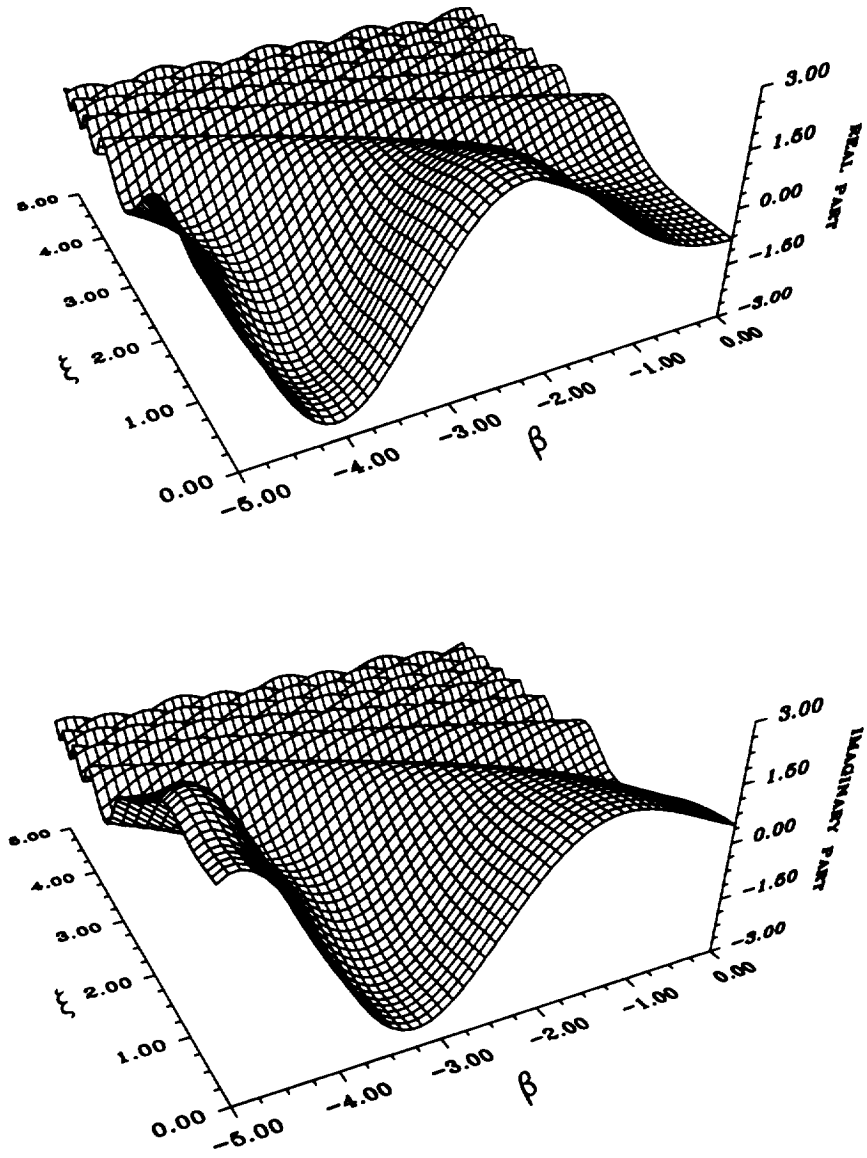

Figure B.11: Plots of the real and imaginary parts of the derivative with respect to β of the incomplete Airy function, $g_1(\beta, \xi)$, in the second quadrant of the $\beta\xi$–plane.

Appendix C

The Generalized Incomplete Airy Integral

The generalized incomplete Airy integral serves as a canonical function for the uniform asymptotic approximation of a class of integrals characterized by multiple symmetrically situated stationary phase points that arbitrarily close to one another or to an integration endpoint [22]. It is defined as follows:

$$\overline{K}_{\omega}(\gamma,\zeta,\nu) \triangleq \int_{\zeta}^{\infty} e^{j(\gamma z+z^{\nu}/\nu)}dz\,;\ \ \nu = 3,4,5\cdots\,, \tag{C.1}$$

where γ and ζ are considered real, and the path of integration is any path that goes to infinity in the sector $0 \leq \arg(z) \leq \pi/\nu$. When $\nu = 3$, $\overline{K}_{\omega}(\gamma,\zeta,3)$ in (C.1) is the definition for the incomplete Airy integral [9]. When $\nu = 4$, $\overline{K}_{\omega}(\gamma,\zeta,4)$ is a special case of the incomplete Pearcy integral with the quadratic phase coefficient being equal to zero.

The complex plane topology of the generalized incomplete Airy integral when $\zeta > 0$ is depicted in Figure C.1. Depending on the endpoint location relative to the saddle point $\overline{K}_{\omega}(\gamma,\zeta,\nu)$ may be written as follows:

1. $\gamma + \zeta^{\nu-1} < 0, \zeta > 0$:

$$\overline{K}_{\omega}(\gamma,\zeta,\nu) = \int_{\zeta}^{\infty\exp(-j3\pi/2\nu)} e^{j(\gamma z+z^{\nu}/\nu)}dz + \int_{\infty\exp(-j3\pi/2\nu)}^{\infty\exp(j\pi/2\nu)} e^{j(\gamma z+z^{\nu}/\nu)}dz\,, \tag{C.2}$$

2. $\gamma + \zeta^{\nu-1} > 0, \zeta > 0$:

$$\overline{K}_{\omega}(\gamma,\zeta,\nu) = \int_{\zeta}^{\infty\exp(j\pi/2\nu)} e^{j(\gamma z+z^{\nu}/\nu)}dz\,. \tag{C.3}$$

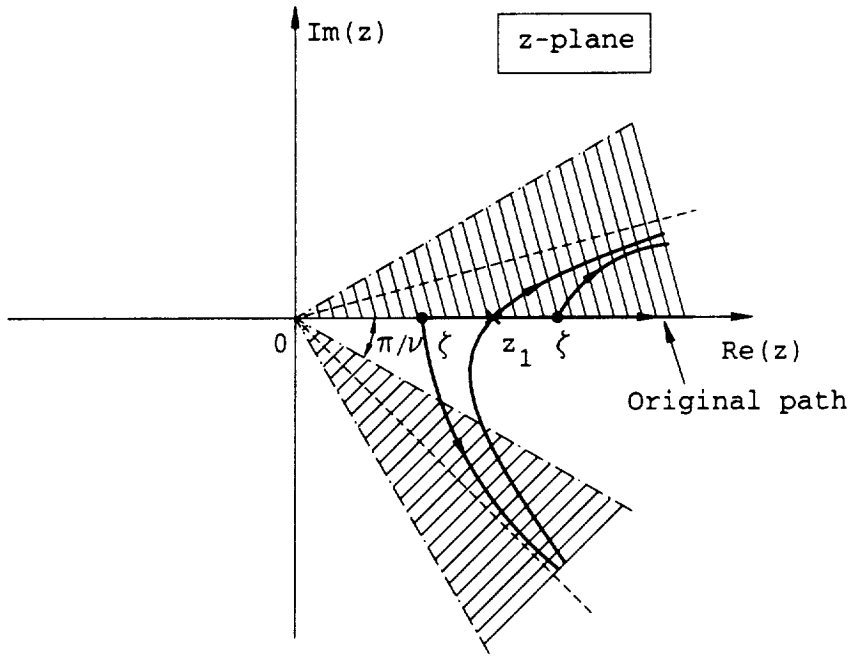

Figure C.1: Complex plane topology of the generalized incomplete Airy integral for $\zeta > 0$

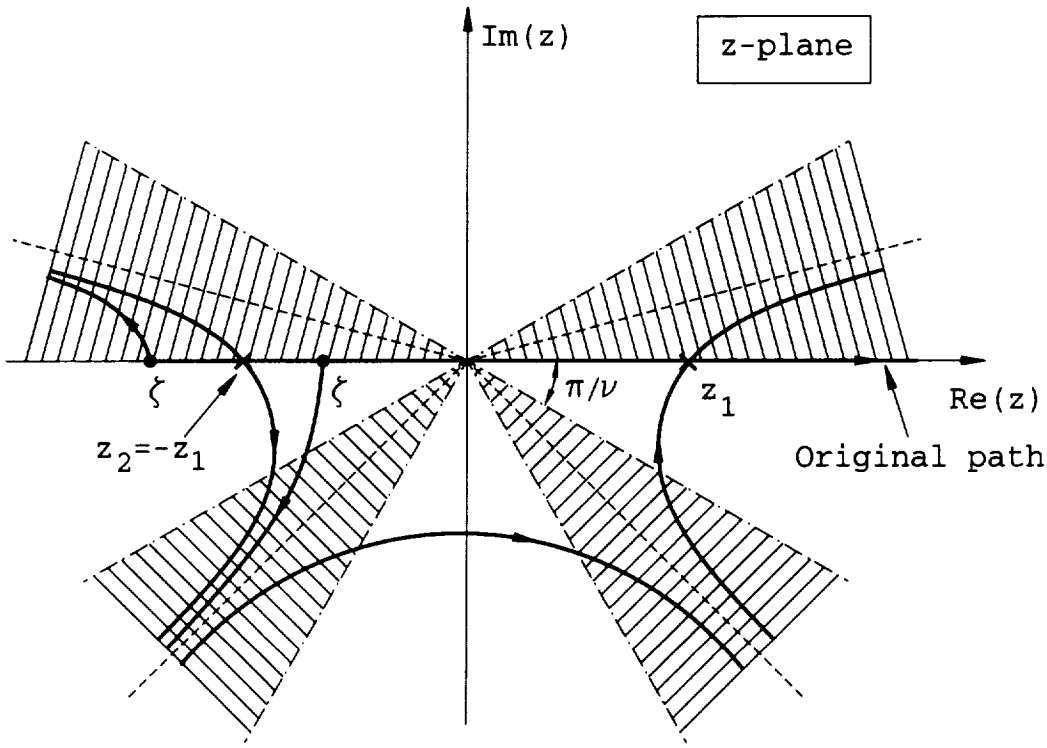

Figure C.2: Complex plane topology of the generalized incomplete Airy integral for $\zeta < 0$ and ν odd.

The complex plane topology of the generalized incomplete Airy integral when $\zeta < 0$ and ν odd or even is depicted in Figures C.2 and C.3, respectively. Depending on the endpoint location relative to the saddle point $\overline{K}_\omega(\gamma, \zeta, \nu)$ may be written as follows:

3. $\gamma + \zeta^{\nu-1} < 0$, $\zeta < 0$, ν is odd:

$$\overline{K}_\omega(\gamma,\zeta,\nu) = \int_\zeta^{\infty \exp[-j(\pi-3\pi/2\nu]} e^{j(\gamma z + z^\nu/\nu)} dz + \int_{\infty \exp[-j(\pi-3\pi/2\nu)]}^{\infty \exp(j\pi/2\nu)} e^{j(\gamma z + z^\nu/\nu)} dz\,, \qquad \text{(C.4)}$$

4. $\gamma + \zeta^{\nu-1} > 0$, $\zeta < 0$, ν is odd:

$$\overline{K}_\omega(\gamma,\zeta,\nu) = \int_\zeta^{\infty \exp[j(\pi-\pi/2\nu]} e^{j(\gamma z + z^\nu/\nu)} dz + \int_{\infty \exp[j(\pi-\pi/2\nu)]}^{\infty \exp(j\pi/2\nu)} e^{j(\gamma z + z^\nu/\nu)} dz\,, \qquad \text{(C.5)}$$

5. $\gamma + \zeta^{\nu-1} < 0$, $\zeta < 0$, ν is even:

$$\overline{K}_\omega(\gamma,\zeta,\nu) = \int_\zeta^{\infty \exp[-j(\pi-\pi/2\nu]} e^{j(\gamma z + z^\nu/\nu)} dz + \int_{\infty \exp[-j(\pi-\pi/2\nu)]}^{\infty \exp(j\pi/2\nu)} e^{j(\gamma z + z^\nu/\nu)} dz\,, \qquad \text{(C.6)}$$

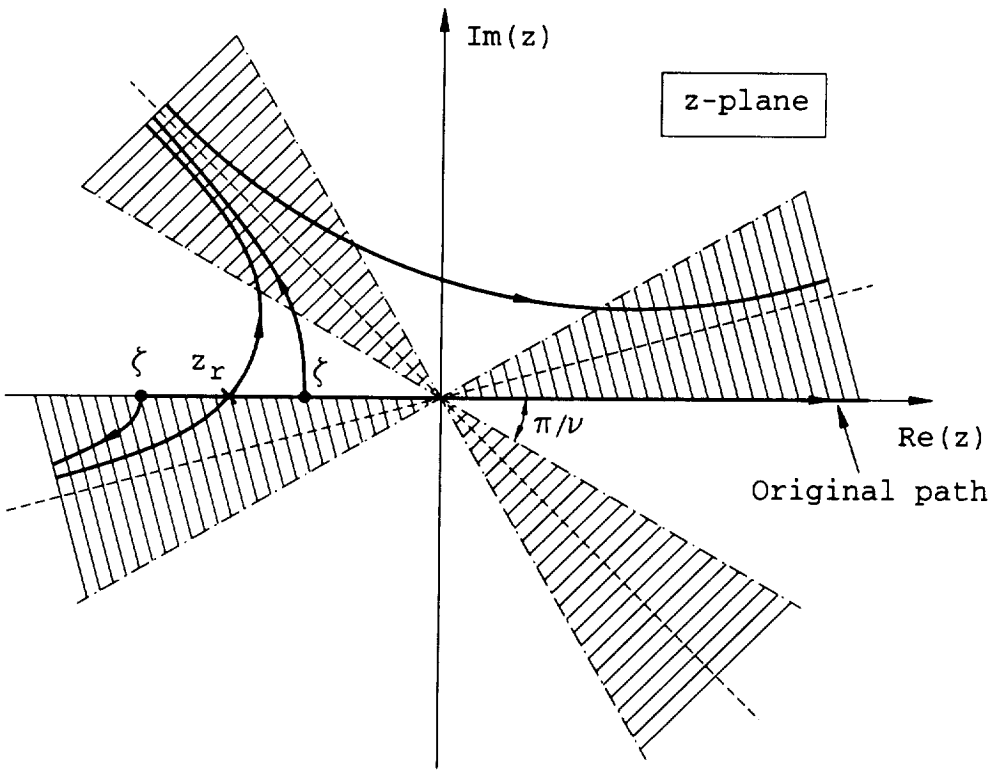

Figure C.3: Complex plane topology of the generalized incomplete Airy integral for $\zeta < 0$ and ν even.

6. $\gamma + \zeta^{\nu-1} > 0$, $\zeta < 0$, ν is even:

$$\overline{K}_\omega(\gamma,\zeta,\nu) = \int_\zeta^{\infty\exp[j(\pi-3\pi/2\nu]} e^{j(\gamma z+z^\nu/\nu)}dz + \int_{\infty\exp[j(\pi-3\pi/2\nu)]}^{\infty\exp(j\pi/2\nu)} e^{j(\gamma z+z^\nu/\nu)}dz\,. \qquad \text{(C.7)}$$

C.1 The incomplete Airy integral

A special case of particular interest for $\overline{K}_\omega(\gamma,\zeta,\nu=3)$ in (C.1) is the incomplete Airy integral which serves as a canonical function for the uniform asymptotic approximation of a class of integrals characterized by two stationary phase points that arbitrarily close to one another or to an integration endpoint [27]. It is defined as follows:

$$\overline{\mathrm{Ai}}(\gamma,\zeta) \triangleq \int_\zeta^\infty e^{j(\gamma z+z^3/3)}dz\,, \qquad \text{(C.8)}$$

where γ and ζ are considered real, and the path of integration is any path that goes to infinity in the sector $0 \le \arg(z) \le \pi/3$.

The complex plane topology of the incomplete Airy integral when the saddle points $z_{1,2} = \pm(-\gamma)^{1/2}$ are real ($\gamma < 0$) is depicted in Figure C.4. There exist three cases depending on the location of the endpoint ζ relative to the saddle points $z_{1,2}$, and $\overline{\mathrm{Ai}}(\gamma,\zeta)$ may be written as follows:

1. $\zeta \le -(-\gamma)^{1/2}$:

$$\begin{aligned}\overline{\mathrm{Ai}}(\gamma,\zeta) &= \int_\zeta^{\infty\exp(j\psi_2)} e^{j(\gamma z+z^3/3)}dz + \int_{L_{23}} e^{j(\gamma z+z^3/3)}dz + \int_{L_{31}} e^{j(\gamma z+z^3/3)}dz \\ &\equiv \mathrm{g}_2(\gamma,\zeta) - j\sqrt{\pi}\,[\mathrm{W}_1(\gamma) - \mathrm{W}_2(\gamma)]\,,\ \gamma < 0\,, \end{aligned} \qquad \text{(C.9)}$$

2. $-(-\gamma)^{1/2} < \zeta \le (-\gamma)^{1/2}$:

$$\begin{aligned}\overline{\mathrm{Ai}}(\gamma,\zeta) &= \int_\zeta^{\infty\exp(j\psi_3)} e^{j(\gamma z+z^3/3)}dz + \int_{L_{31}} e^{j(\gamma z+z^3/3)}dz \\ &\equiv \mathrm{g}_3(\gamma,\zeta) + j\sqrt{\pi}\,\mathrm{W}_2(\gamma)\,,\ \gamma < 0 \end{aligned} \qquad \text{(C.10)}$$

3. $\zeta > (-\gamma)^{1/2}$:

$$\overline{\mathrm{Ai}}(\gamma,\zeta) = \int_\zeta^{\infty\exp(j\psi_1)} e^{j(\gamma z+z^3/3)}dz \equiv \mathrm{g}_1(\gamma,\zeta)\,,\ \gamma < 0\,. \qquad \text{(C.11)}$$

The complex plane topology of the incomplete Airy integral when the saddle points $z_{1,2} = \pm(-\gamma)^{1/2}$ are complex ($\gamma > 0$) is depicted in Figure C.5. There exist two cases

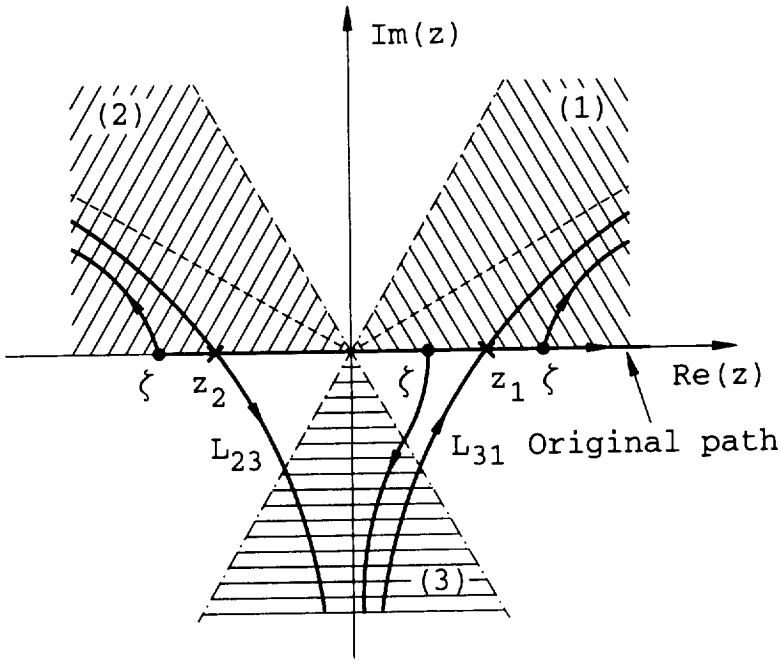

Figure C.4: Complex plane topology of the incomplete Airy integral for $\gamma < 0$.

depending on the sign of the endpoint ζ, and $\overline{\mathrm{Ai}}(\gamma,\zeta)$ may be written as follows:

4. $\zeta < 0$:

$$\begin{aligned}\overline{\mathrm{Ai}}(\gamma,\zeta) &= \int_{\zeta}^{\infty\exp(j\psi_2)} e^{j(\gamma z+z^3/3)}dz + \int_{L_{21}} e^{j(\gamma z+z^3/3)}dz \\ &\equiv g_2(\gamma,\zeta) + 2\pi\,\mathrm{Ai}(\gamma)\,,\ \ \gamma > 0\,,\end{aligned} \tag{C.12}$$

5. $\zeta > 0$:

$$\overline{\mathrm{Ai}}(\gamma,\zeta) = \int_{\zeta}^{\infty\exp(j\psi_1)} e^{j(\gamma z+z^3/3)}dz \equiv g_1(\gamma,\zeta)\,,\ \ \gamma > 0\,. \tag{C.13}$$

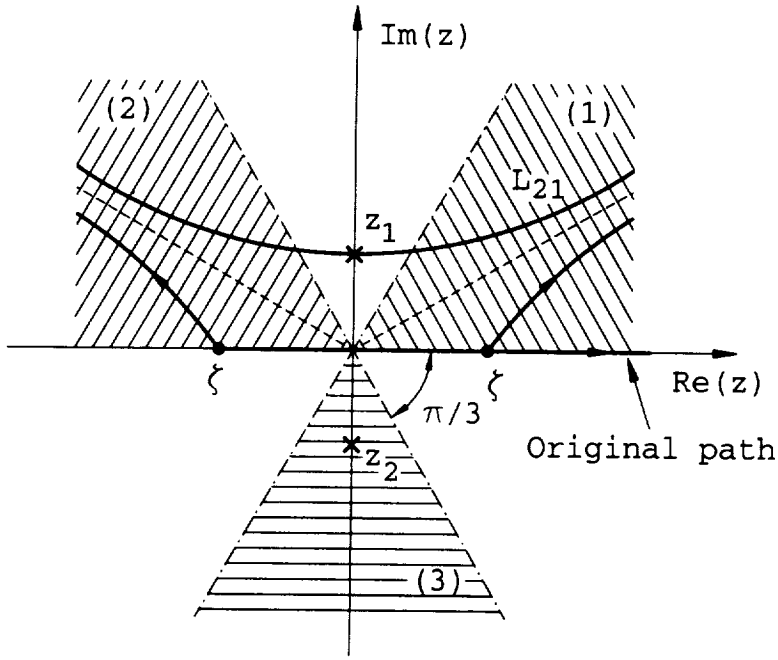

Figure C.5: Complex plane topology of the incomplete Airy integral for $\gamma > 0$.

Appendix D

The UTD Transition Function

The UTD transition function utd is defined as follows:

$$F(x) \triangleq 2j\sqrt{x}\, e^{jx} \int_{\sqrt{x}}^{\infty} e^{-j\tau^2}\, d\tau\,, \tag{D.1}$$

where x is cosidered real, with $\sqrt{x} = |\sqrt{x}|$ if $x > 0$, and $\sqrt{x} = j|\sqrt{x}|$ if $x < 0$. Also, the path of integration in the Fresnel integral is any path that goes to infinity in the fourth quadrant. $F(-|x|)$ may be obtained using the following relation:

$$F(-|x|) = F^*(|x|)\,. \tag{D.2}$$

When $x < 6.0$, $F(x)$ is computed using its power series form, that is

$$F(x) \simeq \sqrt{\pi x}\, e^{j(x+\pi/4)}\, \mathrm{sign}(x) - 2jxe^{jx} \sum_{n=0}^{N(x)} \frac{(-jx)^n}{(2n+1)n!}\,. \tag{D.3}$$

The number of terms in the series, $N(x)$, is given by the empirical formula

$$N(x) = 10\sqrt{x}\,, \tag{D.4}$$

and results in a truncation error of less than 10^{-6}. The large argument form of the Fresnel transition function ($x \geq 6.0$) is given by:

$$F(x) \sim \sum_{m=0}^{5} \frac{(-1)^m 2^m \left(\frac{1}{2}\right)_m}{(2jx)^m}\,, \tag{D.5}$$

where

$$\left(\alpha + \frac{1}{2}\right)_0 = 1, \text{ and } 2^m \left(\alpha + \frac{1}{2}\right)_m = (2\alpha+1)(2\alpha+3)\cdots(2\alpha+2m-1)\,. \tag{D.6}$$

Appendix E

The Fresnel Transition Function of Complex Argument

In this appendix, some properties and formulae for the Fresnel transition function with complex argument are presented. The Fresnel transition function is defined as follows:

$$\tilde{F}(\xi) \triangleq 2j\xi e^{j\xi^2} \int_{\xi}^{\infty} e^{-js^2}\, ds \tag{E.1}$$

where the path of integration in the Fresnel integral is any path that goes to infinity in the fourth quadrant. When ξ is real, $\tilde{F}(\xi) = F(\xi^2)$, where $F(x)$ is the UTD transition function [4]. The complex plane topology of the Fresnel integral is shown in Figure E.1. Also, $\tilde{F}(-\xi)$ may be obtained using the following relation:

$$\tilde{F}(-\xi) = \tilde{F}(\xi) - 2\sqrt{j\pi}\,\xi\, e^{j\xi^2}\,. \tag{E.2}$$

The power series form of $\tilde{F}(\xi)$ used in small argument approximations is given by

$$\tilde{F}(\xi) = \sqrt{j\pi}\,\xi\, e^{j\xi^2} - 2j\xi^2 e^{j\xi^2} \sum_{n=0}^{\infty} \frac{(-j\xi^2)^n}{(2n+1)n!}\,;\ |\xi| \ll 1\,. \tag{E.3}$$

The asymptotic expansion of $\tilde{F}(\xi)$ used in large argument approximations is given by:

$$\tilde{F}(\xi) \sim 2\sqrt{j\pi}\,\xi\, e^{j\xi^2} u(-\eta) + 1 + \sum_{m=1}^{\infty} (-1)^m \frac{1\cdot 3\cdots(2m-1)}{(2j\xi^2)^m}\,;\ |\xi| \gg 1\,, \tag{E.4}$$

$$\eta = \Re(\xi e^{j\frac{\pi}{4}})\,. \tag{E.5}$$

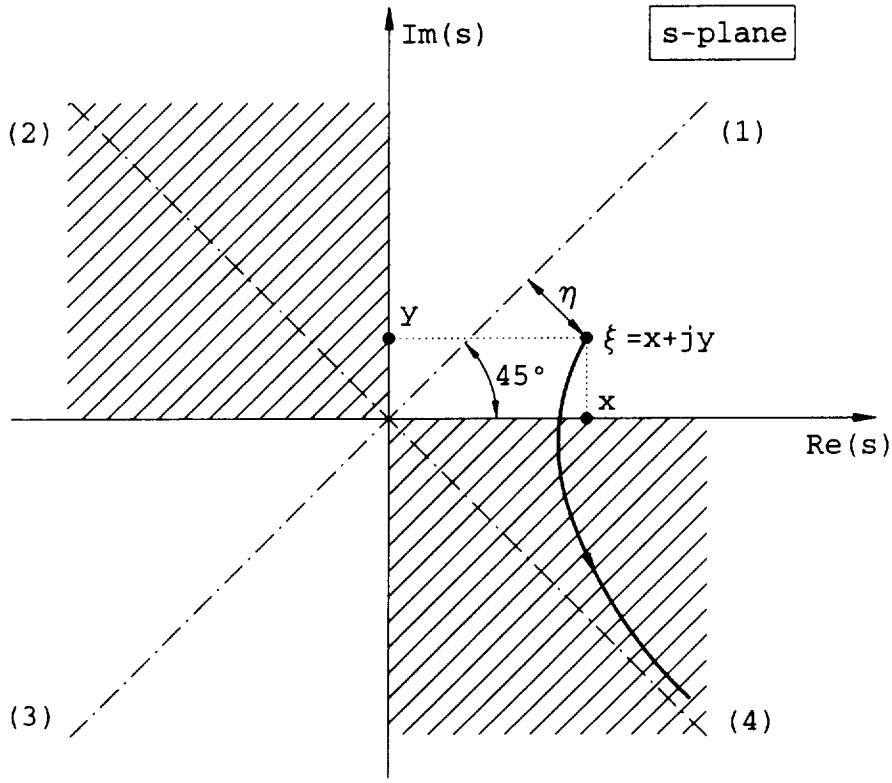

Figure E.1: Complex plane topology of the Fresnel integral with complex argument

Appendix F

Geometric Interpretation of the Phase Derivatives in the 2-D PO Radiation Integral

In this appendix, the phase derivatives in the PO integral formulation for the near-zone EM scattering from a smooth two dimensional curved boundary are expressed in terms of the local geometric parameters of the boundary C as shown in Figure F.1. The phase function $\phi(\ell)$ in the 2–D PO radiation integral is given by

$$\phi(\ell) = s^i(\ell) + R(\ell)\,, \tag{F.1}$$

where

$$\left[s^i(\ell)\right]^2 = \left\{\left[\vec{s}^{\,i}(\ell_0) + \vec{r}(\ell)\right]\cdot\hat{n}(\ell_0)\right\}^2 + \left\{\left[\vec{s}^{\,i}(\ell_0) + \vec{r}(\ell)\right]\cdot\hat{t}(\ell_0)\right\}^2\,, \tag{F.2}$$

$$R^2(\ell) = \left\{\left[\vec{R}(\ell_0) - \vec{r}(\ell)\right]\cdot\hat{n}(\ell_0)\right\}^2 + \left\{\left[\vec{R}(\ell_0) - \vec{r}(\ell)\right]\cdot\hat{t}(\ell_0)\right\}^2\,, \tag{F.3}$$

ℓ_0 is an arbitrary reference point on the boundary C, $\ell = \ell_0 + \delta\ell$ is the arclength, and $\vec{r}(\ell)$ is the natural representation of C.

1. First derivative, $\dot{\phi}(\ell)$:

From Equation (F.1) the first derivative of the phase function is given by

$$\dot{\phi}(\ell) = \dot{s}^{\,i}(\ell) + \dot{R}(\ell)\,. \tag{F.4}$$

Taking the first derivative of both sides of Equation (F.2) we have

$$\begin{aligned} s^i(\ell)\dot{s}^{\,i}(\ell) &= \left\{\left[\vec{s}^{\,i}(\ell_0) + \vec{r}(\ell)\right]\cdot\hat{n}(\ell_0)\right\}\dot{\vec{r}}(\ell)\cdot\hat{n}(\ell_0) \\ &+ \left\{\left[\vec{s}^{\,i}(\ell_0) + \vec{r}(\ell)\right]\cdot\hat{t}(\ell_0)\right\}\dot{\vec{r}}(\ell)\cdot\hat{t}(\ell_0)\,. \end{aligned} \tag{F.5}$$

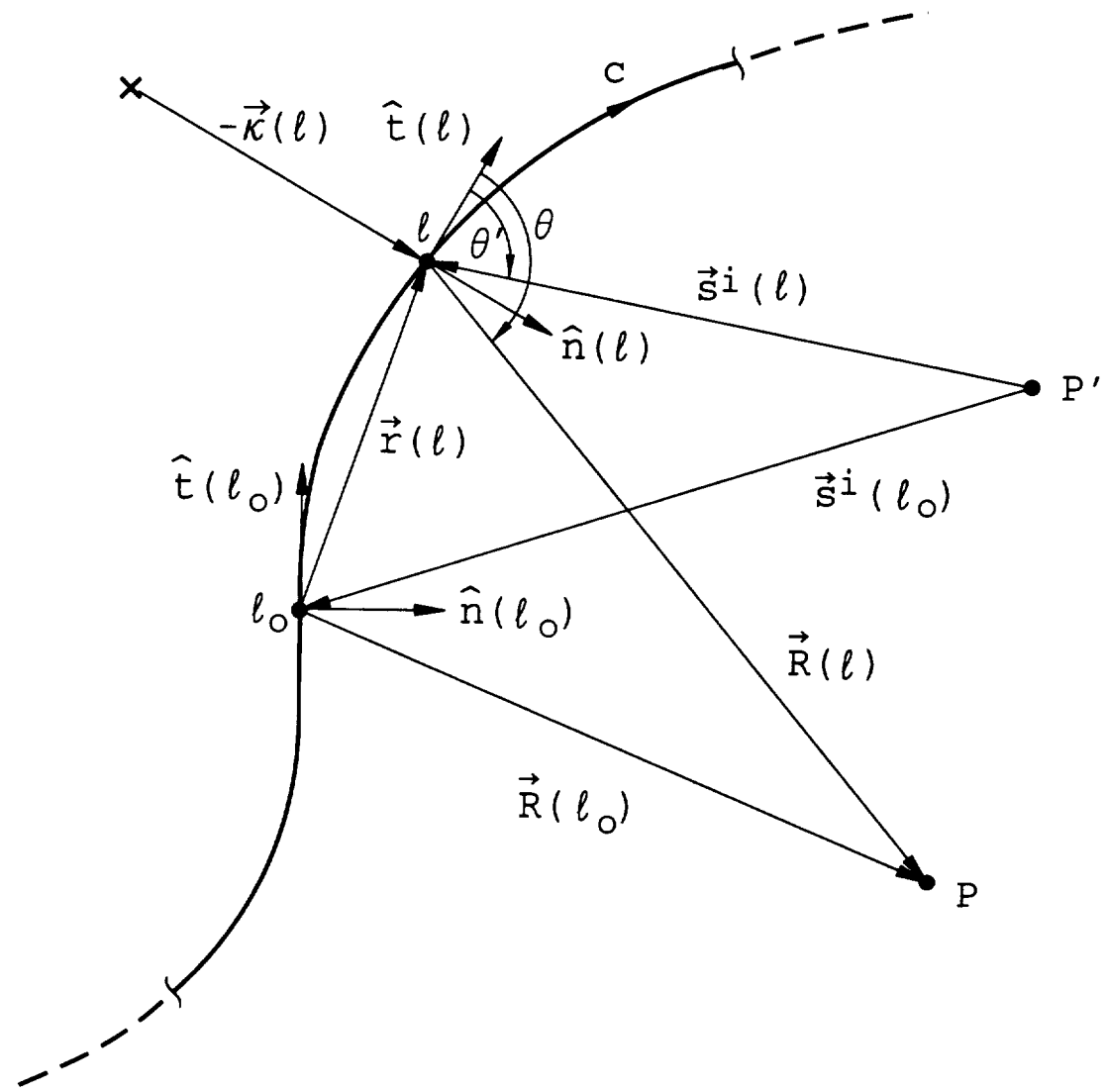

Figure F.1: Geometric parameter definitions for the phase derivatives in the 2–D PO radiation integral

Using the fact that $\dot{\vec{r}}(\ell) = \hat{t}(\ell)$ from the Frenet Equations [28] we have that

$$\dot{s}^{i}(\ell) = \frac{\left\{[\vec{s}^{i}(\ell_0) + \vec{r}(\ell)] \cdot \hat{t}(\ell_0)\right\}}{s^{i}(\ell)}, \tag{F.6}$$

and letting $\delta \to 0$, that is $\ell_0 \to \ell$ we have that

$$\dot{s}^{i}(\ell) = \hat{s}^{i}(\ell) \cdot \hat{t}(\ell), \tag{F.7}$$

and in a similar fashion

$$\dot{R}(\ell) = -\hat{R}(\ell) \cdot \hat{t}(\ell). \tag{F.8}$$

Thus, using Equations (F.7) and (F.8), the first derivative of the phase function is given by

$$\dot{\phi}(\ell) = \left[\hat{s}^{i}(\ell) - \hat{R}(\ell)\right] \cdot \hat{t}(\ell). \tag{F.9}$$

2. Second derivative, $\ddot{\phi}(\ell)$:

From Equation (F.1) the second derivative of the phase function is given by

$$\ddot{\phi}(\ell) = \ddot{s}^{i}(\ell) + \ddot{R}(\ell). \tag{F.10}$$

Taking the derivative of both sides of Equation (F.5) we get

$$\begin{aligned} \left[\dot{s}^{i}(\ell)\right]^2 + s^{i}(\ell)\ddot{s}^{i}(\ell) &= \left[\hat{t}(\ell) \cdot \hat{n}(\ell_0)\right]^2 + \left[\hat{t}(\ell) \cdot \hat{t}(\ell_0)\right]^2 \\ &+ \left\{\left[\vec{s}^{i}(\ell_0) + \vec{r}(\ell)\right] \hat{n}(\ell_0)\right\} \dot{\hat{t}}(\ell) \cdot \hat{n}(\ell_0) \\ &+ \left\{\left[\vec{s}^{i}(\ell_0 + \vec{r}(\ell)\right] \hat{n}(\ell_0)\right\} \dot{\hat{t}}(\ell) \cdot \hat{t}(\ell_0), \end{aligned} \tag{F.11}$$

and using the fact that $\dot{\hat{t}}(\ell) = \vec{\kappa}_g(\ell) = -\hat{n}(\ell)\kappa(\ell)$ from the Frenet Equations [28], where $\kappa_g(\ell)$ denotes the normal surface curvature, and again letting $\delta \to 0$, that is $\ell_0 \to \ell$ along with Equation (F.7) we have that

$$\ddot{s}^{i}(\ell) = -\kappa_g(\ell)\left[\hat{s}^{i}(\ell) \cdot \hat{n}(\ell)\right] + \frac{1}{s^{i}(\ell)} - \frac{\left[\hat{s}^{i}(\ell) \cdot \hat{t}(\ell)\right]^2}{s^{i}(\ell)}. \tag{F.12}$$

In a similar fashion, $\ddot{R}(\ell)$ is given by

$$\ddot{R}(\ell) = \kappa_g(\ell)\left[\hat{R}(\ell) \cdot \hat{n}(\ell)\right] + \frac{1}{R(\ell)} - \frac{\left[\hat{R}(\ell) \cdot \hat{t}(\ell)\right]^2}{R(\ell)}, \tag{F.13}$$

and thus using Equations (F.12) and (F.13), the second derivative of the phase function is given by

$$\ddot{\phi}(\ell) = \frac{\left[\hat{R}(\ell) - \hat{s}^{\,i}(\ell)\right] \cdot \hat{n}(\ell)}{\rho_g(\ell)} + \frac{\left[\hat{s}^{\,i}(\ell) \cdot \hat{n}(\ell)\right]^2}{s^i(\ell)} + \frac{\left[\hat{R}(\ell) \cdot \hat{n}(\ell)\right]^2}{R(\ell)}, \tag{F.14}$$

where $\rho_g(\ell) = 1/\kappa_g(\ell)$ is the surface radius of curvature at ℓ.

3. Third derivative, $\dddot{\phi}(\ell)$:

The third derivative of the phase function is given by

$$\dddot{\phi}(\ell) = \dddot{s}^{\,i}(\ell) + \dddot{R}(\ell). \tag{F.15}$$

Taking the derivatives of both sides of Equation (F.11) we get

$$\begin{aligned} 3\dot{s}^{\,i}(\ell)\ddot{s}^{\,i}(\ell) + s^i(\ell)\,\dddot{s}^{\,i}(\ell) \;=\; & -3\left[\hat{t}(\ell)\cdot\hat{n}(\ell_0)\right]\left[\hat{n}(\ell)\cdot\hat{n}(\ell_0)\right]\kappa_g(\ell) \\ & - \left\{\left[\vec{s}^{\,i}(\ell_0) + \vec{r}(\ell)\right]\cdot\hat{n}(\ell_0)\right\}\left[\dot{\hat{n}}(\ell)\cdot\hat{n}(\ell_0)\right]\kappa_g(\ell) \\ & - \left\{\left[\vec{s}^{\,i}(\ell_0) + \vec{r}(\ell)\right]\cdot\hat{n}(\ell_0)\right\}\left[\hat{n}(\ell)\cdot\hat{n}(\ell_0)\right]\dot{\kappa}_g(\ell) \\ & - 3\left[\hat{t}(\ell)\cdot\hat{t}(\ell_0)\right]\left[\hat{n}(\ell)\cdot\hat{t}(\ell_0)\right]\kappa_g(\ell) \\ & - \left\{\left[\vec{s}^{\,i}(\ell_0) + \vec{r}(\ell)\right]\cdot\hat{t}(\ell_0)\right\}\left[\dot{\hat{n}}(\ell)\cdot\hat{t}(\ell_0)\right]\kappa_g(\ell) \\ & - \left\{\left[\vec{s}^{\,i}(\ell_0) + \vec{r}(\ell)\right]\cdot\hat{t}(\ell_0)\right\}\left[\hat{n}(\ell)\cdot\hat{t}(\ell_0)\right]\dot{\kappa}_g(\ell), \end{aligned} \tag{F.16}$$

and using the fact that $\dot{\hat{n}}(\ell) = \hat{t}(\ell)\kappa_g(\ell)$ from the Frenet Equations [28], and again letting $\delta \to 0$, that is $\ell_0 \to \ell$ along with Equations (F.7) and (F.12) we have that

$$\begin{aligned} \dddot{s}^{\,i}(\ell) \;=\; & -\left[\hat{s}^{\,i}(\ell)\cdot\hat{n}(\ell)\right]\dot{\kappa}_g(\ell) - \left[\hat{s}^{\,i}(\ell)\cdot\hat{t}(\ell)\right]\kappa_g^2(\ell) \\ & + \frac{3\left[\hat{s}^{\,i}(\ell)\cdot\hat{n}(\ell)\right]\left[\hat{s}^{\,i}(\ell)\cdot\hat{t}(\ell)\right]\kappa_g(\ell)}{s^i(\ell)} \\ & - \frac{3\left[\hat{s}^{\,i}(\ell)\cdot\hat{n}(\ell)\right]^2\left[\hat{s}^{\,i}(\ell)\cdot\hat{t}(\ell)\right]}{\left[s^i(\ell)\right]^2}. \end{aligned} \tag{F.17}$$

In a similar fashion, $\dddot{R}(\ell)$ is given by

$$\begin{aligned} \dddot{R}(\ell) \;=\; & \left[\hat{R}(\ell)\cdot\hat{n}(\ell)\right]\dot{\kappa}_g(\ell) + \left[\hat{R}(\ell)\cdot\hat{t}(\ell)\right]\kappa_g^2(\ell) \\ & + \frac{3\left[\hat{R}(\ell)\cdot\hat{n}(\ell)\right]\left[\hat{R}(\ell)\cdot\hat{t}(\ell)\right]\kappa_g(\ell)}{R(\ell)} \\ & + \frac{3\left[\hat{R}(\ell)\cdot\hat{n}(\ell)\right]^2\left[\hat{R}(\ell)\cdot\hat{t}(\ell)\right]}{R^2(\ell)}, \end{aligned} \tag{F.18}$$

and thus using Equations (F.17) and (F.18), the third derivative of the phase function is given by

$$\begin{aligned}\dddot{\phi}(\ell) &= \left[\hat{R}(\ell)-\hat{s}^i(\ell)\right]\cdot\hat{n}(\ell)\dot{\kappa}_g(\ell)-\frac{\left[\hat{s}^i(\ell)-\hat{R}(\ell)\right]\cdot\hat{t}(\ell)}{\rho_g^2(\ell)}\\ &+\frac{3\left[\hat{s}^i(\ell)\cdot\hat{n}(\ell)\right]\left[\hat{s}^i(\ell)\cdot\hat{t}(\ell)\right]}{s^i(\ell)}\left[\frac{1}{\rho_g(\ell)}-\frac{\hat{s}^i(\ell)\cdot\hat{n}(\ell)}{s^i(\ell)}\right]\\ &+\frac{3\left[\hat{R}(\ell)\cdot\hat{n}(\ell)\right]\left[\hat{R}(\ell)\cdot\hat{t}(\ell)\right]}{R(\ell)}\left[\frac{1}{\rho_g(\ell)}+\frac{\hat{R}(\ell)\cdot\hat{n}(\ell)}{R(\ell)}\right]. \qquad \text{(F.19)}\end{aligned}$$

Finally, using the following relations:

$$\hat{s}^i(\ell)\cdot\hat{n}(\ell) = -\sin\theta' \qquad \text{(F.20)}$$

$$\hat{s}^i(\ell)\cdot\hat{t}(\ell) = -\cos\theta' \qquad \text{(F.21)}$$

$$\hat{R}(\ell)\cdot\hat{n}(\ell) = \sin\theta \qquad \text{(F.22)}$$

$$\hat{R}(\ell)\cdot\hat{t}(\ell) = \cos\theta \qquad \text{(F.23)}$$

Equations (F.9), (F.14), and (F.19) can be expressed in terms of the angles θ and θ' defined in Figure F.1, that is

$$\dot{\phi}(\ell) = -(\cos\theta+\cos\theta'), \qquad \text{(F.24)}$$

$$\ddot{\phi}(\ell) = \frac{\sin\theta+\sin\theta'}{\rho_g(\ell)}+\frac{\sin^2\theta'}{s^i(\ell)}+\frac{\sin^2\theta}{R(\ell)}, \qquad \text{(F.25)}$$

$$\begin{aligned}\dddot{\phi}(\ell) &= (\sin\theta+\sin\theta')\dot{\kappa}_g(\ell)+\frac{\cos\theta+\cos\theta'}{\rho_g^2(\ell)}\\ &+\frac{3\sin\theta'\cos\theta'}{s^i(\ell)}\left[\frac{1}{\rho_g(\ell)}+\frac{\sin\theta'}{s^i(\ell)}\right]\\ &+\frac{3\sin\theta\cos\theta}{R(\ell)}\left[\frac{1}{\rho_g(\ell)}+\frac{\sin\theta}{R(\ell)}\right]. \qquad \text{(F.26)}\end{aligned}$$

When ℓ is a reflection point as shown in Figure F.2, Equations (F.24)–(F.26) reduce to the more familiar expressions

$$\dot{\phi}(\ell_r) = (\hat{s}^i-\hat{s}^r)\cdot\hat{t}_r=0, \ \textit{(law of reflection)} \qquad \text{(F.27)}$$

$$\ddot{\phi}(\ell_r) = \cos^2\theta^i\left(\frac{1}{s^r}+\frac{1}{\rho^r}\right)\propto(\text{reflected ray spread factor})^{-2}, \qquad \text{(F.28)}$$

$$\frac{1}{\rho^r} = \frac{1}{s^i}+\frac{2}{\rho_g(Q_r)\cos\theta^i}=(\text{reflected ray caustic distance})^{-1}, \qquad \text{(F.29)}$$

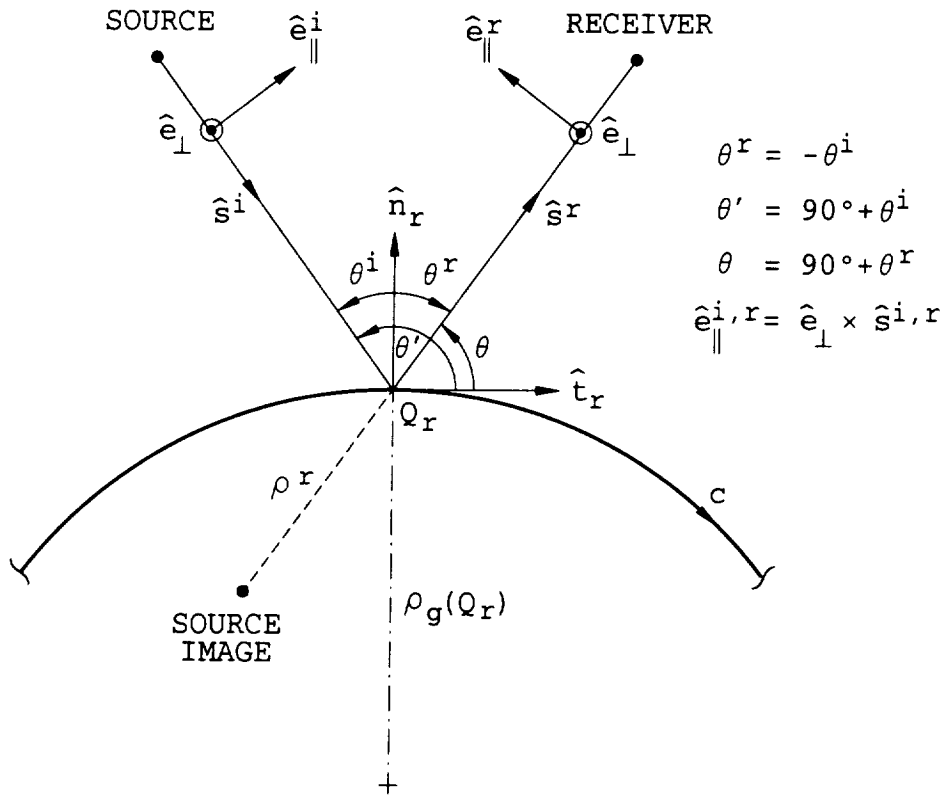

Figure F.2: Reflection from a 2–D curved boundary

$$
\begin{aligned}
\bar{\bar{\phi}}\,(\ell_r) &= 2\cos\theta^i \kappa_g'(Q_r) - \frac{3\cos^2\theta^i \sin\theta^i}{s^i}\left[\frac{1}{\rho_g(Q_r)\cos\theta^i} + \frac{1}{s^i}\right] \\
&- \frac{3\cos^2\theta^r \sin\theta^r}{s^r}\left[\frac{1}{\rho_g(Q_r)\cos\theta^r} + \frac{1}{s^r}\right] \qquad \text{(F.30)} \\
&\propto \text{(reflected ray spread factor near a caustic)}^{-3}\,.
\end{aligned}
$$

Appendix G

Geometric Interpretation of the Phase Derivatives in the 3-D PO Radiation Integral

In this appendix, the phase derivatives in the PO integral formulation for the near-zone EM scattering from a smooth three dimensional curved surface are expressed in terms of the local geometric parameters of the surface S as shown in Figure G.1. The phase function $\phi(\ell,\tau)$ in the 3-D PO radiation integral is given by

$$\phi(\ell,\tau) = s^i(\ell,\tau) + R(\ell,\tau)\,, \tag{G.1}$$

where

$$\begin{aligned}\left[s^i(\ell,\tau)\right]^2 &= \left\{\left[\vec{s}_0^{\,i} + \vec{r}(\ell,\tau)\right]\cdot\hat{\ell}_0\right\}^2 + \left\{\left[\vec{s}_0^{\,i} + \vec{r}(\ell,\tau)\right]\cdot\hat{\tau}_0\right\}^2 \\ &+ \left\{\left[\vec{s}_0^{\,i} + \vec{r}(\ell,\tau)\right]\cdot\hat{n}_0\right\}^2\,, \qquad \text{(G.2)}\\ R^2(\ell,\tau) &= \left\{\left[\vec{R}_0 - \vec{r}(\ell,\tau)\right]\cdot\hat{\ell}_0\right\}^2 + \left\{\left[\vec{R}_0 - \vec{r}(\ell,\tau)\right]\cdot\hat{\tau}_0\right\}^2 \\ &+ \left\{\left[\vec{R}_0 - \vec{r}(\ell,\tau)\right]\cdot\hat{n}_0\right\}^2\,, \qquad \text{(G.3)}\end{aligned}$$

$\hat{\ell}_0$, $\hat{\tau}_0$, and $\hat{n}_0$ are the principal unit tangents and unit normal vector at the reference point (ℓ_0,τ_0) forming a local surface orthogonal coordinate system, $\ell = \ell_0 + \delta\ell$ and $\tau = \tau_0 + \epsilon\tau$ are the arclengths from (ℓ_0,τ_0) to (ℓ,τ) along the principal coordinate curves of S which are always orthogonal, and the surface vector $\vec{r}(\ell,\tau)$ is therefore a natural representation of S for which the first and second fundamental forms are given by the following expressions [29]:

$$I(d\ell, d\tau) = d\ell^2 + d\tau^2\,, \tag{G.4}$$

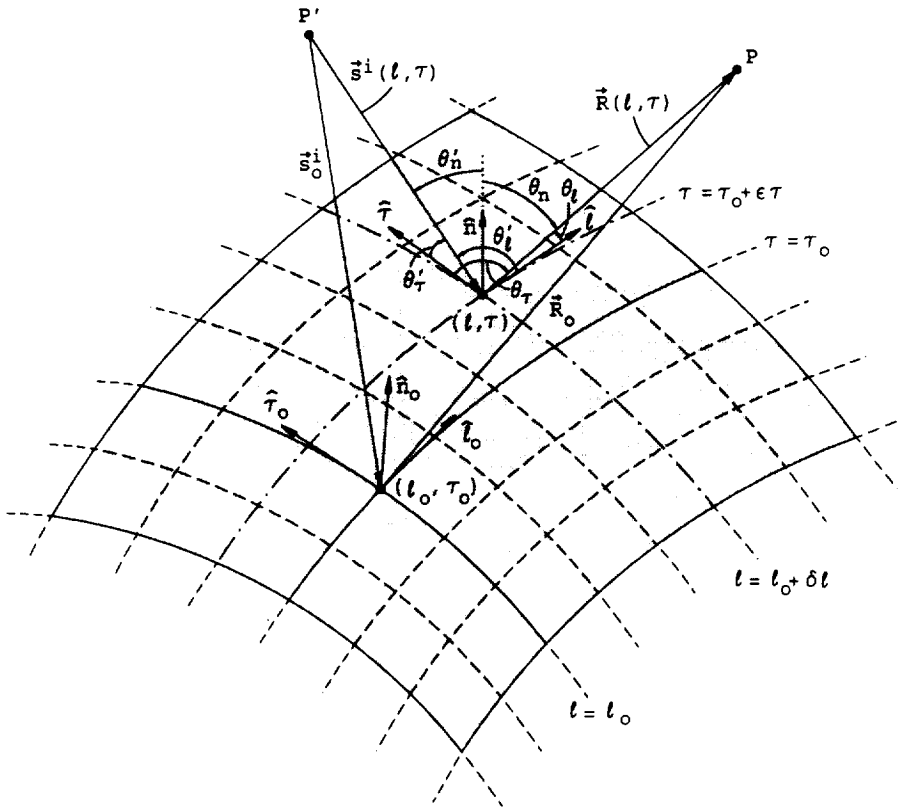

Figure G.1: Geometric parameter definitions for the phase derivatives in the 3–D PO radiation integral

$$II(d\ell, d\tau) = -\kappa_1(\ell,\tau)d\ell^2 - \kappa_2(\ell,\tau)d\tau^2\,, \tag{G.5}$$

where $\kappa_{1,2}$ are the principal curvatures along the principal surface directions $\hat{\ell}$ and $\hat{\tau}$, respectively. Equations (G.4) and (G.5) imply the following relations:

$$\dot{\vec{r}}_\ell(\ell,\tau)\cdot\dot{\vec{r}}_\ell(\ell,\tau) = 1\,, \tag{G.6}$$

$$\dot{\vec{r}}_\ell(\ell,\tau)\cdot\dot{\vec{r}}_\tau(\ell,\tau) = 0\,, \tag{G.7}$$

$$\dot{\vec{r}}_\tau(\ell,\tau)\cdot\dot{\vec{r}}_\tau(\ell,\tau) = 1\,, \tag{G.8}$$

$$\ddot{\vec{r}}_{\ell\ell}(\ell,\tau) = -\hat{n}(\ell,\tau)\kappa_1(\ell,\tau)\,, \tag{G.9}$$

$$\ddot{\vec{r}}_{\ell\tau}(\ell,\tau) = 0\,, \tag{G.10}$$

$$\ddot{\vec{r}}_{\tau\tau}(\ell,\tau) = -\hat{n}(\ell,\tau)\kappa_2(\ell,\tau)\,. \tag{G.11}$$

1. First derivatives, $\dot{\phi}_\ell(\ell,\tau)$ and $\dot{\phi}_\tau(\ell,\tau)$:

From Equation (G.1) the first derivatives of the phase function are given by

$$\dot{\phi}_\ell(\ell,\tau) = \dot{s}^i_\ell(\ell,\tau) + \dot{R}_\ell(\ell,\tau)\,, \tag{G.12}$$

$$\dot{\phi}_\tau(\ell,\tau) = \dot{s}^i_\tau(\ell,\tau) + \dot{R}_\tau(\ell,\tau)\,. \tag{G.13}$$

Taking the first derivative with respect to ℓ of both sides of Equation (G.2) we have

$$\begin{aligned} s^i(\ell,\tau)\dot{s}^i_\ell(\ell,\tau) &= \left\{\left[\vec{s}^i_0 + \vec{r}(\ell,\tau)\right]\cdot\hat{\ell}_0\right\}\dot{\vec{r}}_\ell(\ell,\tau)\cdot\hat{\ell}_0 \\ &+ \left\{\left[\vec{s}^i_0 + \vec{r}(\ell,\tau)\right]\cdot\hat{\tau}_0\right\}\dot{\vec{r}}_\ell(\ell,\tau)\cdot\hat{\tau}_0 \\ &+ \left\{\left[\vec{s}^i_0 + \vec{r}(\ell,\tau)\right]\cdot\hat{n}_0\right\}\dot{\vec{r}}_\ell(\ell,\tau)\cdot\hat{n}_0\,. \end{aligned} \tag{G.14}$$

Using the fact that $\dot{\vec{r}}_\ell(\ell,\tau) = \hat{\ell}$ from (G.6) and (G.7) and letting $\delta,\epsilon \to 0$, that is $(\ell_0,\tau_0) \to (\ell,\tau)$, Equation (G.14) becomes

$$\dot{s}^i_\ell(\ell,\tau) = \hat{s}^i(\ell,\tau)\cdot\hat{\ell}\,, \tag{G.15}$$

and in a similar fashion $\dot{R}_\ell(\ell,\tau)$ is given by

$$\dot{R}_\ell(\ell,\tau) = -\hat{R}(\ell,\tau)\cdot\hat{\ell}\,. \tag{G.16}$$

Furthermore, using the fact that $\dot{\vec{r}}_\tau(\ell,\tau) = \hat{\tau}$ from (G.7) and (G.8) we have

$$\dot{s}^i_\tau(\ell,\tau) = \hat{s}^i(\ell,\tau)\cdot\hat{\tau} \quad\text{and}\quad \dot{R}_\tau(\ell,\tau) = \hat{R}(\ell,\tau)\cdot\hat{\tau}\,, \tag{G.17}$$

thus, the first derivatives of the phase function $\dot{\phi}_\ell(\ell,\tau)$ and $\dot{\phi}_\tau(\ell,\tau)$ are given by

$$\dot{\phi}_\ell(\ell,\tau) = \left[\hat{s}^i(\ell,\tau) - \hat{R}(\ell,\tau)\right]\cdot\hat{\ell}\,, \tag{G.18}$$

$$\dot{\phi}_\tau(\ell,\tau) = \left[\hat{s}^i(\ell,\tau) - \hat{R}(\ell,\tau)\right]\cdot\hat{\tau}\,. \tag{G.19}$$

In terms of the angles $\theta'_{\ell,\tau}$ and $\theta_{\ell,\tau}$ defined in Figure G.1, the first derivatives of the phase function may be written as follows:

$$\dot{\phi}_\ell(\ell,\tau) = -(\cos\theta'_\ell + \cos\theta_\ell)\,, \tag{G.20}$$

$$\dot{\phi}_\tau(\ell,\tau) = -(\cos\theta'_\tau + \cos\theta_\tau)\,. \tag{G.21}$$

2. Second derivatives, $\ddot{\phi}_{\ell\ell}(\ell,\tau)$, $\ddot{\phi}_{\ell\tau}(\ell,\tau)$, and $\ddot{\phi}_{\tau\tau}(\ell,\tau)$:

From Equation (G.1) the second derivatives of the phase function are given by

$$\ddot{\phi}_{\ell\ell}(\ell,\tau) = \ddot{s}^i_{\ell\ell}(\ell,\tau) + \ddot{R}_{\ell\ell}(\ell,\tau)\,, \tag{G.22}$$

$$\ddot{\phi}_{\ell\tau}(\ell,\tau) = \ddot{s}^i_{\ell\tau}(\ell,\tau) + \ddot{R}_{\ell\tau}(\ell,\tau)\,, \tag{G.23}$$

$$\ddot{\phi}_{\tau\tau}(\ell,\tau) = \ddot{s}^i_{\tau\tau}(\ell,\tau) + \ddot{R}_{\tau\tau}(\ell,\tau)\,. \tag{G.24}$$

Taking the derivative with respect to ℓ of both sides of Equation (G.14) we get

$$\begin{aligned}\left[\dot{s}^i_\ell(\ell,\tau)\right]^2 &+ s^i(\ell,\tau)\ddot{s}^i_{\ell\ell}(\ell,\tau) = \left[\dot{\vec{r}}_\ell(\ell,\tau)\cdot\hat{\ell}_0\right]^2 + \left[\dot{\vec{r}}_\ell(\ell,\tau)\cdot\hat{\tau}_0\right]^2 \\ &+ \left[\dot{\vec{r}}_\ell(\ell,\tau)\cdot\hat{n}_0\right]^2 + \left\{\left[\vec{s}^i_0 + \vec{r}(\ell,\tau)\right]\cdot\hat{\ell}_0\right\}\left[\ddot{\vec{r}}_{\ell\ell}(\ell,\tau)\cdot\hat{\ell}_0\right] \\ &+ \left\{\left[\vec{s}^i_0 + \vec{r}(\ell,\tau)\right]\cdot\hat{\tau}_0\right\}\left[\ddot{\vec{r}}_{\ell\ell}(\ell,\tau)\cdot\hat{\tau}_0\right] \\ &+ \left\{\left[\vec{s}^i_0 + \vec{r}(\ell,\tau)\right]\cdot\hat{n}_0\right\}\left[\ddot{\vec{r}}_{\ell\ell}(\ell,\tau)\cdot\hat{n}_0\right]\,.\end{aligned} \tag{G.25}$$

Letting $\delta,\epsilon\to 0$, that is $(\ell_0,\tau_0)\to(\ell,\tau)$ and using (G.9), Equation (G.25) becomes

$$\left[\dot{s}^i_\ell(\ell,\tau)\right]^2 + s^i(\ell,\tau)\ddot{s}^i_{\ell\ell}(\ell,\tau) = 1 - \kappa_1(\ell,\tau)\left[\vec{s}^i(\ell,\tau)\cdot\hat{n}\right]\,. \tag{G.26}$$

Directly from (G.26) one can also infer the following expression:

$$\left[\dot{s}^i_\tau(\ell,\tau)\right]^2 + s^i(\ell,\tau)\ddot{s}^i_{\tau\tau}(\ell,\tau) = 1 - \kappa_2(\ell,\tau)\left[\vec{s}^i(\ell,\tau)\cdot\hat{n}\right]\,. \tag{G.27}$$

Taking the derivative with respect to τ of both sides of Equation (G.14), then letting $\delta,\epsilon\to 0$ and using Equation (G.10) we also get

$$\dot{s}^i_\ell(\ell,\tau)\dot{s}^i_\tau(\ell,\tau) + s^i(\ell,\tau)\ddot{s}^i_{\ell\tau}(\ell,\tau) = 0\,. \tag{G.28}$$

Then, using Equations (G.15), (G.17), and (G.26)-(G.28) we obtain the following expressions:

$$\ddot{s}^i_{\ell\ell}(\ell,\tau) = -\kappa_1(\ell,\tau)\left[\hat{s}^i(\ell,\tau)\cdot\hat{n}\right] + \frac{1-\left[\hat{s}^i(\ell,\tau)\cdot\hat{\ell}\right]^2}{s^i(\ell,\tau)}, \tag{G.29}$$

$$\ddot{s}^i_{\ell\tau}(\ell,\tau) = -\frac{\left[\hat{s}^i(\ell,\tau)\cdot\hat{\ell}\right]\left[\hat{s}^i(\ell,\tau)\cdot\hat{\tau}\right]}{s^i(\ell,\tau)}, \tag{G.30}$$

$$\ddot{s}^i_{\tau\tau}(\ell,\tau) = -\kappa_2(\ell,\tau)\left[\hat{s}^i(\ell,\tau)\cdot\hat{n}\right] + \frac{1-\left[\hat{s}^i(\ell,\tau)\cdot\hat{\tau}\right]^2}{s^i(\ell,\tau)}. \tag{G.31}$$

Similarly, the quantities $\ddot{R}_{\ell\ell}$, $\ddot{R}_{\ell\tau}$, and $\ddot{R}_{\tau\tau}$ are given by

$$\ddot{R}_{\ell\ell}(\ell,\tau) = \kappa_1(\ell,\tau)\left[\hat{R}(\ell,\tau)\cdot\hat{n}\right] + \frac{1-\left[\hat{R}(\ell,\tau)\cdot\hat{\ell}\right]^2}{R(\ell,\tau)}, \tag{G.32}$$

$$\ddot{R}_{\ell\tau}(\ell,\tau) = -\frac{\left[\hat{R}(\ell,\tau)\cdot\hat{\ell}\right]\left[\hat{R}(\ell,\tau)\cdot\hat{\tau}\right]}{R(\ell,\tau)}, \tag{G.33}$$

$$\ddot{R}_{\tau\tau}(\ell,\tau) = \kappa_2(\ell,\tau)\left[\hat{R}(\ell,\tau)\cdot\hat{n}\right] + \frac{1-\left[\hat{R}(\ell,\tau)\cdot\hat{\tau}\right]^2}{R(\ell,\tau)}. \tag{G.34}$$

Finally, using (G.29)-(G.34) the second derivatives of the phase function are given by

$$\begin{aligned}\ddot{\phi}_{\ell\ell}(\ell,\tau) &= \kappa_1(\ell,\tau)\left[\hat{R}(\ell,\tau)-\hat{s}^i(\ell,\tau)\right]\cdot\hat{n} + \frac{1-\left[\hat{s}^i(\ell,\tau)\cdot\hat{\ell}\right]^2}{s^i(\ell,\tau)} \\ &+ \frac{1-\left[\hat{R}(\ell,\tau)\cdot\hat{\ell}\right]^2}{R(\ell,\tau)},\end{aligned} \tag{G.35}$$

$$\ddot{\phi}_{\ell\tau}(\ell,\tau) = -\frac{\left[\hat{s}^i(\ell,\tau)\cdot\hat{\ell}\right]\left[\hat{s}^i(\ell,\tau)\cdot\hat{\tau}\right]}{s^i(\ell,\tau)} - \frac{\left[\hat{R}(\ell,\tau)\cdot\hat{\ell}\right]\left[\hat{R}(\ell,\tau)\cdot\hat{\tau}\right]}{R(\ell,\tau)}, \tag{G.36}$$

$$\begin{aligned}\ddot{\phi}_{\tau\tau}(\ell,\tau) &= \kappa_2(\ell,\tau)\left[\hat{R}(\ell,\tau)-\hat{s}^i(\ell,\tau)\right]\cdot\hat{n} + \frac{1-\left[\hat{s}^i(\ell,\tau)\cdot\hat{\tau}\right]^2}{s^i(\ell,\tau)} \\ &+ \frac{1-\left[\hat{R}(\ell,\tau)\cdot\hat{\tau}\right]^2}{R(\ell,\tau)}.\end{aligned} \tag{G.37}$$

In terms of the angles θ'_n, θ_n, $\theta'_{\ell,\tau}$, and $\theta_{\ell,\tau}$ defined in Figure G.1, the second derivatives of the phase function may be written as follows:

$$\ddot{\phi}_{\ell\ell}(\ell,\tau) = (\cos\theta'_n+\cos\theta_n)\kappa_1(\ell,\tau) + \frac{\sin^2\theta'_\ell}{s^i(\ell,\tau)} + \frac{\sin^2\theta_\ell}{R(\ell,\tau)}, \tag{G.38}$$

$$\ddot{\phi}_{\ell\tau}(\ell,\tau) = \frac{\cos\theta'_\ell\cos\theta'_\tau}{s^i(\ell,\tau)} + \frac{\cos\theta_\ell\cos\theta_\tau}{R(\ell,\tau)}, \tag{G.39}$$

$$\ddot{\phi}_{\tau\tau}(\ell,\tau) \;=\; (\cos\theta'_n + \cos\theta_n)\kappa_2(\ell,\tau) + \frac{\sin^2\theta'_\tau}{s^i(\ell,\tau)} + \frac{\sin^2\theta_\tau}{R(\ell,\tau)}\,. \qquad \text{(G.40)}$$

3. Third derivatives, $\bar{\bar{\phi}}_{\ell\ell}(\ell,\tau)$, $\bar{\bar{\phi}}_{\ell\tau}(\ell,\tau)$, $\bar{\bar{\phi}}_{\tau\tau\ell}(\ell,\tau)$, and $\bar{\bar{\phi}}_{\tau\tau\tau}(\ell,\tau)$:

From Equation (G.1) the third derivatives of the phase function are given by

$$\bar{\bar{\phi}}_{\ell\ell}(\ell,\tau) \;=\; \bar{\bar{s}}^{\,i}_{\ell\ell}(\ell,\tau) + \bar{\bar{R}}_{\ell\ell}(\ell,\tau)\,, \qquad \text{(G.41)}$$

$$\bar{\bar{\phi}}_{\ell\tau}(\ell,\tau) \;=\; \bar{\bar{s}}^{\,i}_{\ell\tau}(\ell,\tau) + \bar{\bar{R}}_{\ell\tau}(\ell,\tau)\,, \qquad \text{(G.42)}$$

$$\bar{\bar{\phi}}_{\tau\tau\ell}(\ell,\tau) \;=\; \bar{\bar{s}}^{\,i}_{\tau\tau\ell}(\ell,\tau) + \bar{\bar{R}}_{\tau\tau\ell}(\ell,\tau)\,, \qquad \text{(G.43)}$$

$$\bar{\bar{\phi}}_{\tau\tau\tau}(\ell,\tau) \;=\; \bar{\bar{s}}^{\,i}_{\tau\tau\tau}(\ell,\tau) + \bar{\bar{R}}_{\tau\tau\tau}(\ell,\tau)\,. \qquad \text{(G.44)}$$

Taking the derivative with respect to ℓ of both sides of Equation (G.25) we get

$$\begin{aligned}
3\dot{s}^i_\ell(\ell,\tau)\ddot{s}^{\,i}_{\ell\ell}(\ell,\tau) \;+\; & s^i(\ell,\tau)\,\bar{\bar{s}}^{\,i}_{\ell\ell\ell}(\ell,\tau) = 3\left[\dot{\vec{r}}_\ell(\ell,\tau)\cdot\hat{\ell}_0\right]\left[\ddot{\vec{r}}_{\ell\ell}(\ell,\tau)\cdot\hat{\ell}_0\right] \\
+\; & 3\left[\dot{\vec{r}}_\ell(\ell,\tau)\cdot\hat{\tau}_0\right]\left[\ddot{\vec{r}}_{\ell\ell}(\ell,\tau)\cdot\hat{\tau}_0\right] + 3\left[\dot{\vec{r}}_\ell(\ell,\tau)\cdot\hat{n}_0\right]\left[\ddot{\vec{r}}_{\ell\ell}(\ell,\tau)\cdot\hat{n}_0\right] \\
+\; & \left\{\left[\vec{s}^{\,i}_0 + \vec{r}(\ell,\tau)\right]\cdot\hat{\ell}_0\right\}\left[\bar{\bar{\vec{r}}}_{\ell\ell\ell}(\ell,\tau)\cdot\hat{\ell}_0\right] \\
+\; & \left\{\left[\vec{s}^{\,i}_0 + \vec{r}(\ell,\tau)\right]\cdot\hat{\tau}_0\right\}\left[\bar{\bar{\vec{r}}}_{\ell\ell\ell}(\ell,\tau)\cdot\hat{\tau}_0\right] \\
+\; & \left\{\left[\vec{s}^{\,i}_0 + \vec{r}(\ell,\tau)\right]\cdot\hat{n}_0\right\}\left[\bar{\bar{\vec{r}}}_{\ell\ell\ell}(\ell,\tau)\cdot\hat{n}_0\right]\,. \qquad \text{(G.45)}
\end{aligned}$$

Next, from Equations (G.6)–(G.11) one can show that $\bar{\bar{\vec{r}}}_{\ell\ell\ell}(\ell,\tau)$ is given by

$$\bar{\bar{\vec{r}}}_{\ell\ell\ell}(\ell,\tau) = -\kappa_1^2(\ell,\tau)\hat{\ell} - \left[\hat{\ell}\cdot\nabla\kappa_1(\ell,\tau)\right]\hat{n}\,, \qquad \text{(G.46)}$$

and letting $\delta,\epsilon \to 0$ Equation (G.45) becomes

$$\begin{aligned}
3\dot{s}^i_\ell(\ell,\tau)\ddot{s}^{\,i}_{\ell\ell}(\ell,\tau) + s^i(\ell,\tau)\,\bar{\bar{s}}^{\,i}_{\ell\ell\ell}(\ell,\tau) \;=\; & -\kappa_1^2(\ell,\tau)\left[\vec{s}^{\,i}(\ell,\tau)\cdot\hat{\ell}\right] \\
& -\; \hat{\ell}\cdot\nabla\kappa_1(\ell,\tau)\left[\vec{s}^{\,i}(\ell,\tau)\cdot\hat{n}\right]\,. \qquad \text{(G.47)}
\end{aligned}$$

Directly from (G.47) one can also infer the following expression:

$$\begin{aligned}
3\dot{s}^i_\tau(\ell,\tau)\ddot{s}^{\,i}_{\tau\tau}(\ell,\tau) + s^i(\ell,\tau)\,\bar{\bar{s}}^{\,i}_{\tau\tau\tau}(\ell,\tau) \;=\; & -\kappa_2^2(\ell,\tau)\left[\vec{s}^{\,i}(\ell,\tau)\cdot\hat{\tau}\right] \\
& -\; \hat{\tau}\cdot\nabla\kappa_2(\ell,\tau)\left[\vec{s}^{\,i}(\ell,\tau)\cdot\hat{n}\right]\,. \qquad \text{(G.48)}
\end{aligned}$$

Next, taking the derivative of Equation (G.28) with respect to ℓ and τ we obtain the following expressions:

$$2\dot{s}^i_\ell(\ell,\tau)\ddot{s}^i_{\ell\tau}(\ell,\tau) + \dot{s}^i_\tau(\ell,\tau)\ddot{s}^i_{\ell\ell}(\ell,\tau) + s^i(\ell,\tau)\,\overline{\overline{s}}^i_{\ell\ell\tau}(\ell,\tau) = 0, \qquad \text{(G.49)}$$

$$2\dot{s}^i_\tau(\ell,\tau)\ddot{s}^i_{\ell\tau}(\ell,\tau) + \dot{s}^i_\ell(\ell,\tau)\ddot{s}^i_{\tau\tau}(\ell,\tau) + s^i(\ell,\tau)\,\overline{\overline{s}}^i_{\tau\tau\ell}(\ell,\tau) = 0. \qquad \text{(G.50)}$$

Then, using (G.15), (G.17), (G.29)–(G.31), and (G.47)–(G.50) the quantities $\overline{\overline{s}}^i_{\ell\ell}$, $\overline{\overline{s}}^i_{\ell\tau}$, $\overline{\overline{s}}^i_{\tau\tau\ell}$, and $\overline{\overline{s}}^i_{\tau\tau\tau}$ are given by

$$\begin{aligned}
\overline{\overline{s}}^i_{\ell\ell}(\ell,\tau) &= -\kappa_1^2(\ell,\tau)\left[\hat{s}^i(\ell,\tau)\cdot\hat{\ell}\right] - \hat{\ell}\cdot\nabla\kappa_1(\ell,\tau)\left[\hat{s}^i(\ell,\tau)\cdot\hat{n}\right] \\
&\quad + \frac{\hat{s}^i(\ell,\tau)\cdot\hat{\ell}}{s^i(\ell,\tau)}\left\{3\kappa_1(\ell,\tau)\left[\hat{s}^i(\ell,\tau)\cdot\hat{n}\right] - \frac{1-\left[\hat{s}^i(\ell,\tau)\cdot\hat{\ell}\right]^2}{s^i(\ell,\tau)}\right\}, \qquad \text{(G.51)} \\
\overline{\overline{s}}^i_{\ell\tau}(\ell,\tau) &= \frac{\hat{s}^i(\ell,\tau)\cdot\hat{\tau}}{s^i(\ell,\tau)}\left\{\kappa_1(\ell,\tau)\left[\hat{s}^i(\ell,\tau)\cdot\hat{n}\right] - \frac{1-3\left[\hat{s}^i(\ell,\tau)\cdot\hat{\ell}\right]^2}{s^i(\ell,\tau)}\right\}, \qquad \text{(G.52)} \\
\overline{\overline{s}}^i_{\tau\tau\ell}(\ell,\tau) &= \frac{\hat{s}^i(\ell,\tau)\cdot\hat{\ell}}{s^i(\ell,\tau)}\left\{\kappa_2(\ell,\tau)\left[\hat{s}^i(\ell,\tau)\cdot\hat{n}\right] - \frac{1-3\left[\hat{s}^i(\ell,\tau)\cdot\hat{\tau}\right]^2}{s^i(\ell,\tau)}\right\}, \qquad \text{(G.53)} \\
\overline{\overline{s}}^i_{\tau\tau\tau}(\ell,\tau) &= -\kappa_2^2(\ell,\tau)\left[\hat{s}^i(\ell,\tau)\cdot\hat{\tau}\right] - \hat{\tau}\cdot\nabla\kappa_2(\ell,\tau)\left[\hat{s}^i(\ell,\tau)\cdot\hat{n}\right] \\
&\quad + \frac{\hat{s}^i(\ell,\tau)\cdot\hat{\tau}}{s^i(\ell,\tau)}\left\{3\kappa_2(\ell,\tau)\left[\hat{s}^i(\ell,\tau)\cdot\hat{n}\right] - \frac{1-\left[\hat{s}^i(\ell,\tau)\cdot\hat{\tau}\right]^2}{s^i(\ell,\tau)}\right\}, \qquad \text{(G.54)}
\end{aligned}$$

Similarly, the quantities $\overline{\overline{R}}_{\ell\ell}$, $\overline{\overline{R}}_{\ell\tau}$, $\overline{\overline{R}}_{\tau\tau\ell}$, and $\overline{\overline{R}}_{\tau\tau\tau}$ are given by

$$\begin{aligned}
\overline{\overline{R}}_{\ell\ell}(\ell,\tau) &= \kappa_1^2(\ell,\tau)\left[\hat{R}(\ell,\tau)\cdot\hat{\ell}\right] - \hat{\ell}\cdot\nabla\kappa_1(\ell,\tau)\left[\hat{R}(\ell,\tau)\cdot\hat{n}\right] \\
&\quad + \frac{\hat{R}(\ell,\tau)\cdot\hat{\ell}}{R(\ell,\tau)}\left\{3\kappa_1(\ell,\tau)\left[\hat{R}(\ell,\tau)\cdot\hat{n}\right] + \frac{1-\left[\hat{R}(\ell,\tau)\cdot\hat{\ell}\right]^2}{R(\ell,\tau)}\right\}, \qquad \text{(G.55)} \\
\overline{\overline{R}}_{\ell\tau}(\ell,\tau) &= \frac{\hat{R}(\ell,\tau)\cdot\hat{\tau}}{R(\ell,\tau)}\left\{\kappa_1(\ell,\tau)\left[\hat{R}(\ell,\tau)\cdot\hat{n}\right] + \frac{1-3\left[\hat{R}(\ell,\tau)\cdot\hat{\ell}\right]^2}{R(\ell,\tau)}\right\}, \qquad \text{(G.56)} \\
\overline{\overline{R}}_{\tau\tau\ell}(\ell,\tau) &= \frac{\hat{R}(\ell,\tau)\cdot\hat{\ell}}{R(\ell,\tau)}\left\{\kappa_2(\ell,\tau)\left[\hat{R}(\ell,\tau)\cdot\hat{n}\right] + \frac{1-3\left[\hat{R}(\ell,\tau)\cdot\hat{\tau}\right]^2}{R(\ell,\tau)}\right\}, \qquad \text{(G.57)} \\
\overline{\overline{R}}_{\tau\tau\tau}(\ell,\tau) &= \kappa_2^2(\ell,\tau)\left[\hat{R}(\ell,\tau)\cdot\hat{\tau}\right] + \hat{\tau}\cdot\nabla\kappa_2(\ell,\tau)\left[\hat{R}(\ell,\tau)\cdot\hat{n}\right] \\
&\quad + \frac{\hat{R}(\ell,\tau)\cdot\hat{\tau}}{R(\ell,\tau)}\left\{3\kappa_2(\ell,\tau)\left[\hat{R}(\ell,\tau)\cdot\hat{n}\right] + \frac{1-\left[\hat{R}(\ell,\tau)\cdot\hat{\tau}\right]^2}{R(\ell,\tau)}\right\}, \qquad \text{(G.58)}
\end{aligned}$$

Finally, using Equations (G.41)–(G.44), and (G.51)–(G.58) the third derivatives of the phase function are given by

$$\begin{aligned}
\ddot{\phi}_{\ell\ell}(\ell,\tau) &= \left[\hat{R}(\ell,\tau)-\hat{s}^i(\ell,\tau)\right]\cdot\left\{\kappa_1^2(\ell,\tau)\hat{\ell}+\left[\hat{\ell}\cdot\nabla\kappa_1(\ell,\tau)\right]\hat{n}\right\} \\
&+ \frac{\hat{s}^i(\ell,\tau)\cdot\hat{\ell}}{s^i(\ell,\tau)}\left\{3\kappa_1(\ell,\tau)\left[\hat{s}^i(\ell,\tau)\cdot\hat{n}\right]-\frac{1-\left[\hat{s}^i(\ell,\tau)\cdot\hat{\ell}\right]^2}{s^i(\ell,\tau)}\right\} \\
&+ \frac{\hat{R}(\ell,\tau)\cdot\hat{\ell}}{R(\ell,\tau)}\left\{3\kappa_1(\ell,\tau)\left[\hat{R}(\ell,\tau)\cdot\hat{n}\right]+\frac{1-\left[\hat{R}(\ell,\tau)\cdot\hat{\ell}\right]^2}{R(\ell,\tau)}\right\}, \qquad \text{(G.59)} \\
\ddot{\phi}_{\ell\tau}(\ell,\tau) &= \frac{\hat{s}^i(\ell,\tau)\cdot\hat{\tau}}{s^i(\ell,\tau)}\left\{\kappa_1(\ell,\tau)\left[\hat{s}^i(\ell,\tau)\cdot\hat{n}\right]-\frac{1-3\left[\hat{s}^i(\ell,\tau)\cdot\hat{\ell}\right]^2}{s^i(\ell,\tau)}\right\} \\
&+ \frac{\hat{R}(\ell,\tau)\cdot\hat{\tau}}{R(\ell,\tau)}\left\{\kappa_1(\ell,\tau)\left[\hat{R}(\ell,\tau)\cdot\hat{n}\right]+\frac{1-3\left[\hat{R}(\ell,\tau)\cdot\hat{\ell}\right]^2}{R(\ell,\tau)}\right\}, \qquad \text{(G.60)} \\
\ddot{\phi}_{\tau\tau\ell}(\ell,\tau) &= \frac{\hat{s}^i(\ell,\tau)\cdot\hat{\ell}}{s^i(\ell,\tau)}\left\{\kappa_2(\ell,\tau)\left[\hat{s}^i(\ell,\tau)\cdot\hat{n}\right]-\frac{1-3\left[\hat{s}^i(\ell,\tau)\cdot\hat{\tau}\right]^2}{s^i(\ell,\tau)}\right\} \\
&+ \frac{\hat{R}(\ell,\tau)\cdot\hat{\ell}}{R(\ell,\tau)}\left\{\kappa_2(\ell,\tau)\left[\hat{R}(\ell,\tau)\cdot\hat{n}\right]+\frac{1-3\left[\hat{R}(\ell,\tau)\cdot\hat{\tau}\right]^2}{R(\ell,\tau)}\right\}, \qquad \text{(G.61)} \\
\ddot{\phi}_{\tau\tau\tau}(\ell,\tau) &= \left[\hat{R}(\ell,\tau)-\hat{s}^i(\ell,\tau)\right]\cdot\left\{\kappa_2^2(\ell,\tau)\hat{\tau}+\left[\hat{\tau}\cdot\nabla\kappa_2(\ell,\tau)\right]\hat{n}\right\} \\
&+ \frac{\hat{s}^i(\ell,\tau)\cdot\hat{\tau}}{s^i(\ell,\tau)}\left\{3\kappa_2(\ell,\tau)\left[\hat{s}^i(\ell,\tau)\cdot\hat{n}\right]-\frac{1-\left[\hat{s}^i(\ell,\tau)\cdot\hat{\tau}\right]^2}{s^i(\ell,\tau)}\right\} \\
&+ \frac{\hat{R}(\ell,\tau)\cdot\hat{\tau}}{R(\ell,\tau)}\left\{3\kappa_2(\ell,\tau)\left[\hat{R}(\ell,\tau)\cdot\hat{n}\right]+\frac{1-\left[\hat{R}(\ell,\tau)\cdot\hat{\tau}\right]^2}{R(\ell,\tau)}\right\}, \qquad \text{(G.62)}
\end{aligned}$$

In terms of the angles θ'_n, θ_n, $\theta'_{\ell,\tau}$, and $\theta_{\ell,\tau}$ defined in Figure G.1, the third derivatives of the phase function may be written as follows:

$$\begin{aligned}
\ddot{\phi}_{\ell\ell}(\ell,\tau) &= (\cos\theta'_\ell+\cos\theta_\ell)\kappa_1^2(\ell,\tau)+(\cos\theta'_n+\cos\theta_n)\left[\hat{\ell}\cdot\nabla\kappa_1(\ell,\tau)\right] \\
&+ \frac{\cos\theta'_\ell}{s^i(\ell,\tau)}\left[3\cos\theta'_n\kappa_1(\ell,\tau)+\frac{\sin^2\theta'_\ell}{s^i(\ell,\tau)}\right] \\
&+ \frac{\cos\theta_\ell}{R(\ell,\tau)}\left[3\cos\theta_n\kappa_1(\ell,\tau)+\frac{\sin^2\theta_\ell}{R(\ell,\tau)}\right], \qquad \text{(G.63)} \\
\ddot{\phi}_{\ell\tau}(\ell,\tau) &= \frac{\cos\theta'_\tau}{s^i(\ell,\tau)}\left[\cos\theta'_n\kappa_1(\ell,\tau)+\frac{1-3\cos^2\theta'_\ell}{s^i(\ell,\tau)}\right] \\
&+ \frac{\cos\theta_\tau}{R(\ell,\tau)}\left[\cos\theta_n\kappa_1(\ell,\tau)+\frac{1-3\cos^2\theta_\ell}{R(\ell,\tau)}\right], \qquad \text{(G.64)}
\end{aligned}$$

$$\ddot{\phi}_{\ell\tau\tau}(\ell,\tau) = \frac{\cos\theta'_\ell}{s^i(\ell,\tau)}\left[\cos\theta'_n\kappa_2(\ell,\tau)+\frac{1-3\cos^2\theta'_\tau}{s^i(\ell,\tau)}\right] + \frac{\cos\theta_\ell}{R(\ell,\tau)}\left[\cos\theta_n\kappa_2(\ell,\tau)+\frac{1-3\cos^2\theta_\tau}{R(\ell,\tau)}\right], \tag{G.65}$$

$$\ddot{\phi}_{\tau\tau\tau}(\ell,\tau) = (\cos\theta'_\tau+\cos\theta_\tau)\kappa_2^2(\ell,\tau)+(\cos\theta'_n+\cos\theta_n)\left[\widehat{\tau}\cdot\nabla\kappa_2(\ell,\tau)\right] + \frac{\cos\theta'_\tau}{s^i(\ell,\tau)}\left[3\cos\theta'_n\kappa_2(\ell,\tau)+\frac{\sin^2\theta'_\tau}{s^i(\ell,\tau)}\right] + \frac{\cos\theta_\tau}{R(\ell,\tau)}\left[3\cos\theta_n\kappa_2(\ell,\tau)+\frac{\sin^2\theta_\tau}{R(\ell,\tau)}\right]. \tag{G.66}$$

When (ℓ,τ) is a reflection point $Q_r=(\ell_r,\tau_r)$, as shown in Figure G.2, one can use the derivatives of the phase function in the PO radiation integral to derive some familiar expressions involved in the reflected field from a 3–D surface. The first derivatives of the phase function given in (G.18) and (G.19) evaluated at Q_r represent the *law of reflection,* that is

$$\begin{cases}\dot{\phi}_\ell(\ell_r,\tau_r)=(\widehat{s}^{\,i}-\widehat{s}^{\,r})\cdot\widehat{\ell}_r=0\\ \dot{\phi}_\tau(\ell_r,\tau_r)=(\widehat{s}^{\,i}-\widehat{s}^{\,r})\cdot\widehat{\tau}_r=0\,,\end{cases} \tag{G.67}$$

which can be written in a more familiar form as follows:

$$\begin{cases}(\widehat{s}^{\,i}-\widehat{s}^{\,r})\cdot\widehat{n}_r=0\\ (\widehat{s}^{\,i}-\widehat{s}^{\,r})\times\widehat{n}_r=0\,.\end{cases} \tag{G.68}$$

The second derivatives of the phase function given in (G.38)–(G.40) evaluated at Q_r with (G.67) being employed are related to the spread factor of the reflected wavefront through the following expression:

$$\ddot{\phi}_{\ell\ell}(\ell_r,\tau_r)\ddot{\phi}_{\tau\tau}(\ell_r,\tau_r)-\ddot{\phi}^2_{\ell\tau}(\ell_r,\tau_r) = \cos^2\theta^i\left(\frac{1}{s^r}+\frac{1}{\rho^r_\ell}\right)\left(\frac{1}{s^r}+\frac{1}{\rho^r_\tau}\right) \propto (\text{reflected ray spread factor})^{-2}, \tag{G.69}$$

where θ^i is the usual angle of incidence, and $\rho^r_{\ell,\tau}$ are the radii of curvature of the reflected wavefront due to spherical wave illumination and are given by

$$\frac{1}{\rho^r_{\ell,\tau}} = \frac{1}{s^i}+\frac{1}{\cos\theta^i}\left[\kappa_1(Q_r)\sin^2\theta_\tau+\kappa_2(Q_r)\sin^2\theta_\ell\right] \pm\sqrt{\frac{1}{\cos^2\theta^i}\left[\kappa_1(Q_r)\sin^2\theta_\tau+\kappa_2(Q_r)\sin^2\theta_\ell\right]^2-4\kappa_1(Q_r)\kappa_2(Q_r)}\,, \tag{G.70}$$

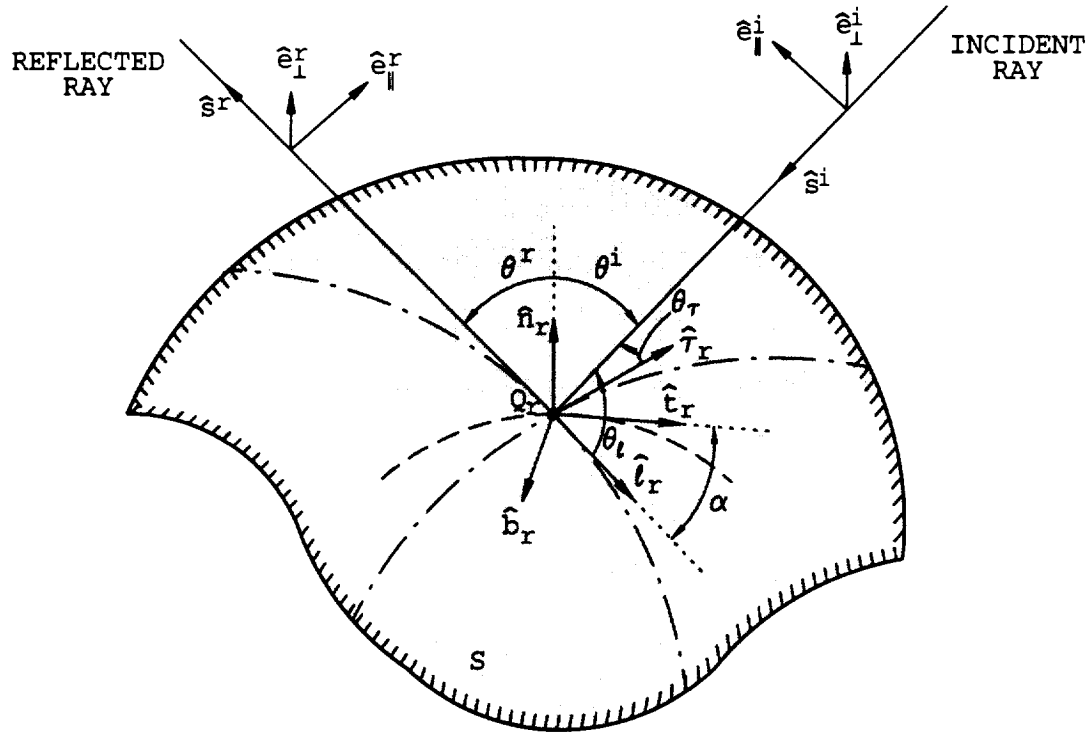

Figure G.2: Reflection from a 3-D curved surface

where the angles $\theta_{\ell,\tau}$ are defined in Figure G.2 and $\kappa_{1,2}(Q_r)$ are the principal surface curvatures at Q_r in the directions of $\hat{\ell}_r$ and $\hat{\tau}_r$, respectively. An alternative expression for $\rho^r_{\ell,\tau}$ is as follows:

$$\frac{1}{\rho^r_{\ell,\tau}} = \frac{1}{s^i} + \frac{f\,\kappa_g(Q_r)}{\cos\theta^i}\left[1 \pm \sqrt{1 - \frac{4\kappa_1(Q_r)\kappa_2(Q_r)\cos^2\theta^i}{f^2\kappa_g(Q_r)}}\right], \tag{G.71}$$

$$f = 1 + \frac{\kappa_t(Q_r)}{\kappa_g(Q_r)}\cos^2\theta^i, \tag{G.72}$$

where $\kappa_g(Q_r)$ is the normal surface curvature along the plane of incidence, $\kappa_t(Q_r)$ is the normal surface curvature along the transverse plane defined by the unit normal vector $\hat{n}_r$ and the unit binormal vector $\hat{b}_r$, and they can be found using *Euler's theorem* [29], that is

$$\kappa_g(Q_r) = \kappa_1(Q_r)\cos^2\alpha + \kappa_2(Q_r)\sin^2\alpha, \tag{G.73}$$

$$\kappa_t(Q_r) = \kappa_1(Q_r)\sin^2\alpha + \kappa_2(Q_r)\cos^2\alpha, \tag{G.74}$$

where α is the angle between $\hat{t}_r$ and $\hat{\ell}_r$ as shown in Figure G.2. The third derivatives of the phase function given in (G.63)–(G.66) evaluated at Q_r with (G.67) being employed are related to the spread factor of the reflected wavefront when the observation point is near a caustic ($\rho^r_\ell = -s^r$) through the following expression:

$$\begin{aligned} m(Q_r) &= \dddot{\phi}_{\ell\ell\ell}(\ell_r,\tau_r) - \frac{\ddot{\phi}_{\ell\tau}(\ell_r,\tau_r)}{\ddot{\phi}_{\tau\tau}(\ell_r,\tau_r)} \\ &\quad \cdot \left[3\,\dddot{\phi}_{\ell\ell\tau}(\ell_r,\tau_r) - \frac{\ddot{\phi}_{\ell\tau}(\ell_r,\tau_r)\,\dddot{\phi}_{\ell\tau\tau}(\ell_r,\tau_r)}{\ddot{\phi}_{\tau\tau}(\ell_r,\tau_r)}\right] \\ &\propto (\text{reflected ray spread factor near a caustic})^{-3}, \end{aligned} \tag{G.75}$$

where

$$\begin{aligned} \dddot{\phi}_{\ell\ell\ell}(\ell_r,\tau_r) &= 2\cos\theta^i\left[\hat{\ell}_r\cdot\nabla\kappa_1(Q_r)\right] \\ &\quad + \frac{\cos\theta'_\ell}{s^i}\left[3\cos\theta^i\kappa_1(Q_r) + \frac{\sin^2\theta'_\ell}{s^i}\right] \\ &\quad + \frac{\cos\theta_\ell}{s^i}\left[3\cos\theta^r\kappa_1(Q_r) + \frac{\sin^2\theta_\ell}{s^r}\right], \end{aligned} \tag{G.76}$$

$$\ddot{\phi}_{\ell\tau}(\ell_r,\tau_r) = -\cos\theta_\ell\cos\theta_\tau\left(\frac{1}{s^i}+\frac{1}{s^r}\right), \tag{G.77}$$

$$\ddot{\phi}_{\tau\tau}(\ell_r,\tau_r) = 2\cos\theta^i\kappa_2(Q_r) + \sin^2\theta_\tau\left(\frac{1}{s^i}+\frac{1}{s^r}\right), \tag{G.78}$$

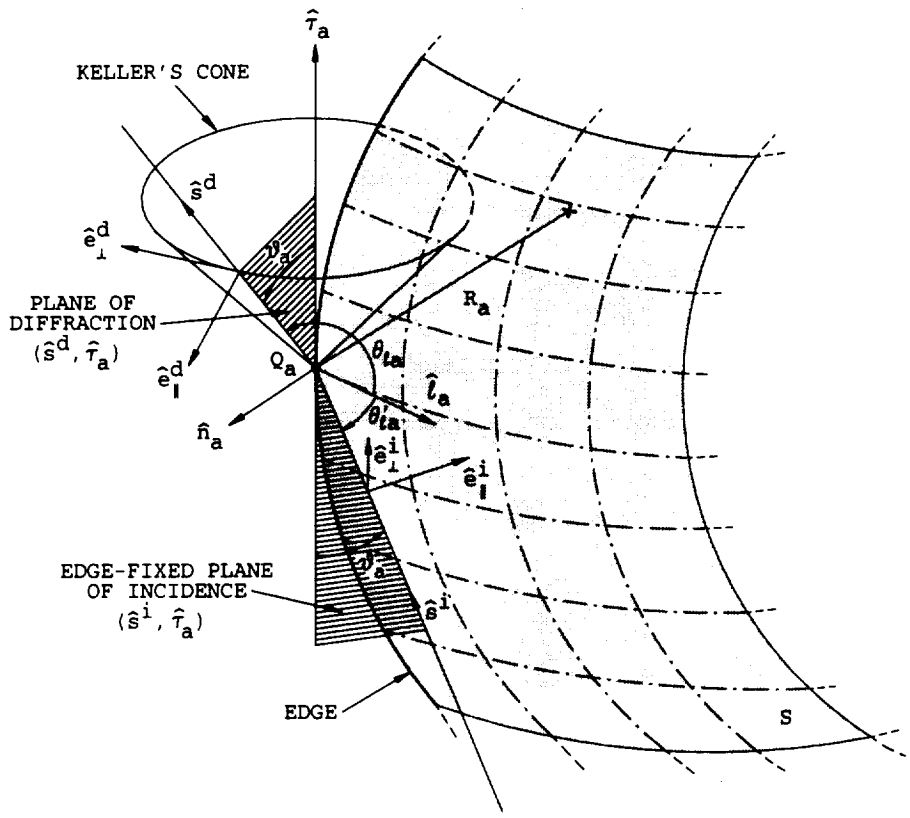

Figure G.3: Diffraction from a curved edge in 3–D surface (side view)

$$\bar{\bar{\phi}}_{\ell\tau}(\ell_r,\tau_r) = \frac{\cos\theta'_\tau}{s^i}\left[\cos\theta^i\kappa_1(Q_r)+\frac{1-3\cos^2\theta'_\ell}{s^i}\right] + \frac{\cos\theta_\tau}{s^i}\left[\cos\theta^r\kappa_1(Q_r)+\frac{1-3\cos^2\theta_\ell}{s^r}\right], \tag{G.79}$$

$$\bar{\bar{\phi}}_{\ell\tau\tau}(\ell_r,\tau_r) = \frac{\cos\theta'_\ell}{s^i}\left[\cos\theta^i\kappa_2(Q_r)+\frac{1-3\cos^2\theta'_\tau}{s^i}\right] + \frac{\cos\theta_\ell}{s^i}\left[\cos\theta^r\kappa_2(Q_r)+\frac{1-3\cos^2\theta_\tau}{s^r}\right]. \tag{G.80}$$

When (ℓ,τ) is an edge diffraction point $Q_a=(\ell_a,\tau_a)$ as shown in Figure G.3, one can use the derivatives of the phase function to derive some familiar expressions involved in the diffracted field from a curved edge in a 3–D surface. It is assumed here for convenience that the edge extends along the surface coordinate curve τ. The first derivative of the phase function along τ given in (G.19) evaluated at Q_a represents Keller's *law of edge diffraction*, that is

$$\dot{\phi}_\tau(\ell_a,\tau_a) = \left(\widehat{s}_a^{\,i} - \widehat{s}_a^{\,d}\right)\cdot\widehat{\tau}_a = 0\,, \tag{G.81}$$

where $\widehat{\tau}_a$ is the associated unit tangent to the edge at Q_a. The second derivative of the phase function along τ given in (G.40) evaluated at Q_a with (G.81) being employed is related to the spread factor of the diffracted wavefront, that is

$$\begin{aligned}\ddot{\phi}_{\tau\tau}(\ell_a,\tau_a) &= \sin^2\vartheta_a\left(\frac{1}{s_a^d}+\frac{1}{\rho_a^d}\right) \\ &\propto \text{(diffracted ray spread factor)}^{-2}\,,\end{aligned} \tag{G.82}$$

where ϑ_a is the angle of diffraction defined in Figure G.2, and ρ_a^d is the distance from the caustic at Q_a and the second caustic of the diffracted ray and is given by

$$\frac{1}{\rho_a^d} = \frac{1}{s_a^i} + \frac{\left(\widehat{s}_a^{\,d} - \widehat{s}_a^{\,i}\right)\cdot\widehat{n}_a}{R_a\sin^2\vartheta_a}\,, \tag{G.83}$$

where $\widehat{n}_a$ is the associated unit normal vector to the edge at Q_a directed away from the center of curvature, and $R_a > 0$ is the radius of curvature of the edge at Q_a. The third derivatives of the phase function given in (G.63)-(G.66) evaluated at Q_a with (G.81) being employed are related to the distance parameter for the EUTD transition function, that is

$$\begin{aligned}L_d(Q_a) &= \dddot{\phi}_{\ell\ell\tau}(\ell_a,\tau_a) - \frac{\ddot{\phi}_{\ell\tau}(\ell_a,\tau_a)}{\ddot{\phi}_{\tau\tau}(\ell_a,\tau_a)} \\ &\quad\cdot\left[3\,\dddot{\phi}_{\ell\ell\tau}(\ell_a,\tau_a) - \frac{\ddot{\phi}_{\ell\tau}(\ell_a,\tau_a)\,\dddot{\phi}_{\ell\tau\tau}(\ell_a,\tau_a)}{\ddot{\phi}_{\tau\tau}(\ell_a,\tau_a)}\right],\end{aligned} \tag{G.84}$$

where

$$\begin{aligned}\dddot{\phi}_{\ell\ell\ell}(\ell_a,\tau_a) &= (\cos\theta_{\ell a}+\cos\theta'_{\ell a})\kappa_1^2(Q_a) \\ &+ \sin\vartheta_a(\sin\varphi'_a+\sin\varphi_a)\left[\widehat{\ell}_a\cdot\kappa_1(Q_a)\right] \\ &+ \frac{\cos\theta'_{\ell a}}{s_a^i}\left[3\kappa_1(Q_a)\sin\vartheta_a\sin\varphi'_a+\frac{\sin^2\theta'_{\ell a}}{s_a^i}\right] \\ &+ \frac{\cos\theta_{\ell a}}{s_a^d}\left[3\kappa_1(Q_a)\sin\vartheta_a\sin\varphi_a+\frac{\sin^2\theta_{\ell a}}{s_a^d}\right],\end{aligned} \tag{G.85}$$

$$\ddot{\phi}_{\ell\tau}(\ell_a,\tau_a) = \frac{\cos\theta'_{\ell a}\cos\theta'_{\tau a}}{s_a^i} + \frac{\cos\theta_{\ell a}\cos\theta_{\tau a}}{s_a^d}\,, \tag{G.86}$$

$$\dddot{\phi}_{\ell\ell\tau}(\ell_a,\tau_a) = \frac{\cos\theta'_{\tau a}}{s_a^i}\left[\kappa_1(Q_a)\sin\vartheta_a\sin\varphi'_a+\frac{1-3\cos^2\theta'_{\ell a}}{s_a^i}\right]$$

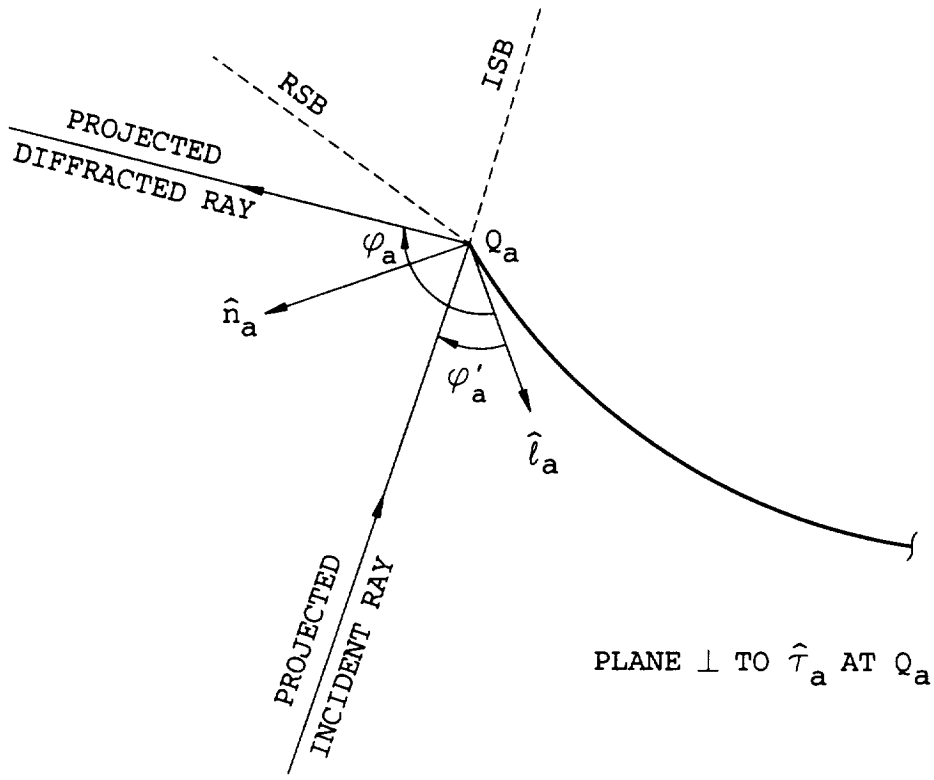

Figure G.4: Diffraction from a curved edge in a 3–D surface (top view)

$$+ \quad \frac{\cos\theta_{\tau a}}{s_a^d}\left[\kappa_1(Q_a)\sin\vartheta_a\sin\varphi_a + \frac{1-3\cos^2\theta_{\ell a}}{s_a^d}\right], \qquad \text{(G.87)}$$

$$\ddot{\phi}_{\ell\tau\tau}(\ell_a,\tau_a) = \frac{\cos\theta'_{\ell a}}{s_a^i}\left[\kappa_2(Q_a)\sin\vartheta_a\sin\varphi'_a + \frac{1-3\cos^2\theta'_{\tau a}}{s_a^i}\right]$$

$$+ \quad \frac{\cos\theta_{\ell a}}{s_a^d}\left[\kappa_2(Q_a)\sin\vartheta_a\sin\varphi_a + \frac{1-3\cos^2\theta_{\tau a}}{s_a^d}\right]. \qquad \text{(G.88)}$$

The angles φ'_a and φ_a are the angles between the projected directions of incidence and observation (on a plane perpendicular to $\hat{\tau}_a$) and $\hat{\ell}_a$ as shown in Figure G.4.

Bibliography

[1] M. Klein and I. W. Kay, *Electromagnetic Theory and Geometrical Optics.* Interscience Publishers, 1965.

[2] H. Ikuno and L. B. Felsen, "Real and complex rays for scattering from a target with inflection points," *Radio Science,* vol. 22, No. 6, pp. 952–958, Nov. 1987.

[3] H. Ikuno and L. B. Felsen, "Complex ray interpretation of reflection from concave-convex surfaces," *IEEE Trans. Antennas Propagat.,* vol. 36, pp. 1260–1271, Sept. 1988.

[4] R. G. Kouyoumjian and P. H. Pathak, "A uniform geometrical theory of diffraction for an edge in a perfectly conducting surface," *Proc. of IEEE,* vol. 62, pp. 1448–1461, Nov. 1974.

[5] J. B. Keller, "Geometrical theory of diffraction," *J. Opt. Soc. Am.,* vol. 52, pp. 116–130, 1962.

[6] R. F. Harrington, *Time Harmonic Electromagnetic Fields.* New York: McGraw–Hill, p. 127, 1961.

[7] C. Chester, B. Friedman, and F. Ursell, "An extension of the method of steepest descent," *Proc. Cambridge Philosoph. Soc.,* vol. 53, pp. 599–611, 1957.

[8] L. B. Felsen and N. Marcuvitz, *Radiation and Scattering of Waves.* Englewood Cliffs, NJ: Prentice Hall, 1973.

[9] L. Levey and L. B. Felsen, "On incomplete Airy functions and their application to diffraction problems," *Radio Science,* vol. 4, No. 10, pp. 959–969, Oct. 1969.

[10] M. H. Rahnavard and W. V. T. Rusch, "Surface-curvature-induced microwave shadows," *IEEE Trans. Antennas Propagat.,* vol. 30, pp. 83–88, Jan. 1982.

[11] N. C. Albertsen, P. Balling, and N. E. Jensen, "Caustics and caustic corrections to the field diffracted by a curved edge," *IEEE Trans. Antennas Propagat.,* vol. 35, pp. 297–303, May 1977.

[12] V. P. Maslov, *Perturbation Theory and Asymptotic Method.* Paris, France: Dounod, 1972 (in French).

[13] R. W. Ziolkowski and G. A. Deschamps, "Asymptotic evaluation of high frequency fields near a caustic: An introduction to Maslov's method," *Radio Science,* vol. 17, pp. 1181–1191, 1984.

[14] P. H. Pathak and M. C. Liang, "On a uniform asymptotic solution valid across smooth caustics of rays reflected by smoothly indented boundaries," *IEEE Trans. Antennas Propagat.,* Vol. 38, No. 8, pp. 1192–1203, Aug. 1990.

[15] R. M. Lewis and J. Boersma, "Uniform asymptotic theory of edge diffraction," *J. Math. Phys.,* Vol. 10, pp. 2291–2305, 1968.

[16] N. A. Logan and K. S. Yee, *Electromagnetic Waves,* edited by R. E. Langer, University of Wisconsin Press, Madison, 1962

[17] M. Abramowitz and I. A. Stegun, *Handbook of Mathematical Functions.* New York: Dover, 1972, p. 446.

[18] H. Ihuno, "Calculation of far-scattered fields by the method of stationary phase," *IEEE Trans. Antennas Propagat.,* Vol. AP–27, pp. 199–202, Mar. 1979.

[19] P. Ya. Ufitsev, "The method of fringe waves in the physical theory of diffraction," *Sovyetskoye Radio,* Moscow, 1962. Now translated and available from the US Air Force Foreign Technology Division, Wright Patterson AFB, Dayton, OH, USA.

[20] G. L. James, *Geometrical Theory of Diffraction for Electromagnetic Waves.* London, UK: Peter Peregrinus Ltd., 1976, p. 150.

[21] M. Abramowitz and I. A. Stegun, *Handbook of Mathematical Functions.* New York: Dover, 1972, p. 260.

[22] E. D. Constantinides and R. J. Marhefka, "On a class of complete and incomplete generalized Airy functions and their application to high-frequency scattering and diffraction problems," paper presented at the 1992 IEEE AP-S/URSI Symposium, Chicago, IL.

[23] G. B. Airy, "On the intensity of light in the neighborhood of a caustic," *Trans. Cambridge Phil. Soc.,* Vol. 6, p. 379, 1838.

[24] V. A. Fock, *Electromagnetic Diffraction and Propagation Problems.* Oxford, England: Pergamon, 1965.

[25] R. M. Lewis, "Asymptotic theory of transients," *Electromagnetic Wave Theory,* edited by J. Brown. Oxford, England: Pergamon, 1967, pp. 864–869.

[26] A. Erdélyi, *Asymptotic Expansions.* New York: Dover, 1956, pp. 41–43.

[27] N. Bleistein, "Uniform asymptotic expansions of integrals with many nearby stationary points and algebraic singularities," *J. Math. Mech.,* Vol. 17, pp. 533–559, 1967.

[28] M. M. Lipschutz, *Differential Geometry,* Schaum's Outline Series in Mathematics, McGraw–Hill, 1969.

[29] D. J. Struick, *Lectures on Classical Differential Geometry,* Addison–Wesley, 1950.